THE UNIVERSITY
of EDINBURGH

Targeting cellular nuclear export to inhibit influenza A virus replication

Rebecca Amy Dewar

Doctor of Philosophy

The University of Edinburgh

2017

Acknowledgments

Firstly, I would like to express my sincere gratitude to Professor Paul Digard for the continuous support, patience, motivation and immense knowledge throughout my PhD studies. Thank you - I could not have wished for a better supervisor. I was also fortunate to have a secondary supervisor Professor Bernadette Dutia, who's support, and advice was immensely appreciated, especially at the writing stage of my research.

Besides my supervisors, I would like to thank the rest of my thesis committee; Dr Lonneke Vervelde and Dr Xavier Donadeu for their encouragement and insightful comments during committee meetings which incented me to examine my research from different perspectives.

I would also like to thank the funders Moredun Scientific and Karyopharm Therapeutics for their endorsement of this project.

Special thanks also to Dr Darren Shaw, who helped advise on the statistical analysis throughout this thesis.

I am also extremely grateful to Dr Helen Wise, Dr Nikki Smith, Dr Saira Hussain, Dr Lita Murphy, Dr Lilian Chung and Dr Elly Gaunt for their constant help, support and inspiration during my PhD studies. Your contributions were invaluable.

I was very privileged to work alongside best friends during my studies - Dr Seema Jasim, Anabel Clements, Dr Matty Turntables, Rute Pinto, Carina Conceição and Dr Mariya Goncheva. I am so grateful to have met some of the most amazing people in my life. Friday bar, 2-hour coffee breaks, Waiting Room gossips, Popworld, Portuguese nights, the list could go on… my PhD would not have been half as much fun without you all.

A massive thanks to my best Glaswegian friend Clare for always being there for me (and for much needed nights out).

Thanks to BMF training for maintaining my sanity during the writing stage and to Caroline for getting muddy with me.

I would also like to thank my MRes/CVR friends Antonio, Pranav, Eva, Jo and Alice and my MRes supervisors' Dr Frazer Rixon and Dr Chris Boutell who allowed me to discover my love for research and who gave me the confidence to pursue a PhD.

Finally, the biggest thanks to my small but perfect family - my Mum, Gran and Grandpa. I cannot begin to express on paper how much your support and encouragement means to me - without you, this would not have been possible. I am incredibly lucky.

Declaration

I declare that this thesis was composed by myself, that the work contained herein is my own except where stated otherwise in the text, and that this work has not been submitted for any other degree or professional qualification.

Rebecca Amy Dewar

Lay summary

Commonly known as ‘the flu’, influenza is an infectious disease caused by viruses. Three types of influenza viruses infect people; A, B, and C. Influenza A virus (IAV) poses the most threat to human populations as it has the potential to cause pandemic outbreaks which can spread to millions of people worldwide. Vaccines are developed annually to treat influenza virus during ‘flu season’, which typically occurs during the winter months. Unfortunately, vaccines are not always successful as the influenza virus can change between seasons. Therefore, as a secondary line of defence to treat influenza, antiviral drugs are administered. Currently only two classes of antivirals have been licensed in the US and Europe for use against influenza virus in humans; one class has been rendered ineffective and another is beginning to lose effectiveness. Thus, it is necessary to investigate new antivirals for IAV infection.

Like all viruses, IAV uses cells to produce more virus. In this thesis, a set of inhibitors, called selective inhibitors of nuclear export (SINE) that target a human cell pathway dependent on the CRM1 protein, were assessed as potential influenza antivirals. CRM1 facilitates the transport of proteins from the nucleus to the cytoplasm for normal cell functions. IAV also uses CRM1 to move its genome from the nucleus to the cytoplasm to allow production of new virus particles. SINE compound, KPT-335 was effective against many influenza viruses with little toxic effect on cells. To determine if IAV would become resistant to KPT-335, resistant viruses were developed in cells and the virus was sequenced to determine any changes that occurred. This revealed that KPT-335 resistance occurred by a single mutation in one of the virus proteins

(NP). However, the resistant viruses did not grow as well in cells and were susceptible to an immune factor found in humans (MxA), that recognises and defends the body against viruses. Altogether the results of this study demonstrate that KPT-335 could be a successful broad-spectrum novel antiviral therapy.

Abstract

Influenza A virus (IAV) is a global health threat, causing seasonal epidemics and potential pandemics leading to morbidity, death and economic losses. Currently, there are two main classes of licensed antivirals against IAV available in the US and Europe; adamantanes and neuraminidase inhibitors, both of which are hindered by the generation of resistant virus variants. The viral polymerase has a high error rate leading to mutations that allow the virus to overcome selection pressures directed at its own genome from conventional antivirals. The prospect of inhibiting host proteins that the virus exploits to facilitate its replication is of increasing interest as an antiviral strategy as the emergence of resistance has been predicted to be slower when targeting a host cellular factor.

IAV utilizes the host nuclear export protein CRM1 to transport viral ribonucleoproteins (vRNPs) from the nucleus to the cytoplasm of an infected cell, a critical late stage of the influenza lifecycle. Leptomycin B (LMB), a Streptomyces metabolite, has been previously shown to target this pathway, resulting in reduced viral propagation; however, LMB's potent cytotoxicity has limited its use as a therapeutic agent. This thesis examined two novel selective inhibitors of nuclear export (SINE), KPT-335 and KPT-185, with less cytotoxicity. *In vitro,* KPT-335 inhibited replication of human and animal IAV strains in a dose-dependent manner with minimal cytotoxicity. To assess the resistance potential of KPT-335, IAV viruses were serially passaged in the presence of a sub-optimal concentration of the compound and assayed for the development of resistance. Resistance to KPT-335 became evident at 8-10

rounds of passage. Sequencing analysis of independently derived resistant virus clones identified 4 single amino acid changes on a surface exposed patch of the viral nucleoprotein (NP). Introduction of these amino acid changes, into otherwise wild type viruses by reverse genetics, confirmed that changes Q311R and N309T conferred a drug-resistant phenotype. However, these substitutions came at a fitness cost to virus replication. The molecular basis for resistance was unclear but Q311R and N309T NP-mutant viruses produced increased levels of M1 during infection as well as producing virus particles with increased M1:NP ratios. Furthermore, the KPT-335-resistance mutations were surprisingly similar to NP sequence polymorphisms previously associated with susceptibility to the innate defence protein MxA. Consistent with this, viruses harbouring the Q311R mutation displayed increased susceptibility to MxA inhibition compared to wild-type virus. Altogether this study confirms that SINEs have the potential to be successful therapeutic agents against IAV replication and that although resistance could be generated, it may be difficult for the virus to overcome both drug selection pressures and the human innate immune response restrictions by escape mutations.

Table of contents

List of figures and tables

Chapter 3 Generating an influenza A virus strain resistant to nuclear export inhibitor, KPT-335.

Chapter 4 Investigating the genetic basis of resistance of influenza A virus to a selective inhibitor of nuclear export, KPT-335

Chapter 7 Material and Methods

Abbreviations

ATP	Adenosine triphosphate
CAS	Cytoplasmic accumulation signal
CC_{50}	50% Cytotoxicity Concentration
CDC	The Centers for Disease Control and Prevention
cDNA	Complementary DNA
CI	Confidence interval
CPE	Cytopathic effect
CRM1	Chromosomal maintenance 1
cRNA	Complementary RNA
DAPI	4',6-diamidino-2-phenylindole
DIPs	*Defective interfering particles*
DMSO	Dimethyl sulfoxide
DNA	Deoxyribonucleic acid
dsRNA	Double stranded-RNA
FDA	*Food and Drug Administration*
FLUBV	Influenza B virus
HA	Hemagglutinin
HIV	H*uman immunodeficiency virus*
IAV	Influenza A virus
IC_{50}	50% Inhibitory Concentration
IF	Immunofluorescence
IFN	Interferon
IIV	Inactivated influenza vaccine
ISG	IFN stimulated gene
IV	Intravenous
LAIV	Live attenuated influenza vaccine
LMB	Leptomycin B
M1	Matrix protein 1

M2	M2 proton channel
MOI	Multiplicity of infection
mRNA	Messenger RNA
Mx	Myxovirus resistance gene
NA	Neuraminidase
NAbs	Neutralising antibodies
NAIs	Neuraminidase inhibitors
NEP	Nuclear export protein
NES	Nuclear export signal
NFX1	Nuclear Transcription Factor
NLS	Nuclear localisation signal
NP	Nucleoprotein
NPC	Nuclear core complex
NS1	Non-structural protein 1
NS2	Non-structural protein 2
NTZ	Nitazoxanide
ORF	Open reading frame
p.i.	Post infection
PA	Polymerase acidic protein
PB1	Polymerase basic protein 1
PB2	Polymerase basic protein 2
PCR	Polymerase chain reaction
PFU	Particle forming units
PKR	Protein kinase RNA-activated
pPCR	*Quantitative polymerase chain reaction*
PRR	Pathogen recognition receptor
R^2	Coefficient of determination
Rab11	RAs-related protein
RAN-GDP	RAs-related Nuclear protein- Guanosine diphosphate
RAN-GTP	RAs-related Nuclear protein- Guanosine-5'-triphosphate
RANGAP	*Ran GTPase* activating protein
RANGEF	Ran Guanine nucleotide Exchange Factor

RCC1	Regulator of chromosome condensation 1
RdRp	*RNA-dependent RNA polymerase*
RNA	Ribonucleic acid
RNP	Ribonucleoprotein
S.D	Standard deviation
S.E.M	Standard error of the mean
SDS-PAGE	Sodium dodecyl sulfate polyacrylamide gel electrophoresis
SI	Selective index
SINE	Selective inhibitor of nuclear export
ssRNA	Single-stranded RNA
UTR	Untranslated region
vRNA	Viral RNA
vRNP	Viral RNP
WHO	The World Health Organisation
WT	Wild type
XPO1	Exportin 1
YB-1	Y box binding protein 1

Chapter 1 Introduction

1.1 Influenza A virus classification and hosts

Influenza viruses, belonging to the *Orthomyxoviridae* family, have a negative sense single-stranded eight segmented RNA genome and are classified into four genera: A-D (Hause *et al.*, 2013). Influenza A virus (IAV) poses the greatest threat to society as it can cause severe, widespread and uncontrolled disease in both humans and livestock. The primary host of IAV is waterfowl belonging to the Anseriformes and Charadriiformes (Webster *et al.,* 1992), although wild birds and domestic poultry are also important reservoirs of infection. Avian IAV replication takes place in the gut epithelium of birds where the disease is largely asymptomatic. It can then spread via the faecal-oral route to other vertebrate hosts where it manifests as a respiratory illness (Webster *et al.,* 1978). The virus undergoes adaption after crossing the species barrier to infect a varied collection of hosts, including humans, cats, dogs, horses, cattle, seals, whales, mink, camel and penguins (reviewed in Joseph *et al*., 2016). Human IAV typically targets epithelial cells of the respiratory tract and is transmitted via airborne droplets and/or fomite contact (reviewed in Killingley *et al., 2*013).

IAV are further categorised into subtypes based on the glycoproteins presented on the virus surface; hemagglutinin (HA) and neuraminidase (NA). There are currently 18 identified types of HA and 11 identified types of NA. Each IAV strain contains one subtype each of HA and NA, all of which have been isolated from aquatic birds apart

from two chiropteran-specific subtypes of HA (H17, 18) and NA (N10, 11), found only in bat isolates (Tong *et al.*, 2012; 2013). To date, only H1, H2 and H3 subtypes are confirmed to infect and transmit between humans. H5, H6, H7, H9 and H10 subtypes are rarely found in humans and are generally transmitted via direct contact from domesticated birds with limited transmission between humans (Schrauwen and Fouchier, 2014). However, infections in humans caused by H5N1, H5N6 and H7N9 viruses have increased in recent years, with mortality rates reaching 30-50 % (WHO, 2017). This highlights the need for control and preventative measures such as antivirals and vaccines to effectively protect the population against emerging viruses.

1.2 Influenza A virion structure

1.2.1 Virion shape

IAV can be described as a pleomorphic virus as infections do not produce single well-defined virion sizes. Lab-adapted IAV strains classically produce 'spherical' virions that have a diameter of ~120 nm (Harris *et al.*, 2006; Yamaguchi *et al.,* 2008) (Fig. 1.1.A). Spherical strains also often produce elongated virions which are <250 nm long (Calder *et al*., 2010; Harris *et al*., 2006; Wasilewski *et al*., 2012; Yamaguchi *et a*l., 2008) and are termed bacilliforms (Vijayakrishnan *et al*., 2013). Clinical isolates of IAV contain not only spherical and bacilliform virions but also produce very long particles known as filaments (Fig. 1.1.D). A filamentous virion is typically >250 nm in length although some can reach up to 30 µm (Cox *et al*., 1980; Roberts *et al*., 1998). A recent study where filaments were selected for during intranasal passage of a highly lab-adapted spherical strain in guinea pigs (Seladi-Schulman *et al*., 2013), highlighted

the relevance of filamentous particles in nature. Additionally, filaments have shown to be advantageous for transmission between co-housed ferrets and guinea pigs (Campbell *et al*., 2014; Lakdawala *et al*., 2011).

1.2.2 Virion composition

The IAV virion is an enveloped particle that derives its lipid bilayer from the plasma membrane of the host cell (Palese and Shaw, 2007). The viral envelope is composed of three viral proteins; HA, NA and M2 as well as the incorporation of some host cell proteins. The two main viral glycoproteins, HA and NA are found at the surface of influenza virus particles comprising 80 % and 17 % of the envelope protein composition, respectively (Webster *et al.,* 1998). M2 is a minor component of the viral envelope with ~20 molecules per virion (Nayak *et al*., 2009). Additionally, host cell proteins have been reported to be incorporated into the virus envelope including two members of the tetraspanin family: CD9 and CD81 (Shaw *et al.*, 2008 ;Hutchinson *et al.*, 2014). The glycoproteins display a fringe like appearance as shown by electron microscopy and/or tomography of spherical and filamentous viruses (Fig. 1.1.C). On filamentous structures, the glycoproteins are orderly dispersed, suggesting an arranged interaction with the matrix layer beneath (Wasilewski *et al*., 2012). The M1 protein oligomerizes to form the matrix layer, which is bound to an internal surface of the viral membrane. The organisation of the M1 helical matrix influences virion morphology (Calder *et al*., 2010). Lattices of multimerized M1 form a rigid cylindrical helix along the length of a filamentous virion whereas in spherical virions, M1 forms a less ordered structure (Calder *et al*., 2010). Under the matrix layer lies the viral genome which consists of 8 segments of viral RNA bound to a trimeric complex composed of the

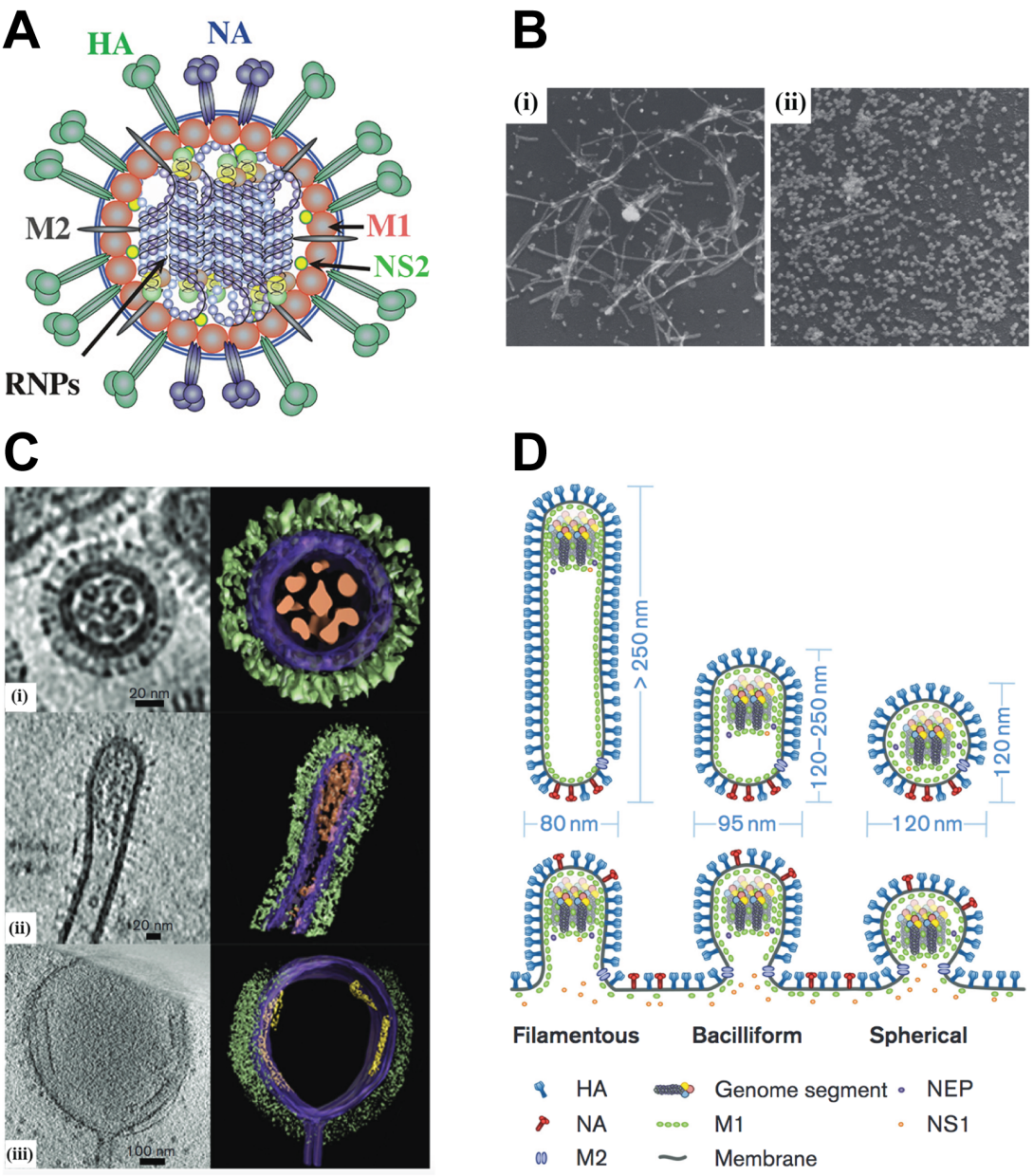

Fig. 1.1 Structure of IAV. **(A)** Cartoon of a spherical influenza A virion. Cartoon drawn by Prof. Paul Digard. **(B)** Filamentous virions are lost after laboratory passage. (i) Two passages of the clinical isolate A/Rockefeller Institute/1/1957 (H2N2), presenting a visible filamentous morphology. However, this morphology was lost after 12 passages as shown in (ii). (Originally published in The Journal of Experimental Medicine. 112:945–952. **(C)** Electron tomograms bacilliform and filamentous influenza virions. Electron tomograms of virion 'slices' (left panels) and segmented images (right panels). Viral glycoproteins are shown in green, membrane and matrix proteins are shown in purple and the genome is highlighted in brown (Vijayakrishnan *et al.,* 2013). **(D)** Schematic of budding and released filamentous, bacilliforms and spherical virions. Images B, C and D taken and adapted from Dadonaite *et al.,* 2016.

viral polymerase proteins; PB2, PB1 PA and multiple nucleoprotein (NP) molecules (Neumann *et al.,* 2009; Portela and Digard, 2002). The vRNA-polymerase-NP subunit is collectively known as a viral ribonucleoprotein (vRNP) complex. Small amounts of NS1 and NS2 are incorporated into spherical virions along with the vRNP complexes (Hutchinson *et al*., 2014). The presence of NS1 and NS2 in filamentous viruses has not yet been examined.

1.2.3 The vRNP complex

The structure of the vRNP complex is shown in Figure 1.2. NP binds with high affinity to the vRNA phosphate backbone, thereby leaving the RNA bases exposed for base pairing or genome replication (Baudin *et al*., 1994; Compans *et al*, 1972; Scholtissek *et al.,* 1971). The vRNA genomic ends are not bound to NP but fold back and base pair to form a partially double stranded structure which is bound together by PB1, PB2 and PA; the polymerase complex (Fodor, 2013; Hsu *et al.,* 1987). The rest of the vRNA is coated by NP monomers (Compans *et al.,* 1972). Electron microscopy has revealed that that internal vRNPs are twisted and that the antiparallel double helix of vRNPs complexes is maintained by interaction with NP (Wu *et al.,* 2009; Compans *et al.,* 1972, Jennings *et al.,* 1983). The vRNA forms a loop at the end opposite the polymerase bound end.

1.2.4 The IAV genome and gene products

The IAV genome is 13.5 kB in size and consists of 8 segments of negative sense viral RNA (vRNA). The vRNA segments share a similar structure. They contain a long central antisense coding region which is flanked by short untranslated regions

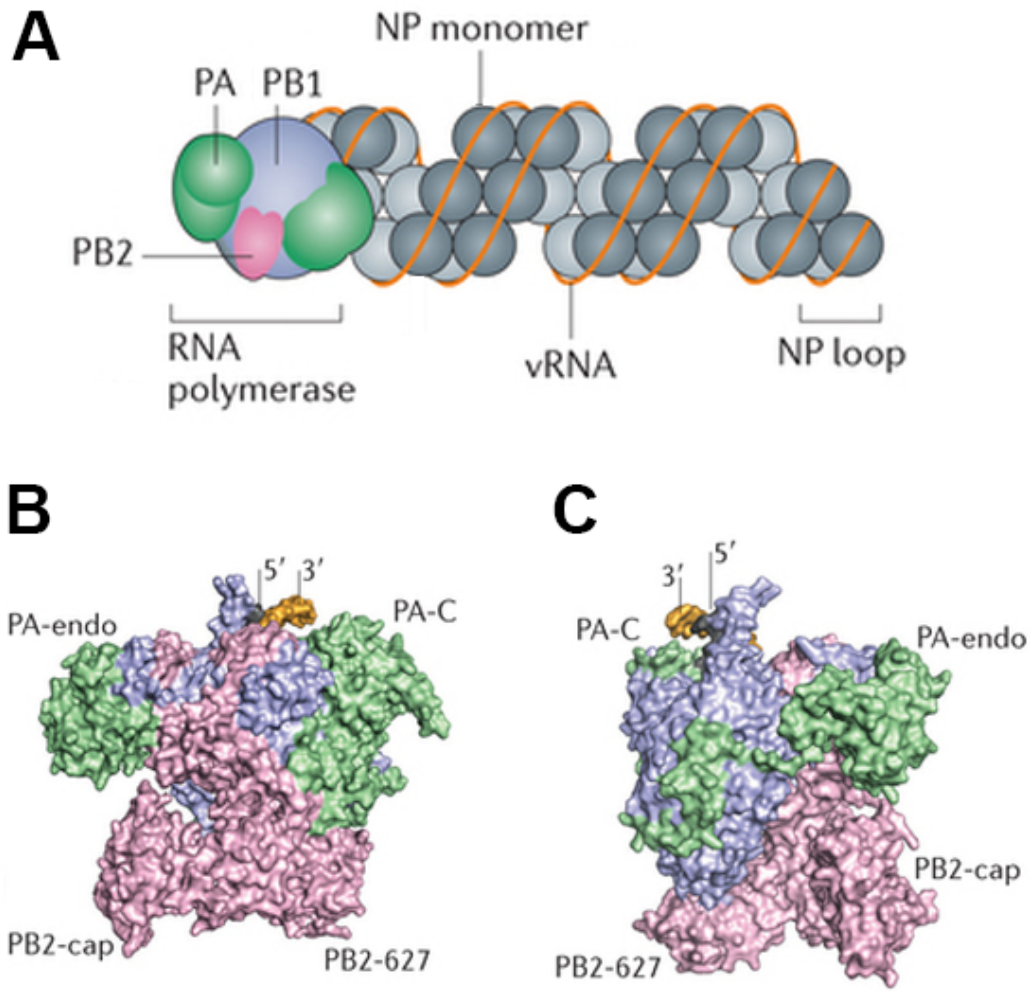

Fig. 1.2. The IAV vRNP complex and polymerase trimer structure. (A) Model of a vRNP complex. The vRNA is bound by its 5' and 3 termini by a trimeric RNA polymerase and the remaining exposed vRNA is coated by multiple NP monomers. The complex is twisted into an antiparallel double helix. **(B)** Front and **(C)** side view of IAV RNA polymerase structure (Protein DATA Bank; 4WSB). PB1, PB2 and PA are coloured in purple, pink and green, respectively. The PB2 cap-binding domain (PB2-cap), PB2 627-domain (PB2-627), PA endonuclease domain (PA-endo) and PA C-terminal domain (PA-C) are indicated. The 5′ and 3′ termini of a vRNA are shown in yellow. (Figure taken and adapted from Velthuis and Fodor, 2016).

(UTRs). Each segment encodes at least one protein but some can encode more than one protein. Individual vRNAs contain one major open reading frame (ORF) which is translated into a single protein following faithful transcription of mRNA. IAV employs mRNA splicing, ribosomal frame-shifting and alternative translation initiation mechanisms to encode further proteins from the same vRNA segment (details of each mechanism are described in section *1.3.3.2 mRNA processing, transport and translation*). The 8 segments encode at least 19 recognised proteins, 14 of which have known functions (Table 1.1). IAV gene products are displayed in Fig.1.3 and the roles for the characterised polypeptides and their corresponding mechanism of expression are detailed in Table 1.1.

1.3 Influenza A virus replication and lifecycle

IAV has evolved many mechanisms to facilitate its ability to invade and hijack host cell machinery for successful propagation. Unlike most negative strand RNA viruses, which transcribe RNA in the host cytoplasm, influenza virus genome transcription and replication takes place in the nucleus (Jackson *et al.,* 1982). The life cycle can be divided into the following stages: entry into the host, viral uncoating, import of vRNPs into the nucleus, transcription and replication/mRNA processing, protein synthesis and processing, export of vRNPs into the cytoplasm and assembly and budding at the cellular plasma membrane. Each stage of the viral replication cycle is briefly described, with more emphasis on the RNP nuclear export stage to compliment the topic of this thesis.

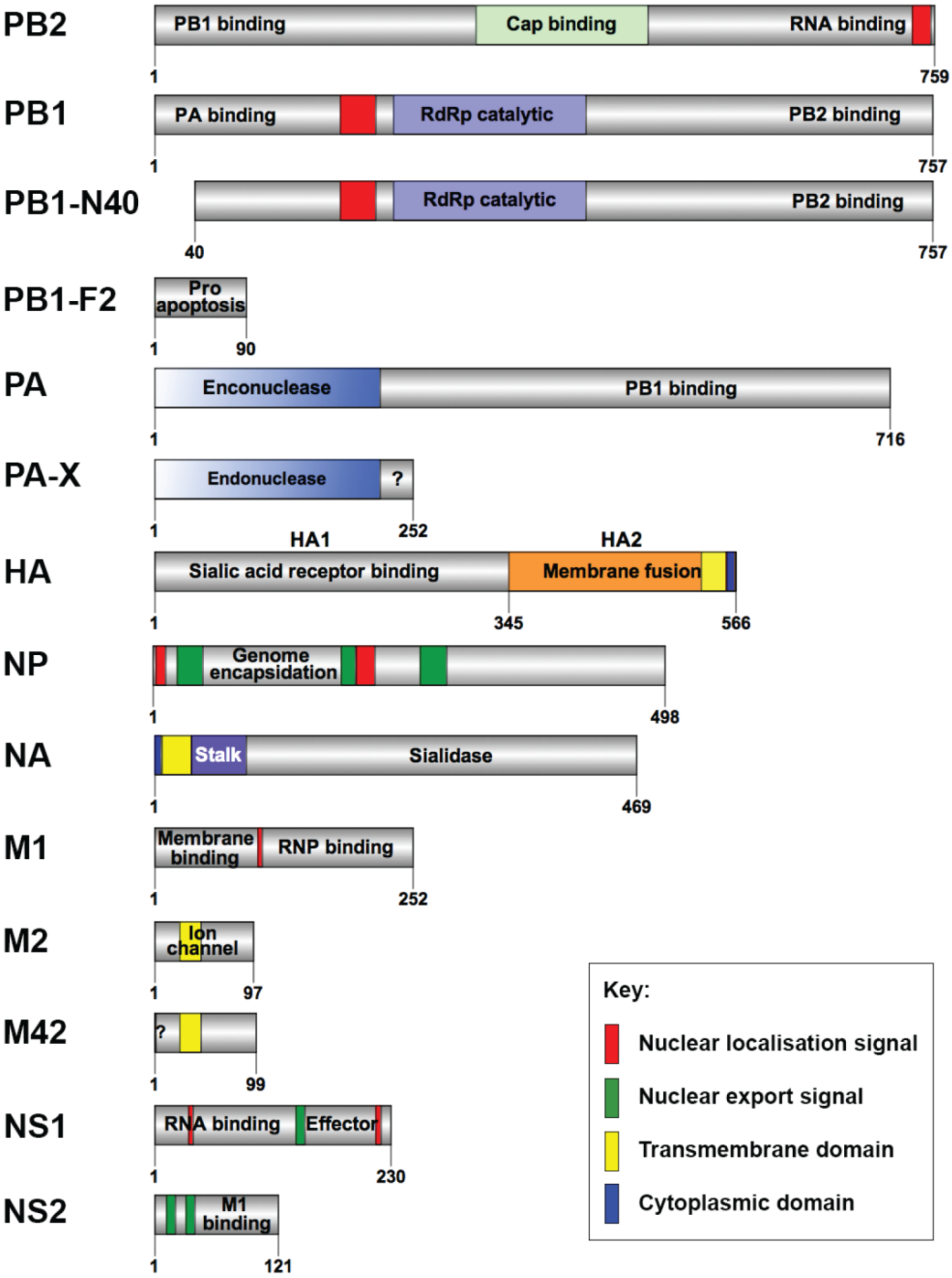

Fig. 1.3 Influenza A virus gene products. Major structural and/or functional domains are indicated along with nucleocytoplasmic trafficking motifs. PB2-S1 excluded as functional domains are unknown. See table 1.1. for mechanism in which the proteins are expressed and their major functions.

Table 1.1 IAV proteins*

Segment		Gene product	Mechanism by which expressed	Protein size (AA)	Main function(s)
No.	**Name**				
1	**PB2**	PB2	Main ORF	759	Part of heterotrimeric polymerase which binds to 5' cap from host RNA during 'cap snatching' (Blass *et al.*, 1982)
		PB2-S1	Spliced mRNA	508	Inhibits RIG-I signalling (Yamayoshi *et al*., 2015)
2	**PB1**	PB1	Main ORF	757	Part of the heterotrimeric polymerase which drives elongation of mRNA (Braam *et al.*, 1983)
		PB1-F2	Alternative AUG site	87	Virulence factor (Chen *et al*., 2001)
		PB1-N40	Alternative AUG site	718	Unknown (Wise *et al.,* 2009)
3	**PA**	PA	Main ORF	716	Part of the heterotrimeric polymerase with endonuclease activity involved in 'cap snatching' (Dias *et al.*, 2009)
		PA-X	Ribosomal frameshift	152	Endonuclease activity involved in host cell shut-off (Jagger *et al.*, 2012)
		PA-N155	Alternative AUG site	562	Unknown (Muramoto *et al.,* 2013)
		PA-N182	Alternative AUG site	535	Unknown (Muramoto *et al*., 2013)
4	**HA**	HA	Main ORF		Mediates receptor binding, virus entry and budding
5	**NP**	NP	Main ORF	498	Encapsidation of vRNA to form vRNP complexes
6	**NA**	NA	Main ORF	454	Possesses sialidase activity which mediates release of progeny virus and facilities virus attachment
7	**M**	M1	Main ORF	252	Major structural protein involved in viral budding and assembly
		M2	Spliced mRNA	97	Acts as proton ion channel; during virus entry and required for membrane scission at the stage of budding
		M42	Spliced mRNA and alternative AUG site	99	Variant of M2 (Wise *et al.,* 2012)
8	**NS**	NS1	Main ORF	230	IFN antagonist (Hale *et al*., 2008)
		NS2 (NEP)	Spliced mRNA	121	Involved in nuclear export of vRNPs (O'Neill *et al.,* 1998)
		NS3	Spliced mRNA	187	Unknown (Selman *et al.,* 2012)
		tNS1	Alternative AUG site	150/152	Involved in IRF inhibition (Kuo *et al.,* 2016)

*segments and protein sizes based on A/Puerto Rico/8/1934 (H1N1)

1.3.1 Entry

IAV enters the host cell by attaching to sialic acid on the cell surface via the HA glycoprotein (Gottschhalk, 1959). Host sialic acids are associated with underlying galactose by α2,3 or α2,6 linkages. Human HA subtypes bind to α2,6-linked sialic acid while avian HA subtypes bind to α2,3 receptors. One amino acid mutation in HA can change receptor binding specificity significantly; accordingly, HA is an important factor regarding host tropism (Edinger *et al*., 2014; Hamilton *et al*., 2012). Once bound to the sialic acids, virions are internalised by dynamin-dependent clathrin-mediated endocytosis (Eierhoff *et al*., 2010). However, micropinocytosis has been suggested as the main route for the non-selective uptake of filamentous virions (Rossman *et al*, 2010). Before fusion of the host and viral membranes, the HA undergoes post-translation processing. HA is synthesised as an inactive precursor (HA0). HA0 is then cleaved by cellular proteases into two functional subunits: HA1 and HA2. HA1 initiates endocytosis, while HA2 primes the virus to fuse its membrane with the cellular endosomal membrane (Hamilton *et al.*, 2012). Acidification of the late endosome triggers the cleaved HA2 to undergo a pH-dependent conformational change. This allows insertion of the fusion peptide, which lies at the N-terminus of HA2, into the endosome membrane. Subsequently, several HA molecules cluster to form a fusogenic unit, which undergoes a further conformational change to bring the two opposing membranes together (reviewed in Hamilton *et al*., 2012). The M2 ion channel then acidifies the viral core to allow M1 to dissociate from vRNPs for their release into the cytoplasm (Fig. 1.4; (1)).

1.3.2 Nuclear import

Once released from the late endosomes, vRNPs are transported from the cytoplasm to the nucleus. vRNPs are too large to passively diffuse through the nuclear pore complex (NPC) and therefore are actively transported using a signal-dependent nuclear import pathway; importin-α-importin-ß. The exposed nuclear localisation sequences (NLS) on NP molecules associate with importin-α, which in turn associates with importin-ß (O'Neill *et al.*, 1995). A non-classical NLS (not arginine or lysine rich) is found within the first 13 amino acids of NP (Fig. 1.3) and is essential for vRNP import and virus replication (Cros *et al*., 2005). Once bound to importin-α, RAN-GTP binds to importin-ß at the NPC to allow for RAN GTPase to dissociate the importin-α-vRNP complex, thereby allowing vRNP release into the nucleus, where viral transcription and genome replication take place (Fig. 1.4; (2)).

1.3.3 Transcription, translation and genome replication

1.3.3.1 Transcription

After translocation into the nucleus, each of the eight vRNPs of the IAV genome are transcribed to produce mRNA; known as transcription. Transcription is primed by a process called 'cap-snatching', which involves the binding and cleavage of 10-13 nucleotide RNA fragments containing a 5' 7-methylguanosine cap (m7GpppXm) from host precursor mRNA (pre-mRNA) (Bouloy *et al.*, 1978; Plotch *et al*., 1979; Plotch *et al*, 1981). The host pre-mRNA 5' cap binds to the polymerase complex via the PB2 subunit (Blass *et al.,* 1982) and the cap is cleaved via the interaction with the PA endonuclease domain (Hara *et al.*, 2006). The PB1 subunit catalyses RNA elongation by reading vRNA as a template from the 3' to 5' direction (Braam *et al.*, 1983). The

mRNA is then polyadenylated by reiterative copying of a poly U sequence motif near the conserved 5' end of the vRNA template (Poon *et al*., 1999; Robertson *et al*., 1981). The viral mRNA therefore resembles a host mRNA with a 5' cap and a 3' poly(A) tail. Viral mRNA then assembles into messenger RNPs (mRNPs) and utilises cellular host cell machinery for export (see later) and translation for protein expression (Fig. 1.4; (3)).

1.3.3.2 Genome replication

In contrast to transcription, genome replication involves a non-capped, non-poly(A) positive-sense full length copy of vRNA. First, the vRNA is replicated to complimentary RNA (cRNA) which acts as an intermediate template. Second, the cRNA is copied into vRNA. Genome replication requires newly synthesised NP and polymerase proteins to stop the degradation of cRNA (Vreede *et al*., 2004). Both cRNA and vRNA contain a triphosphate nucleotide at the 5'end suggesting that transcript initiation for genome replication is primer independent (McCauley *et al.*, 1983). Additionally, genome replication can be initiated *in trans* by polymerase complexes that are unbound from the template vRNP complex (Jorba *et al*., 2014) (Fig. 1.4; (4)).

As described, the polymerase has two distinct functions and therefore must regulate the frequency in which it generates mRNA versus the replication process. However, the mechanism by which the polymerase switches between these two activities is not fully understood. Previous studies show that during the early stages of infection there

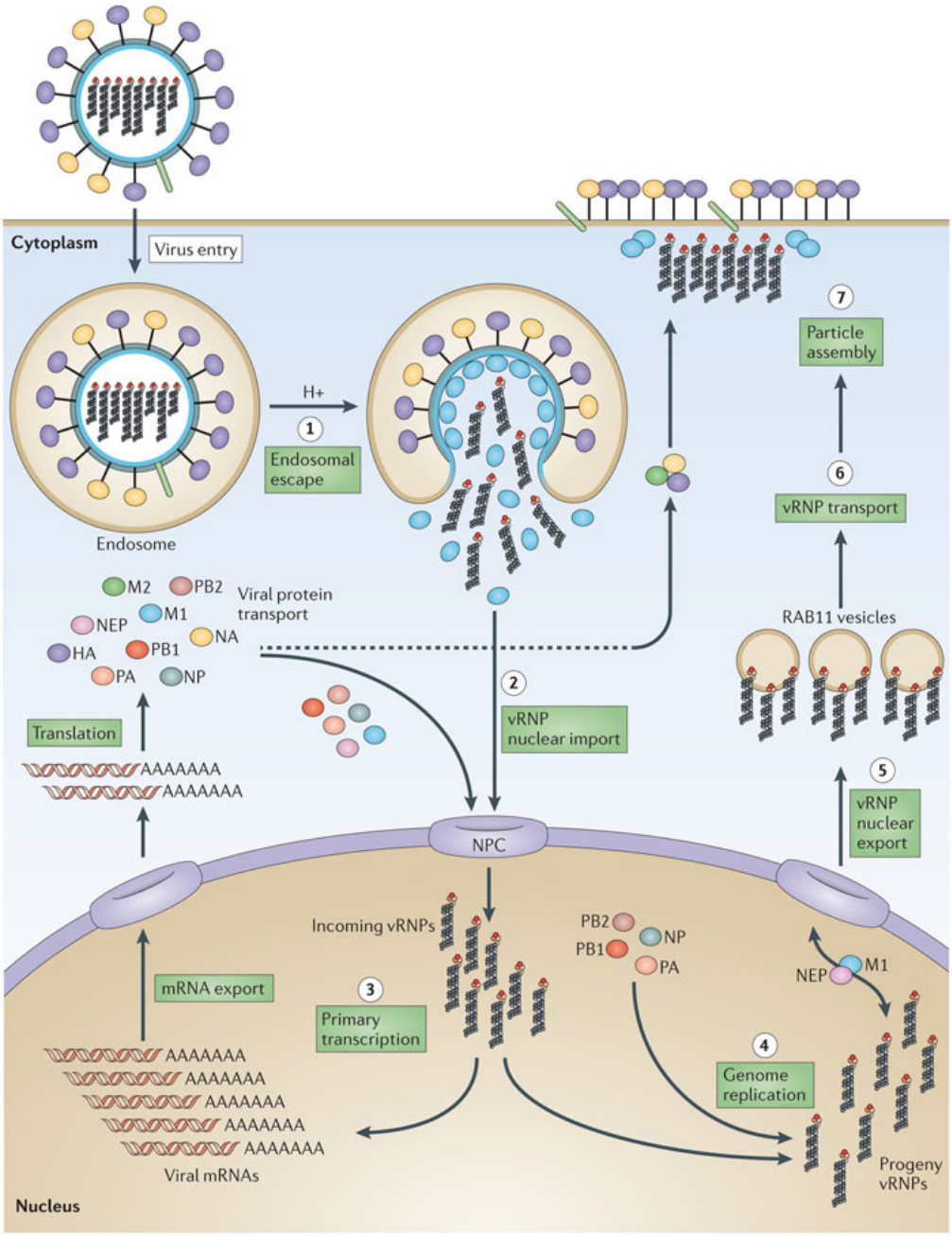

Fig. 1.4. Schematic of the IAV life-cycle. IAV attaches to host cell sialic acid receptors via the virus surface glycoprotein HA and subsequently enters via clathrin-mediated endocytosis (or micropinocytosis). HA is cleaved by cellular proteases to allow fusion between the viral envelope and the endosomal membrane **(1).** Acidification of the endosome opens the M2 ion channel to allow uncoating of RNP complexes and for pH-dependent HA fusion to allow for the release of vRNPs **(2).** vRNPs are translocated to the nucleus where the viral RNA-dependent RNA polymerase transcribes and replicates the –vRNA **(3+4).** Viral mRNAs are exported to the cytoplasm for translation. Viral proteins that are required in transcription and replication are translocated back to nucleus. Progeny vRNPs are exported to the cytoplasm **(5)** where the vRNPs are transported via cellular Rab11 vesicles **(6)** and packaged for release from the host cell **(7)** (Figure is taken from Eisfeld *et al*, 2014).

are higher amounts of mRNA compared to cRNA (Taylor *et al.,* 1977; Robb *et al.,*2009) and at later stages of infection similar amounts of mRNA and cRNA are observed alongside vRNA. One switching model suggests that both mRNA and cRNA are produced early in infection, but the unprotected cRNA is exposed to host nucleases and is degraded, however the polyadenylated and capped mRNA is protected (Vreede *et al*., 2007; Vreede *et al*., 2004). At later stages, the polymerase and NP have been made and protect the cRNA from degradation. It has also been suggested that NS2 may interact with the polymerase complex which may play a role in the polymerase switching from transcription to replication (Robb *et al.,* 2009).

1.3.3.3 mRNA processing, transport and translation

The viral mRNAs are thought to be recognised similarly to host mRNA; thus, after transcription they are (partially) spliced, exported and translated in a similar process to the cellular mRNA (Amorim *et al.*, 2011; Read *et al.*, 2010; Bier *et al.,* 2011; Hao *et al.*, 2008). Post-transcription modification processes take place such as IAV utilising the host cell splicing machinery to splice M and NS viral transcripts to alternative mRNAs; M1/M2/M42 and NS1/NS/NS3 respectively. Additionally, PB1-F2 and PB1-N40 can be expressed by translation of segment 2 (PB1) mRNA, which has several start codons downstream of the conventional AUG, thus initiating alternative translation events (Chen *et al*., 2001 Wise *et al*., 2009). The current mechanism by which influenza mRNA nuclear export takes place is not fully understood. However, it has been established that the main host protein involved in export of cellular mRNA is the nuclear export factor 1 (NXF1) (Read & Digard, 2010; Larsen *et al.,* 2014). Once exported to the cytoplasm, viral mRNAs are translated by cellular ribosomes. At this

stage, most viruses produce viral proteins by translation downstream of the primary ORF, however some viruses can express PA-X following a ribosomal frameshift in which segment 3 (PA) mRNA is translated from the +1 reading frame (Jagger *et al*., 2012). The protein components of the vRNP complex are then imported back into the nucleus where newly synthesised vRNPs assemble.

1.3.4 RNP nuclear export

In late stages of infection, newly synthesised vRNPs are transported from the nucleus to the cytoplasm for packaging of progeny virus particles. IAV utilises the cellular host protein chromosomal maintenance 1 (CRM1) (also known as exportin 1 (XPO1)) to mediate nucleocytoplasmic transport of vRNPs (Elton *et al.,* 2001; Watanabe *et al.*, 2001). Cellular CRM1 recognises proteins that contain a leucine-rich nuclear export signal (NES) domain (reviewed in Dong *et al.,* 2009). CRM1 interacts with the NES motif within cargo proteins and, in association with RAN GTPases, the cargo its transported from the nucleus across the NPC. The RAN GTPase-activating protein (RANGAP) within the cytoplasmic side of the NPC, hydrolyses RAN-GTP to RAN-GDP to facilitate the dissociation of the CRM1-protein-RAN-GTP complex and release the cargo protein into the cytoplasm. RAN-GDP translocates back to the nucleus and the GDP is exchanged for GTP by RAN guanine nucleotide exchange factor (RANGEF) for subsequent rounds of nuclear-cytoplasmic transport of proteins (reviewed in Hutten *et al.*, 2007). The energy required for CRM1 export is generated by high RanGTP concentration gradient in the nucleus, which drives the transport of cargo proteins to the cytoplasm (Monecke *et al*., 2009).

In the presence of leptomycin B (LMB), a specific CRM1 inhibitor, vRNPs are retained in the nucleus of infected cells (Elton *et al.*, 2001; Ma *et al.*, 2001; Watanabe *et al*., 2001), therefore indicating that the CRM1 pathway is essential for vRNP nuclear export. Influenza infection lacking M1 and NS2 proteins results in inefficient export of NP (Bui *et al*., 2000; Martin and Helenius, 1991, Neumann *et al.*, 2000), signifying their involvement during the nuclear export process. Mutating the NES domain of the M1 protein results in impaired nuclear export of vRNPs; however the M1 NES is not sensitive to LMB treatment suggesting M1 does not directly interact with CRM1 (Sakaguchi *et al*., 2003). NS2 can directly interact with CRM1 via its two NES domains (Huang *et al*., 2012; Neumann *et al*., 2000; O'Neill *et al*., 1998). Although there is a strong link to suggest a CRM1-NS2 interaction, at present there is no evidence to indicate that NS2 directly interacts with vRNPs. M1, however, has been described to directly interact with NS2 via its NLS motif (Yasuda *et al*., 1993; Akarsu *et al*., 2003; Shimizu *et al*., 2011). Consequently, it has been suggested that M1 forms a bridge between the vRNPs and NS2. Thus, a daisy chain model has been proposed as follows; vRNP-M1-NS2-CRM1 for export of the viral genome during late stages of infection. However, NP can undergo nuclear export in the absence of other viral proteins in both infected and transfected cells (Elton *et al.,* 2001; Watanabe *et al.,* 2001). Thus, suggesting the possibility of M1 and NS2 independent vRNP export. Additionally, NP has three NES motifs, one of which directly interacts with CRM1 (Elton *et al.*, 2001). NP has also been shown to bind directly to CRM1 in two further studies (Chutiwitoonchai *et al.*, 2014; Kakisaka *et al.*, 2015). Nevertheless, the exact role NP plays during vRNP export remains unclear.

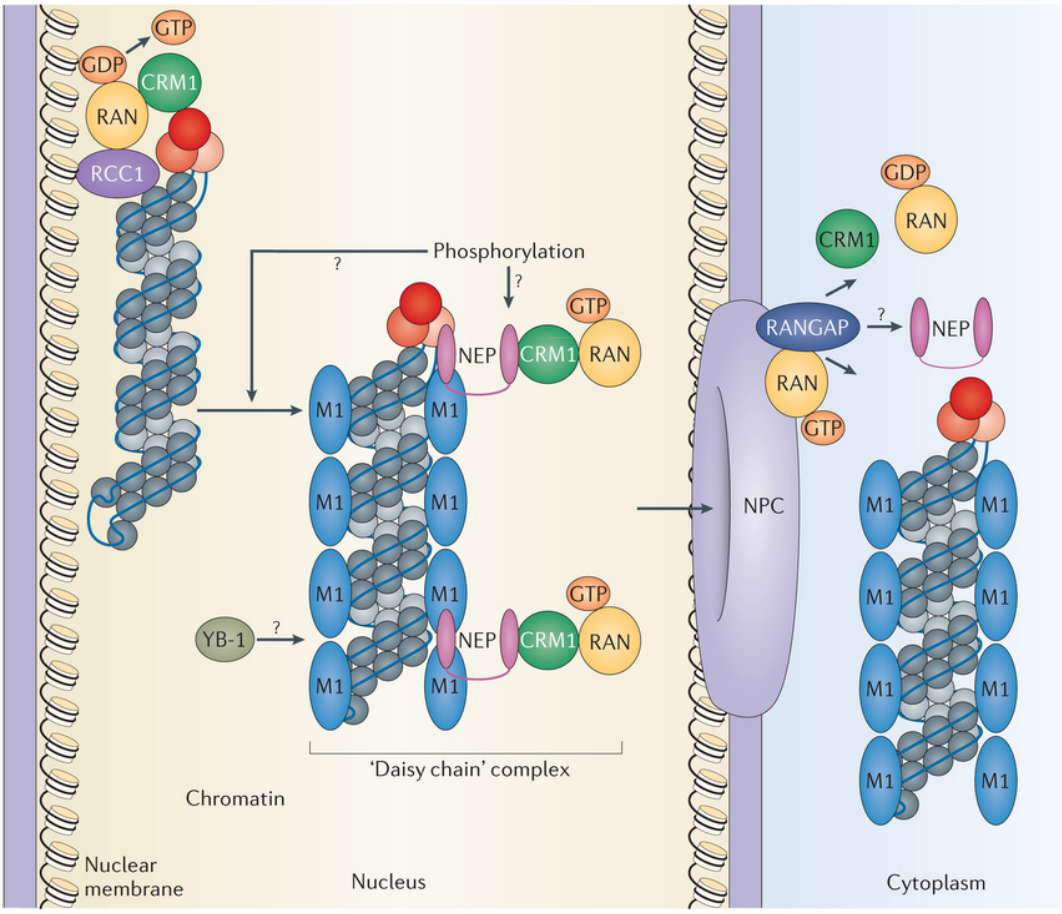

Fig. 1.5 Model for vRNP nuclear export. During late stages of infection, newly synthesized vRNPs are transported from nucleus to the cytoplasm for packaging into new virions. vRNPs localise with chromatin at the nuclear membrane and associates with CRM1. Phosphorylation may trigger signal transduction necessary to release vRNPs from chromatin. vRNPs are thought to be exported via a 'daisy chain' complex in which viral NS2 (labelled as NEP), containing a NES recognised by CRM1, acts as an adaptor between CRM1 and M1-vRNP. At the cytoplasmic side of NPC, RAN-GTP is hydrolysed by RANGAP to release vRNPs into the cytoplasm. Cellular Yb-1 protein is thought to be transported with vRNPs. M1 remains associated with vRNPs whereas the location of NS2 after export is unclear. (Figure is taken from Eisfeld *et al.*, 2014).

1.3.4.1 Other cellular factors involved in vRNP export

Some nuclear vRNPs are associated with cellular chromatin, also at the nuclear periphery of infected cells, implying that vRNPs bound to chromatin could be an intermediate nuclear export step (Chase *et al.,* 2011). Chromatin is also associated with regulator of chromosome condensation 1 (RCC1), a guanine-nucleotide releasing factor that promotes exchange of RAN-bound GDP by GTP; vRNPs have also been shown to form complexes with RCC1. As well as vRNPs, M1 is associated with chromatin (Chase *et al*., 2011; Kurokawa *et al*., 1990). This evidence would support the hypothesis that M1 triggers vRNP release from chromatin before undergoing nuclear export. A cellular host protein involved in transcription and translation, Y-box-binding protein (YB-1) (Wolffe, 1998) is imported into the nucleus and accumulates with vRNPs, M1 and NS2 after LMB treatment suggesting that YB-1 is also associated with vRNP export (Kawaguchi *et al*, 2012). Cellular kinase activity affects nuclear export as treatment with protein kinase C inhibitors (Bui *et al*., 2000), a RAF-MEK-ERK mitogen-activated protein kinase (MAPK) inhibitor (Pleschka *et al.*, 2001), a receptor of tyrosine kinase inhibitor (Kumar *et al*., 2011), and a serum/glucocorticoid regulated kinase 1 inhibitor (Alamares-Sapuay *et al*., 2013) impairs RNP nuclear export, suggesting phosphorylation of a viral or cellular factor is necessary for the nuclear export process. Additionally, vRNP export is enhanced by HA-mediated activation of MAPK signalling pathway when HA reaches the plasma membrane (Marjuki *et al*., 2006; 2007), indicating an indirect role for HA promoting vRNP export.

1.3.5 Assembly and budding

Once released into the cytoplasm, vRNPs are transported through the cytoplasm to the host cell plasma membrane which forms the virus envelope thus, releasing progeny virus particles to infect neighbouring cells. vRNPs associate with the cellular microtubule network by access to the Rab11-dependent vesicle-trafficking pathway to transport through the cytoplasm (Eisfeld *et al*., 2011; Amorim *et al*., 2011; Eisfeld *et al*., 2014; Momose *et al*., 2011). The vRNPs are thought to 'piggyback' on recycling endosomes (RE) to transport through the cytoplasm via an interaction between cellular Rab11 and viral PB2 (Amorim *et al*., 2011). In the cytoplasm, all 8 RNA segments must be packaged into a virion particle. There are two methods that have been hypothesised to explain packaging of the viral genomic segments into virion particles; randomly and specifically. The later model is favoured as packaging signals have been identified in non-coding and coding 5' and 3' regions of vRNA (Fujii *et al*., 2005; Fujii *et al*., 2003; Liang *et al*., 2005; Watanabe *et al*., 2003). Additionally, an electron microscopy study produced further evidence for the selective packaging model by establishing that influenza virions contain 8 vRNP segments in a 7+1 formation; 1 central vRNP and 7 others in a surrounding circle (Noda *et al*., 2006).

Virus budding is initiated by insertion of HA and NA into the plasma membrane. The glycoproteins target cholesterol and sphingolipid enchiridion regions of the plasma membrane known as lipid rafts, which are thought to serve as platform for the concentration of proteins (Brown *et al.,* 1992; Simons and Toomre, 2000). The M1 protein possibly crosslinks with the cytoplasmic tails of HA and NA to help mediate incorporation into the budding virion (Jin *et al*., 1997). M1 also binds to the M2 ion

channel protein by binding via the M2 cytoplasmic tail (McCown *et al.,* 2006). M2 performs membrane scission by localising its cytoplasmic tail to the plasma membrane and changing the membrane curvature, thus inducing the budding process (Rossman *et al.,* 2010). The enzymatic activity of NA, on the surface of the plasma membrane as well as the particle, initiates cleavage of the sialic acid receptors to allow release of the newly formed virion from the host cell (Palese *et al.*, 1974).

1.3.6. Involvement of the innate immune system during IAV replication

IAV enters through the oral or nasal passages to the mucosal layer that covers the respiratory epithelium; the host's initial defence barrier to IAV infection. If successful at surpassing the mucous layer, the virus invades the respiratory cells via sialic acid receptors (as described in section *1.3.1 Entry*). After successful replication, the virus can spread to both immune and non-immune cells. The vRNA present in infected cells is detected by pattern recognition receptors (PRRs). IAV is recognised by at least three classes of PRRs; Toll-like receptors (TLR) (TLR3; dsRNA, TLR7 and 8; ssRNA), retinoic acid-inducible gene I (RIG-I) (5'triphosphate RNA) and NOD-like receptors (nucleotide-binding oligomerization domain-like receptors) (various stimuli) (reviewed in Iwasaki and Pillai, 2014). RIG-I and NOD-like receptors recognise the virus within the cytoplasm of cells whereas TLR3 and TLR7 detect vRNA in endosomes (reviewed in Iwasaki and Pillai, 2014). Each receptor triggers individual signalling pathways for upregulation of innate immune factors as shown in Figure 1.6. Generally, once the virus is recognised by a PRR, the host cells can secret Type I interferons (IFN-I), chemokines, pro-inflammatory cytokines and eicosanoids (Hogner *et al.,* 2013; Kallfass *et al.,* 2013; Jewell *et al.*, 2007). IFN-I, whether

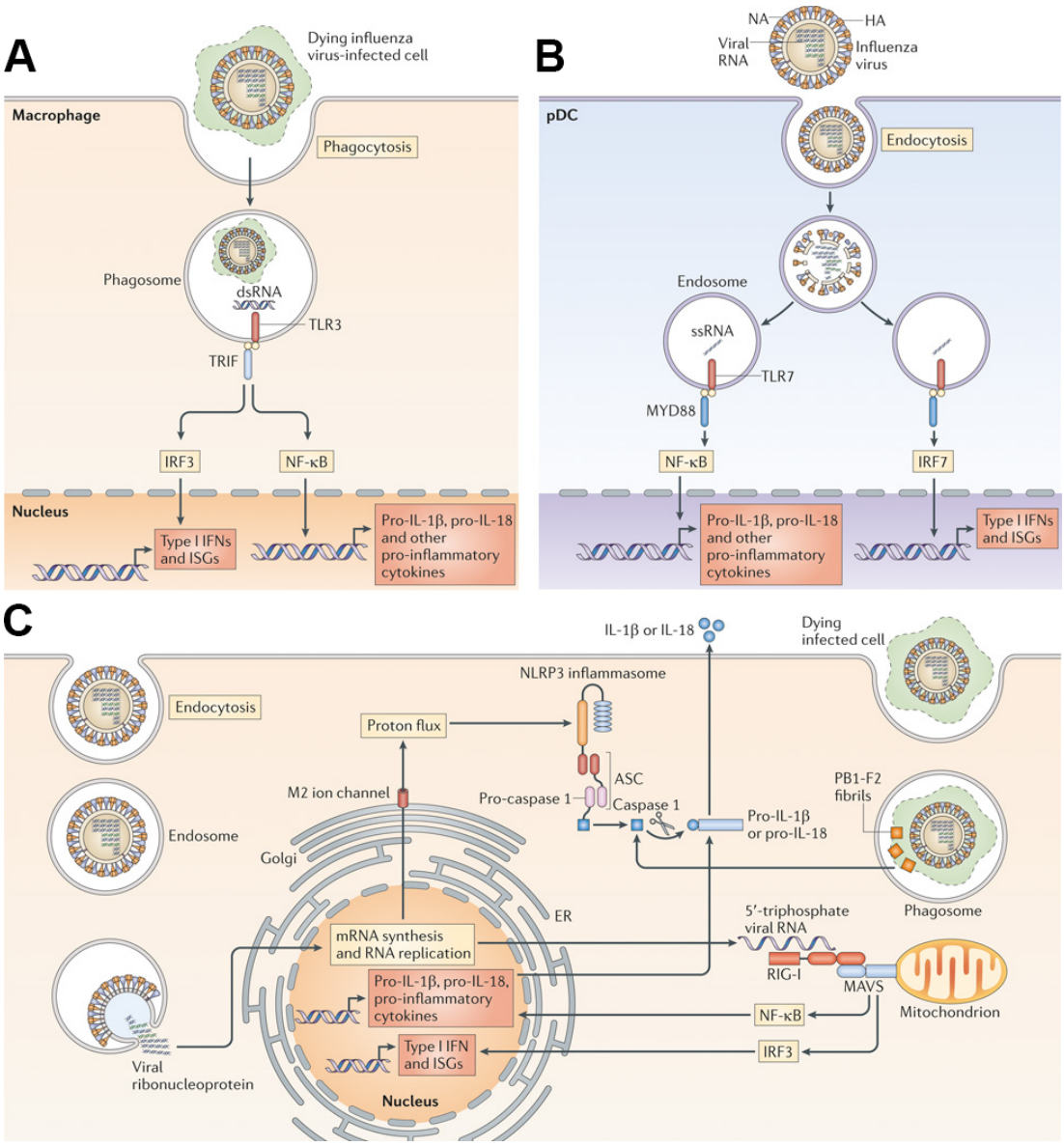

Fig. 1.6. Innate immune recognition during IAV infection. (A) Infected cells are phagocytosed by macrophages for recognition of double-stranded RNA (dsRNA) by Toll-like receptor 3 (TLR3), which leads to the induction of the expression of NF-κB-dependent pro-inflammatory cytokines and of IFN-I and ISGs downstream of IFN-regulatory factor 3 (IRF3) **(B)** Incoming genomic single-stranded RNA (ssRNA) that is contained within the virion is released via the degradation of the viral membrane and capsid within acidified endosomes, and ssRNA is recognized by TLR7 in plasmacytoid dendritic cells (pDCs). TLR7 signalling induces NF-κB-dependent genes from the NF-κB endosome, and IRF7 activation from the IRF7 endosome. **(C)** Within infected cells, vRNA in the cytosol is recognized by RIG-I, which, through the activation of mitochondrial antiviral signalling protein(MAVS), leads to the induction of pro-inflammatory cytokines and IFN-I. M2 ion channel activity in the Golgi stimulates formation of the NOD-, LRR- and pyrin domain-containing 3 (NLRP3) inflammasome, which results in caspase 1 activation and the release of the cytokines IL-1β and IL-18. (Image and figure legend taken and adapted from Iwasaki and Pillai, 2014).

produced by non-immune or immune cells such as macrophages and dendritic cells (DCS), stimulates the expression of hundreds of genes known as IFN-stimulated genes (ISGs) in neighbouring cells, including myxovirus (Mx) proteins, protein kinase R (PKR), 2'-5'-oligoadenylate synthetase (OAS) and interferon-induced transmembrane protein 1 (IFITM) proteins, which mediate antiviral activity (reviewed in Iwasaki and Pillai, 2014). Chemokines can recruit additional immune cells to site of infection such as monocytes, natural killer (NK) cells and neutrophils (Hwang *et al.,* 2012). Pro-inflammatory cytokines and eicosanoids induce local and systemic inflammation and are connected to the adaptive immune response (reviewed in Dennis *et al.*, 2015). The regulation of adaptive immunity to IAV is out of the scope of this study and therefore is not discussed in detail.

1.4 The impact of influenza A virus on human health

IAV is a successful, persistent and unpredictable human pathogen. Transmission of influenza virus through aerosol causes acute febrile disease in humans, which can present as a severe infection in individuals with underlying medical conditions (such as cardiopulmonary disease), infants/young children and the elderly. These high-risk individuals are more likely to obtain complications such as pneumonia and bronchitis, which can result in hospitalisation and even death. IAV is a major burden on the global population, increasing mortality and morbidity rates and causing significant economic losses. It has been estimated that ~20 % of children and ~5 % of adults present with symptomatic influenza A and B virus infection every year (Turner *et al.,* 2003).

According to the World Health Organisation (WHO), approximately 1 billion people are infected and 250,000 to 500,000 people die annually from an influenza infection (WHO, 2016).

1.4.1 Seasonal epidemics

Influenza epidemics occur annually during the winter months; November-April in the Northern hemisphere and May-October in the Southern hemisphere (influenza epidemics in tropical regions are not well defined). The current circulating strains that infect humans during seasonal epidemics include IAVs H1N1pdm09 and H3N2 and influenza B virus (FLUBV) from Victoria and Yamagata lineages. Epidemics can present when point mutations occur in the epitope region of the viral surface antigens (HA and NA) which is known as antigenic drift. The novel antigenic virus variants can evade immune recognition leading to seasonal outbreaks. Antigenic drift occurs due to the lack of the viral RNA polymerase 'proof reading' function, which for most smaller RNA viruses, results in unavoidable virus variance. This error prone activity of IAV poses a problem for both seasonal vaccines and antiviral therapy (as discussed in section; *1.5 Strategies to combat human influenza infections*). Additionally, epidemics can occur if the seasonal vaccine efficacy is suboptimal (reviewed in Paules *et al*.,2018). A reduction in vaccine effectiveness can result in limited heard immunity within a population. A sufficient heard immunity reduces the spread of disease where a high proportion of the population are immune to the disease, particularly through vaccination. A person's prior exposure to influenza, vaccine history, age and co-existing conditions can affect vaccine effectiveness as well as vaccine mismatches, where the circulating influenza strains differ from those in the vaccine formulations.

Table 1.2 Influenza A virus pandemics*

Name	Year	Subtype	Source
Spanish flu	1918	H1N1	Avian (?)
Asian flu	1957	H2N2	Avian
Hong Kong flu	1968	H3N2	Avian
Russian flu	1977	H1N1	Laboratory (?)
Swine flu	2009	H1N1	Swine

*Information adapted from the WHO pandemic influenza website (WHO, 2016).

1.4.2 Pandemics

An influenza pandemic occurs when a novel IAV subtype emerges suddenly by antigenic shift. The segmented nature of the IAV genome facilitates the reassortment during coinfection with both human and non-human viruses. Antigenic shift can occur when genes encoding at least the HA glycoprotein are to 'reassort' their genetic material to form a 'new' virus. The new reassortant virus is antigenically different from preceding human viruses. However, the novelty alone is insufficient for the emergence of a pandemic influenza virus. The virus must adapt to successfully replicate in humans, transmit within from person to person and a susceptible population is also required (reviewed in Nicholson *et al.,* 2003).

Five confirmed pandemic outbreaks have occurred in humans since the 20th century (each of which are summarised in table 1.2). The most famous influenza pandemic outbreak was the 1918 "Spanish flu" in which at least 40 million people died; estimated to be around 3-6 % of the world population at the time. Unlike most influenza outbreaks, which affect young, elderly and immunosuppressed, the 1918

pandemic predominately caused morbidity in otherwise healthy young adults. Thus, it is the most aggressive IAV outbreak to date (Worobey *et al*., 2014). All subsequent human pandemic strains are caused by viruses derived from this pandemic strain and variants continue to be endemic in humans (Taubenberger and Morens, 2006). The first pandemic of the 21st century was caused by a swine origin H1N1 virus in 2009 (H1N1pdm09) in which the virus spread over 215 countries (Nelson *et al.*, 2015) with an estimate of ~284,500 deaths in the US (Nguyen *et al.,* 2013). The virus mostly only produced mild infections in humans but spread well within the population. The HA, NP and NS proteins were derived from an H1N1 strain circulating in pigs in North America (Taubenberger and Morens, 2006). The NA and M segments were originally derived from an avian virus that adapted in pigs in Europe and Asia (Scoltissek *et al.,* 1983) and finally the PB2, PB1 and PA proteins came from a linage of swine flu that had a reassortment of avian, swine and human origin viruses (Garten *et al.,* 2009). The H1N1pdm09 strain has replaced the 1977 Russian H1N1 virus and is still currently circulating in humans.

1.5 Strategies to combat human influenza infections

1.5.1 Vaccination

Vaccination is the primary strategy to combat human influenza infections. The main goals of influenza vaccine administration are to provide protection against influenza infection and disease symptoms and to prevent transmission within a population (Salk and Salk, 1977; Pronker *et al.*, 2012). Vaccines elicit an adaptive immune response by administering viral antigens. The main antigen that elicits this immune response is the

HA glycoprotein (NA can also elicit an immune response but to a lesser degree). In the UK, the seasonal immunisation programme offers protection to individuals who are most at risk of serious illness or death should they develop an influenza infection. At risk individuals include patients >65 years, pregnant women, health care workers, immunosuppressed individuals and patients with underlying health condition such as long-term heart or respiratory disease (http://www.nhs.uk/Conditions/vaccinations-/Pages/who-should-have-flu-vaccine.aspx).

Currently, three types of influenza vaccine are recommended by the WHO for human use; inactivated virus, recombinant viral HA and live-attenuated virus (Belshe *et al*., 2007; Cox *et al*., 2008; Pronker *et al*., 2012). Any type of seasonal influenza vaccine contains antigens from at least three circulating influenza strains: two IAV subtypes: H1N1_pdm09, H3N2 and a FLUBV strain from the Victoria-like or Yamagata-like lineage (Pronker *et al.*, 2012). The composition of the 2016-2017 trivalent vaccine was recommended to contain an A/California/7/2009 (H1N1) pdm09-like virus, an A/Hong Kong/4801/2014 (H3N2)-like virus and a B/Brisbane/60/2008-like virus (Victoria lineage) (The Green Book, 2008). Additionally, quadrivalent vaccines were recommended to contain a fourth FLUBV virus, B/Phuket/3073/2013-like virus (Yamagata lineage). The most common type of vaccine is the inactivated influenza vaccine (IIV). IIV are administrated intramuscularly and produce neutralising antibodies that target HA epitopes, thus eliciting a protective humoral immune response (Belongia *et al*., 2009; Osterholm *et al*., 2011). IIVs can be classed as whole virus vaccines or split vaccines (Belshe *et al*., 2007). The influenza whole virus vaccines were first developed by growing influenza virus in embryonated hen eggs

which was purified and chemically inactivated with formaldehyde (reviewed in Wong and Webby, 2013). Split vaccines contain a non-ionic detergent treatment step, which exposes all viral proteins upon dissociation of the virion (Duxbury *et al*., 1968). Currently, most influenza vaccines in Europe and the US are egg-grown, formaldehyde-inactivated and treated with non-ionic detergent. Another type of IIV are vaccines that contain subunits of purified HA or HA/NA proteins without any other viral components (Cox *et al*., 2008). These subunits can be generated using baculovirus expression systems or recombinant DNA technologies to allow production of large quantities of HA and NA (Baxter *et al.*, 2011). Live-attenuated vaccines (LAIV) were first developed in the 1960s by serial passaging IAV in eggs at sub-optimal temperature conditions thus resulting in temperature sensitive, cold-adapted and attenuated stains (Mills, 1969). The variants grew at 25 ˚C but not at temperatures >35 ˚C, which is similar to the lower respiratory tract and therefore when administrated, virus replication was restricted to the upper respiratory tract and induced local protective immune responses (Belshe *et al*., 2007; De Villiers *et al*., 2009). LAIV have been available in the US since 2003 and are administered intranasally to mimic the natural route of infection which can come with certain risks and benefits in comparison to the IIV. In the UK in 2014, the Joint Committee on Vaccination and Immunisation (JCVI) recommended administration of a universal childhood vaccine programme with a newly licensed LAIV. The childhood LAIV programme recommends that all children between the ages of 2-4 years receive a live attenuated nasal vaccine (Fluenz Tetra). LAIV can elicit a more rapid and efficient innate and adaptive immune response (Belshe *et al.*, 2007), provide cross-reactive T-cell-mediated protection against multiple influenza viruses (Gorse *et al.*, 1996; Pica

and Palese, 2013) and provide a longer lasting immune response (Couch *et al*., 1997). However, due to the inherent risk of immunising with live viruses, LAIV are not recommended for immunosuppressed, asthmatic patients (Greenhawt, 2014), and children under two years of age (Belshe *et al*., 2007).

1.5.2 Antivirals

Annual vaccines have successfully reduced the impact of seasonal influenza epidemics; however, they are not without their significant restrictions. The most obvious limitation of the annual vaccination is that they only prevent the spread of infection and offer no therapeutic benefit. Additionally, the unpredictable antigenic changes of the viral surface glycoproteins in circulating IAV strains can render the seasonal vaccine ineffective. Furthermore, developing a vaccine to a newly emerging strain is a time-consuming process and thus vaccination programs are of limited use in preventing the initial spread of infection from a new pandemic strain. Consequently, antiviral drugs are critical as a short-term resource to regulate and prevent transmission and illness caused by both seasonal and pandemic influenza viruses. The necessity for antiviral therapy was clearly demonstrated with the emergence of the recent H1N1pdm09 strain in which the antiviral drug, oseltamivir was heavily used while a vaccine was under development (Miller *et al.*, 2013). To date, only two classes of antiviral have been approved by the FDA in the US and Public Health England (PHE) in the UK as a treatment for influenza infections; M2 ion channel blockers and neuraminidase inhibitors (NAIs).

1.5.2.1 M2 ion channel blockers

Amantadine was the first drug used against influenza infection in the 1960s as a prophylactic against Asian IAV infection (Davies, 1964). Amantadine (Symmetrel) and rimantadine (Flumadine), both belonging to the drug class: adamantanes, were first approved in 1976 for use as a prophylactic and therapeutic agent against IAV infection. Adamantanes block the action of the viral M2 ion channel which is responsible the conductance of protons to acidify the viral interior, thereby facilitating the dissociation of the matrix protein from vRNPs – required for unpacking of the viral genome (Helenius *et al.*, 1992). Adamantanes bind to M2 and inhibit its proton conduction mechanism, either directly or allosterically, and subsequently preventing the uncoating of the virion and inhibiting vRNP release/viral replication (Hay *et al.,* 1985; Cady *et al*., 2011; Schnell and Chou, 2008; Stouffer *et al*., 2008). Adamantanes possess no inhibitory effect against FLUBV, as they do not contain M2 but a homologue protein, that although shares functional homology with IAV M2, differs in sequence. In past seasons, the emergence of adamantane resistance in IAV strains has become prevalent. 99 % of H3N2 and H1N1pdm09 viruses are resistant to both amantadine and rimantadine (according to surveillance data provided by CDC, Atlanta, GA). Since 2006 the CDC has recommended the cessation of adamantanes as treatment against current circulating strains of IAV. Development of novel M2 ion channel blockers are underway; however the new compounds were still inactive against the viruses containing the adamantane-resistant mutation, S31N (Balgi *et al*., 2013).

1.5.2.2 Neuraminidase (NA) inhibitors

Development of neuraminidase inhibitors (NAIs) commenced in the late 1960s with the synthetic compound Neu5Ac2en (DANA) (Edmond *et al*., 1966); although the compound exhibited low specificity and potency. The three-dimensional crystal structure exposing the catalytic sites of NA was resolved in the 1980s (Varghese *et al.,* 1983), which facilitated the design of current NAIs (Colman, 1994). To date, there are three FDA-approved NAIs for treatment against IAV infection; oseltamivir (Tamiflu) and zanamivir (Relenza) and newly licensed peramivir (Rapivab) (Alame *et al*., 2016). NA is required to help release progeny virus particles by digesting the HA receptors from the cell membrane (Palese *et al*., 1974) and can also help the spread of infection by facilitating movement though the respiratory tract by digesting neuraminic acid in respiratory mucus (Calfee *et al.,* 1998). NAIs competitively inhibit the viral NA sialidase activity, thus consequently blocking the release of newly synthesised virions. Unlike adamantanes, NAIs are effective against both IAV and FLUBV strains, as the NA active site is highly conserved across all influenza viruses. Oseltamivir is the most commonly administered NAI due to the ease of oral delivery, whereas zanamivir is usually administered via inhalation and peramivir is delivered intravenously (IV), thus providing an alternative route of delivery for patients unable to inhale and/or take medication orally. In recent years, there has been a debate on the effectiveness of NAIs as an antiviral treatment. The 2014 Cochrane Collaboration study (Jefferson *et al.*, 2014) and the 2015 Multiparty Group for Advice on Science (MUGAS) report (Dobson, 2015) reviewed randomized placebo-controlled trials with patients receiving NAI treatment within a 48 h onset of 'flu-like' symptoms. The Cochrane and MUGAS studies concluded that oseltamivir decreased 'flu like' symptoms on average 16.8 h

(95% confidence interval (CI) 8.4-25.1) and described the reduction as "small". Additionally, Jefferson *et al*., stated that there was insufficient evidence for NAI effectiveness against influenza infection complications such a pneumonia and that oseltamivir increases the risk of adverse effects such as nausea and vomiting. However, the lack of clinical trials including the severely ill and hospitalised patients reduced the reliability of the analyses of NAI efficacy presented in both studies as the success of treatment outcomes was not well represented. Thus, the European Centre for Disease Prevention and Control (ECDC) expert panel concluded in 2016 that they still endorsed the current policy on the use of NAI as a treatment for influenza virus infection along with support from the WHO (ECDC, 2016).

1.5.2.3 Other antivirals

In addition to the WHO-approved influenza antivirals, other therapeutic agents are approved and available in other countries. Laninamivir, also a NAI, is approved for treatment in Japan, but is still currently in clinical trials in the US (Kashiwagi *et al*, 2016). Arbidol, a membrane fusion inhibitor that acts by binding to the HA2 subunit and preventing the conformational change required for membrane fusion (Leneva *et al.*, 2009), is currently only licensed for use in Russia and China. An influenza polymerase inhibitor Favipiravir (T-705) has been approved for use in Japan and is currently undergoing Phase III clinical trials in US and Europe (Furuta *et al.*, 2013). Other potential virus-acting therapeutic agents are undergoing clinical trials. These include PA endonuclease inhibitors; AL-794 and S-033188 and a small molecule inhibitor of PB2 cap-binding; VX-787 currently undergoing phase II human trials in Belgium (Table 1.3). In addition, human monoclonal antibodies (HuMAbs) prepared

from vaccinated donors and/or patients with viral infections could have therapeutic use, with several HuMAbs displaying broad neutralising activities against a range of HA subtypes (Table 1.3). Finally, a small number of host-targeting potential IAV drugs are also currently being evaluated clinically (Table 1.3) and are discussed in detail in section *1.5.4.2 Targeting cellular host factors*

1.5.3 Antiviral resistance

The emergence of antiviral drug resistance in IAV has been a growing problem in the past few years, with many circulating strains accumulating drug-resistant mutations. The ability of influenza viruses to overcome certain selection pressures such as drug inhibition is most likely due a viral error-prone RdRp which introduces mutations and thus produces a high abundance of viral variants. The inappropriate use of antivirals within hospitals and clinics, such as misdiagnosis or overuse, has also be speculated to contribute to the rapid increase in resistance observed over the past few decades.

1.5.3.1 Genetic barriers to resistance and fitness cost

The number and type of mutations necessary to generate resistance differ dependant on the antiviral class and target; which is referred to as the genetic barrier to resistance (Gotte, 2012). Some older classes of antivirals have been described to have a low genetic barrier, in which the viruses only require one or two mutations to gain resistance such as the first generation HIV antivirals, RT inhibitors (Perno *et al.,* 2008). The genetic barrier will affect the rate at which resistance to a drug will occur. For example, if one resistance pathway only requires one mutation and another pathway

require multiple mutations, the former would likely occur more often. Thus, the ideal antiviral drug would have a high genetic barrier so resistance would not arise easily.

Established resistance mutations are often not maintained in a population after drug treatment has ceased. This is usually because of the fitness costs associated with the drug-resistance mutations. When under a selection pressure, the mutations would produce a benefit (becoming resistant) but carry a cost as a result of the fitness gain in a drug dependant environment. Examples of these cost/benefit trade-offs include thymidine kinase mutations in HSV to gain resistance to acyclovir, resulting in decreased enzyme production (Piret and Boivin, 2014) and resistance to thymine analogue HIV inhibitors by removal of chain-terminating function, which results in lower replication titres (Hu *et al.,* 2006). However, these trade-offs are not always present. In the case with the influenza H1N1 2009 strain, containing oseltamivir resistance mutation H274Y had little to no cost to virus fitness (Renzette et al., 2014; Hauge et al., 2009) (as discussed in more detail below).

1.5.3.1 Adamantine resistance

Early resistance to adamantanes was revealed in the 1990s, where during clinical use, amantadine and rimantadine resistant strains emerged in 30 % of patients after 2-3 days of treatment (Hayden,1992). Furthermore, in the late 1980s, it was determined that drug-resistant virus variants did not lose pathogenicity and could still transmit efficiently between individuals (Belshe *et al*, 1988). After 50 decades of effective use of adamantanes, global drug resistance has increased drastically. In the US, the frequency of adamantane resistance at the end of the 2003-2004 influenza season was

1.9 %. This increased to 14.5 % between 2004-2005 and at the beginning of 2006, 92 % of circulating H3N2 strains were adamantane-resistant (Bright, 2006). The mutations for IAV to escape the M2 ion channel blocker have been well characterised. Mutations identified to cause adamantane resistance (L26F, V27A, A30T/V, S31N, G34E and L38F) are found within the M2 transmembrane domain (Cheung *et al*., 2006; Hayden, 1992). The S31N substitution renders viruses highly resistant, with >97 % of strains harbouring this mutation (Bright *et al*, 2006; Deyde *et al*., 2007; Frederick and Hayden, 2006). Mutations within the M2 transmembrane domain that line the channel pore (V27A, A30T/V and G34E) lead to an increase in M2 pore size and hydrophilicity, whereas mutations in the tetramer helix-helix packaging region (L26F, L38F and S31N) destabilise the helix assembly, therefore narrowing the M2 pore size (reviewed in Hussain *et al*., 2017). Currently, > 99 % of circulating influenza strains are thought to be resistant to adamantanes, which has subsequently led the CDC to change their recommendation for the use of adamantanes as treatment against IAV infection. Thus, NAIs have been made the antiviral treatment of choice for influenza infection.

1.5.3.2 NAI resistance

Due to the rapid emergence of adamantane-resistant virus variants, preclinical *in vitro* resistance studies were performed to determine the prevalence of NAI-resistant IAV strains. Drug-resistant mutations E119G/A/D/V and R292K were found in NA after *in vitro* passage with NAIs and in patients treated with both oseltamivir and zanamivir (McKimm-Breschkin, 2000). Additionally, two drug resistant viruses containing the mutation H274Y in NA, were isolated from healthy volunteers that were infected with

IAV and administered oseltamivir (Gubareva *et al.*, 2001). In 1999, a global Neuraminidase Inhibitor Susceptibility Network (NISN) was established to monitor the clinical IAV resistance to NAIs (Zambon and Hayden, 2001). The first few reports from 1999 to 2006, determined that IAV strains remained relatively susceptible to NAIs, with the expectation of a few rare cases of resistant variants (Monto *et al*., 2006). However, between 2007-2008, oseltamivir resistance presented in seasonal H1N1 viruses with a 7 % increase of strains containing the drug-resistant escape mutation H274Y (Sheu *et al*., 2008). By the 2008-2009 season, >90 % of circulating H1N1 viruses were resistant to oseltamivir; however all strains were still sensitive to zanamivir and all H3N2 viruses were still susceptible to oseltamivir and zanamivir (Baranovich *et al*., 2010; Matsuzaki *et al*., 2010). The emergence of the novel pandemic H1N1 2009 strain replaced the pre-pandemic oseltamivir-resistant H1N1 subtype. Global analyses of clinical isolates from April 2009 to January 2010 demonstrated that almost all post-pandemic strains were susceptible to NAIs (Dapat *et al*., 2013; Okomo-Adhiambo *et al*., 2010). IAV continues to be largely susceptible to NAIs with >98 % of pandemic H1N1 and H3N2 strains sensitive to NAIs (Hurt *et al*., 2016).

1.5.4 Methods of preventing antiviral resistance

The establishment of the M2 escape mutation S31N in IAV has rendered adamantanes ineffective as an anti-influenza treatment after ~50 years of use. Luckily, the majority of circulating H1N1 and H3N2 subtypes are still sensitive to NAIs. However, if the same timeline of viral adamantane resistance was applied to NAIs, first approved for clinical use in 1990s, circulating strains could be resistant to NAIs by 2030.

Consequently, investigation into new strategies for the control of viral drug resistance are essential. Proper diagnosis of respiratory illness will reduce the use of unnecessary/over-use of prescription of antivirals and potentially decrease the prevalence and speed of resistant strain emergence. Physicians often fail to correctly diagnosis influenza infection or associate 'flu-like' symptoms with another respiratory illness. In 2006, a study concluded that most children that were either hospitalized or

1.5.4.1 Combination therapy

The emergence of drug-resistant virus variants can be reduced with treatment of two or more drugs that target the virus and/or a cellular host factor, in which the mechanism of inhibition differs. This combination therapy presents the virus with two or more genetic barriers to adapt to and overcome and therefore may reduce the likelihood that a drug-resistant strain will develop. Additionally, the use of combination therapy clinically may allow physicians to reduce the doses of individual drugs necessary for potent antiviral activity thereby reducing dose-related side effects. Combination treatment to avoid the selection of resistant viruses has been a successful strategy for antiretroviral therapy (ART) against HIV (Lohse *et al.,* 2007; Taiwo *et al.*, 2010).

Since the mid to late 1990s it has been known that simultaneous treatment with three antivirals against HIV blocks viral replication and decreases the probability of resistance by effectively establishing a chemicogenetic barrier. The multiple HIV therapy can keep viral plasma loads below detectable levels, prevent the likelihood of resistant viral variants and allow successful management of HIV-infected patients (Gulick, 2002; Raboud *et al.*, 2002). Additionally, treatment with pegylated interferon

Table 1.3 Summary of influenza antivirals currently licenced or in clinical trials*

Virus/host targeted	Class	Name	Development stage
Virus targeting	M2 ion channel blockers	Amantadine	Licensed in 1976 - no longer recommended
		Rimantadine	Licensed in 1976 - no longer recommended
	NA inhibitors	Oseltamivir carboxylate	Approved in US and UK (1999)
		Zanamivir	Approved in US and UK (1999)
		Laninamivir	Approved in Japan (2010)
		Peramivir	Approved in Japan, Korea and US (2016)
	Nucleoside analogues for RNA-dependent RNA polymerase	Favipiravir	Approved in Japan (2014) and in phase III in US and Europe
		Ribavirin	Phase II as a combination therapy in US
	Membrane fusion inhibitors	Arbidol	Approved in Russia (2005)
	Small molecules that inhibit PB2 cap-binding	JNJ-63623872 aka VX-787	Phase IIb in Belgium
	PA endonuclease inhibitors	AI-794	Phase I in UK
		S-033188	Phase III in Japan
	Monoclonal HA antibodies	CR261	Phase I in Holland
		CR8020	Phase II in Holland
		MEDI8852	Phase II in US
		MHAA4549A	Phase II in UK
		VIS410	Phase II in UK
Host targeting	Attachment	Fludase (DAS181)	Phase II in US
	Attachment	Nitazoxanide	Phase II in US
	Nuclear export inhibitors	KPT-335)	Phase I in Australia

*Data from clinicaltrials.gov accessed on 1/06/17

(IFN) in combination with ribavirin has been used as a therapy for severe hepatitis C infections and respiratory syncytial virus infection (Cacoub *et al.*, 2005).

Exploiting combination antivirals is not a novel pharmacological rationale to control influenza virus infection. Many investigations study the activity of drug combinations against influenza virus *in vitro* and *in vivo.* The effects of the interactions of two or more drugs can be defined as synergistic, additive or antagonistic; depending on if the combined effect exceeds, equals or is less than the overall sum of the antiviral effects of each drug, respectively. Synergistic drug combinations are more advantageous, as the drugs can enhance each other's mechanism of action and therefore may result in a dose reduction, a decrease in cellular toxicity/side effects and permit greater cost-effectiveness. Synergistic interactions between combinations of current anti-influenza drugs amantadine, oseltamivir and ribavirin have been found to be more efficacious prophylatically than monotherapy *in vitro* and *in vivo* (Nguygen *et al.*, 2012; Govorkova *et al,* 2004; Ilyushina *et al*., 2008; Ilyushina *et al*, 2007; Smee *et al*., 2006). Several influenza studies, which tested the compounds in animal models*,* show enhanced antiviral activity when used in combination; the success of influenza antiviral combinations are detailed in Table 1.4. However, clinical applications of combination therapy against influenza virus are limited, possibly due to the development of resistance to the current antiviral class of adamantanes, thus limiting the number of other classes of approved antivirals for use. Two randomised clinical trials tested the combination of oseltamivir and zanamivir treatment against H3N2 and H1N1pdm09 viruses but failed to indicate an additive effect of the combination

Table 1.4. Outcome of double drug combinations on influenza virus infection in animal models

Drug combination	Influenza subtype	Drug interactions	Reference
Oseltamivir + Amantadine	H1N1	Enhanced protection	(Masihi *et al*., 2007)
	H3N2	Enhanced protection	(Masihi *et al*., 2007)
	H5N1	Greater protection than monotherapy	(Ilyushina *et al*., 2007)
	H5N1	Greater protection than monotherapy	(Smee *et al*., 2009)
Oseltamivir + Rimantadine	H9N2	Greater protection than monotherapy	(Leneva *et al*., 2009)
	H3N2	Synergistic	(Galabov *et al*., 2016)
Oseltamivir + Ribavirin	H1N1	No added benefit	(Smee *et al*., 2006)
	FLUBV	Synergistic	(Smee *et al*., 2006)
	H5N1	Greater protection than monotherapy	(Smee *et al*., 2009)
	H5N1	Additive at some concentrations	(Ilyushina *et al*., 2008)
	H5N1	Additive at some concentrations	(Ilyushina *et al*., 2008)
Amantadine + Ribavirin	H5N1	Greater protection than monotherapy	(Smee *et al*., 2009)
Peramivir + Ribavirin	H1N1	Additive-synergistic	(Smee *et al*., 2002)
Oseltamivir + T-705	H1N1	Strong synergy	(Smee *et al*., 2010)
	H3N2	Strong synergy	(Smee *et al*., 2010)
	H5N1	Strong and minor synergy	(Smee *et al*., 2010)

therapy (Duval *et al.*, 2010; Escuret *et al.*, 2012). In another study, a comparison between a triple combination with amantadine, ribavirin and oseltamivir vs oseltamivir monotherapy was examined (Kim *et al*., 2011). Results indicated that the mortality rate was lower in patients receiving triple therapy compared to the monotherapy (17 % versus 35 %). Notably, two trials comparing zanamivir/oseltamivir combination and oseltamivir alone resulted in reduced clinical efficacy, potentially as a result of competitive antagonism (Dunning *et al.,* 2014; Duval *et al.,* 2010). Currently, another randomised clinical trial is underway, testing a triple combination of amantadine, ribavirin and oseltamivir vs oseltamivir alone (Dunning *et al*., 2014).

1.5.4.2 Targeting cellular host factors

Targeting cellular factors involved in influenza virus replication signifies a novel antiviral strategy that could potentially slow the emergence of viral drug resistance. It is hypothesised that the virus would find it more challenging to escape inhibition of host-encoded target compared to inhibition of a viral protein (Watanabe and Kawaoka, 2015). Influenza virus replication takes place in non-immune (respiratory epithelial cells) and immune cells (alveolar macrophages and dendritic cells) and relies on numerous host cell factors (reviewed in Hale *et al.,* 2010). Many host factors have been identified using genome-wide siRNA screening and genomic/proteomic bioinformatics approaches; however, development and validation of compounds with antiviral properties against novel cellular targets can be a time consuming and expensive approach. Nevertheless, if a host targeting antiviral could counteract viral drug resistance it could be cost effective in the long-term. One of the major difficulties when developing a cellular targeting antiviral is the potential for the compound to cause adverse effects on host cells. This difficulty may explain why there are currently

no licenced influenza antiviral therapies that inhibit cellular factors. However, the severity of the disease may outweigh the consequences of overt toxicity. For example, one host-targeting antiviral drug, Maraviroc (a CCR5 chemokine receptor antagonist) has been FDA-approved for the treatment of HIV, which presents itself as persistent, life threatening disease. Influenza antivirals are often administered to immunosuppressed individuals that have acquired influenza virus as a secondary infection and thus present with more serious illness than in a healthy individual. Accordingly, it is important to take in to consideration the severity of disease and determine the benefits and risks of administration of the cellular targeting therapy. Nonetheless, the area of cellular drug targets is advancing. Recently, a few potential antivirals, that block host factors, have been developed with lower toxicity and are currently being tested experimental *in vitro/in vivo,* with some advancing to human clinical trials (Table 1.4).

To date, nitazoxanide (NTZ) is the most successful cell-targeting compound to proceed in clinical trials. NTZ was originally developed and licensed for treatment against protozoa and helminth infection (White, 2004). It was first identified to have antiviral properties during a clinical trial for Cryptosporidium treatment in patients with HIV infection (Capparelli and Syed, 2008). Since then, NTZ has been shown to inhibit a range of both bacterial and viral infections (reviewed in Rossingnol, 2014). For influenza infection, NTZ inhibits replication by impairing HA assembly through disruption of HA transportation from the endoplasmic reticulum (ER) to Golgi, thus preventing the exit of virus particles from infected cells (Rossingnol *et al*., 2009). *In vitro* studies have shown broad-spectrum antiviral activity of NTZ (Rossingnol *et al.*,

2009) and a synergistic effect when used in combination with oseltamivir (Belardo *et al.*, 2015). A recent phase IIb human clinical trial demonstrated reduced influenza symptoms by 36 hours (treatment started 48 h after the onset of symptoms) (Haffizulla *et al.,* 2014). Currently, four phase II and III trials are underway including a 4-way comparison trial of NTZ vs oseltamivir vs NTZ/oseltamivir vs placebo (NCT01610245: study identification number obtained from the https://clinical-trials.gov/ database). Additionally, there is encouraging *in vitro* data to suggest that serial passage of influenza virus in the presence of NTZ failed to select for drug resistance virus variants (Belardo *et al*., 2015).

Fludase (DAS18) is another successful cell-targeting compound to proceed to phase II clinical studies. Fludase is a recombinant fusion protein containing a sialidase catalytic domain, derived from *Actinomyces viscosus*, fused with a cell surface anchoring domain. The compound cleaves sialic acid receptors from the airway epithelium and therefore prevents virus attachment (Malakhov *et al.*, 2006). Preclinical *in vitro* and *in vivo* studies have demonstrated that Fludase possesses potent broad-spectrum antiviral efficacy and cell protective properties when administered long term. In 2007, the first phase I clinical trial of Fludase was carried out in healthy adults to determine the safety and tolerability of the drug. The study concluded in 2009 and revealed that the drug was well tolerated at all dosage levels tested (Triana-Baltzer *et al*., 2009). Since then, multiple successful phase I trials have been carried out on healthy adults and on those suffering from asthma and bronchiolitis (NCT01113034). Thus far, one phase II study has been performed with patients who were otherwise healthy but suffering from IAV infection. Fludase was well tolerated with slightly more mild to moderate adverse

effects in the treatment than the placebo group (Moss *et al*., 2012). Further testing of Fludase is currently underway to evaluate its safety and tolerability during influenza infected individuals that have known chronic health conditions.

Other cellular targeting antiviral compounds, yet to advance to clinical testing, are currently under experimental investigation in both *in vitro* and *in vivo*, such as protease, phospholipase and V-ATPase inhibitors, compounds that target various cellular signalling pathways including Raf/MEK/ERK, mechanistic target of rapamycin (mTOR) and epidermal growth factor receptor (eGRF) and inhibitors against immunomodulatory factors such as cyclooxygenase, angiotensin converting enzyme (ACE), angiotensin receptors and AMP activated protein kinase (AMPK) (see Table 1.5 for details). A few of these compounds are approved for treatment against other diseases; however, thus far none have successfully proceeded to clinical-stage trials regarding treatment of influenza virus infection. NTZ and Fludase are the only two cellular inhibitors to date that have proceeded to phase II clinical testing against IAV. KPT-335 (also known as verdinexor), is a cellular inhibitor that targets host cell factor CRM1, which has recently completed an initial phase I clinical trial. Investigations into the preclinical efficacy of KPT-335 will be the focus of this thesis.

Table 1.5 Potential anti-IAV therapeutics targeting host cell factor

Drug target	Drug name	Mechanism of action	Current development stage
Attachment	Fludase (DAS181)	Removes sialic acid receptors from respiratory epithelial cells thus preventing attachment of the virus to the host cell surface	Successfully inhibits influenza A viruses *in vivo* (Belser *et a*l., 2007) Currently in Phase II clinical trials (http://www.drugdevelopment-technology.com) (US)
Attachment	Nitazoxanide	Interferes with assembly of viral HA	Clinical Phase III (US) NCT02612922
Membrane fluidity	Fattiviracin FV-8	Alters the fluidity of the plasma membrane thus may restrict effect virus entry	Broad spectrum antiviral activity against enveloped viruses (Harada *et al.,* 2007)
Transcription/ replication	Viramidine	Inosine-5'-monophosphate dehydrogense	Influenza A virus inhibition in vitro and in vivo (Sidwell *et al*., 2005)
Nuclear export	Verdinexor (KPT-335)	Targets host cell export protein CRM1 which the virus utilizes for nucleocytoplasmic transport of vRNPs	Inhibits various influenza A and B strains *in vitro* (Perwitasari *et al*., 2014) Reduced influenza replication in mice and ferrets (Perwitasari *et al.,* 2016) Currently in Phase I clinical trials (www.karyopharm.com)
Protease inhibitors	Nafamostat, Leupeptin, Aprotinin and Camostat	Inhibits the host proteases ability to splice mRNA which determines whether species specificity and virulence of the virus	Protease inhibitors have shown to block infection at viral entry (reviewed in Kido *et al*., 2017)
Phospholipase inhibitors	ML395	Inhibits catalyzation of phosplipase which plays a role in metabolic pathways,	Broad-spectrum activity against influenza strains (O'Reilly *et al*., 2014)
V-ATPase inhibitors	NorakinR, ParkopanR, AntiparkinR and AkinetonR	Thought to increase internal pH of the pre-lysyosome thus inhibiting conformational transformation of HA	Parkinson treatments that contain the adamantine scaffold shown to have an inhibitory effect against influenza A and B viruses (Schroeder *et al*., 1985)
Raf/MEK/ERK pathway	U0126	Inhibits Raf signalling resulting in nuclear retention of vRNPs	Inhibition of influenza A virus in vitro (Pleschka *et al.,* 2001)
mTOR pathway	Rapamycin	Potent immunosuppressive and antiproliferative properties	Treatment lead to protection from multiple influenza subtypes (McMichael and Haynes, 2013)
eGFR pathway	PPQ-B	May down regulate NF-κB and MAPK pathways to inhibit replication and inflammatory responses	Suppressed replication of influenza A viruses in vitro (Wang *et al*., 2017)
Immunomodulatory agents	Cyclooxygenase inhibitors, ACE inhibitors, angiotensin receptors blockers, AMPK agonists	Reduce levels of LDL-cholesterol and improve inflammatory changes this reduce the mortality of influenza infection	Reduced mortality in mouse models (reviewed in Fedson, 2009) and patients with pneumia (Mortensen *et al*., 2012)
Immune dysregulation	Celecoxib Mesalazine	Targets COX-1 and COX-2 pathways; modulators of the immune response	Approved as anti-inflammatory drugs COX-1 plays a role in controlling thermoregulatory response to IAV in mice (Carey *et al.,* 2010; Zheng *et al*., 2008)
Immune dysregulation	Statins	Targets HMG-CoA which helps modulate the immune response	Approved as cardio-protective drugs. Possibly help control immune system cytokine overexpression during IAV infection (Mehrbod *et al*., 2014)

1.6 Selective inhibitors of nuclear export (SINEs)

1.6.1 CRM1, the major nuclear export receptor

NPCs mediate the exchange of macromolecules between the nucleus and the cytoplasm. NPCs permit the passive diffusion of small molecules (<~40 kDa), while larger cargos (greater than 40 kDa) are selectively transported by signal-mediated pathways, driven by the RANGTP/GDP cycle (reviewed in Beck and Hurt, 2017). There are currently 7 members of the karyopherin superfamily of importin and exportin nucleocytoplasmic transport receptors. CRM1 is the most versatile cellular export protein that lies within the NPC and facilitates the nuclear export of >240 proteins and RNA molecules (reviewed in Wente and Roul, 2010). CRM1 interacts with a NES domain on the nuclear-cytoplasmic shuttling cargo (Matsuyama *et al.*, 2006). The initial understanding that CRM1 mediated nuclear export of proteins was significantly influenced by studies with the HIV-1 REV protein (Pollard and Malim, 1998). REV recognised and stimulated export of unspliced/ partially spliced mRNA and was one of the first proteins identified to contain a NES domain (Fischer *et al.*, 1995). Investigations of the REV NES motif subsequently led to the identification of the CRM1 pathway.

1.6.1.2 CRM1 structure and LMB binding

The CRM1 structure is conserved between species including yeast, fungi, mice and humans (Fung and Chook, 2014). The 120 kDa ring-shaped protein is composed of 21 tandem HEAT repeats and contains a pair of anti-parallel helices A and B that form the outer and inner surfaces (Dickmanns et al., 2015). The highest sequence identity

between CRM1 and other karyopherin superfamily members has been shown in the first 3 HEAT repeats and the CRIME domain (Fig. 1.7.A), thus indicating their functional importance (Fornerod et al., 1997; Monecke et al., 2014). The NES binding groove is located between HEAT proteins 11 and 12 (Dong et al., 2009; Monecke et al., 2009). CRM1 binds to cargoes at the outer surfaces anchoring to five key hydrophobic residues (Φ1–Φ5) in the NES region (Fig. 1.7.B). The cysteine residue 528 (yellow circle) is the major target for CRM1 inhibitors. LMB was the first compound identified as the potent CRM1 inhibitor. LMB is a 540 Da polyketide which contains an α,β-unsaturated δ-lactone ring (Fig. 1.8.A). Structure analysis has revealed that LMB bind to the NES domain by occupying 4 of the 5 hydrophobic pockets leaving Φ4 vacant (Fig. 1.7.C). The α,β-unsaturated δ-lactone ring covalently binds to Cys528 of human CRM1 through a Michael reaction. The hydrolysis of the lactone ring (catalysed by CRM1) renders the binding irreversible, thus responsible LMB's cytotoxic effects.

1.6.2. Karyopharm therapeutics

Karyopharm Therapeutics is a clinical-stage US-based pharmaceutical company that have developed first-in-class novel selective inhibitors of nuclear export (SINE). The discovery and development of the novel compounds was performed using an *in silico* molecular modelling system to screen a virtual library containing compounds predicted to bind to the NES groove of the human CRM1 protein (Dong *et al.,* 2009). The compounds were further validated and confirmed to disrupt binding between CRM1 and NES proteins. SINEs have been designed to transiently bind to the CRM1

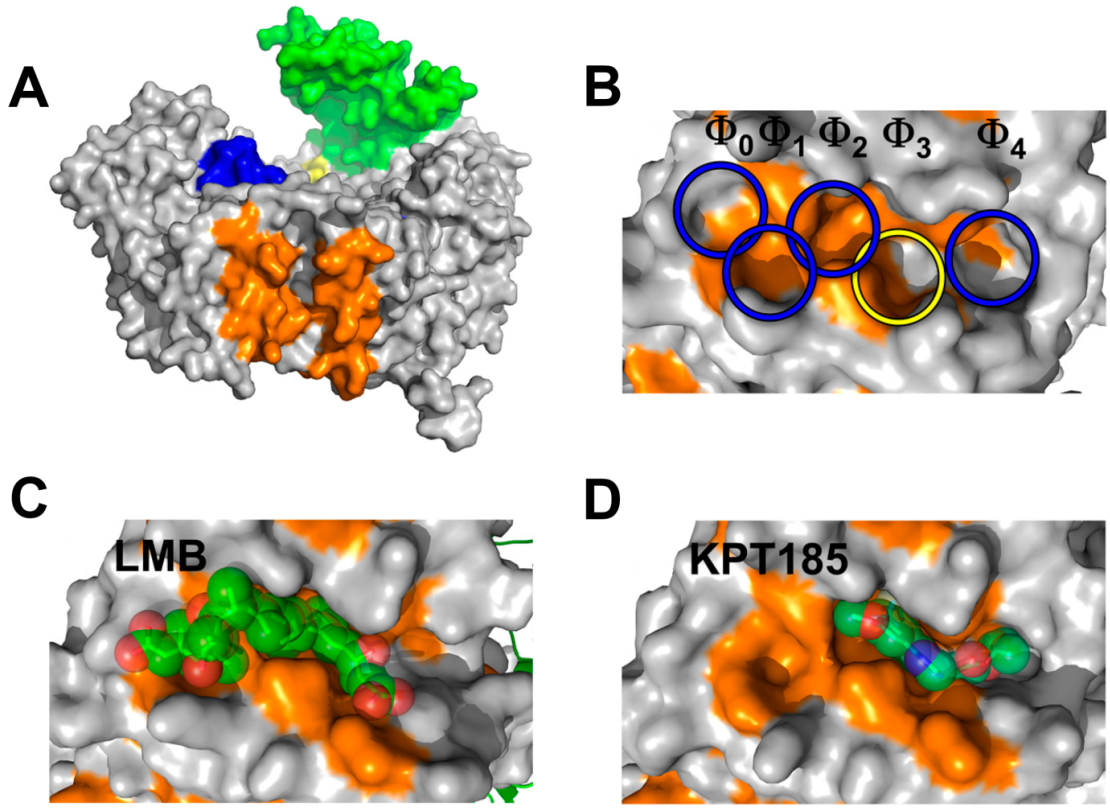

Figure 1.7. Structure of CRM1 and inhibitors binding via the NES-binding cleft. **(A)** The structure of CRM1 (grey) showing the CRIME-domain (green), the acidic loop (blue), the C-terminal helix (HEAT helix 21B (red)) and the NES-binding cleft (orange) **(B)** The 5 interacting residues (hydrophobic pockets) of the NES region indicated by circles. The yellow circle indicates the position of Cys-528 in human CRM1. LMB **(C)** and KPT-185 **(D)** molecules binding to the NES region of CRM1. Figure taken and adapted from Dickenmanns *et al.,* 2015.

cargo binding site, which blocks CRM1-mediated transport for ~12-24 h (London *et al.*, 2014). SINE's transient binding properties have been designed to reduce potential adverse toxic side effects that can be caused by the cellular inhibitors.

SINE inhibitors contain a trifluoromethly pheyl triazole scaffold (Fig. 1.8.C.D) and have been crystallized in complex with CRM1 (Lamalobella et al., 2012; Tai et al., 2014). The crystal structure analysis revealed that they occupy three of the five hydrophobic pockets (Φ2–Φ4) leaving Φ0 and Φ1 sites vacant (Fig. 1.7.D). The Michael acceptors (an isopropyl acrylate) are not hydrolysed when bound to CRM1, thus bind in a reversible fashion to NES which may explain their reduced side effects in contrast to the irreversible cytotoxic inhibitor, LMB.

Karyopharm originally developed SINEs as therapeutic cancer agents as they retain tumour suppressor proteins such as p53, forkhead box O (FOXO), retinoblastoma protein (RB1) and cyclin dependent kinase inhibitor 1A (CDKN1A), within the nucleus of a cell (Das *et al*., 2015; Parikh *et al.,* 2014; Zhang *et al*., 2013). Accumulation of these proteins allows the functional activation of tumour necrosis factor (TNF) proteins thus limiting oncogenesis. CRM1 also exports anti-inflammatory protein IκB which inhibits nuclear factor kappa-light-chain enhancer of activated B cells (NF-κB). NF-κB is associated with cancer metastasis and resistance to chemotherapy, therefore nuclear sequestration of IκB by SINEs reduces metastasis growth and help overcome chemotherapy resistance (Nair *et al.,* 2017). Currently, Karyopharm have five main SINE compounds in their drug development pipeline: KPT-330 (Selinexor), KPT-350, KPT-8601, KPT-9274 and KPT-335 (Verdinexor)

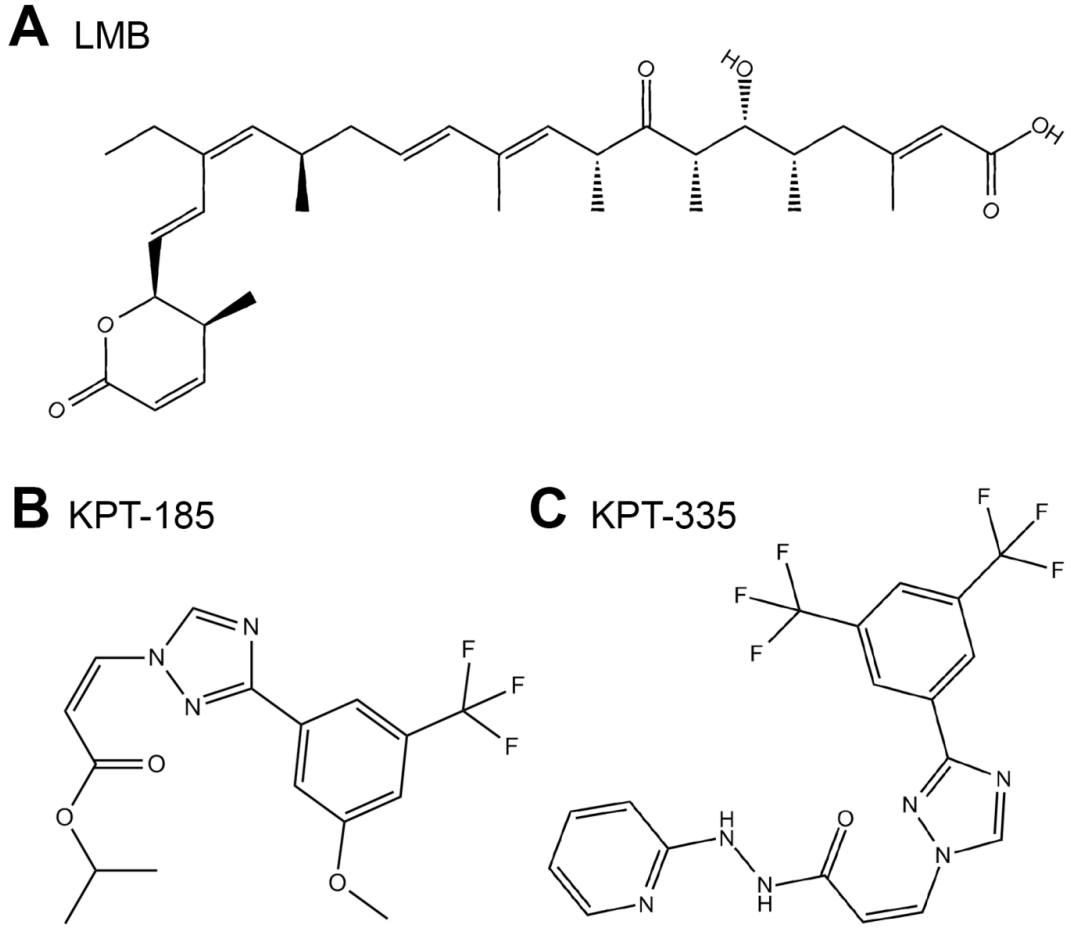

Figure 1.8. Chemical structures of CRM1 inhibitors; LMB, KPT-185 and KPT-335. (A) Chemical structure of LMB ($C_{33}H_{48}O_6$, MW = 540.74 g/mol). LMB contains α,β-unsaturated δ-lactone, two conjugated dienes, a β-hydroxy-ketone moiety and a terminal carboxylate **(B, C)** Chemical structure of SINEs; KPT-185 ($C_{16}H_{16}F_3N_3O_3$, MW = 355.31 g/mol) and KPT-335 ($C_{18}H_{12}F_6N_6O$, MW = 442.325 g/mol). Both inhibitors contain a trifluoromethyl phenyl triazole (4-phenyl-5-(trifluoromethyl)-2H-triazole, $C_9H_6F_3N_3$). (Chemical structure taken and adapted from sellechchem.com)

(https://www.karyopharm.com/pipeline/). KPT-330 is the most successful SINE to date, with >2000 patients administered treatment thus far. The compound is well tolerated and many patients are receiving long term therapy to treat multiple myeloma and B-cell lymphoma (Kuruvilla *et al.,* 2017; Muz *et al.*, 2017). KPT-350 and KPT-8601 are second generation SINE compounds and are currently in phase I clinical trials for treatment against MM, myelodysplastic syndrome, colorectal cancer, prostate cancer, solid tumours and lymphoma (Turner *et al.*, 2016). KPT-335 is the lead compound in development for treatment of viruses (www.karopharm.com-/pipeline/oral-verdinexor-kpt-335/).

1.6.3. KPT-335 as an antiviral agent

Many viruses exclusively utilise the host protein, CRM1, for nuclear-cytoplasmic transport of cargos for virus replication. IAV hijacks the CRM1 pathway to transport vRNPs from the nucleus to cytoplasm as shown previously by use of the specific CRM1 inhibitor LMB, as well as by other approaches (*1.3.4 Nuclear export*). The first study to report KPT-335's efficacy against IAV was by Perwitasari *et al.,* (2014). KPT-335 inhibited vRNP export and had antiviral activity against both influenza A and B virus strains *in vitro*. Additionally, prophylactic and therapeutic treatment of KPT-335 protected mice against influenza disease pathology and reduced viral lung loads. A second study, published in 2016, further evaluated *in vivo* efficacy of KPT-335 in two animal models of influenza infection: mice and ferrets (Perwitasari *et al.*, 2016). KPT-335 reduced virus shedding and pro-inflammatory cytokine expression in both animal models. Additionally, KPT-335 has also been shown to have antiviral

activity against Venezuelan equine encephalitis (VEEV) by retaining the viral capsids in the nucleus of the host cell (Lundberg *et al.*, 2016).

The success of KPT-335 in pre-clinical *in vitro* and *in vivo* studies warranted its development as a novel therapeutic agent against influenza infection. Subsequently, in 2015, a phase I clinical trial was conducted in healthy human volunteers. The randomized, double-blind, placebo controlled, dose-escalating trial was designed to evaluate the safety and tolerability of KPT-335 (NCT02431364). KPT-335 was generally well tolerated with mild to moderate AE. Karyopharm are continuing clinical development of KPT-335 as treatment against IAV (www.karopharm.com/-pipeline/oral-verdinexor-kpt-335/). The KPT-335 pipeline is demonstrated in Fig. 1.9.

Figure. 1.9. KPT-335 therapeutic pipeline

BASIC RESEARCH	PROTOTYPE DESIGN /DISCOVERY	PRECLINICAL	CLINICAL DEVELOPMENT			FDA APPROVAL (PHASE IV)
			PHASE I	PHASE II	PHASE III	
Establishing a potential drug target	*De novo drug design, predication made of chemical that might interact with active site of target protein*	*Testing drug efficacy in vitro and in vivo*	*Screening for safety*	*Establishing drug efficacy*	*Final confirmation of safety and efficacy*	*Safety studies during sales*
KPT-335 (Verdinexor)						
CRM1 interacts with proteins containing NES domain (Fornerod et al., 1997) LMB prevents nuclear export via inhibition of CRM1 (Wolff et al., 1997) CRM1 activity discovered to be essential during influenza replication (Elton et al., 2001)	*In silico* molecular modelling based on the structural model of the NES groove of CRM1 as a framework for selection of a virtual library of small molecule inhibitors of nuclear export (SINEs) (Dong et al., 2009) SINE compounds (KPT-335) validated (Etchin et al., 2013, Lapalombella et al., 2012)	Inhibited replication of both influenza A and B viruses in vitro (Perwitasari et al., 2014) Efficacious against influenza A virus infection in vivo (mice and ferrets) (Perwitasari et al., 2016) **Work reported in this thesis**	Randomised, double-blind, placebo-controlled dose-escalating clinical trial in healthy human volunteers (Karyopharm)			
2001	2009	2013	2015		Estimated time	
	0	4	6	8	10	12

1.7 Aims

The aim of this project was to investigate the potential of two SINE compounds, KPT-335 (verdinexor) and KPT-185 as novel therapeutic agents against IAV infection. Chapter 1 characterises pre-clinical efficacy of the compounds including investigations into cytotoxicity, antiviral efficacy and confirmation of the drugs mechanism of action. Subsequent chapters investigate the potential for emergence of drug-resistant virus variants *in vitro*. Although determining the potential for drug-resistant is not a requirement for pre-clinical development of a therapeutic agent, the FDA recommend that the drug resistance threshold for novel compounds should be considered before proceeding to clinical trials. This work aimed to support the ongoing development of KPT-335 as a potential influenza therapeutic agent as well as help enhance current knowledge of the CRM1-mediated nuclear export process during IAV infection.

Chapter 2 Characterising the antiviral activity of selective inhibitors of nuclear export against influenza A virus *in vitro*.

2.1 Introduction

CRM1, also known as XPO1, is a eukaryotic protein involved in the nuclear-cytoplasmic transport of proteins containing leucine-rich sequences termed nuclear export signals (NES) (reviewed in Hutten & Kehlenbach, 2007). Influenza viruses exploit the cellular CRM1 protein to achieve nuclear export of their viral genome, in the form of vRNP complexes, to the cytoplasm for propagation of progeny viruses. The current 'daisy-chain' model for CRM1-mediated export of vRNPs suggests the viral NP within the vRNP complex binds to the M1 protein, which in turns interacts with the NS2 protein (also known as the nuclear export protein (NEP)). NS2 contains a leucine-rich NES which is then subsequently recognised by CRM1 (reviewed in Eisfeld *et al.,* 2014). In part, the knowledge that influenza viruses utilise this cellular pathway comes from use of a natural inhibitor of CRM1, the fungal toxin leptomycin B (LMB) (Kudo *et al.*, 1999; Nishi, Yoshida, & Fujiwara, 1994). Influenza virus-infected cells treated with LMB displayed nuclear retention of vRNPs, indicating that their normal nuclear-cytoplasmic transport had been blocked (Elton *et al.*, 2001; Ma, Roy, & Whittaker, 2001; Watanabe *et al.*, 2001). Not unexpectedly, LMB is a potent cytotoxin, as displayed by numerous studies, which indicate significant potency *in vitro* but poor tolerability *in vivo* (reviewed by Mutka *et al.*, 2009). LMB's overt

toxicity is thought to be due to the covalent and irreversible nature of its interaction with the CRM1, thus hindering its use as a potential therapeutic antiviral agent.

Karyopharm Therapeutics, a clinical-stage US pharmaceutical company, specialise in the discovery and development of novel drugs directed against cellular nuclear transport. They succeeded in developing CRM1 inhibitors with lower toxicity and greater oral bioavailability than LMB, known as Selective Inhibitors of Nuclear Export (SINEs). These compounds have been described to inhibit CRM1-mediated nuclear-cytoplasmic transport by selectively and transiently binding to CRM1's cargo binding site, cysteine residue 529 (Turner and Sullivan, 2008). Although primarily focused on developing anti-cancer agents for veterinary and human applications, Karyopharm recognise that SINEs also have potential as antiviral agents and have preliminary data indicating that their compounds inhibit influenza A virus (IAV) (Perwitasari *et al*., 2014; 2016).

The aim of this section was to test the efficacy and mechanism of action of the Karyopharm compounds KPT-185 and KPT-335 (as well as an inactive chiral enantiomer control to KPT-185; KPT-301) alongside LMB, which was used as a positive control for inhibition of nuclear export. Initially, cytotoxic effects caused by the compounds were assessed and subsequently their antiviral efficacy was analysed against a human lab-adapted IAV strain and then against a range of both human and animal isolates of IAV. The mechanism of action of the compounds was also investigated with respect to the intracellular trafficking of IAV.

2.2 Results

2.2.1 Antiviral activity of SINEs

Prior to testing the activity of SINEs against IAV, the cytotoxicity of KPT-185, KPT-335 and an inactive control (KPT-301) was examined in cell culture. A549 or MDCK cells were treated with 2-fold dilutions of the compounds starting from 5 μM and the ATP content was measured 24 h later to assess cell viability. The assay determines the number of viable cells in culture based in quantification of ATP, which indicates the presence of metabolically active cells. Thus, a reduction of ATP in the presence of compound would signal a cytotoxic effect of the drug. KPT-301 displayed a 20-30 % reduction in ATP levels at concentrations >1 μM indicating the inactive compound was slightly toxic to both A549 and MDCK cells at the higher concentrations tested (Fig. 2.1. A.B). Little toxicity was observed at concentrations between 0.15 μM and 1 μM for both KPT-185 and KPT-335 in A549 and MDCK treated cells (Fig. 2.1. A.B). As dose response curves are generally sigmoidal, EC_{50} values (the half maximal effective concentrations) were determined using a non-linear regression model. From the dose-response analysis, the concentrations required for 50 % cytotoxicity (CC_{50} value) were determined as 2.7 μM and 2.9 μM for KPT-185 and 2.6 μM and 9.8 μM for KPT-335 in A549 and MDCK cells, respectively (Table 2.1). All forthcoming experiments were carried out with drug concentrations ≤1 μM to ensure that inhibition of virus replication observed was not caused by adverse cellular toxicity.

To analyse the efficacy of SINEs against IAV, A549 cells were infected with a laboratory-adapted human H1N1 virus, A/PR/8/34 (PR8), at either high (3) or low

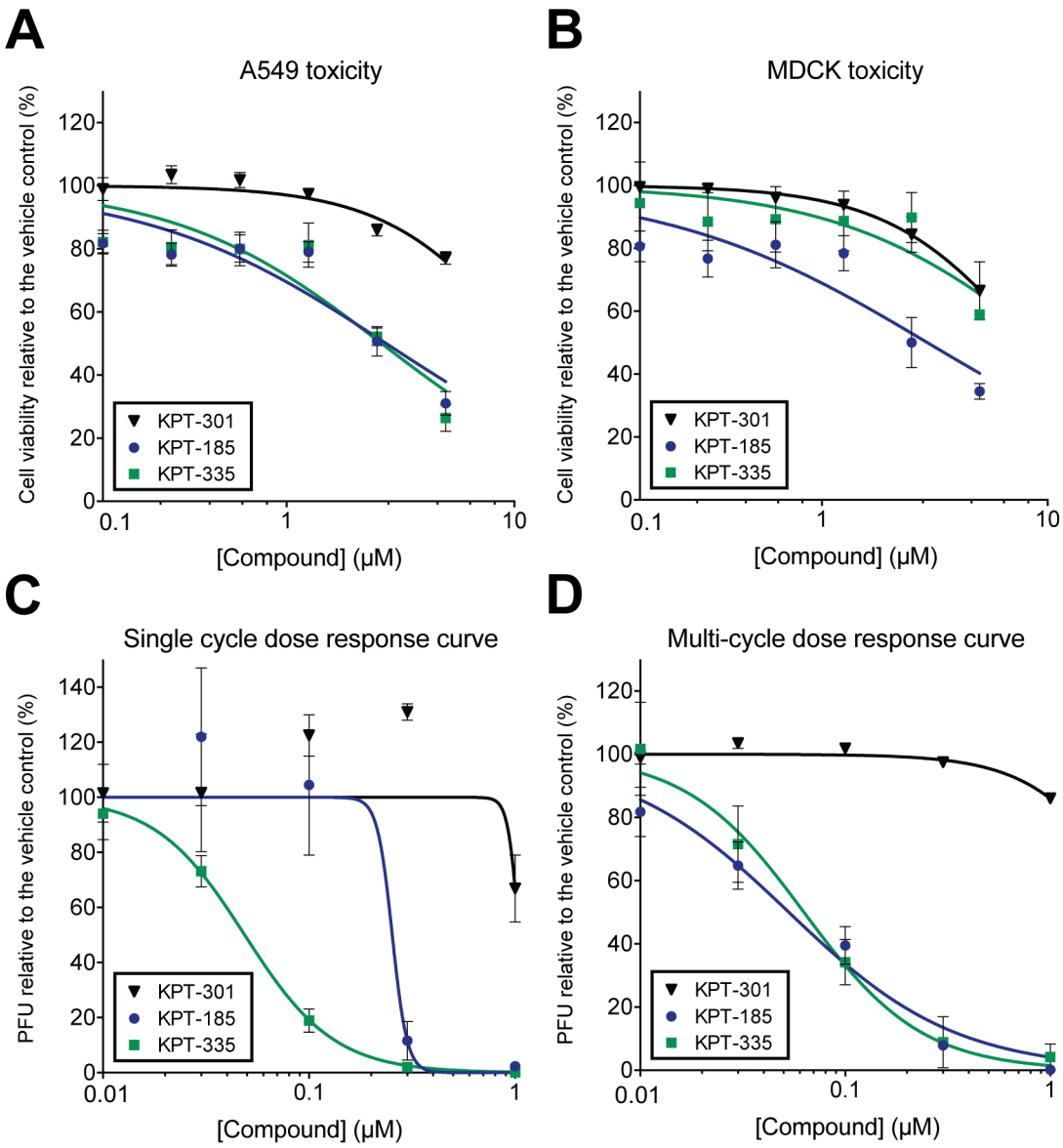

Fig. 2.1. Efficacy of SINEs against IAV *in vitro*. (A, B) Cytotoxicity of SINEs. A549 or MDCK cells were treated with either the vehicle control (DMSO) or SINEs in 2-fold dilutions. 24 h post-treatment, cells were assayed for ATP content to determine cell viability. Data are the mean ± S.D of two independent assays, each measured in triplicate. Curves were fitted using a non-linear regression model. **(C, D)** Dose-response efficacy of SINEs against IAV. A549 cells were infected with PR8 virus at (C) MOI 3 or (D) MOI 0.01 and treated with increasing concentrations of SINEs. Virus supernatant was taken 24 h p.i. and titred by plaque assay. Data are the mean ± SEM of three independent experiments. Curves were fitted using a non-linear regression model. This analysis assumes a standard slope where the response goes from 10% to 90% of maximal as concentration increase over ~2 log units.

(0.01) multiplicities of infection (MOI) and treated with SINEs, starting at a concentration of 0.01 μM and increasing in 0.5-log_{10} increments to 1 μM. Supernatants were collected at 16 h (MOI=3) or 24 h (MOI=0.01) post-infection (p.i.) for viral titre determination by plaque assay, as previously described (Turnbull *et al.,* 2016). The inactive compound, KPT-301, had little effect on virus replication at concentrations < 0.3 μM tested in both single and multi-cycle replication assays. At concentrations >1 μM, KPT-301 appears to reduce viral titre by ~30 % during single cycle infection and ~10% in a multi-cycle assay. (Fig. 2.1. C, D).

Both KPT-185 and KPT-335 successfully inhibited virus replication in a dose-dependent manner at both the low and high MOI infection conditions (Fig. 2.1.C.D). Under multi cycle replication conditions, KPT-185 and KPT-335 had similar 50 % inhibitory concentration (IC_{50}) values of 0.05 μM and 0.06 μM, respectively (Table 2.1). Under single cycle conditions, an IC_{50} value of 0.04 μM was determined for KPT-335 inhibition, which was similar to the value obtained for multi-cycle infections (Table 2.1). However, curve fitting for the rather variable KPT-185 data, obtained under single cycle conditions, determined an estimate (~) IC_{50} value of ~0.26 μM, with wide 95 % confidence intervals (CI) (Table 2.1). Thus, these results indicated that the SINE compounds effectively inhibited replication *in vitro* at concentrations below that exhibiting cytotoxicity and that KPT-335 was the most potent inhibitory compound under both conditions.

To provide a point of comparison with previous work, cytotoxicity and dose-response assays were performed in a similar manner to the SINE compounds with the natural

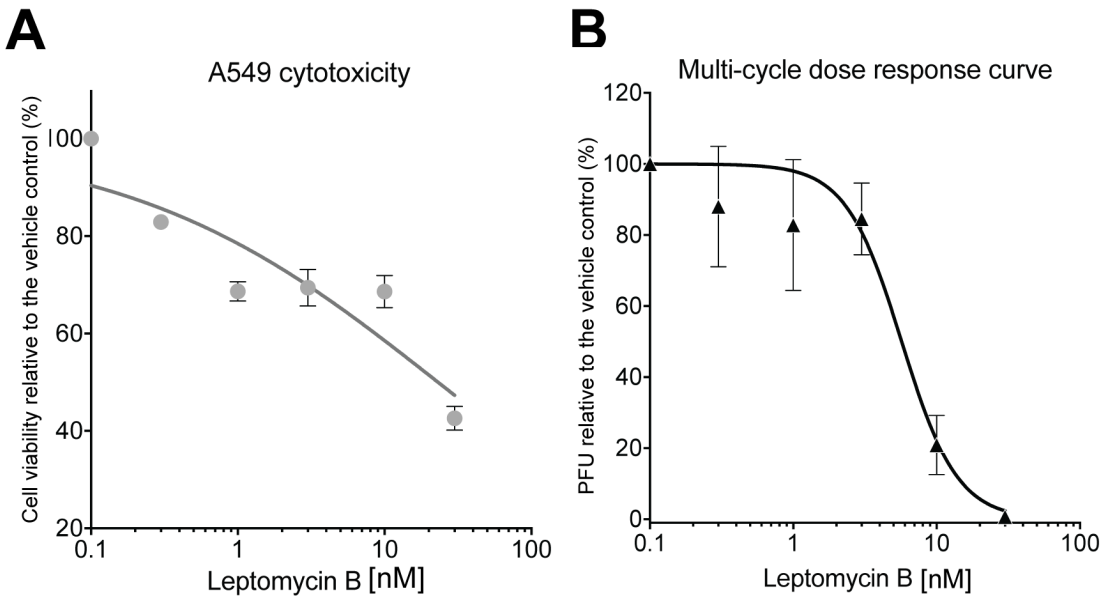

Fig. 2.2. Efficacy of LMB against IAV *in vitro*. (A) Cytotoxicity of LMB. A549 cells were treated with either the vehicle control (DMSO) or LMB in 2-fold dilutions. 24 h post-treatment, cells were assayed for ATP content to determine cell viability. Data are the mean ± S.E.M of three independent assays, each measured in triplicate. Curve was fitted using a non-linear regression model. **(B)** Dose-response efficacy of LMB against IAV. A549 cells were infected with PR8 virus at MOI 0.01 and treated with increasing concentrations of LMB. Virus supernatant was taken 24 h p.i. and titred by plaque assay. Data are the mean ± SEM of two independent experiments. Curve was fitted using non-linear regression model.

CRM1 inhibitor, LMB (Fig. 2.2). Cell viability was assessed by treating A549 cells with 2-fold dilutions of LMB, starting from 30 nM and the ATP content was measured 24 h later. Substantial cytotoxic effects were observed at concentrations as low as 1 nM with a 40 % decrease in cell viability compared to the untreated cells. A 60 % reduction in cell viability was observed at the highest concentration tested (30 nM) (Fig. 2.2.A). A CC_{50} value of 2 nM (0.02 μM) was determined by non-linear regression model analysis (Table 2.1). To determine the concentration at which LMB was antiviral, A549 cells were infected with PR8 at a low MOI (0.01) and treated with increasing concentrations of LMB, starting at a concentration of 0.03 nM and increasing in 0.5-log_{10} increments to 30 nM. Supernatants were collected at 24 h p.i., for viral titre determination by plaque assay. LMB inhibited virus replication in a dose-dependent manner (Fig. 2.3.B) and had a resulting IC_{50} value of 6 nM (0.006 μM) (Table 2.1). However, at the IC_{50} concentration, LMB caused around a 30 % loss of cell ATP content, suggesting that overt cytotoxic damage to cells may contribute to the observed reduction in virus titre. These data confirmed that LMB would likely be excessively toxic to be used as an antiviral agent.

The CC_{50} and IC_{50} values established from the data presented in Figs. 2.1 and 2.2 along with corresponding 95 % CI and R^2 values are presented in Table 2.1. All 95% CI calculated were small apart from the aforementioned wide range CI obtained for KPT-185 under single cycle infection conditions. Aside from KPT-185 single cycle infection and KPT-335 MDCK cytotoxicity, all R^2 values were ≥ 0.7 indicating that the IC_{50} determinations from curve fitting could be considered reasonably accurate. Accordingly, selective indexes (SI) were determined for KPT-185, KPT-335 and

Table 2.1 *In vitro* efficacy of SINEs and LMB against IAV

Compound	Cell type	CC_{50} (μM)[D]	95% CI (μM)	R^2 [C]	Infection	IC_{50} (μM)[A]	95% CI (μM)[B]	R^2 [C]	SI[E]
KPT-185	A549	2.7	2.0 to 4.0	0.8	Single[1]	~0.26	Very wide	0.6	10
	MDCK	2.9	1.6 to 5.2	0.8	Multi[2]	0.05	0.04 to 0.07	1.0	52
KPT-335	A549	2.6	2.01 to 3.6	0.7	Single	0.04	0.03 to 0.08	0.9	65
	MDCK	9.8	3.2 to 30.2	0.5	Multi	0.06	0.04 to 0.11	0.9	37
LMB	A549	0.02	0.01 to 0.05	0.7	Multi	0.006	0.004 to 0.008	0.9	<1

[1] High multiplicity infection to determine drug inhibition after a single replication cycle in A549 cells

[2] Low multiplicity infection to determine drug inhibition after multiple replication cycles in A549 cells

[A] IC_{50} - Represents the concentration of drug that is required for 50% virus inhibition

[B] 95% confidence interval (CI) - probability that a value will fall between an upper and lower bound of a probability distribution (0.95)

[C] R^2 **-** statistical measure of how close the data are to the fitted regression line. R^2 value =1 indicates a 'perfect fit'

[D] CC_{50} - Represent the concentration of drug that is required for 50% cytotoxicity

[E] Selective index (SI) – A549 CC_{50}[1]/IC_{50}

LMB under the single or multicycle infection conditions by calculating the ratio of the CC_{50} values (from A549 cells) to the IC_{50} values. Also described as the therapeutic window, this number represents the comparison of the concentration of compound that causes an antiviral effect to the concentration that causes cytotoxicity. Accordingly, is preferable to have a wide therapeutic window i.e. a high SI index value. KPT-335 had the greatest SI for single cycle infection (SI=65) and KPT-185 had a higher index for multi cycle infection (SI=52). Both SINE compounds had a considerably higher SI value than LMB which was <1. Overall, these results indicate that the SINE compounds effectively inhibited PR8 replication *in vitro* at concentrations well below that exhibiting cytotoxicity, leading to a desirable high SI value much greater than their toxic counterpart LMB.

2.2.2 Effect SINEs have on intracellular localisation of viral proteins

To determine whether SINEs inhibited viral replication at the stage of vRNP nuclear export, the intracellular localisation of viral NP was examined by immunofluorescence (IF). NP (the main component of the vRNP complex) localisation can act as a marker to determine whether the virus genome has undergone nuclear export late post-infection (Amorim *et al*., 2011; Martin *et al*., 1999: Elton *et al.*, 2005). A549 cells were mock infected or infected with PR8 at an MOI of 3 and incubated in the absence of compound (vehicle control; DMSO) or presence of an inhibitory concentration of SINEs (1 μM). LMB (10 nM) was used as a positive control for inhibition of vRNP nuclear export (Elton *et al*., 2001; Ma *et al.*, 2001; Watanabe *et al*., 2001). At 8 h p.i., cells were permeabilized and immunofluorescently stained for viral NP (green) and cellular DNA (blue). Mock infected cells, in the absence (DMSO) or presence of drug

treatment, showed no NP staining (Fig. 2.3.A), indicating that the compounds did not induce any unspecific background noise. NP was not present in all cells analysed, indicating a lower than expected infection level for an MOI of 3 infection. This may be due to a discrepancy in the original titre of the PR8 stock used to calculate the MOI. As expected, in the absence of inhibitors, NP localised predominantly in the cytoplasm of infected cells, indicating nuclear export of the replicated viral genome had taken place. A similar pattern was observed with the inactive compound, KPT-301. In contrast, both KPT-185 and KPT-335 treated infected cells displayed mainly nuclear staining of NP. This NP nuclear localisation was comparable to the LMB treated cells, thus suggesting both KPT-185 and KPT-335 blocked the export of vRNPs.

To assess the reproducibility of this effect, NP localisation was examined over a range (0.01 μM to 1 μM) of compound concentrations. Cells were imaged at random and infected cells were scored for whether NP was predominantly localised in the nucleus or the cytoplasm. No treatment, DMSO and KPT-301 controls showed <10 % of cells with NP nuclear retention, indicating that most had already exported the virus genome after the 8 h infection (Fig. 2.3.B). Almost all cells displayed NP nuclear retention at the higher concentrations of KPT-185 and KPT-335, as well as the LMB positive control. Intermediate amounts of the active drugs resulted in some, but not all, cells showing NP nuclear retention. By this measurement the IC_{50} concentration for NP nuclear export for KPT-185 and KPT-335 was ~0.09 μM and ~0.07 μM, respectively, comparable to the IC_{50} values established for single cycle virus replication (~0.26 μM and 0.04 μM) and multicycle infection (0.05 μM and 0.6 μM) (Fig. 2.1.A, Table 2.1). Overall these data suggest that SINEs block the export of vRNPs during later stages

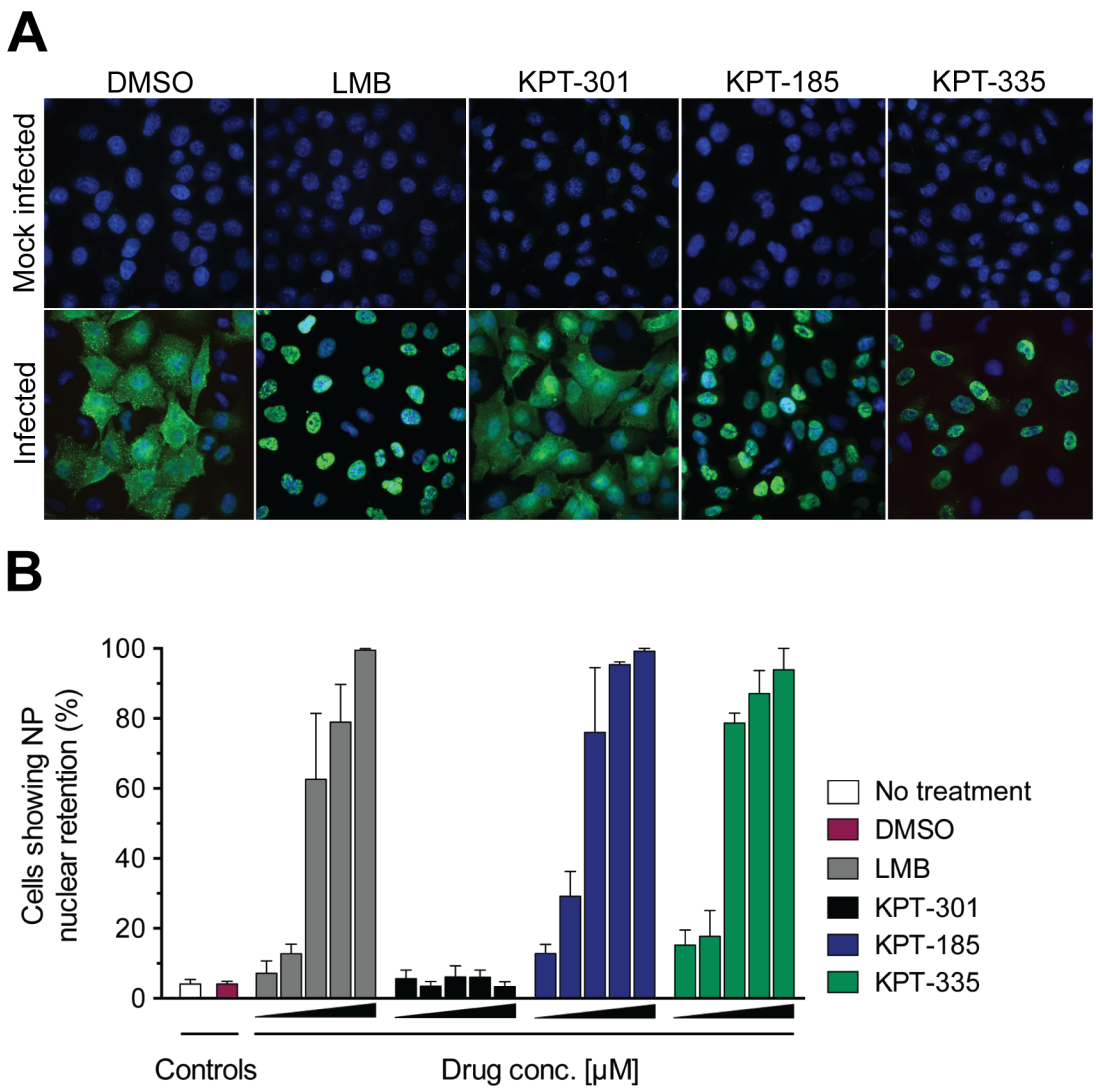

Fig. 2.3. Effect of SINEs on intracellular localisation and accumulation of IAV NP. (A) SINEs block nuclear export of NP. A549 cells were mock infected or infected with PR8 virus at MOI 3 in the presence of SINEs (1 µM), LMB (10 nM) or the vehicle control (DMSO). 8 h p.i. cells were fixed, permeabilised and stained with anti-NP (green) as well as a nuclear stain (DAPI; blue) and imaged by confocal microscopy. Single optical slices are shown. **(B)** Quantification of NP nuclear retention after SINE/LMB treatment. A549 cells were infected as (A), and treated with increasing concentrations of SINEs or LMB (0.01 µM to 1 µM or 1 nM to 10 nM in 0.5 $\log_{10}$ increments, respectively) and imaged as in (A). Cells with predominantly nuclear NP were scored. Counts were taken from three images per drug concentration from two independent experiments and are plotted as mean ± S.D..

of infection: a similar mechanism to previously published reports with LMB (Elton *et al*., 2001; Ma *et al*., 2001; Watanabe *et al.*, 2001). Previously published work with LMB demonstrates conflicting observations to whether CRM1 inhibition leads to nuclear retention of other viral proteins that contain a nuclear export signal (NES) and/or are involved in RNP nuclear export (Cao *et al*., 2012; Elton *et al.,* 2001; Huang *et al*., 2012; Ma *et al.,* 2001; Watanabe *et al*., 2001). To determine whether translocation of viral proteins other than NP were affected by treatment with SINEs, PB2, M1, NS2 and NS1 protein localisation was examined by IF. The HA and NA proteins were not examined due to the lower likelihood that these proteins would change in localisation in response to KPT-335 treatment Similar to the previous experiment (Fig. 2.3), A549 cells were mock infected or infected with PR8 at an MOI of 3 and incubated in the presence of the vehicle control (-drug) or KPT-335 (1 μM). At 8 h p.i. cells were fixed, permeabilised and immunofluorescently stained with anti-NP, PB1, M1, NS2 and NS1. Mock infected cells incubated with the various primary antibodies displayed little to no unspecific background staining for any of the proteins examined. Cells stained with anti-NP (green) were used as a positive control for drug efficacy at the concentration used. As previously observed (Fig. 2.3.), NP was predominately localised to the cytoplasm in the absence of KPT-335, whereas in the presence of compound it localised to the nucleus of cells, indicating successful blockade of nuclear export. PB2, part of the vRNP complex, was examined as an example of a polymerase protein. PB2 localisation remained unchanged in the presence of KPT-335 with the polypeptide mainly localised to the nucleus of infected cells. M1 and NS2, both mediators involved in nuclear export of vRNPs (Eisfeld *et al.*, 2014), showed no difference in localisation in the presence of compound,

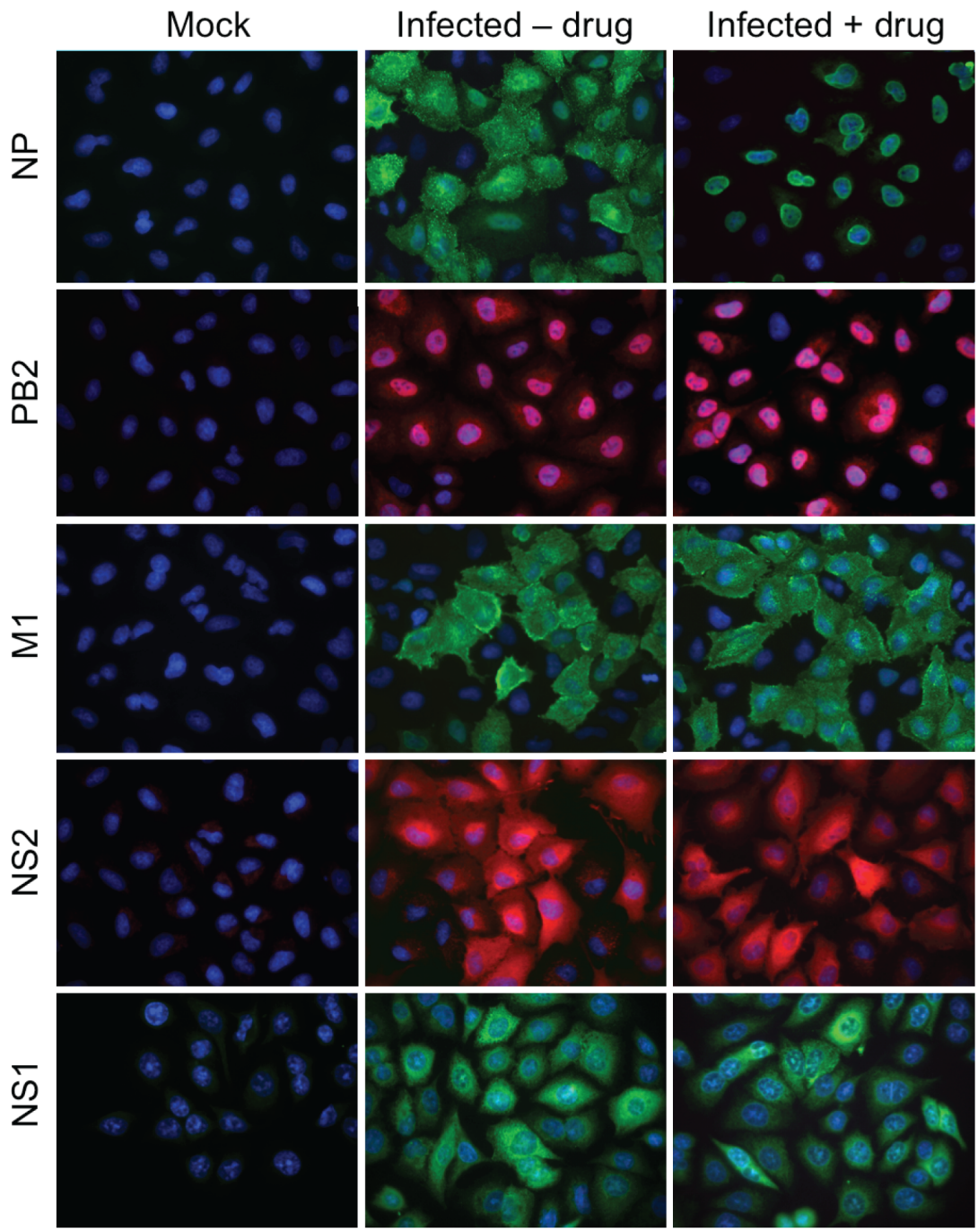

Fig. 2.4. Effect of KPT-335 on localisation of IAV viral proteins. A549 cells were infected with PR8 virus at MOI 3 and treated with 1 μM of KPT-335. 8 h p.i. cells were fixed, permeabilised and stained with anti-NP (green), PB2 (red), M1 (green), NS2 (red) or NS1(green) and a nuclear stain DAPI (blue). Images were taken as single optical slices. Data are representative of 2 independent experiments.

displaying a mixed nuclear and cytoplasmic staining pattern similar to that of NP without compound. Although NS1 contains a NES, there is limited published evidence to suggest its involvement in CRM-mediated transport (Huang *et al.*, 2012; Tynell *et al.,* 2014). Similar to M1 and NS2 localisation, NS1 also displayed unchanged nuclear/cytoplasmic location after drug treatment. Thus, of the viral proteins examined, only NP localisation was affected by KPT-335 treatment. Although the other proteins analysed have been reported to be involved in nuclear export, the nuclear/cytoplasmic localisation of M1, NS2 and NS1 and the nuclear localisation of PB2 was unaltered after treatment with the compound. This data supports the hypothesis that NP is the most suitable viral protein to be used for determination of whether the virus genome has undergone nuclear export during late stages of infection.

2.2.3 Time dependent efficacy of KPT-335

The hypothesis that SINEs act by blocking nuclear export of the viral genome predicts that the compounds should act only when added during the first half of the virus lifecycle. Accordingly, a time of drug-addition assay was performed, where KPT-335 was added at various time points during virus infection and NP localisation as well as overall virus replication examined. A549 cells were mock infected or infected with PR8 at an MOI of 3 and KPT-335 was added before (-1 h), at the time of infection (0 h) or at varying times post-infection (+1, 2, 4, 6 and 8 h). Mock infected and infected but untreated (no drug) cells were included as controls. For IF analysis, the infection was stopped at 9 h p.i., while virus supernatant was harvested at 16 h p.i. for titre analysis. As expected, mock infected cells showed no NP staining and infected untreated cells displayed mostly cytoplasmic staining as observed previously (Fig.

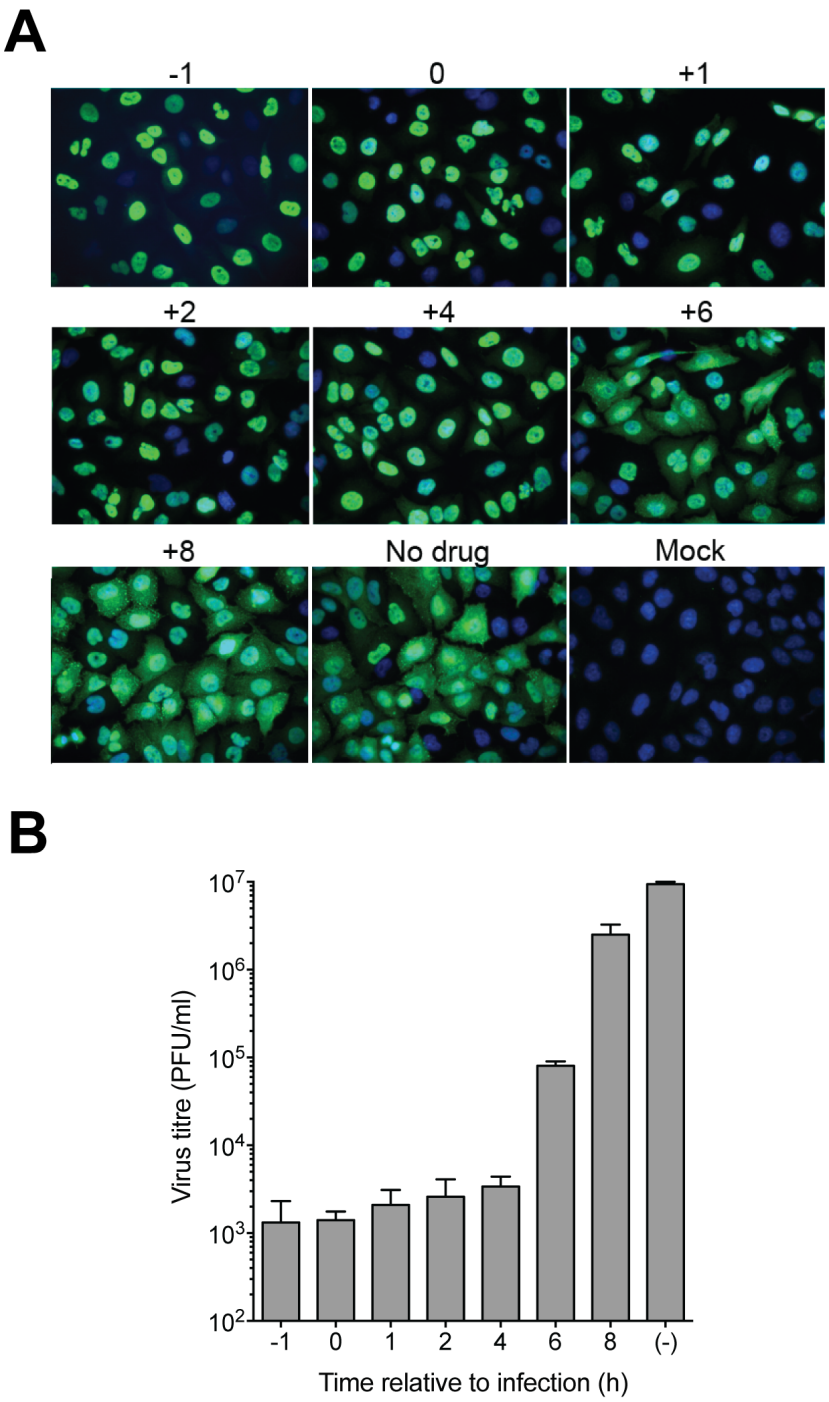

Fig. 2.5. Time-dependent efficacy of KPT-335. A549 cells were infected or (mock infected) with PR8 virus at MOI 3. Drug (0.3 μM) was added before infection (-1 h), at the time of infection (0 h) or at 1, 2, 4, 6 and 8 h p.i, as well as a no drug control. **(A)** NP localisation after addition of KPT-335. 9 h p.i. cells were fixed, permeablised and stained with anti-NP (green) and a nuclear stain (DAPI; blue). **(B)** Virus titres after addition of KPT-335. Cell supernatants were harvested at 16 h p.i. and virus titres determined by plaque assay. Data are the mean ± S.D. of 2 independent experiments.

2.5.A). NP was retained in the nucleus of infected cells when KPT-335 was added before (-1), during (0 h) and up to 4 h p.i.. However, when compound was added at 6 h or 8 h p.i., NP staining was seen in both the nucleus and the cytoplasm of infected cells, similar to the localisation of NP in the no drug-treated control cells. The corresponding titre data showed that addition of the drug at any time point prior to and including 4 h p.i. led to highly effective suppression of virus replication, whereas drug addition at 6 h p.i. was less effective and drug added at 8 h p.i. caused only a minor decrease in viral titre (Fig. 2.5.B). Since previous studies indicated that nuclear export of replicated vRNPs begins after ~5 h p.i. (Elton *et al*., 2005; Elton *et al*., 2001 Martin *et al.,* 1991), these data are consistent with the drug acting by inhibiting nuclear export of the viral genome. These data further support the conclusion drawn from the NP IF analysis in Fig. 2.4., that SINEs were acting at the stage of RNP nuclear export.

2.2.4 Viral gene expression after treatment with SINEs

Nuclear localisation of NP at later times of infection can reflect a block to nuclear export of the viral genome, but can also suggest slower kinetics of virus replication, with NP acting as a visual 'clock' of virus infection (Elton *et al.,* 2005; Martin *et al.,* 1991) . To assess whether SINEs were inhibiting viral gene expression, accumulation of NP, M1 and NS2 was examined by western blotting. A549 cells were mock infected or infected with PR8 at an MOI of 3 and treated with increasing concentrations of KPT-335 or left untreated (-). LMB and KPT-301 were included as controls. At 8 h p.i., total cell lysates were harvested and blotted for NP, M1, NS2 as well as cellular tubulin as a loading control. Mock infected samples did not contain viral proteins, as expected (Fig. 2.6). All drug-treated infected samples contained similar amounts of

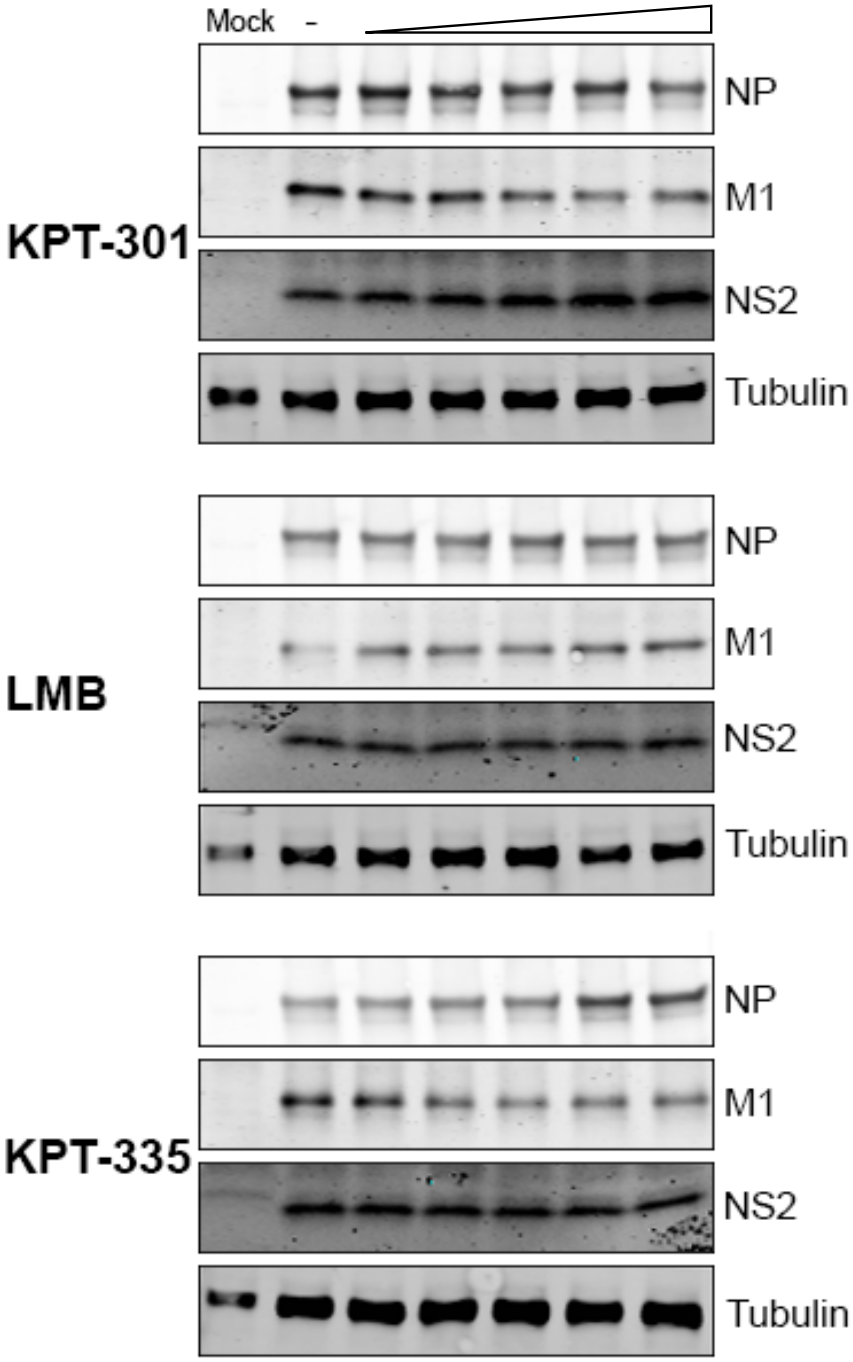

Fig. 2.6. Viral gene expression after SINE treatment in a single cycle growth assay. A549 cells were infected (or mock infected) with PR8 virus (MOI 3), treated with increasing concentrations of KPT-335/KPT-301, LMB (0.01 μM to 1 μM or 1 nM to 10 nM in 0.5 $\log_{10}$ increments, respectively (as depicted with white triangle)) or with a DMSO control (-). Cells were harvested at 8 h p.i. and total cell lysates analysed by SDS-PAGE and western blotting for viral NP, M1 and NS2 as well as cellular tubulin as a loading control.

NP, M1 and NS2 protein compared to the untreated infected samples as well as similar amounts of viral proteins between treatment groups. Thus, as previously defined for LMB (Elton *et al.*, 2001), SINEs did not generally inhibit IAV gene expression in a single round of replication.

2.2.5 KPT-185 has a lower antiviral efficacy compared to KPT-335 in plaque reduction assays

To assess the efficacy of SINE compounds against IAV infection further, plaque reduction assays were performed. Optimisation of this assay was central to future drug resistance investigations presented in subsequent chapters. This assay determines drug efficacy by observing the compounds' direct effects on the plaque number and/or the plaque size in tissue culture. MDCK cells were infected with 100 plaque forming units (PFU)/ml of PR8. After 1 h incubation with the virus, cells were grown under inhibitory concentrations (1 μM) of KPT-185, KPT-335 or KPT-301 or in the presence of DMSO. At 48 h p.i., cells were fixed and stained with toluidine blue to visualise plaque formation. Consistent with previous results, KPT-301 had no effect on the number of plaques when compared to DMSO-treated control (Fig. 2.7.A). Infection in the presence of 1 μM of KPT-185 gave around a 50 % reduction in plaque number compared to the DMSO-treated cells, while cells treated with KPT-335, at the same concentration, almost totally eliminated plaque formation. No obvious difference in plaque size was observed for any drug treatment. These results suggested KPT-335 was the most potent inhibitor by this method.

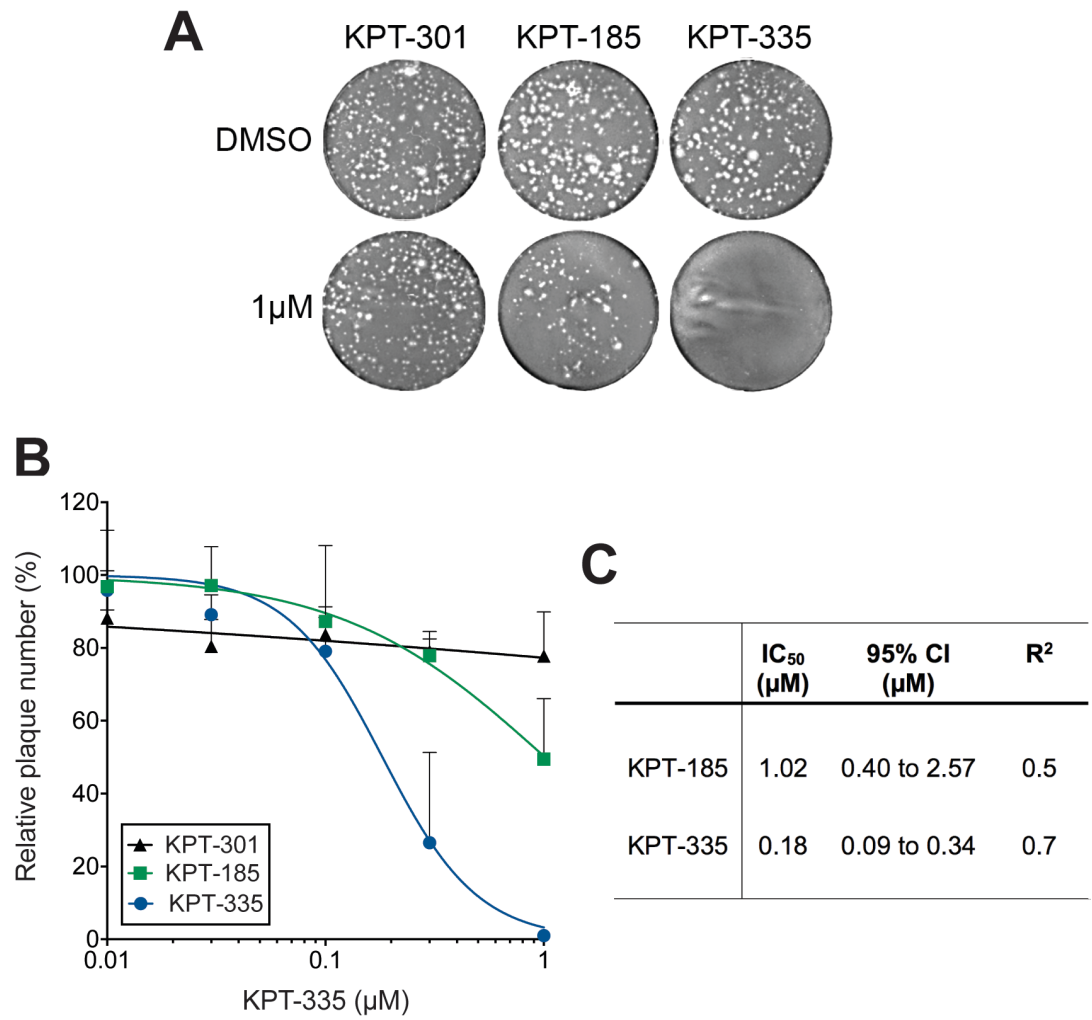

	IC_{50} (μM)	95% CI (μM)	R^2
KPT-185	1.02	0.40 to 2.57	0.5
KPT-335	0.18	0.09 to 0.34	0.7

Fig. 2.7. Efficacy of SINEs by plaque reduction assay. MDCK cells were infected with PR8 virus at 100 PFU/well in the presence of increasing concentration of SINEs. **(A)** Plaque reduction assay. 48 h p.i. cells were stained with toluidine blue and imaged. **(B)** Relative plaque numbers. Plaque counts were taken from three independent experiments and data plotted as mean ± S.D.. Curves were fitted using a non-linear regression model. **(C)** IC_{50}, 95 % CI and R^2 values obtained from the curves fitted in (B).

To determine the reproducibility of these results, the plaque reduction assays were carried out over a range of compound concentrations. Infected cells were treated with increasing concentrations of compounds, starting at 0.01 μM and increasing in 0.5-$\log_{10}$ increments to 1 μM. As expected, KPT-301 had no effect on plaque number over the range of drug concentrations tested (Fig. 2.7.B). As a reduction in plaques was not observed a non-linear regression model could not be fitted and thus an IC_{50} value could not predicted for this data set. Unexpectedly, KPT-185 only suppressed plaque number at the highest concentration (1 μM), with a ~50 % reduction in plaques compared to the DMSO control. An IC_{50} value of 1.02 μM (with a wide range of uncertainty) was determined by fitting the data to a non-linear regression model (Fig. 2.7.C). This was contradictory to the dose-response replication data exhibited in Fig. 2.1, which showed KPT-185 to be inhibitory at concentrations substantially lower than 1 μM with an IC_{50} value of 0.05 μM. In comparison, KPT-335 reduced plaque number by ~60 % at a concentration of 0.3 μM and completely inhibited plaque formation at 1 μM with a subsequent IC_{50} value of 0.18 μM; a value more comparable to the tire data in Fig. 2.1., which gave an IC_{50} of 0.06 μM. However, for both compounds, measuring drug susceptibility by plaque reduction did not appear to be as sensitive an assay as measuring the titre of replicated virus from liquid supernatant. Based on the above data, the decision was made to remove KPT-185 from further experimentation and continue with KPT-335 only.

2.2.6 Efficacy of KPT-335 against a panel of human and animal IAV strains

To establish whether KPT-335 had general antiviral potency against a variety of influenza strains, the compound was tested against a panel of human and animal (equine, avian and swine) isolates of IAV, by measuring the endpoint titres of multicycle replication assays. As described previously for PR8 (Fig. 2.1.D), A549 cells were infected with virus at an MOI of 0.01 and treated with increasing concentrations of KPT-335. The compound was tested against a swine (H1N1), two duck (H4N6, H5N3) and an equine (H3N8) derived viruses as well as a human isolate (H3N2). Sensitivity to a recombinant virus, PR8 MUd, was also analysed as this virus would be used in drug-resistant investigations in the subsequent chapter. At 24 h p.i., cell supernatants were taken and virus titre determined by plaque assay. Dose-response curves were fitted to the data (Fig. 2.8) and IC_{50} values were determined. Selective indexes were calculated using the A549 CC_{50} value obtained from data analysis in Fig. 2.1.A. and results are shown in Table 2.2. KPT-335 was found to be antiviral against all strains tested, displaying dose-dependent inhibition of virus replication, with subsequent IC_{50} values ranging between 0.004-0.03 μM (Table 2.2). Additionally, selective indexes were high for all strains, varying from 87 to 650. Both the IC_{50} values and selective indexes were comparable to the values calculated previously for the human lab-adapted strain PR8 (0.04 μM). To quantify the sensitivity of KPT-335 between viruses, non-linear regression curves were fitted to the data. Results were inconclusive due to the curve fits for some strains (in particular A/duck/England/62 and A/equine/Miami/63); thus any differences in drug-sensitivity between strains could not be reliably determined. Nevertheless, none of the IC_{50} values

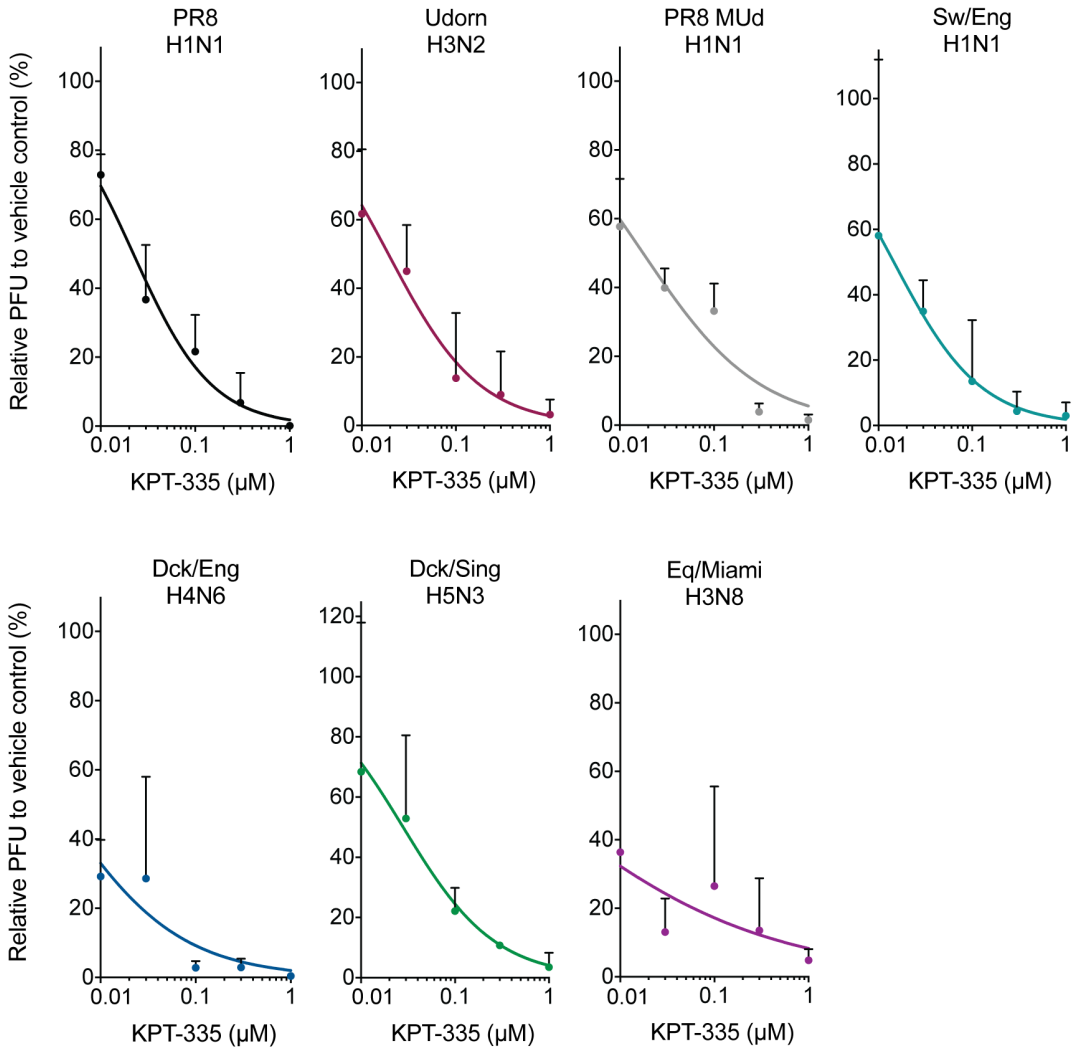

Fig. 2.8. Efficacy of KPT-335 against human and animal IAV strains. A549 cells were infected with indicated viruses at MOI 0.01 and treated with increasing concentrations of KPT-335 from 0.01 μM. Virus supernatant was taken 24 h p.i. and titred by plaque assay. Data are the mean ± S.D. of two independent experiments. Curves were fitted using a non-linear regression model.

Table 2.2. *In vitro* efficacy of KPT-335 against influenza A virus strains

IAV strain	Subtype	Host species	IC_{50} (μM) [A]	95% CI (μM) [B]	R^2 [C]	SI [D]
A/PuertoRico/8/34	H1N1	Human (lab)	0.02	0.02 to 0.03	0.9	130
A/Udorn/72	H3N2	Human	0.02	0.01 to 0.04	0.8	130
PR8 MUd	H1N1	PR8 containing seg7 from Udorn	0.02	0.01 to 0.03	0.9	130
A/swine/England/453/06	H1N1	Swine (Eurasian)	0.02	0.004 to 0.4	0.6	130
A/duck/England/62	H4N6	Avian	0.004	0.004 to 0.03	0.5	650
A/duck/Singapore/5/97	H5N3	Avian	0.03	0.01 to 0.07	0.7	87
A/equine/Miami/63	H3N8	Equine	0.01	9e-5 to 0.2	0.3	260

[A] IC_{50} - the concentration of drug that is required for 50 % virus inhibition

[B] 95 % confidence interval (CI) - probability that a value will fall between an upper and lower bound of a probability distribution (0.95)

[C] R^2 **-** statistical measure of how close the data are to the fitted regression line

[D] Selective index (SI) – A549 CC_{50}[1]/IC_{50}

[1] A549 CC_{50} value[2] = 2.6 μM

[2] CC_{50} - the concentration of drug that is required for 50 % cytotoxicity

were significantly different even between those strains with better R^2 values and narrower CI limits for the IC_{50} estimates. Overall, these results demonstrate a relatively broad anti-influenza A virus activity of KPT-335 *in vitro*. Evidence for general activity against IAV was important data to obtain to justify further development of this compound as a therapeutic agent.

2.3 Discussion

In this chapter, the antiviral activity of selective inhibitors of nuclear export (SINEs) against IAV were characterised *in vitro*. The company, Karyopharm, developed SINEs KPT-185 and KPT-335 to transiently bind to the CRM1 cargo binding site and subsequently inhibit export of proteins exploiting this pathway with less cytotoxic effects than their fungal toxic counterpart, LMB. Although SINEs were initially developed as anti-cancer agents, Karyopharm acquired evidence to suggest SINEs inhibited influenza virus infection. Subsequently, in collaboration with Karyopharm, tests were carried out to confirm this hypothesis.

The inhibitors, KPT-185 and KPT-335, successfully reduced replication of the laboratory-adapted human H1N1 virus (PR8) replication in a dose-dependent manner with little toxic effect on a human lung cell line (A549) and as well as on the 'gold-standard' mammalian cell line (MDCK) for growing IAV (Fig. 2.1.A, B). Typically, compounds that target a host cell factor are suspected to have greater toxic side effects. The low cytotoxicity observed for SINEs may be explained by the mechanism in which SINEs transiently bind to CRM1. Although this reversible interaction would also block host proteins that utilise the CRM1 export pathway, they would not be blocked permanently. The covalent nature of the LMB-CRM1 interaction is likely the reason why LMB is so overtly toxic as it would essentially bind indefinitely to CRM1, thus affecting host cell export functions in the long term.

This study was supported by Karyopharm, who also supported studies in Professor Ralph Tripp's laboratory (USA). The Tripp group has published two papers on this subject since 2014. The first paper by Perwitasari *et al*., (2014) investigated the efficacy of the novel SINE compound KPT-335 *in vitro*. They determined an IC_{50} value of 0.02 μM for the human H1N1pdm09 strain, A/California/04/09, which was very similar to the KPT-335 multicycle IC_{50} of 0.04 μM determined for the H1N1 PR8 strain in this study. The Perwitasari study determined an KPT-335 CC_{50} value of 26.8 μM, which was 10 times greater than the CC_{50} value determined in this study: 2.6 μM. Perwitasari *et al*., used a Toxilight (Adenylate kinase (AK) enzyme quantification) assay to determine cytotoxicity whereas in this study the CellTiter-Glo (ATP quantification) was used. An evaluation study of commercial cytotoxicity assays indicated that the CellTiter-Glo assay was ~50 % more sensitive than the Toxilight assay (Peternel *et al.,* 2009). Additionally, CellTiter-Glo was found to be the most reproducible cytotoxicity assay in comparison to other assays tested. These data suggest that CellTiter-Glo assay is more a more accurate assay to determine CC_{50} and thus may explain the discrepancy in the CC_{50} values between the Perwitasari study and this one.

The low cytotoxicity and low inhibitory concentration values of the SINEs led to a desirable high selective index (Table 2.1). For KPT-335, this was over 15 times higher than its toxic counterpart LMB, indicating its potential as a therapeutic agent. KPT-335's antiviral activity against a range of human and animal IAV strains confirmed that the compound could be used as an effective broad-spectrum antiviral (Fig. 2.8). No significant differences were observed between the IC_{50} values of the range of

strains tested which included human, avian, equine, and swine origin. There was a slight discrepancy in the Eq/Miami and Dck/Sing strains due to the poor curve fits as indicated by the low R^2 values. The avian/equine virus replication was performed in a human cell line (A549 cells) and may be suboptimal growth conditions, explaining the poor curve fits. The use of a suitable animal cell line (i.e. avian and equine) would perhaps have been a better model to measure the drug efficacy against these strains. This may also explain why these subtypes were slightly more sensitive to the compound at lower concentrations compared to the other strains examined. Nevertheless, both viruses displayed reduced overall growth in A549 cells compared to PR8 and the other strains examined. These results are supported by previously published work (Perwitasari *et al.,* 2014) in which KPT-335 was tested against a wide range of IAV strains including human (H1N1, H3N2) and avian (H5N1, H7N3, H7N9) viruses as well as, influenza B strains. The authors found little to no differences in efficacy of the compound between the strains tested, with an IC_{50} value range between 0.01-0.4 μM, comparable to the IC_{50} values in this study (0.004-0.03 μM). Their data support the findings in this chapter suggesting that all IAV strains make use of the CRM1 export pathway irrespective of their subtype and origin. If use of the CRM1 pathway is a general feature of IAV infection, KPT-335 would be a highly desirable antiviral candidate especially when considering pandemic outbreaks, where the subtypes and host source cannot be predicted.

The Tripp group's second paper, by Perwitasari *et al*., (2016), investigated KPT-335 efficacy further by examining its antiviral activity against IAV infection in two animal models; mice and ferrets. The study, which used A/California/04/09 (H1N1 – a 2009

pandemic strain), concluded that KPT-355 reduced virus shedding, pro-inflammatory cytokines and inflammatory cell infiltration in a mouse model, as well as limiting IAV replication, lung pathology and inflammation in ferrets. The Perwitasari *et al*., data provided further evidence for KPT-335's potential as a successful therapeutic antiviral agent against IAV infection.

The mechanism by which the SINE compounds inhibit IAV was hypothesised to be the same as LMB, as their development was based on the fungal-derived inhibitor, which has been previously shown to block export of vRNPs via CRM1 inhibition (Elton *et al*., 2001; Kudo *et al*., 1999; Nishi *et al*., 1994). By IF analysis, both KPT-185 and KPT-335 were found to inhibit nuclear export of vRNPs as effectively as LMB (Fig. 2.3.A). IF examination of infected SINE-treated cells showed accumulation of NP in the nucleus, indicating inhibition of virus export, which was reproducible in dose-response experiments (Fig. 2.3.B). IC_{50} values for NP nuclear retention efficacy were comparable to the dose-dependent inhibitory concentrations calculated for Fig. 2.1.A.B. Further confirmation that the SINE compounds were targeting nuclear export of viral proteins was determined by a time of drug-addition assay. Virus replication was suppressed (Fig. 2.5.B) and NP export blocked (Fig. 2.5.A) when KPT-335 was added any time point prior to and including 4 h p.i. Previously published work indicates nuclear export of the viral genome takes place around 5 h p.i. (Elton *et al*., 2001), therefore these data support the IF data presented in Fig. 2.3., i.e. that the compound was acting at the stage of nuclear export the vRNPs.

IF analysis of other viral proteins revealed no difference in the localisation of NS1, PB2, M1 or NS2 after treatment with KPT-335. NS1 is known to be involved in interaction with mRNA export machinery pathways including NXF1, Tap15 and Rae1 (Larsen *et al*., 2014; Satterly *et al.*, 2007; Wang *et al.,* 2015, Pereira *et al.,* 2017), however currently there is limited evidence to suggest its direct involvement in CRM1-mediated export. All NS1 proteins have a well-conserved leucine rich-NES motif (Tynell *et al.*, 2014), therefore it may be hypothesised that NS1 could be directly recognised by CRM1 through this domain. However, a FRET analysis conducted by Han *et al*., (2010) revealed that a transiently expressed NS1 protein did not directly interact with CRM1. Additionally, Tynell *et al.,* (2014), examined the localisation of NS1 during IAV infection after LMB treatment by IF using NP as a positive control for nuclear retention. The authors discovered little difference in the localisation of NS1 in the untreated and LMB-treated cells with most cells displaying both nuclear and cytoplasmic NS1 staining. These data are comparable to the results found in Fig. 2.5, where KPT-335 did not alter the nuclear/cytoplasmic localisation of NS1. This suggests CRM1-inhibition was inefficient at blocking nuclear export of NS1, indicating that the export of this protein is possibly independent or only partially dependent on CRM1.

Similarly to what was observed for NS1, KPT-335 did not alter PB2's localisation (Fig. 2.5.). However, in contrast to NS1, PB2 staining appeared to be predominantly nuclear. There is some evidence to suggest that the bulk of the polymerase proteins in the nucleus may not be RNP-associated (Loucaides *et al*., 2009). If most PB2

molecules are not RNP-associated, then any change in the localisation of the minority population bound to vRNPs after KPT-335 treatment may not be detected.

M1 and NS2 have been implicated as adaptor proteins involved during CRM1-mediated export of vRNP complexes. Both M1 and NS2 nuclear/cytoplasmic localisation was unaltered after KPT-335 treatment (Fig. 2.5) which is comparable to previous studies using LMB, which also found that the intracellular distribution of M1 was not changed by LMB during infection (Elton *et al*., 2001; Ma *et al.,* 2001). Additionally, Cao *et al*., (2012), found that the localisation of a GFP-M1-NES recombinant protein was also unaltered after LMB treatment. These data and the results displayed in this study, suggest M1 is not necessarily exported with RNPs in a detectable amount as analysed by IF. A previous study demonstrated that a virus lacking the NES1 of NS2 was retained in the nucleus of the cell after treatment with LMB, suggesting NES1 within the NS2 protein is necessary for CRM1-dependent export (Huang *et al*., 2012). However, similar to M1, NS2 localisation also remained unchanged after treatment with LMB (Ma *et al*., 2001), suggesting that vRNP nuclear export does not involve the bulk of M1 and NS2. The unchanged location of NS2 may suggest there is an excess of NS2 in nucleus with only a minor fraction of NS2 required for CRM1-export, or that the transport of NS2-RNP complexes is too transitory to be examined by IF.

CRM1 generally actively transports molecules over 42 kDa through the nuclear pore complex (NPC) (Hutten & Kehlenbach, 2007). Given that M1 and NS2 are 28 kDa and 11 kDa in size, respectively (NP = 52kDa), they may export via an CRM1-

independent pathway, possibly by passive diffusion. Therefore, another potential explanation for the unchanged M1 and NS2 localisation may be that a larger proportion of these proteins are transported out the nucleus via passive diffusion and, as mentioned previously, a smaller proportion of M1 and NS2 are required for CRM1-mediated export. Arguing against this notion, a previous study by (Zhao *et al.,* 1998) found that newly synthesised M1 oligomerizes into both dimers and mulitrimers *in vivo,* therefore exceeding the molecular mass limit (>40 kDa) for passive diffusion. Therefore, another explanation for the unchanged M1 location could be that inhibition of CRM1 does not stop M1 transport as the compounds do not block M1 and CRM1 binding, if they are interacting directly, or perhaps M1 may interact with other undefined cellular adapters. Consequently, differentiating between M1 and NS2 transported by CRM1 as part of the vRNP complex or whether they have been transported by passive diffusion would not be possible by the IF method presented and therefore the effect SINEs had on the localisation of these proteins would be undetectable.

Western blotting analysis revealed that inhibition of nuclear export by SINEs did not affect viral gene expression (Fig. 2.6), suggesting inhibitors are not slowing virus replication kinetics upstream of the nuclear export process under single cycle replication conditions. The data were comparable to previously published work for LMB, where there were no differences in the level of protein synthesis of HA_0, NP or M1 between treated and untreated PR8 infected BHK cells (Elton *et al*., 2001), confirming that there is no evidence to suggest CRM1-inhibitors act by altering viral protein levels. The direct or indirect effect the natural CRM1 inhibitor, LMB, has on

other export functions is undefined, whereas Karyopharm state SINE compounds were designed to act specifically by targeting CRM1 with no off-target effects (https://www.karopharm.com). Published reports indicate that CRM1 is not utilised by influenza mRNAs for export from the nucleus. This has been examined in multiple cell lines including MDCK, BHK, 293T and A549 cells (Amorim *et al.,* 2006; Elton *et al*., 2001; Hughes, 2000; Larsen *et al*., 2014; Read & Digard, 2010; Satterly *et al*., 2007; Wang *et al.*, 2015). These data and the data presented in this section supports Karyopharm's claim, as SINEs inability to inhibit protein synthesis suggests the compounds directly target CRM1 and other cellular nuclear export pathways, such as those used to transport mRNAs, remain unaffected.

Antiviral activity of SINEs analysed by plaque reduction assay revealed that KPT-185 was less potent against IAV replication compared to KPT-335 (Fig. 2.7). The reduced efficacy of KPT-185 may be explained by a possible loss in stability of the compound over the longer time-period of this assay (48 h) as the previous multi-cycle and single infection assays were carried out over 16-24 h (Fig. 2.1.C (24 h), Fig. 2.2.D (16 h)), implying KPT-185's *in vitro* effective-life to be <48h. However, no further investigation was performed to validate this notion. As stated previously, plaque reduction assays performed with a sub-optimal inhibitory concentration were a key experimental approach for future investigations into potential drug-resistance of the compounds. Therefore, further experimentation in this thesis was conducted with KPT-335 only. Furthermore, since the start of this study, Karyopharm Therapeutics removed KPT-185 from their pipeline and defined KPT-335 as their lead compound in development for the treatment of viral infections, available at

https://www.karopharm.com [Accessed on 06/2015]. This information, combined with the plaque reduction data, supported the decision to continue only with KPT-335.

The data described in this chapter determine that SINEs inhibit IAV at the stage of nuclear export by targeting the cellular CRM1 protein and that SINE KPT-335 was effective at inhibiting a broad-range of IAV strains. As previously described in chapter 1, the emergence of drug-resistant escape variants is a major problem hindering the effectiveness of existing antiviral therapies. Therefore, the potential of a drug-resistant IAV mutant emerging should be examined *in vitro* when considering a novel antiviral therapy. The next line of investigation was to determine the ability for a KPT-335-resistant virus strain to develop *in vitro.*

Chapter 3 Generating an influenza A virus strain resistant to the nuclear export inhibitor, KPT-335.

3.1 Introduction

Present anti-influenza virus therapies are hindered by the rapid generation of resistance. The lack of a 'proofreading' function in the influenza virus polymerase results in a high error rate, leading to mutations that allow the virus to overcome certain selection pressures and develop resistant variants to current antivirals such as amantadine and oseltamivir. Amantadine was the first antiviral shown to inhibit IAV, working by blocking ion channel activity of the M2 and it has been used for >30 years. This has led to the rapid emergence of drug-resistant viruses that result from by single amino acid substitutions within the M2 protein. Consequently, amantadine is no longer recommended as antiviral agent (Dong *et al.*, 2015). To combat this problem, there is growing interest in the prospect of inhibiting cellular targets as, if the toxicity problem can be solved, the generation of resistance will be predicted to be slower (Watanabe & Kawaoka, 2015). As described in chapter 2, KPT-335 is a broad-spectrum nuclear export inhibitor exhibiting relatively low cytotoxicity *in vitro*. The US-based pharmaceutical company, Karyopharm Therapeutics, are aiming to develop their clinical stage anti-cancer drug, KPT-335, as a potential antiviral drug.

The US Food and Drug Administration (FDA) recommend that the *in vitro* selection of resistant viruses to a potential antiviral therapy should be examined before commencing with clinical studies of infected patients (www.fda.gov, guidance for

industry #213, 2013). Although resistance data generated *in vitro* will not necessarily predict the potential for clinical resistance, selection of drug-resistant virus variants can provide an insight into whether the genetic threshold for resistance to develop is high or low, as well as providing understanding of the proposed mechanism of action of the investigational compound. Investigation into the genetic barrier for a given target may help determine if single or multiple mutations are required for resistance and if the resistance gain will affect viral fitness. Although *in vitro* resistance development may not correlate to a similar pattern clinically, these types of studies will help the understanding of the resistance potential of drug, which in turn will help select viral traits that should be targeted in order to avoid rapidly developing resistance. Therefore, the next step for development of KPT-335 as an antiviral for IAV was to determine the compound's resistance potential.

The aim of this chapter was to test whether viral variants resistant to the CRM1-inhibitor KPT-335 could be generated upon serial passage of an H1N1 lab-adapted IAV in the presence of sub-optimal concentrations of the drug. Potential drug-resistant viruses were then characterised phenotypically by plaque reduction assays and IF analysis. Genotypic analysis was then carried out by sequencing relevant IAV genes to identify any mutational changes. An outline of the experimental strategy used in this chapter is described in Fig. 3.1.

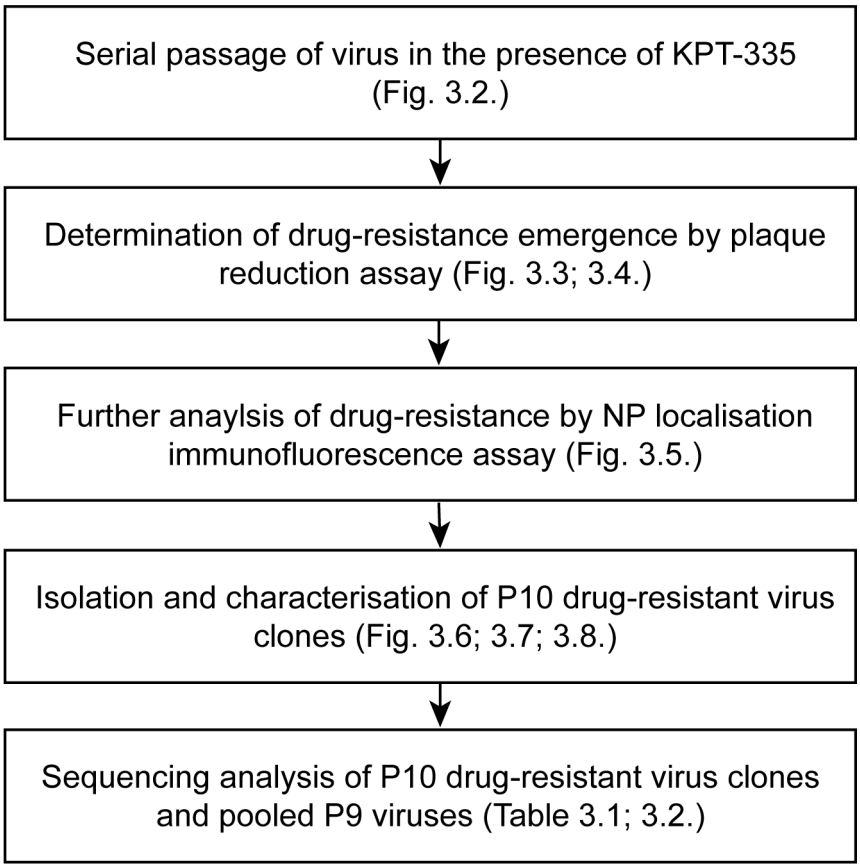

Fig. 3.1. Flow diagram describing the experimental strategy for producing a KPT-335 resistant IAV strain.

3.2 Results

3.2.1 Serial passage of IAV in the presence of KPT-335

To assess whether it was possible to develop a KPT-335 resistant IAV strain, multi-passage experiments were performed. Five independent passages were carried out, designated R1-R5, in the presence of either 0.15 μM or 0.3 μM KPT-335. Amantadine was used as a positive control (AC) for selection of drug-resistant virus variants since resistance is readily produced (Hurt *et al.,* 2016). PR8 is already resistant to amantadine, therefore a PR8 reassortant virus which contains an M segment from Udorn that confers amantadine susceptibility (as well as a filamentous budding phenotype) (Noton *et al.*, 2007) was used for serial passage with amantadine in the first 3 serial passage experiments (R1-R3). For reasons that will become apparent, two further passage experiments (R4 and R5) were subsequently carried out with WT PR8 and only KPT-335 as the selective pressure. A549 cells were infected with viruses at an MOI of 0.001 in the presence of the vehicle control (DMSO), amantadine or KPT-335. A very low MOI was used to perform the serial passage under multi-cycle infection conditions and reduce the likelihood of the production of DIPs (as discussed later). Details of the conditions for each passage experiment are described in Table 3.1. After 48 h p.i., supernatant was harvested and viral titre determined by plaque assay. The progeny viruses were then passaged again under the same conditions for a total of 10 (R1-R3) or 9 (R4, R5) passages. As the two blocks of serial passages were carried out independently, each set had a matching DMSO control. As expected, virus passaged in the presence of DMSO generally replicated well, producing titres that fluctuated around 10^7-10^8 PFU/ml over the course of the two blocks of experiments

Table 3.1 Conditions for multi-passage experiments (R1-R5)

EXP.	IAV STRAIN	DRUG	CONC.(μM)	PASSAGES PERFOMED
AC	PR8 MUd	Amantadine	30	10
DMSO (1)	PR8 MUd	DMSO	-	10
R1	PR8 MUd	KPT-335	0.15	10
R2	PR8 MUd	KPT-335	0.15	10
R3	PR8 MUd	KPT-335	0.3	10
DMSO (2)	PR8	DMSO	-	9
R4	PR8	KPT-335	0.15	9
R5	PR8	KPT-335	0.3	9

(AC/R1-R3 and R4/R5) (Fig. 3.2). Treatment with amantadine initially inhibited virus replication to 10^5 PFU/ml at passages 1 and 2 (P1, 2) but the titre then increased to 10^7 PFU/ml at P3 (Fig. 3.2 AC). Apart from a dip in viral tire at P8 (potentially due to a technical error) the virus appeared unaffected by amantadine treatment thereafter, suggesting that the virus was resistant to the drug (discussed further in section 3.3). For the five serial passages carried out with KPT-335, the drug initially suppressed viral titre at P1, as expected. For passages performed with 0.15 μM KPT-335 (R1, R2, R4), replication was initially knocked down to 10^5 PFU/ml and for passages performed with 0.3 μM drug (R3 and R5), inhibited to 10^3 PFU/ml. Thereafter, all KPT-335 passages produced rises in titre up until P3. However, with the exception of R4 (which kept generally high titres up until P10), decreases in titre were then observed at P4-5, followed by fluctuating titres that mostly produced a final increase in titre from P8 to P9 (R4 and R5) and P10 (R2 and R3). These patterns of rising and falling titres were unexpected, but nevertheless suggested the viruses were no longer susceptible to KPT-335 by the end of the passage experiments.

3.2.2 Determination of drug-resistant IAV by plaque reduction assay

To establish at what stage the R1-R5 viruses became resistant to the compound, KPT-335 drug sensitivity at early (P3), middle (P6) and late passages (P9/10) was assayed by plaque reduction experiments. MDCK cells were infected with 100 PFU/ml of DMSO-passaged virus or R1-R5 viruses from the multi-passage experiments and incubated in the presence of DMSO (-) or KPT-335 at 0.3 μM (+) or 1 μM (++). At 48 h p.i., cells were fixed and stained with toluidine blue to visualise plaque formation. As expected, plaque formation was inhibited by KPT-335 in cells infected with the

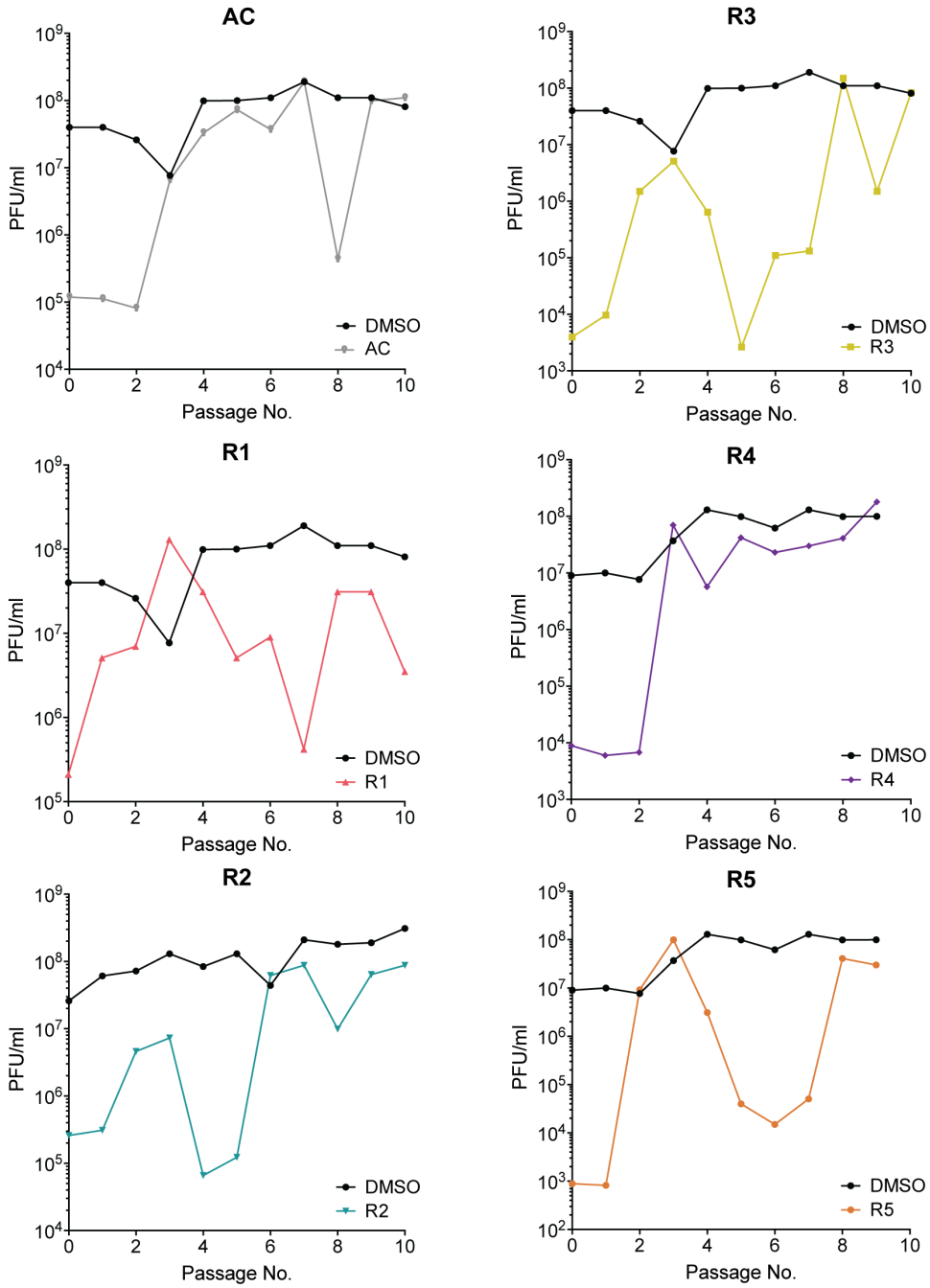

Fig. 3.2. Serial passage of IAV in the presence of a sub-optimal inhibitory concentration of KPT-335. A549 cells were infected with PR8 MUd or PR8 (MOI = 0.001) in the presence of 0.3 μM (R3 and R5) or 0.15 μM (R1, R2 and R4) of KPT-335, as well as the vehicle control (DMSO). 9 or 10 passages were carried out and after each, the virus titre (PFU/ml) was determined by plaque assay before setting the next passage up. 5 independent serial passages were performed in two blocks, named (R1-R3 and R4, R5 respectively) as well as an amantadine control (AC, 30 μM)

DMSO (P3 and P6) viruses at both drug concentrations, while all viruses gave abundant numbers of plaques in the absence of drug (Fig. 3.3). However, phenotypic differences were apparent in the plaque morphology of the R1-R4 pools, with the viruses producing noticeably smaller and/or hazier foci of CPE than the control passaged virus. R1 and R2 virus pools at P3 formed few plaques in the presence of 0.3 μM of drug (+) and little to no plaques were observed after treatment with 1 μM (++) of KPT-335. Infections with R3-R5 virus pools harvested at P3 displayed little to no plaques at either of the drug concentrations tested. Thus, although all virus pools replicated to notably higher titres at P3 than P0, this did not correspond with a drug-resistant phenotype as assessed by plaque reduction assay. At P6, R1-R5 viruses remained mostly susceptible to the compound although R1, R2 and R4 presented ~10-20 plaques under the growth of the lower concentration of compound. No P6 virus presented unambiguous plaques at the higher concentration of drug. However, by this point all drug-passaged virus pools had a small plaque phenotype in the absence of compound, with the R1 population in particular producing poor CPE in comparison to the large, clearer plaques demonstrated by the DMSO control virus, suggestive of a fitness loss in the absence of the drug. Overall, these data indicated that although the P6 viruses had been altered by the selection pressure, they were still susceptible to the compound and true drug resistance had not yet developed.

To determine if the concluding P9 (R4 and R5) and P10 (R1-R3) viruses were resistant to KPT-335, plaque reduction assays were carried out as before. Once again, DMSO (P10) virus plaque formation was inhibited at both concentrations of KPT-335 (Fig. 3.4). However, the R1-R4 viruses produced abundant plaques in the presence of 0.3

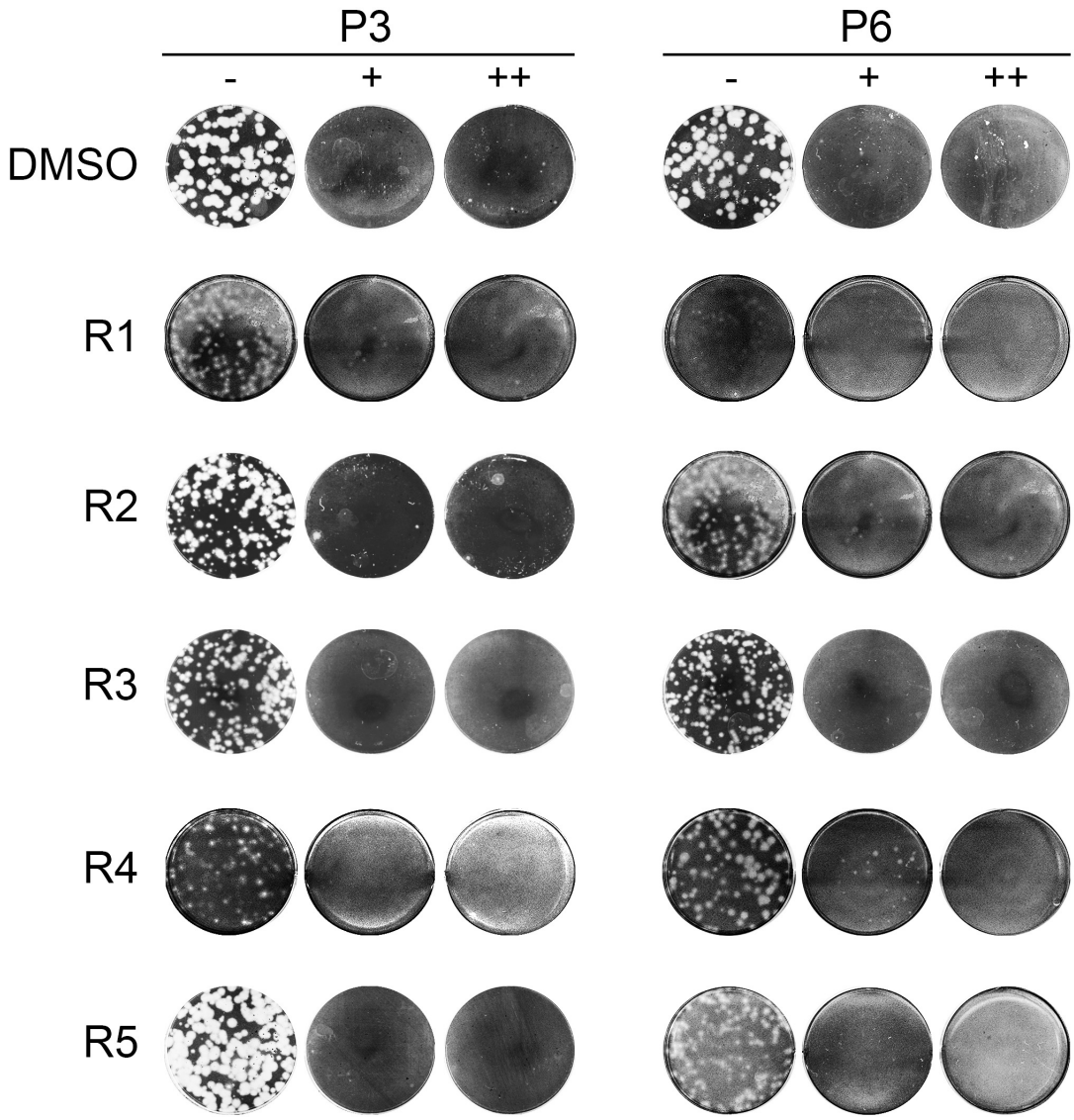

Fig. 3.3. Determination of drug-resistant IAV at P3 and P6 by plaque reduction assay. MDCK cells were infected with 100 PFU/well of virus harvested at passage 3 and 6 (P3, P6) for each independent serial passage (R1-R5) as well as the DMSO vehicle control (DMSO). Infected cells were grown in the presence of KPT-335 at a concentration of 0.3 µM (+) or 1 µM (++) or in the absence of compound (-). 48 h p.i. cells were fixed and stained with toluidine blue and imaged. Images representative of 2 independent experiments.

μM of KPT-335, in similar numbers to the corresponding untreated controls. The R3 population gave smaller plaques in the presence of the compound, while R4 pool plaques were not obviously different in size. Curiously however, the R1 and R2 virus pools displayed clearer plaques in the presence of 0.3 μM of compound compared to the untreated control. R1 and R2 viruses also produced smaller numbers of unambiguous plaques in the presence of 1μM of drug, while the R3 and R4 populations gave a few foci of possible CPE. R5 infected cells did not produce plaques in the presence of both 0.3 μM and 1 μM of compound, with a similar phenotype to the DMSO control virus.

Overall, these data provided substantial evidence that serially passaged viruses R1-R4 had become resistant to KPT-335 by passages P9/10, while the variance in numbers and morphologies of plaques between the serial passages suggested differences in the degree of resistance. Although R5 appeared to be less sensitive to the compound in the multi-cycle growth experiment (Fig. 3.2.), by plaque reduction assay this virus population did not present a clear resistant phenotype. Additionally, R1, R2 and R4 resistance was associated with a small plaque phenotype in the absence of compound suggesting the gain of resistance had reduced the fitness of these viruses.

3.2.3 NP localisation of drug-resistant IAV after KPT-335 treatment

As presented in the previous chapter, KPT-335 inhibits IAV replication by blocking vRNP nuclear export. To determine if the P10 drug-resistant viruses had escaped this repressive mechanism, NP intracellular localisation in the presence and absence of compound was analysed. A549 cells were mock infected or infected with P10 R1 or

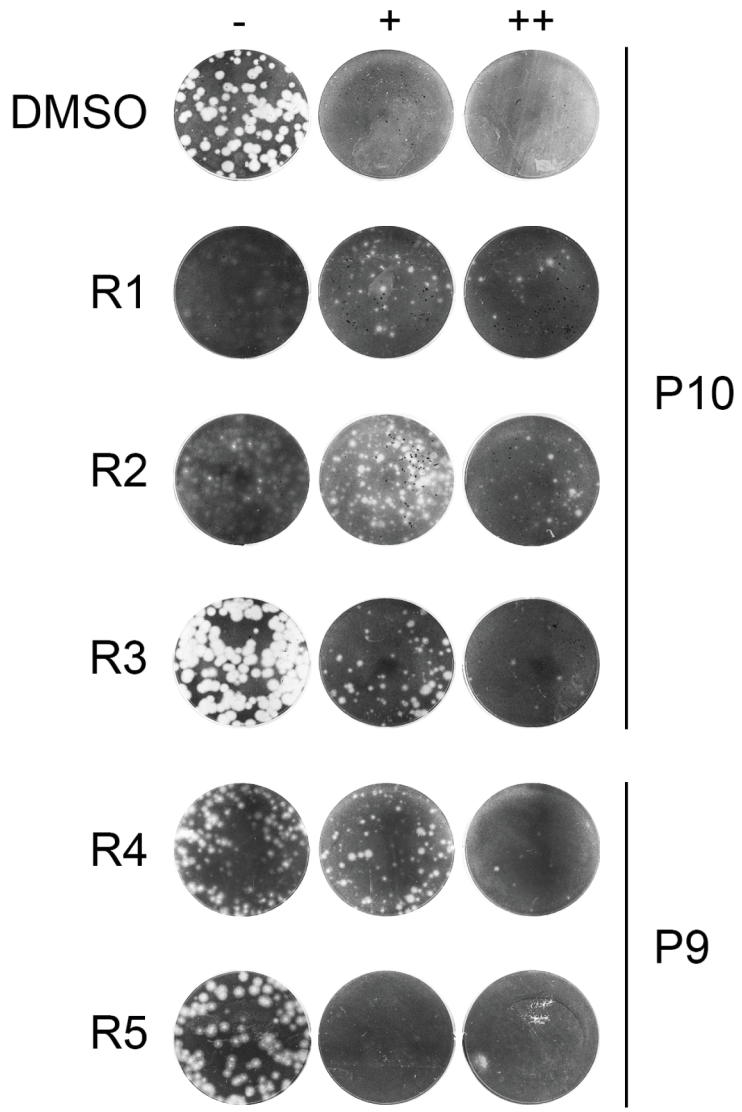

Fig. 3.4. Confirmation of drug-resistant IAV at passages 9 and 10. MDCK cells were infected with 100 PFU/well of virus harvested at passage 10 (R1-R3) or passage 9 (R4, R5) as well as the DMSO vehicle control. Infected cells were grown in the presence of KPT-335 at a conc. of 0.3 μM (+) or 1 μM (++) or in the absence of compound (-). 48 h p.i. cells were fixed and stained with toluidine blue and imaged.

R3 virus stocks or with a DMSO-passaged P10 virus as a control and grown in the presence of DMSO only or (0.3 μM or 1 μM) KPT-335. At 8 h p.i., cells were fixed, permeabilized and stained immunofluorescently for viral NP (green) and cellular DNA (blue). As expected, mock-infected untreated and treated cells did not show NP staining while, infection with the DMSO P10 (positive control) virus in the absence of compound produced cytoplasmic NP staining (Fig. 3.5), indicating normal export of vRNPs had taken place. Complete nuclear retention of DMSO P10 virus NP was observed after treatment with 1 μM of KPT-335 and partial retention at 0.3 μM, indicating that the drug had inhibited nuclear-cytoplasmic transport the of the viral genome. In contrast, for both P10 R1 and R3 virus pools, NP was no longer fully retained in the nucleus at 1 μM KPT-335m unlike the control virus (DMSO P10). These results support the resistant phenotype displayed by the plaque reduction data in Fig. 3.3 and suggests that P10 viruses were no longer inhibited at the stage of nuclear export.

3.2.4 Isolation and characterisation of drug-resistant viral clones

Next, the potential genetic changes responsible for KPT-335 resistance were investigated. However, serial passaging an influenza virus under selective pressure may well result in a mixed population of genotypes/phenotypes. Consequently, sequencing pooled virus supernatants would give a mixed consensus sequence of the whole population, which could be difficult to interpret. Accordingly, to isolate drug-resistant virus clones for sequencing, plaque purification of the P10 R1-R3 viruses was performed. As depicted in Fig. 3.6, serial passaged viruses harvested at P10 (including a DMSO-passaged control virus) were used to infect MDCK cells and

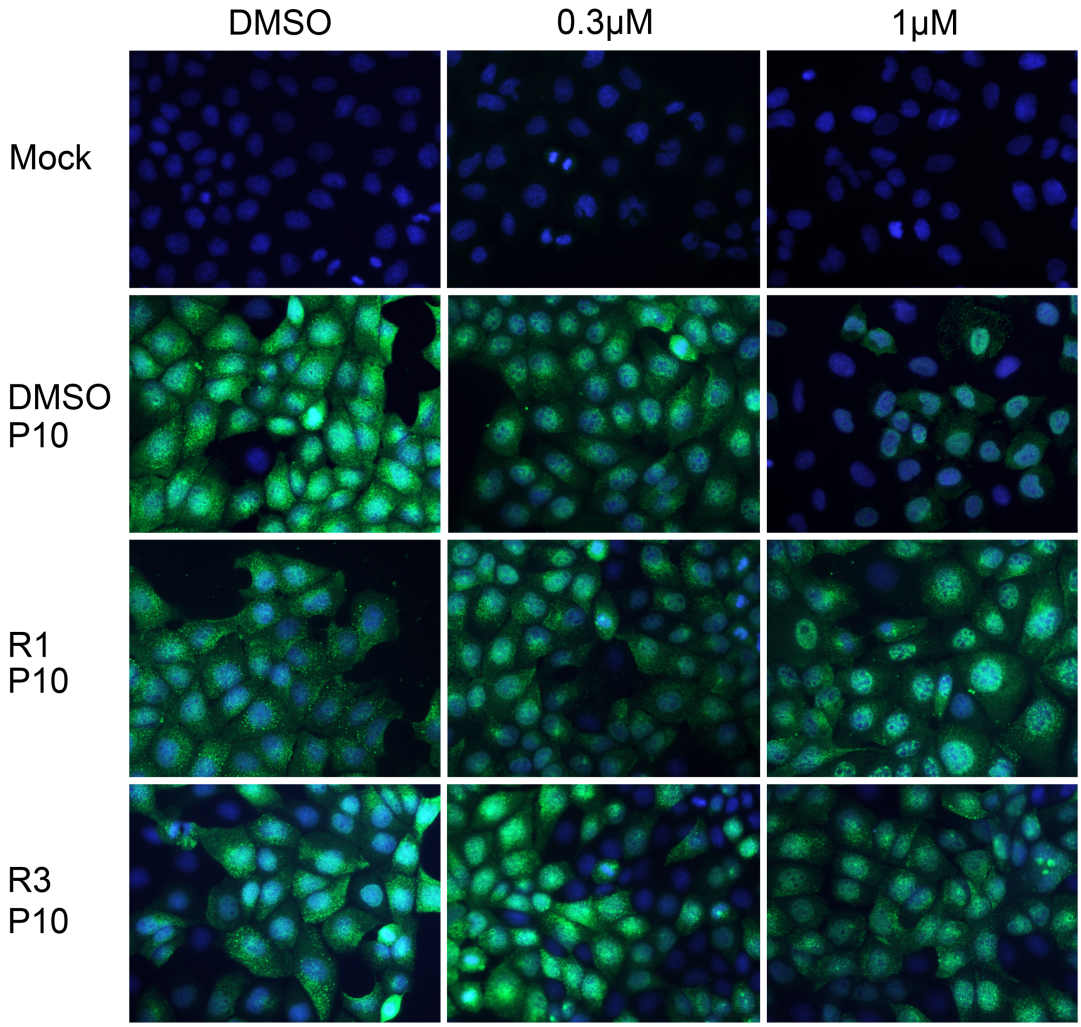

Fig. 3.5. Effect of KPT-335 on intracellular localisation of NP after infection with P10 viruses. A549 cells were infected with DMSO, R1 or R3 (P10) viral supernatants at MOI 3 in the presence (0.3 μM or 1 μM) or absence (DMSO control) of KPT-335. 8 h p.i. cells were fixed and stained with anti-NP (green) and a nuclear stain (DAPI, blue). Images were taken as optical slices through the middle of the cells using a Leica fluorescence microscope.

grown in the presence of KPT-335 (1 μM) under an agarose overlay. 48 h p.i., plaques formed in the presence of compound were isolated from the agarose and transferred to fresh MDCK cells and grown for a further 24 h in the presence of compound (0.3 μM). 8 plaques were isolated per serial passage experiment (R1-R3) and subjected to further experimentation before genotypic analyses. As an example, Fig. 3.7. displays outcomes of the set of experiments carried out to characterise the 8 plaque isolates from R3 (P10). Similar sets of experiments were also performed for the R1 and R2 P10 plaque pick viruses (data not shown). Initially, the 8 viral clones were grown in the presence and absence of the compound to determine the difference in titre and establish the most phenotypically resistant isolates for sequencing. MDCK cells were infected with the isolates in the absence (-drug) or presence (+ drug, 0.3 μM) of KPT-335. At 24 h p.i., viral titre was determined by plaque assay. In the absence of compound, DMSO (P10) virus grew to 10^8 PFU/ml, whereas the isolates grew to ~10^7 PFU/ml (Fig. 3.7.A). This difference in titre may be due to the isolates containing drug dependent adaptations, which as mentioned previously, usually come at a fitness cost to the virus. The DMSO (P10) virus in the presence of compound, displayed a 2-$\log_{10}$ reduction in titre (10^6 PFU/ml) in the presence of compound compared to the untreated control. All R3 plaque isolates grown in the presence of compound displayed <1-$\log_{10}$ reduction in titre in comparison to the untreated control, indicating that all plaque picks (PP) were partially drug-resistant. Isolates 3, 6 and 7 from P10, experiment R3 (re-designated PP1, 2 and 3), displayed the smallest differences in virus titre, suggesting they were the least susceptible to drug and therefore were selected for further analysis.

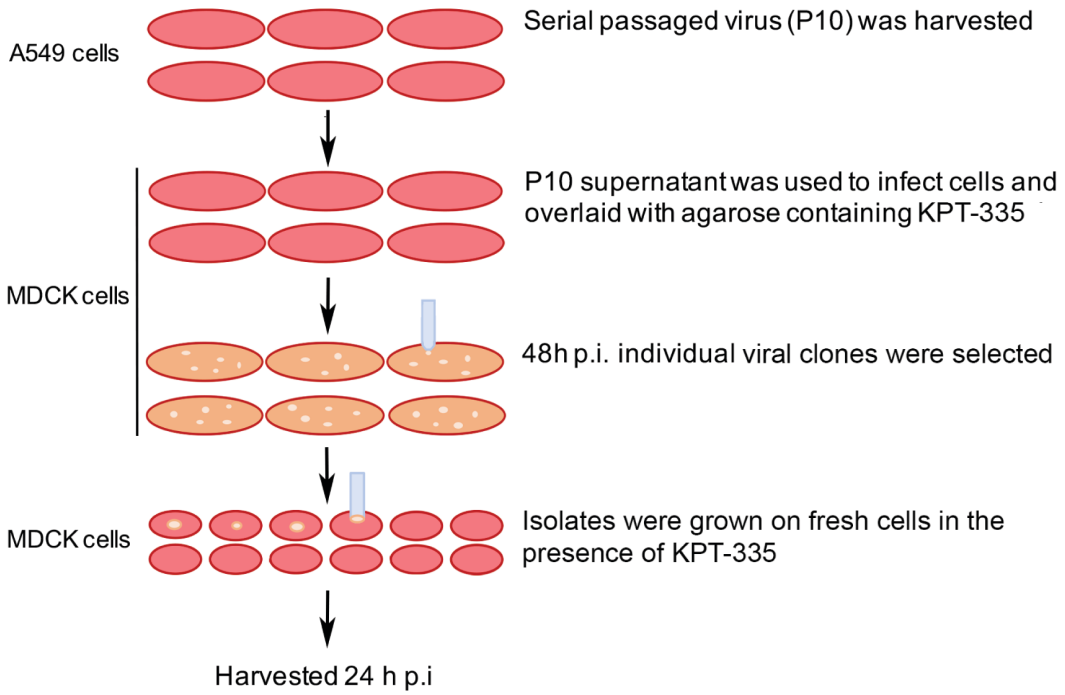

Fig. 3.6 Isolation of drug-resistant viral clones from serial passage experiments R1-R3. Viral supernatants harvested from serial passage (P10) were used to infect MDCK cells at 100 PFU/well. Cells were overlaid with agarose containing 1 μM of KPT-335. 48 h p.i. individual plaques were isolated from the agarose using a cut pipette tip. 8 plaques were picked from each serial passage experiment; R1, R2 and R3. Isolates were grown on fresh MDCK cells in the presence of 0.3 μM of compound. 24 h p.i. supernatant was harvested for further experiments.

To test whether the individual plaque picked virus clones were truly resistant, PP1-3 were tested by a dose response assay similar to those performed in chapter 2 (Fig. 2.1.D). A549 cells were infected with the isolates (PP1, 2 and 3) and a DMSO PP control at an MOI of 0.01 and treated with increasing concentrations of compound. At 24 h p.i., supernatants were harvested and virus titres were determined by plaque assay. As expected, the control DMSO PP was inhibited by the compound in a dose-dependent manner (Fig. 3.7.B). In contrast, the three isolates (PP1-PP3) from the resistant virus stock were not suppressed by the compound at any of the concentrations tested. The drug susceptibility of the three isolates was also checked by plaque reduction assay as performed previously. MDCK cells were infected with the DMSO PP or the isolates at 100 PFU/ml and were left untreated (0 μM) or treated with (0.3 μM or 1 μM) of KPT-335. At 48 h p.i., cells were stained with toluidine blue to visualise plaques. As previously observed, plaque formation by the DMSO PP was inhibited at both 0.3 μM and 1 μM concentrations of the compound (Fig. 3.7.C). All three R3 isolates displayed a slightly hazy small plaque phenotype in absence of compound but the numbers of plaques formed in the presence of 0.3 μM of drug were similar to the numbers observed in the untreated control, indicating resistance to the compound at this concentration. However, little to no plaques were observed at the higher concentration of 1 μM, similarly to the DMSO virus, suggesting that although the isolates were not susceptible to KPT-335 at 0.3 μM, they were not resistant to higher concentrations of the compound. The same set of experiments were performed for the plaques picked for the P10 R1 and R2 serial passaged experiments, in which the outcomes were similar (data not shown). Thus, overall these data indicated the successful isolation of drug-dependent viral isolates.

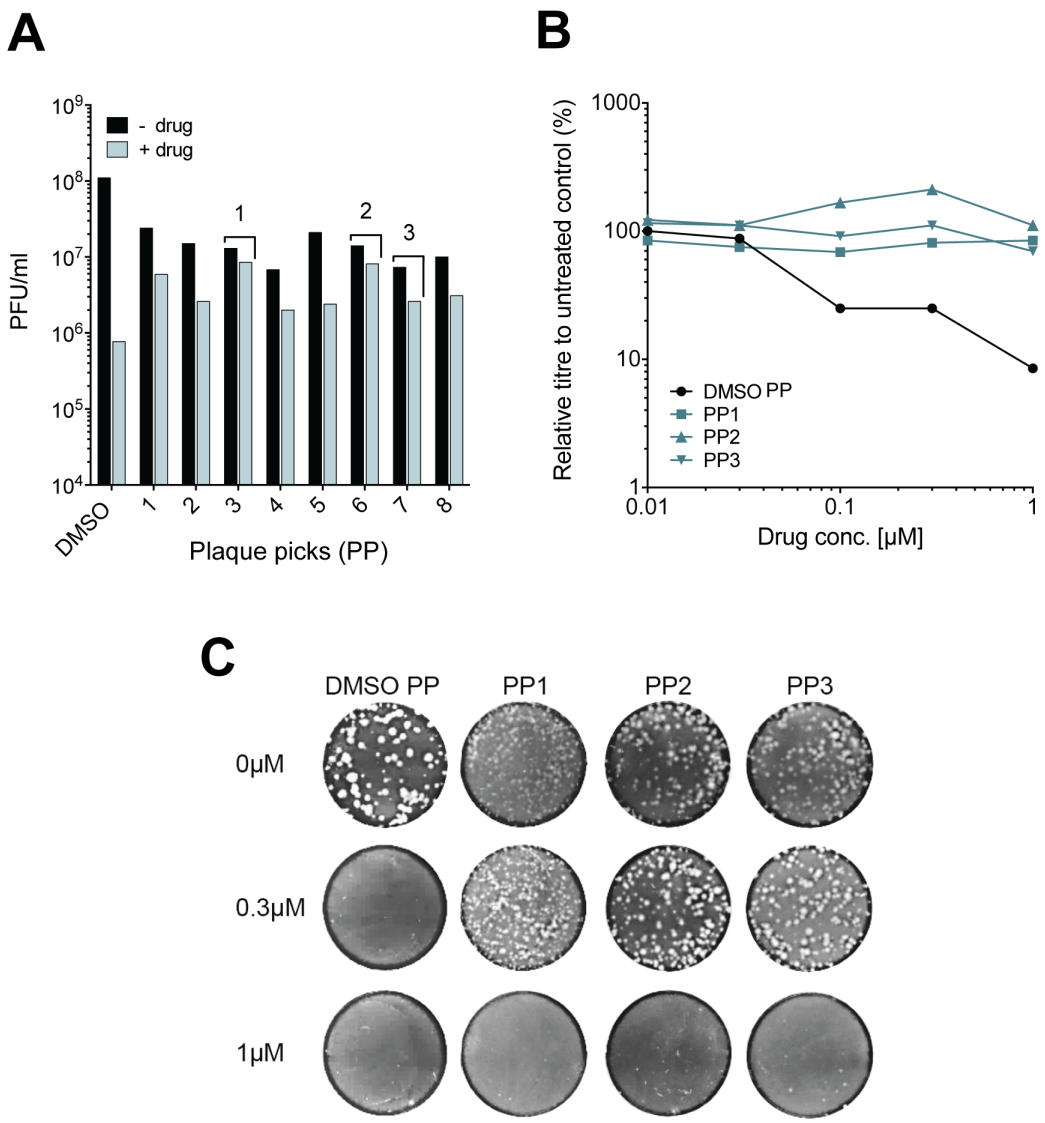

Fig. 3.7. Experimental method to characterise drug-resistant virus isolates for sequencing (using R3 as an example). **(A)** Growth of viral isolates in the presence and absence of compound. MDCK cells were infected with isolates (MOI = 0.01) in the presence (0.3 µM) or absence (0 µM) of compound. 24 h p.i. virus supernatant was titred by plaque assay. The three plaques picks with the smallest difference in titre (indicated by numbers) were selected for further experimentation (B, C). **(B)** Dose-response curve with KPT-335. A549 cells were infected with virus isolates (MOI = 0.01) and treated with increasing concentrations of KPT-335. 24 h p.i. viral supernatant was titred by plaque assay. **(C)** Plaque reduction assay with selected viral isolates. MDCK cells were infected with 100 PFU/well of PP3, 6, and 8, as well as a DMSO vehicle control. Infected cells were treated with KPT-335 at a conc. of 0, 0.3 µM or 1 µM or with no drug (0 µM). 48 h p.i. cells were stained with toluidine blue and imaged.

As a further phenotypic test of the cloned resistant viruses, NP localisation in the presence of compound was assessed by IF assay. Example data are shown for two isolates, one from R1 and one from R2. A549 cells were infected with DMSO PP or the resistant isolates at an MOI of 3 in the absence (0 μM) or the presence (0.3 μM or 1 μM) of compound. 8 h p.i. cells were fixed, permeabilised and immunofluorescently stained for NP (green) and DAPI (blue). Confocal images were taken at high magnification as single optical slices through the middle of the cell. The DMSO PP virus and the isolates, in absence of compound, displayed punctate cytoplasmic staining, as expected, indicating RNP nuclear export had taken place (Fig. 3.8). In the presence of 0.3 μM and 1 μM of KPT-335, the DMSO virus predominantly displayed NP staining in the cell nuclei, with stronger staining at 1 μM indicating enhanced retention at the higher drug concentration, as previously observed. In addition, NP staining concentrated around the edge of the nucleus in a ring-like formation, similar to previous reports with LMB (Elton *et al.,* 2005; Elton *et al.,* 2001; Ma *et al.,* 2001). For both plaque isolates, NP gave stronger cytoplasmic staining in the presence of compound than the DMSO PP, suggesting persistence of RNP nuclear export, although some nuclear retention of NP was nevertheless still evident. Interestingly, this nuclear NP localisation differed from the ring-like staining displayed by the DMSO PP, forming large intranuclear bodies throughout the organelle.

These results indicated that the R1-R3 isolated viral clones were resistant to the KPT-335 compound, at least to some extent. The dose-response data suggested that the isolates were unaffected at any of the drug concentrations, indicating they were fully resistant. However, the plaque reduction assays indicated a resistant phenotype only

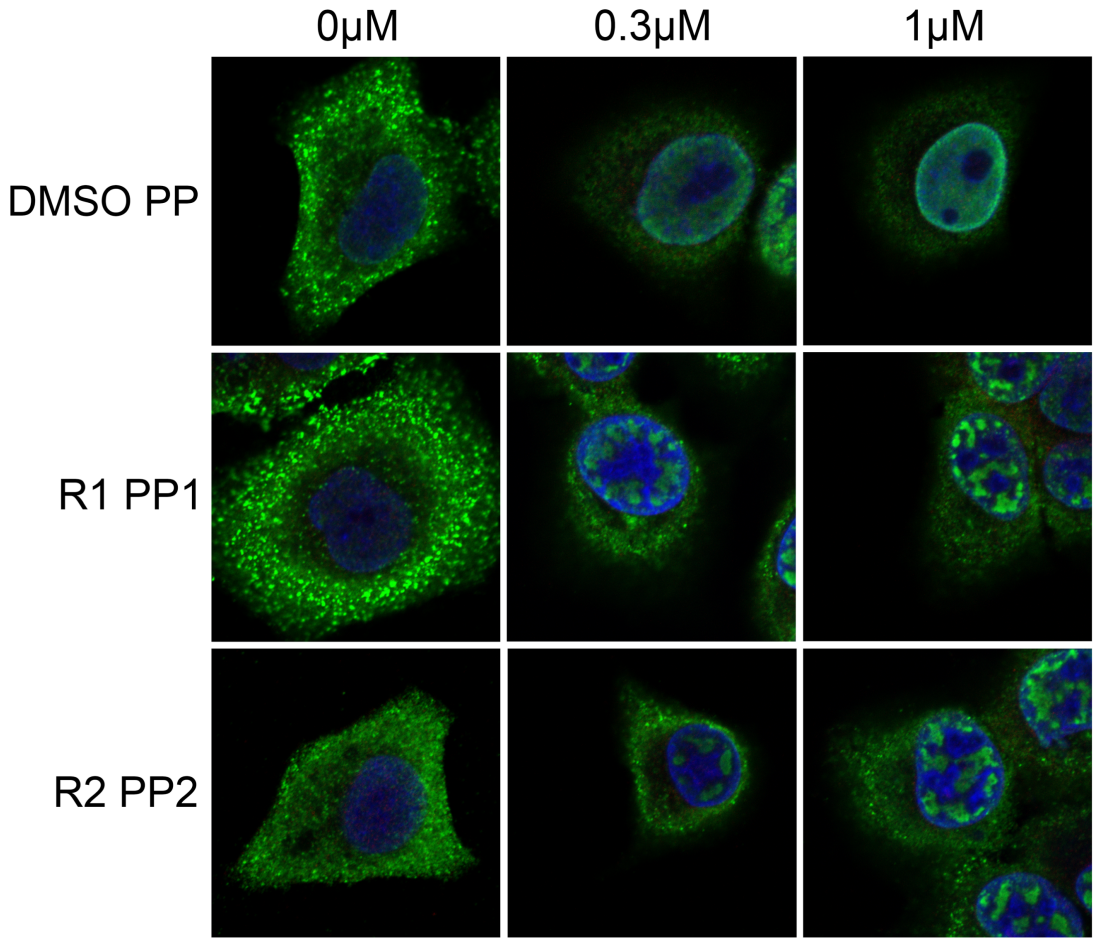

Fig. 3.8. Effect of KPT-335 on intracellular localisation of drug-resistant virus isolates. A549 cells were infected with virus isolates (R1, PP3 and R2, PP2), as well as a DMSO (PP) control (MOI =3). Infections were carried out in the presence (0.3 μM, 1 μM) or absence (0 μM) of KPT-335. 8 h p.i. cells were stained with anti-NP (green) and a nuclear stain (DAPI; blue). Images were taken as single optical slices by confocal microscopy. Data are representative of 2 independent experiments.

at sub-inhibitory concentrations of the compound (0.3 μM), suggesting there was a threshold concentration of drug for resistance.

3.2.5 Sequencing analysis of KPT-335-selected IAV

Genotypic analysis of drug-resistant variants would be expected to reveal mutational changes that may be responsible for a resistant phenotype. To characterise genotypic alterations in the KPT-335-selected viruses, Sanger sequencing of the relevant influenza genes was performed. Viral RNA was extracted and cDNA obtained by reverse transcription reactions carried out with an IAV universal oligonucleotide primer (*5'-AGCAAAAGCAGG-3'*). The post reverse transcriptase (RT) reactions (cDNA) were then amplified with terminal primers specific for PA, PB1, PB2, NP, M and NS segments as well as with sets of internal primers for PA, PB1 and PB2 to amplify the middle regions of these larger genes. The PCR products were purified, size checked on a DNA gel and then sequenced commercially (GATC Biotech, Constance, Germany). The HA and NA genes were not sequenced because of the lower likelihood that these proteins would accumulate functionally important changes in response to KPT-335 treatment. The three characterised clonal isolates from each of experiments R1-R3 as well as a DMSO PP were sequenced. Pooled R4 and R5 P9 samples as well as a DMSO P9 control virus were also sequenced. Sequencing of PR8-WT virus P1 stock was included as a reference sequence (details of the samples processed for sequencing are indicated in Table 3.2).

Sequence analysis revealed genotypic changes present in all serial passaged viruses. Details of changes in the coding regions are shown in Table 3.3. PR8 MUd (P1) and PR8-WT (P1) stocks were used as a reference sequence to compare any amino acid

Table 3.2 Drug-resistant samples sequenced

Virus	Virus population [A]	No. [B]	Passage No. [C]
PR8-WT	Stock	1	P1
DMSO (1)	PP	1	P10
R1	PP	3	P10
R2	PP	3	P10
R3	PP	3	P10
DMSO (2)	Pool	1	P9
R4	Pool	1	P9
R5	Pool	1	P9

[A] Virus population sequenced; the initial virus stock (stock), plaque pick (PP) or pooled virus population (pool)
[B] The number of stock virus, plaque isolates or pooled virus populations selected for sequencing.
[C] The number of passages the virus underwent before sequencing.

changes found in the serial passaged viruses. Sequence analysis of the DMSO PP (the control from the R1-R3 experiments) revealed a few mutational changes (shown in blue in Table 3.3), which possibly arose from adaption to infection in A549 cells during the serial passage (the PR8 clone used was an MDCK-cell adapted one; de Wit *et al.,* 2004). These mutations were also found in some of the R1-R3 plaque isolates. However for simplicity, these mutations were excluded from further analysis as they were expected to not contribute to the drug-resistant phenotype. For each of the three plaque isolates from the R1-R3 passages, amino acid changes were found in all genes analysed. Several nucleotide changes resulted in silent mutations and therefore the probability of them functionally contributing to the resistant phenotype was expected to be low (presented in italics in Table 3.3). Additionally, even though the R1-R3 isolates had been clonally purified, several mutations contained a heterozygous base as established by the analysis of the sequencing chromatograms (traces); these changes are depicted in grey in Table 3.3. These sequence polymorphisms could have resulted from contamination at the plaque pick stage and/or arisen during subsequent amplification steps, but either way, since they had not gone to fixation in the virus population, they were discounted from further analysis. Other potential compensatory drug resistant mutations that had apparently been fixed but were found in only one or two of the three isolated clones are as follows; PB2, F551S (R2+R3), PB1, R363G (R3) and NP, A178T (R2). However, for R1-R3, the only nucleotide changes which had a strong homozygous base and that were conserved between all three plaque isolates within a passage series were discovered in the NP gene. Amino acid changes Q311R, N309T and Y296H (highlighted in red in Table 3.3) were found in passages R1, R2 and R3, respectively. The presence of these mutations in all three clonal

Table 3.3. Sequencing analysis of drug-selected plaque isolates (R1-R3)

	DMSO	R1			R2			R3		
PP	1	1	2	3	1	2	3	1	2	3
PB2		R561S *Y576*	F551S R561S		F551S *Y576*	F551S *Y576*				
PB1			*P444*	*P444*		R363G				
PA									A396H	
NP	S377N	Q311R	Q311R A178T	Q311R	N309T	N309T	N309T	Y296H	Y296H V364I	Y296H V364I
M*	A33T G82R	A33T *S70* *L84*			G82R				*I152*	
NS		Mixed, all in intron						*S190*	*S190*	

Table 3.4. Sequencing analysis of drug-selected pooled viruses (R4 and R5)

	DMSO	R4	R5
PB2			R258K
PB1			
PA		L470C	
NP		P283S	C333S I388M *L166* S9Y
M			
NS			

Blue text = mutations found in DMSO serial passaged control virus
Grey text = mixed nucleotide trace
Italic text = silent mutational change
Red text = mutations identified all 3 plaque isolates (R1-R3) or mutations with a homozygous nucleotide trace in pooled viruses (R4, R5)
* Udorn M sequence "mutated" to PR8 M sequence for DMSO and R1-R3 all PP (discussed in section 3.3)

isolates proposed a convincing argument that these amino acid changes contributed to the drug-resistant phenotype. For R4 and R5, the whole P9 virus population was sequenced rather than individual plaque-picked clones, as well as the matching DMSO P9 control virus. Therefore, as expected, sequencing analysis was 'noisier' with the presence of multiple peaks and poorly defined peaks in the trace analysis, leading to difficulty in confidently identifying single nucleotide changes at some positions. No mutations were found in the DMSO-passaged P10 virus. Five 'mixed' sequences were discovered in R4 and R5 as presented in grey in Table. 3.4. However, two changes with a homozygous nucleotide trace were present in the NP gene: P283S and C333S in R4 and R5, respectively. Applying the same logic as above to the sequencing analysis to the R4 and R5 virus populations, suggested that these mutations in NP were most likely to contribute to possible KPT-335 resistance.

Chromatograms of sections within the NP gene where the five amino acid mutations were identified are displayed in Fig. 3.9. All chromatograms where nucleotide changes were discovered displayed well defined and sharp peaks with no (or in the case of R4, minimal) background interference present at the peak baseline; therefore, mutations observed from these trace analyses could be considered as accurate data.

In summary, genotypic analysis of the serially passaged viruses (R1-R5) revealed consistent amino acid substitutions within the NP gene. The NP mutations found were conserved between the three plaque isolates from each of the R1-R3 serial passages and evidently at or near fixation in passages R4 and R5. Mutations found in the other genes analysed were either silent, mixed within a virus pool or not conserved between

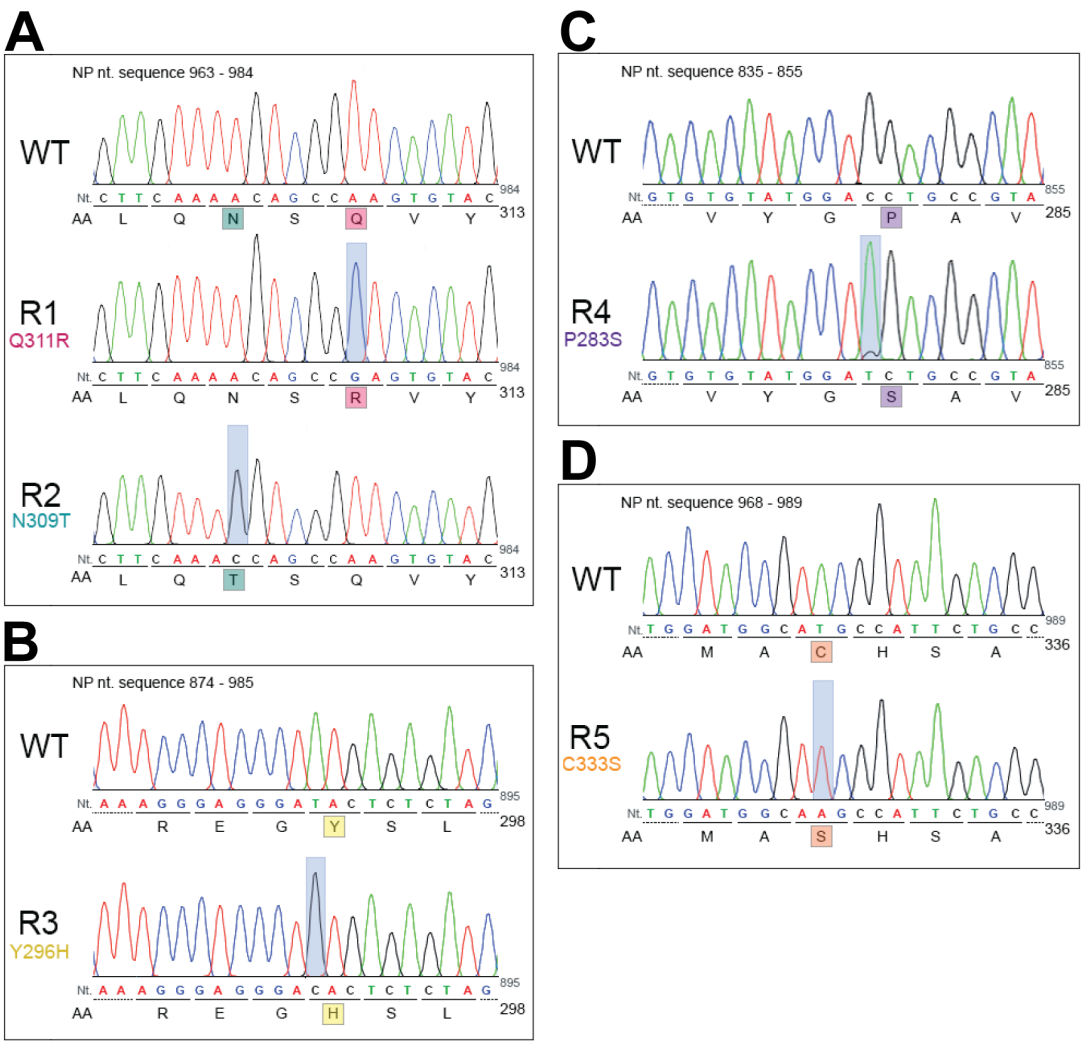

Fig. 3.9. Sequencing chromatograms of sections within the NP gene sequence where 5 amino acid mutations were identified. (A) Chromatogram of NP nucleotide sequence between nucleotides 963 to 984. Nucleotide change found in R1, A977G translated to amino acid change Q311R (highlighted in pink). Nucleotide change found in R2, A971C, translated to N309T (highlighted in turquoise). **(B)** Chromatogram of NP nucleotide sequence between 874 to 895. Nucleotide change found in R3, T886C, translated to Y296H (highlighted in yellow). **(C)** Chromatogram of NP nucleotide sequence between 835 to 855. Nucleotide change found in R4, C847T, translated to P283S (highlighted in purple). **(D)** Chromatogram of NP nucleotide sequence between 968 to 989. Nucleotide change found in R5, T997A, translated to C333S (highlighted in orange). Blue highlighted peaks indicate nucleotide difference from WT virus sequence. Nt. = nucleotide. AA = amino acid.

the isolates sequenced. Thus, the sequencing data strongly indicated that resistance correlated to mutational changes within the NP protein.

3.2.6 Prevalence of KPT-selected NP mutations in human IAV sequences

To determine if the potential drug-resistant NP mutations were found naturally in other human IAV strains, a widespread analysis of full-length segment 5 sequences was conducted. Sequences were obtained by a NCBI database search (conducted on 13/02/17) and gave 18,317 results. The breakdown of subtypes obtained are as follows; 8900 (H3N2), 8862 (H1N1), 193 (H5N1), 119 (H7N9), 91 (H5N6) with remaining sequences other subtypes. Sequences from unknown origins were removed from analysis and any identical sequences were collapsed. An R script was written and provided by Dr Sam Lycett (The University of Edinburgh) and modified by Carina Conceição (PhD student within the Digard group), which separated all sequences into groups of 500 for alignment analysis using FASTA software. Analysis revealed that the KPT-335-selected NP mutations; Q311R, N309T, Y296H, P283S and C333S (Fig. 3.10.B) were not prevalent in the NP protein (data kindly examined by Rute Pinto (PhD student within the Digard group). Additionally, the most predominant amino acid at the NP position of interest was identical to that in the PR8 WT strain. At positions 311 and 296, 99.9 % of sequences had a glutamine (Q) or tyrosine (Y) respectively, with only 0.005 % of sequences displaying either the KPT-335-induced mutant arginine (R) or histidine (H), respectively. At position 333, no sequences were found with a serine (S). At position 283, 57.7 % of sequences matched the PR8 WT proline (P), with 42.3 % containing other amino acids. However, only 0.005 % had the potentially drug-resistant serine (S). Interestingly, 309 was the only amino acid

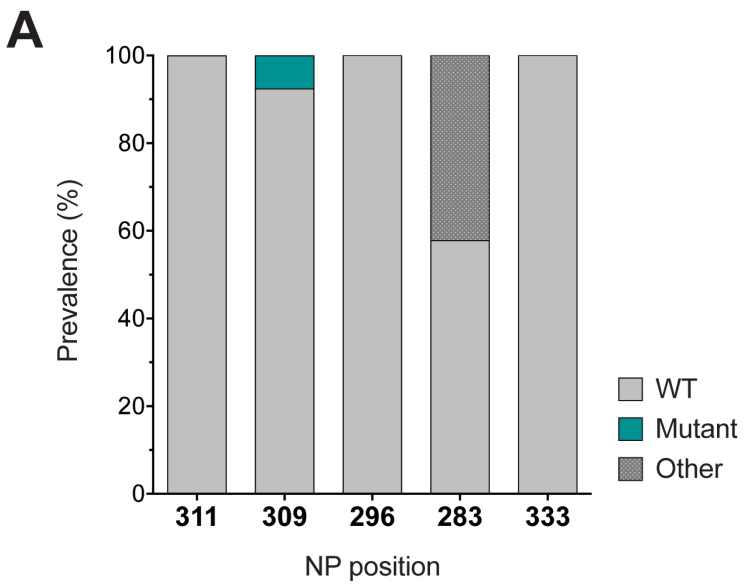

B

Exp.	Nt. change	AA change	Prevalence (%)		
			WT	Mutant	Other
R1	A977G	Q311R	99.9%	0.005%	0.05%
R2	A971C	N309T	92.4%	7.6%	0.07%
R3	T886C	Y296H	99.9%	0.005%	0.02%
R4	C847T	P283S	57.7%	0.005%	42.3%
R5	T997A	C333S	99.9%	0%	0.03%

Fig. 3.10. Prevalence of NP mutations in human IAV sequences. All human full-length NP IAV sequences were downloaded from the NCBI database (18,317) Sequences were then separated into segments of 500 using an Rscript programme written by Dr Sam Lycett. The 500 sequence segments were aligned using MEGA6 and stored as a FASTA file. 10 separate alignments were carried out to determine if the motif had a 'WT' AA or the 'mutant' AA at the 5 different NP positions. Results from the alignments were analysed using excel functions to determine the number of sequences which had an 'X' AA at the NP position of interest (performed by Rute Pinto). **(A)** Bar graph indicating % prevalence of a WT, mutant or another AA at the NP positon specified. (**B)** Table showing the % prevalence values of the AA found at each NP position.

position where a significant number of virus sequences contained the polymorphism of interest. 92.4 % of sequences had a PR8 WT asparagine (N) while 7.6 % matched the mutation to threonine (T). Further analysis revealed that most sequences with a T at 309 were pre-2009 pandemic with ~10 % sequences containing a T before and <3 % containing a T post pandemic 2009 in comparison to the ~11 % with an N pre-pandemic and 75 % post-pandemic (data not shown). These results indicated that the potential drug-resistant mutations were not present in the majority of the previously sequenced human IAV strains, suggesting that other ongoing selective pressures on IAV do not normally select for these potential NP KPT-335-resistant mutations.

3.2.7 Location of drug-selected mutations within the NP protein

To determine where the drug-selected mutations were located within the NP protein, the mutations were mapped onto a linear depiction of the polypeptide together with known intracellular trafficking signals, as well as onto a crystal structure of the trimeric form of the NP protein molecule (Fig. 3.11). The NP protein is 498 amino acids in length and contains at least two nuclear localization signals (NLS) (Neumann *et al.,* 1997; Wang & Palese, 1997), a cytoplasmic accumulation sequences (CAS) (Digard *et al.,* 1999) and three nuclear export signals (NES1, NES2, NES3) (Yu *et al.*, 2012), one of which (NES3) is required for CRM1-mediated nuclear export (Fig. 3.11.A). P283S, Y296H, N309T, Q311R and C333S all appeared in the middle to the C terminal region of the NP polypeptide and as the amino acid numbers suggest, in close proximity to each other. Although not found within the reported CRM1-dependent NES site (NES3; 248-274), they all appear just downstream of this region. Additionally, the C333S mutation from the non-phenotypically resistant virus

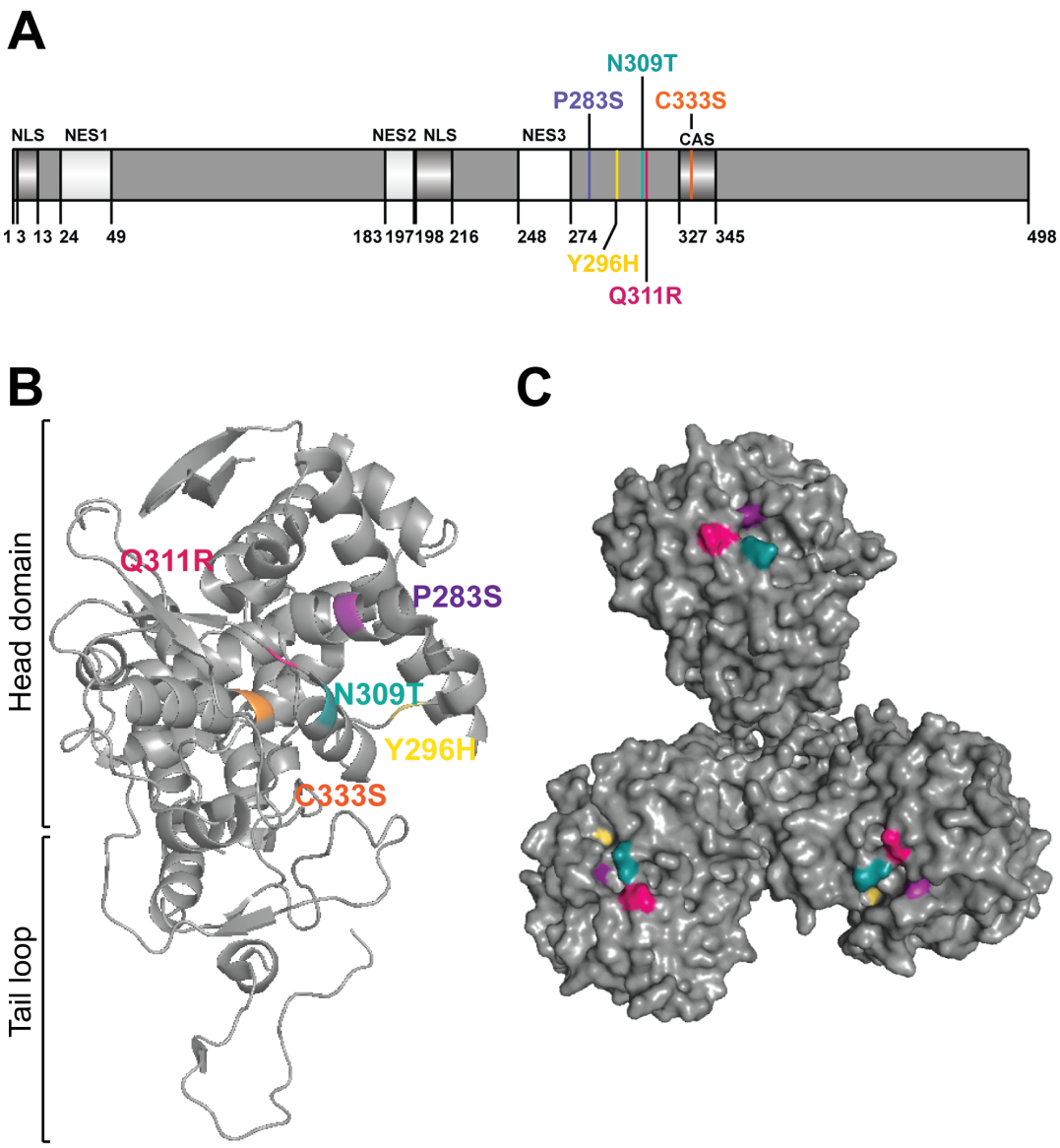

Fig. 3.11. Drug-selected mutations mapped to the structure of NP. (A) NP protein sequence diagram indicating the two nuclear localisation sequences (NLS), a cytoplasmic accumulation signal (CAS) and three nuclear export signal (NES1-3) in relation to the 5 mutations. **(B)** Ribbon structure of the monomer form of NP with amino acids changes mapped in colour. Using Pymol software and the 3.2Å crystal structure sequence from (Ye *et al.,* 2006), NP mutations at positions 283, 296, 309, 311 and 333 were mapped on the structure of the protein. **(C)** Surface structure of NP with 4 (283, 296, 309 and 311) out of 5 mutations visibly mapped to the surface of the trimer form of the protein.

(as shown in R5 (P9) plaque reduction data in Fig. 3.4) was found within the CAS motif associated with cytoplasmic retention of RNPs possibly by tethering NP to the actin cytoskeleton (Digard *et al.,* 1999). Mutations were mapped on a trimeric form of a 3.2Å resolution NP crystal structure obtained from the Protein Data Bank (PDB) under code 2IQH.pdb (published by Ye *et al*., 2006) and the protein structure was annotated using PyMol software. An NP monomer is composed of a head domain, a body domain and a tail loop as depicted in Fig. 3.11.B. Mapping of the NP mutant amino acids onto the monomer crystal structure demonstrated that all five mutations located to a similar region on the body domain (Fig. 3.11.B). Surface visualisation of the trimeric structure revealed that four of the five mutations were located on the surface of the NP molecule (Fig. 3.11.C). P283S (purple), Y296H (yellow), N309T (turquoise) and Q311R (pink) all clustered together at the side of the NP body. C333S (orange), although close to the other four amino acids was not surface exposed.

Thus, all five of the NP mutations were close to each other within the tertiary structure of the protein, although not located within a known NES reported to be involved in CRM1-dependent nuclear export. Importantly, four of the five mutated amino acids were surface exposed on the NP protein, suggesting that if these mutations were responsible for the drug-resistant phenotype, the escape mechanism could involve a change in protein-protein interactions that occur during CRM1-mediated export.

3.3 Discussion

In this chapter, the generation of a KPT-335-resistant IAV was described. Investigating the likelihood of the emergence of drug resistant virus variants is an important pre-clinical step for potential antiviral therapies. Although *in vitro* investigations will not necessarily predict the probability of clinical resistance, it can determine if the genetic barrier for drug resistance would be low or high. Additionally, sequencing of a CRM1-inhibitor resistant virus would be expected to reveal causative mutations within the IAV genome and subsequently expand our knowledge of the CRM1-dependent nuclear export process with regards to influenza virus infection. Therefore, phenotypic and genotypic analyses for potential KPT-resistant variants were performed in cell culture.

KPT-335 resistance was gained by serially passaging H1N1 laboratory strains PR8 MUd and PR8 in A549 cells in the presence of KPT-335, resulting in a selection of isolates showing decreased susceptibility to KPT-335 after 9-10 passages (Fig. 3.2). An amantadine serial passage experiment was initially used as a positive control for the selection of drug-resistant variants. It is widely known from both *in vitro* and *in vivo* studies that the M2 ion channel blocker can easily elicit a variety of drug resistant mutations such as L26F, V27A, A30T/V, S31N, G34E and L38F within the M2 gene of H1N1 viruses (reviewed in Hussain *et al.*, 2017). Therefore, serial passage of an amantadine sensitive virus, such as PR8 MUd, would be expected to result in a drug-resistant variant after few passages in the presence of the compound. Results presented in Fig. 3.2, displayed an increase in virus titre after 3 passages in the presence of

amantadine, suggesting resistance had occurred. However, subsequent sequencing of the M gene revealed that instead of P10 PR8 MUd isolates from the R1-R3 serial passage experiments gaining a specific amantadine resistance mutation, they actually gained a PR8 segment 7 (which already encodes an amantadine-resistant M2) in place of the expected Udorn segment 7 (Table 3.3). A similar replacement of segment 7 had also occurred in the KPT-335-passaged viruses. Sequencing of the PR8 MUd stock and P1 viruses revealed that these viruses contained Udorn segment 7, indicating the original stock was indeed PR8 MUd (data not shown). This suggests that the transformation of the Udorn segment 7 to PR8 segment 7 occurred during the serial passage. PR8 MUd passage experiments were carried out independently from the PR8 passage experiments, which therefore reduced the risk of samples being contaminated with PR8 during the passaging itself. Therefore, it was hypothesised that the initial stock of PR8 MUd contained a low amount of contaminating PR8 virus. This could also be checked by examining the plaque morphology i.e. a mixed population would contain both small (PR8 MUd) and larger (PR8) plaques. Additionally, sequencing the viruses harvested at the various passage points would help determine when the transformation from PR8 MUd to PR8 occurred. To prevent this type of problem occurring in future serial passage experiments with PR8, a single virus clone was isolated to ensure a purified stock before starting the R4 and R5 serial passage experiments.

Perwitasari *et al.,* (2016) investigated the effect of KPT-335 against IAV in two *in vivo* models, as discussed in more detail in chapter 2. They also investigated the potential for drug resistance *in vitro*. The authors serially passaged A/WSN/33 (H1N1) in A549

cells in the absence and presence of KPT-335. In contrast to this study, they found that WSN was still susceptible to KPT-335 even after 10 passages in the presence of the compound. A possible explanation for the discrepancies in results between Perwitasari *et al.,* (2016) and this study may due to the difference in the experimental procedures performed. The serial passage experiment performed by the Perwitasari and colleagues was carried out under selection of 0.2 μM KPT-335, which is a not dissimilar concentration to those assessed in this study (0.15 μM and 0.3 μM). However, to test the susceptibility of the virus harvested at various passages, they used 5 μM KPT-335. Here, it was found that a concentration of 1 μM of drug could completely inhibit WT virus replication (chapter 2, Fig. 2.1), thus suggesting that 5 μM would be too harsh a test and may miss smaller differences in susceptibility to the compound that might be biologically important. Ideally, the KPT-335 serial-passaged virus would benefit from being tested against a sub-optimal drug concentration. Additionally, the authors did not determine virus titre between passages, thus leading to unknown MOIs and possibly increasing the chances of defective inferring particle (DIPs) generation. A DIP influenza virus particle has a large deletion in the central region in one of the eight RNAs and they have been shown to develop upon successive high multiplicity passages of IAV (Magnus, 1954). The presence of many DIPs may interfere with the development of drug resistance as they can affect WT virus function through competitive inhibition during infection (Pathak & Nagy, 2009). Therefore, determining virus quantification between passages to ensure subsequent rounds of passages are performed at low multiplicity, such as performed in this study, would be expected to reduce the presence of DIPs.

Notable fluctuations in virus titre were observed over the course of all three PR8 MUd serial passage experiments (R1, R2 and R3) (Fig. 3.2). To determine whether this was an artefact of the likely contamination with a virus bearing PR8 segment 7, a further two passages were carried out with a plaque-purified PR8 virus (R4 and R5). However, these experiments also gave a similar pattern of fluctuating virus titre over the course of 9 passages. Initially, it was hypothesised that the observed variations in titre could be caused by the production of DIPs (despite controlling the MOI of each passage step), which would interfere with the function of the susceptible WT virus through competitive inhibition. An increase in DIPs can interfere with virus replication and therefore lead to decreases in virus titre. To determine if an increase in DIPs correlated with the decrease in viral titre observed at P3 and/or P6-7, the particle to PFU ratio was estimated by qPCR quantification of segment 7 to derive genome copy: PFU ratios (data not shown). However, these data were inconclusive and did not indicate any convincing differences in the proportion of infectious particles at the passages examined. Although it cannot be ruled out that DIPs did not cause this fluctuation in titre, it can be hypothesised that the low MOI conditions would have reduced this possibility.

Examination of KPT-335 sensitivity of the serial passaged viruses, showed that P3 and P6 viruses were all still largely susceptible to the compound as determined by plaque reduction assay (Fig. 3.3). These results seemed to contradict the increase in titre observed during the multi-passage experiments, which suggested that the viruses were already less susceptible to the compound at these sampling points (Fig. 3.2). Although R1 and R2 did not display a resistant phenotype at P6 (Fig.3.3), they did display a

smaller, less cytopathic plaque phenotype in the absence of drug, similar to the resistant phenotype observed at P10 for these viruses (Fig. 3.4). Thus indicating, that the viruses had phenotypically changed at these early passages and suggesting that KPT-335-resistance may come at a fitness cost to the virus. Further sequencing analysis of P3 and P6 viruses would determine if the potential drug-resistant mutations (Table 3.3) were present at these early passages, but this work was not carried out because of other priorities.

The plaque reduction data clearly revealed that R1-R3 (P10) and R4 (P9) viruses were no longer susceptible to the compound at 0.3 μM, indicating a drug-resistant phenotype. R1 and R2 isolates displayed a larger plaque phenotype in the presence of drug (Fig. 3.4) indicating these two populations were possibly now dependent on the drug and were the most drug-resistant isolates. All viruses were still largely inhibited at 1 μM, suggesting there was a threshold for KPT-335 resistance. The R5 pool of virus did not display a resistant phenotype by plaque reduction assay. Nevertheless, sequencing analysis did reveal a fixed mutational change (C333S) in the NP gene of R5 (P9) virus. IF analysis of P10 viruses (R1 and R3) supported the resistant phenotype observed in the plaque reduction assay data by showing that the drug no longer completely retained NP in the nucleus of the infected cells. Additionally, analysis of NP nuclear export by IF directly indicated that the serial passaged viruses have somehow escaped CRM1 inhibition.

Identifying resistance mutations by DNA sequence analysis of the relevant portions of the virus genome can be useful in predicting clinical outcomes and supporting the

proposed mechanism of action of the compound. It was evident that sequencing of R1-R3 isolates displayed a cleaner trace analysis than the P9 viruses for R4 and R5. Ideally, it would have been beneficial to also plaque purify R4 and R5 for sequencing but as a drug-resistant phenotype was observed and mutations present for R1-R3 this was not followed up. Many of the mutations discovered were discounted to simplify downstream analyses (as detailed in the next chapter). All nucleotide changes that translated to a silent mutation and those presenting heterozygous (mixed) nucleotide traces were not analysed further. The three mutations found in only 1 or 2 of the 3 isolates for R1-R3 (PB2; F551S, PB1; R363G and NP; A178T) were perhaps compensatory drug-resistant mutations and are discussed further in the subsequent chapter. The mutations discovered in all three isolates and in the P10 viruses containing homozygous nucleotide traces (Table 3.3:3.4 Fig. 3.9) were found in the NP gene suggesting that this protein was the major determinant of potential drug-resistance and therefore subsequent analysis was performed with the mutations found in this protein.

Widespread analysis of available IAV sequences revealed that none of the NP mutations were especially prevalent in human IAV strains (Fig. 3.10). In fact, 311R, 296H and 283S appeared in only one sequence and 333S was present in none of the available sequences. 309 was the only amino acid that had a notable number of sequences containing the mutation T (7 %). Interestingly, further analysis revealed that the T309 was mostly present in pre- 2009 pandemic strains (data not shown). These results of the IAV sequence screen suggests viruses containing the NP mutations are not naturally selected for in a biological setting. This would be advantageous if KPT-

335 was developed for use as a clinical antiviral as it suggests the compound would be effective against current circulating strains. Additionally, if KPT-335-resistance occurred in a clinical setting, the drug-resistant mutations found in this study, would result in a less fit virus as also shown by the plaque reduction data for R1 and R2 (Fig. 3.3; 3.4). These mutations would potentially make the virus unstable and therefore their ability to replicate and/or transmit within a population would likely be hindered. A literature search for IAV publications including these NP amino acid mutations was also conducted. Details of this search are presented in chapter 5 (Table 5.1).

NP, a key component of the vRNP complex, is a major determinant for vRNP import and export. Thus far, two nuclear localisations signals (NLS) and a cytoplasmic accumulation signal (CAS) have been identified for their involvement in vRNP transport. As mentioned previously, proteins containing a nuclear export signal (NES), are involved in export of proteins via cellular CRM1. Currently NS2 (NEP), with contains a NES motif, has been deemed the main mediator responsible for directing export of vRNPs. However, primary evidence suggested that exogenous NP can shuttle between the nucleus and cytoplasm (Whittaker *et al.*, 1996). Additionally, Neumann *et al., (*1997) found that the N terminal 38 amino acids of NP were capable of transporting RNPs from the nucleus to the cytoplasm. Since then, (Yu *et al.,* 2012), identified three novel NES motifs within the NP protein, two of which were CRM1-independent NES1 [24-49] and NES2 [183-197], and one CRM1-dependent NES3 [248-274]. The authors found that these motifs were sufficient to direct a GFP-NP-fusion protein from the nucleus to cytoplasm. The potential CRM1-inhibitor resistant mutations found in this study were present downstream of the CRM1-dependent NES

region, suggesting the potential of another unidentified NES motif. Although the Yu et al., study does not exclusively define that this NES motif could not be involved in CRM1-mediated export, it does suggest the hypothesis that vRNPs are unlikely to transport via this NES region alone. Interestingly, the fact that Yu *et al*., identified two NES that were CRM1 independent suggests the possibility that other export pathway may also be involved in the nuclear export of NP.

The NP structure presented in Fig. 3.11.C displays an H5N1 NP protein that was crystallised as a trimer. The NP crystal structure reveals two regions; a head domain and a tail loop region. On the core of the protein, within the head domain, lies a groove comprised of a largely positively charged surface region which forms ionic bonds with the negatively charged backbones of viral cRNA and vRNA. On the opposite side of this binding groove lies a flexible tail loop formed by residues 392-407 (H1N1). The four potential drug-resistant mutations were surface exposed on NP opposite the RNA binding cleft. The surface location of Q311R, N309T, Y296H and P283S suggests drug resistance may have occurred by changing NP's ability to bind directly to another protein involved in the nuclear export process such as CRM1, M1, NS2 or another unknown mediator. As mentioned previously, there is evidence to suggest that NP can bind directly to CRM1. An additional study has shown that overexpression of CRM1 biased transfected NP towards cytoplasmic accumulation and *in vitro*-binding assays determined that these two proteins interact (Elton *et al.*, 2001; Elton *et al.*, 2005). Two subsequent studies confirmed NP-CRM1 interactions in the absence of other IAV proteins (Chutiwitooncahi *et al.,* 2014; Kakisaka *et al*., 2015). Thus, direct interaction of NP with CRM1 may also take place during export of vRNPs. It is currently

hypothesised that nuclear export of vRNPs is mediated by the vRNP-M1-NS2-CRM1 complex. Currently there is no evidence to suggest that NP directly binds to NS2, however studies have indicated that M1 can interact with the vRNP complexes. It has been reported that an M1 NES motif can interact with vRNPs to promote export of the virus (Sakaguchi *et al.,* 2003). Additionally, another study discovered that the C-terminal domain of M1 bound to both RNPs and NP alone (Baudin *et al.,* 2001). Furthermore, by using recombinant proteins *in vitro*, Noton *et al.,* (2007) found that the middle domain of M1 was responsible for binding to NP, in the absence of a RNA interaction. Thus, although there are some discrepancies as to which M1 domain interacts with NP, it is clear that M1 can directly interact with NP in some manner. These data suggest that the NP mutations found in this study could possibly alter interactions with M1; however, a M1-binding region on NP has not yet been defined. Overall the surface exposure of these mutations suggested that the amino acid changes in NP allowed the virus to escape inhibition of CRM1-dependent export by altering an interaction with another protein. Based on current literature, the most likely interaction with NP would be hypothesised to be with CRM1 and/or M1. However, these mutations could also enhance interaction and/or disrupt binding to other proteins involved such as NS2 and/or an unknown mediator or potentially reveal that NP can interact with a novel cellular export pathway.

The data described in this chapter demonstrated that KPT-335-resistant IAVs could be developed after 9-10 passages in the presence of a suboptimal concentration of the compound. Sequencing analysis of potential drug-resistant viruses revealed the most likely mutations contributing to the resistant phenotype were found within the NP gene

and interestingly, four of the five NP-mutants were surface exposed. The next line of investigation was to confirm if these amino acid changes contributed to the resistant phenotype by generating recombinant viruses harbouring the mutations. Chapter 4 will describe the generation of NP-mutant viruses and testing their susceptibility to KPT-335 as well as utilising the recombinant viruses for further investigation into a mechanism of resistance.

Chapter 4 Investigating the genetic basis of resistance of influenza A virus to a selective inhibitor of nuclear export, KPT-335

4.1 Introduction

As described in chapter 3, the ability of IAV to develop resistance to the nuclear export inhibitor, KPT-335, was determined by serial passage of the virus in the presence of the compound. Analysing the coding sequences of the viral proteins thought to be potentially involved in the nuclear export process (PB2, PB1, PA, NP, M and NS) lead to the discovery of five amino acid changes within the NP gene. The changes Q311R, N309T, Y296H, P283S and C333S were found after 9 or more passages in five independent experiments. Reverse genetics allows for the introduction of a desired amino acid change into a wild-type (WT) virus for analysis of its phenotypic effect (Fodor *et al.,* 1999). In this chapter, site-directed mutagenesis was used (on plasmid-borne copies of segment 5) to introduce the NP mutations into the genetic background of a PR8 virus, a standard H1N1 laboratory strain. Determining if the NP amino acid substitutions reduced the virus' susceptibility to KPT-335 would test whether the changes identified in the passaged viruses were responsible for resistance. Further phenotypic analysis with the NP-mutant viruses could also help broaden knowledge of the biology of IAV genome nuclear export. Additionally, investigations into the mechanism of drug-resistance could eventually help the selection of alternative therapies if resistance was to occur and/or provide information into the development of novel antivirals.

The aim of this chapter was to firstly generate recombinant IAVs containing the potential KPT-335 resistant NP-mutations discovered in chapter 3. Initially, the mutant viruses were tested for their susceptibility to KPT-335 and the fungal-derived inhibitor LMB. Further investigations into a potential mechanism of resistance were performed by examining the phenotypic changes of the recombinant viruses compared to the WT PR8 virus. These analyses included examination of plaque size and viral protein localisation in the absence and presence of KPT-335, as well as investigating differences in viral gene expression and virion composition of the mutant viruses.

4.2 Results

4.2.1 Generation of recombinant viruses harbouring the potential KPT-335-resistant NP-mutations

As presented in chapter 3, sequencing analyses of the KPT-335 serial passaged viruses revealed mutations within the IAV NP gene. Although other genotypic changes were discovered, the NP mutations: Q311R, N309T, Y296H, P283S and C333S, were regarded as the most significant, as these substitutions were conserved between clonal isolates from passages R1-R3 and the consensus sequences from pools R4 and R5. Therefore, to simplify phenotypic investigations, the experiments in this chapter were performed with only the five NP amino acid changes. To determine if these mutations would confer a KPT-335-resistant phenotype, recombinant viruses harbouring the NP mutations were generated in a PR8 background. 293T cells were transfected with 8 pDUAL plasmids (Wit *et al.*, 2004), one for each segment of the IAV genome (Fig. 4.1). pDUAL plasmids contain a RNA polymerase II promoter that drives production of mRNA for IAV protein translation and an opposed RNA polymerase I promoter that drives production of 'vRNA-like' RNA for genome replication (Hoffmann *et al.,* 2000). Plasmids containing the potential drug-resistant mutations were generated by site-directed mutagenesis and transfected in place of the WT segment 5 plasmid. Virus supernatant was harvested at 72 h post-transfection and termed the P_0 stock. The P_0 stocks were then used to infect MDCK cells and the virus was propagated a further 48 h to obtain a larger quantity and higher titre of infectious virus. These P_1 stocks were harvested, clarified and the titre determined by plaque assay for use in subsequent experiments. A PR8-WT virus was generated as a positive control and a negative

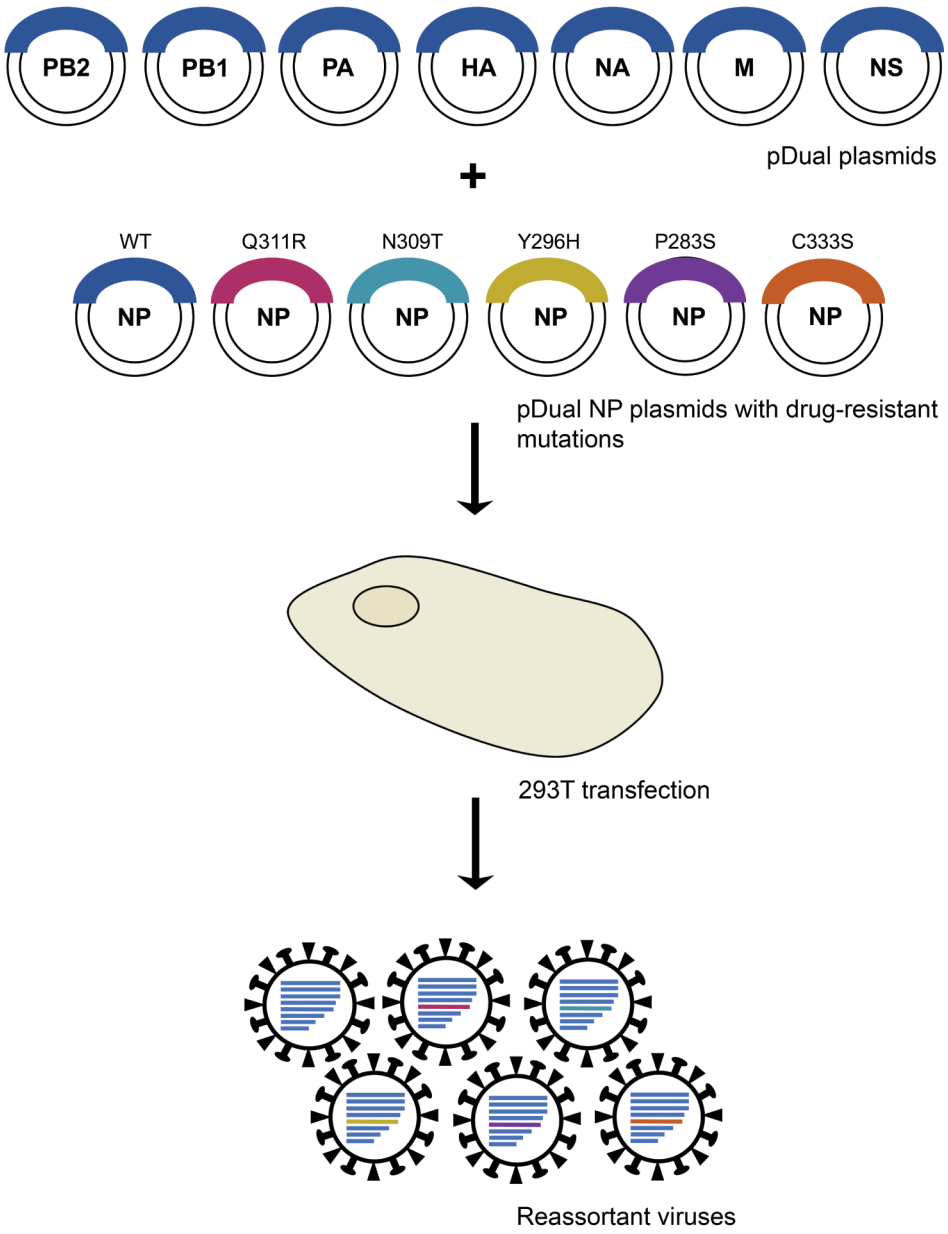

Fig. 4.1. Schematic of the 8-plasmid reverse genetics system to generate IAV strains harbouring KPT-335 selected mutations. 293T cells were co-transfected with 8 pDUAL plasmids, one for each segment of the IAV genome. NP plasmids encoding the mutations of interest were generated by site-directed mutagenesis and were co-transfected instead of the WT NP plasmid. Reassortant viruses were harvested 72 h post-transfection and the infectious virus particles were propagated for a further 48 h in MDCK cells.

control was also included which lacked a PB2 plasmid and therefore was unable to form infectious virus particles. Three independent rescues of the WT and the NP-mutant viruses (hereafter denoted by the amino acid alteration e.g. Q311R, N309T, Y296H, P283S and C333S) were performed to determine the reproducibility of any phenotypes presented. Replicates within the experiments presented in this chapter come from (at a minimum), one experiment performed with each of the three independently generated stocks for each virus. All viruses were confirmed to contain the desired NP substitutions by Sanger sequencing analysis of the cDNA of the NP gene (data not shown).

4.2.2 Replicative fitness of NP-mutant viruses

To determine if the NP amino acid substitutions affected IAV replicative fitness, virus replication was assessed by multi-cycle growth assays. MDCK cells were infected with WT PR8 or the NP-mutant viruses at an MOI of 0.01. At 24 h p.i., viral supernatants were harvested and the titres were determined by plaque assay. WT virus replicated to (on average) $>10^8$ PFU/ml (Fig. 4.2), as expected for PR8 under multi-cycle growth conditions. Q311R displayed a reduction in titre by ~2 $\log_{10}$ in comparison to the WT virus, down to ~10^5 PFU/ml. N309T, Y296H and P283S also presented slight reductions in replication by <1 $\log_{10}$ to ~$10^{7\text{-}8}$ PFU/ml. NP-mutant virus C333S showed little to no decrease in titre compared to the WT virus. However, due to the variability observed across the three independent experiments, none of the decreases were statistically different. Nevertheless, Q311R displayed a substantial reduction in replication in MDCK cells compared to the WT virus suggesting that the change reduced the replicative fitness of the virus.

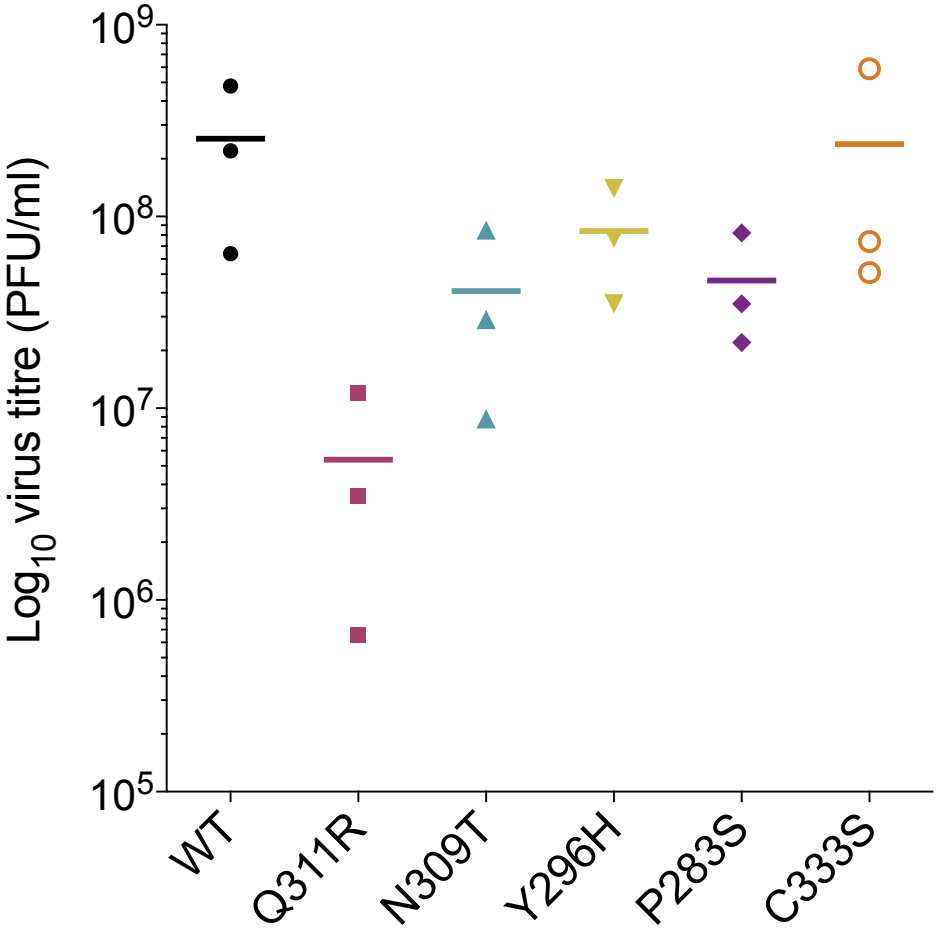

Fig. 4.2. Growth of NP-mutant viruses in MDCK cells. MDCK cells were infected with WT or mutant viruses at MOI 0.01. 24 h p.i. virus was harvested and titred. Data are the individual values and mean of three independently rescued viruses. Differences non-significant by one-way ANOVA.

4.2.3 Susceptibility of NP-mutant viruses to KPT-335

To determine if the NP amino acid substitutions allowed the virus to escape CRM1-inhbition, the susceptibility of the mutant viruses to KPT-335 were examined by dose-response assays as performed in chapter 2 (Fig. 2.1.D). A549 cells were infected with WT or the NP-mutant viruses at an MOI of 0.01 and treated with increasing concentrations of KPT-335, starting at 0.01 μM and increasing in 0.5 $\log_{10}$ increments to 1 μM. At 24 h p.i., virus supernatant was harvested and the titre determined by plaque assay. As expected, the WT virus was inhibited by KPT-335 in a dose-dependent manner, resulting in an IC_{50} value of 0.04 μM (Fig. 4.3), which was identical to the IC_{50} value established in chapter 2 for PR8 multi-cycle dose-response inhibition (Table 2.1). Both Q311R and N309T viruses were considerably less susceptible to KPT-335, giving much higher IC_{50} values of 1.93 μM and 0.68 μM, respectively. However, the lack of an appropriate dose-response inhibition curve resulted in a poor R^2 value of -0.1 for the curve fit used to estimate the IC_{50}, thus, the estimated value for Q311R could not be considered accurate. The N309T dose-response data resulted in a more appropriate curve shape, giving a more desirable R^2 value of 0.5. Here, the IC_{50} value was 17-fold greater than that obtained for the WT virus. Y296H, P283S and C333S viruses were inhibited by KPT-335 in a dose-dependent manner resulting in IC_{50} values of 0.13 μM, 0.18 μM and 0.1 μM, respectively; figures that were slightly (3-4-fold) greater than the WT value. However, as well as the small increase in IC_{50} value, the Y296H virus was noticeably less susceptible to 1 μM drug than WT, with titres decreased on average by less than 10-fold. The P283S virus was also less susceptible than WT to the highest drug concentration although the difference was less marked. In contrast, the C333S virus was apparently more sensitive than WT to higher

drug concentrations (0.3 μM and 1 μM). Overall, the dose response data revealed that Q311R and N309T were substantially less susceptible to KPT-335 than the WT virus with Q311R presenting the most drug-resistant phenotype. Data were less clear-cut for the other viruses but were suggestive of lesser degrees of resistance for Y296H and P283S, and an altered but not clearly resistant susceptibility profile for C333S.

To further characterise the sensitivity of the NP mutant viruses to KPT-335, plaque reduction assays were performed as in chapter 3 (Fig. 3.3;3.4). MDCK cells were infected with WT or the NP-mutant viruses with 100 PFU per well in the presence of DMSO (0 μM) or KPT-335 (0.3 μM or 1 μM). AT 48 h p.i., cells were fixed and stained with toluidine blue to visualise plaque formation. As before, WT virus plaque formation was inhibited in the presence of 0.3 μM and 1μM of KPT-335. Both P283S and C333S viruses were also inhibited by KPT-335 at both drug concentrations (Fig.4.4). In contrast the Q311R, N309T and Y296H viruses presented plaques in the presence of 0.3 μM drug, although plaque formation was still mostly inhibited at 1 μM. The N309T and Y296H viruses generally displayed a smaller plaque phenotype in the presence of the compound compared to the larger plaque phenotype present in the absence of compound, whereas Q311R presented a similar plaque size in both the absence and presence of compound. Notably, in the absence of compound, Q311R displayed a hazy plaque phenotype distinct from the larger and clearer plaques presented by the WT and the other mutant viruses. This phenotype was consistent with the plaque reduction data for the R1 pool of viruses (Fig. 2.3) in which the mutation Q311R was discovered, suggesting that this amino acid change was responsible for the change in plaque morphology. Overall these results showed that Q311R, N309T and

A

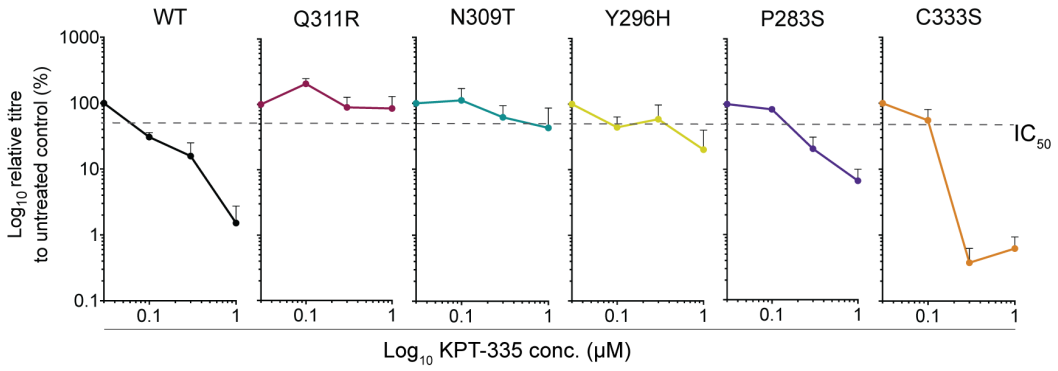

B

Virus	IC_{50} (μM)	95% CI	R^2	IC_{50} fold increase to WT
WT	0.04	0.01 to 0.16	0.7	-
Q311R	1.93	Very wide	-0.1	48
N309T	0.68	0.05 to 8.3	0.5	17
Y296H	0.13	0.001 to 13	0.5	3
P283S	0.18	0.1 to 0.24	0.9	4
C333S	0.10	0.05 to 0.19	0.6	3

Fig. 4.3. Efficacy of KPT-335 against NP-mutant viruses. (A) Dose response efficacy of KPT-335**.** A549 cells were infected with WT or mutant viruses at MOI 0.01 and treated with increasing concentration of KPT-335. 24 h p.i. virus was titred by plaque assay. Data are the mean ± S.E.M of three independent experiments each performed with an independent virus rescue. **(B)** Table displaying IC_{50} values and 95% confidence intervals (CI) for the WT and NP-mutant viruses with their corresponding goodness-of-fit R^2 values. Values were determined by curve fitting with a non-linear regression model. The fold change of the mutant virus IC_{50} values is displayed in comparison to the WT IC_{50} value. Dotted line indicates the ~IC_{50} value on the graph

Y296H viruses were less susceptible to KPT-335 inhibition at 0.3 μM compared to the WT virus, thus indicating that these NP mutations allowed the virus to partially escape CRM1-inhbition. However, all three viruses formed little to no plaques in the presence of the higher compound concentration suggesting the NP mutations did not allow the virus to fully escape CRM1 inhibition. In addition, the susceptibility of P283S and C333S to KPT-335 inhibition was similar to that of WT virus, indicating that these mutations did not elicit drug-resistance measurable by this assay.

The plaque reduction data (Fig. 4.4) suggested a difference in the NP-mutant virus plaque size in the presence and absence of compound. To quantify the difference in cell-to-cell spread, the viruses were grown in the absence or presence of a sub-inhibitory concentration of KPT-335 (0.15μM) and instead of relying on cell lysis and counterstaining of the cell monolayer with toluidine blue to detect gross CPE, immunostaining of viral NP was performed for increased sensitivity and accuracy of measuring plaque size. MDCK cells were infected with 100 PFU/well of WT or the mutant viruses in the absence (DMSO) or the presence of KPT-335 (0.15μM). At 48 h p.i., cells were fixed, permeabilised and stained with anti-NP. Plaque diameter was quantified using ImageJ software and ~20 plaques were measured per well.

In the absence of compound, the WT virus presented the largest plaque phenotype, with all NP-mutant viruses presenting significantly smaller plaques (Fig.4.5 A.B). In the presence of compound, a small plaque size was displayed by all viruses with no significant differences in size between the WT and the NP-mutant viruses (Fig.4.5. AB). The difference in plaque size in the presence and absence of compound was

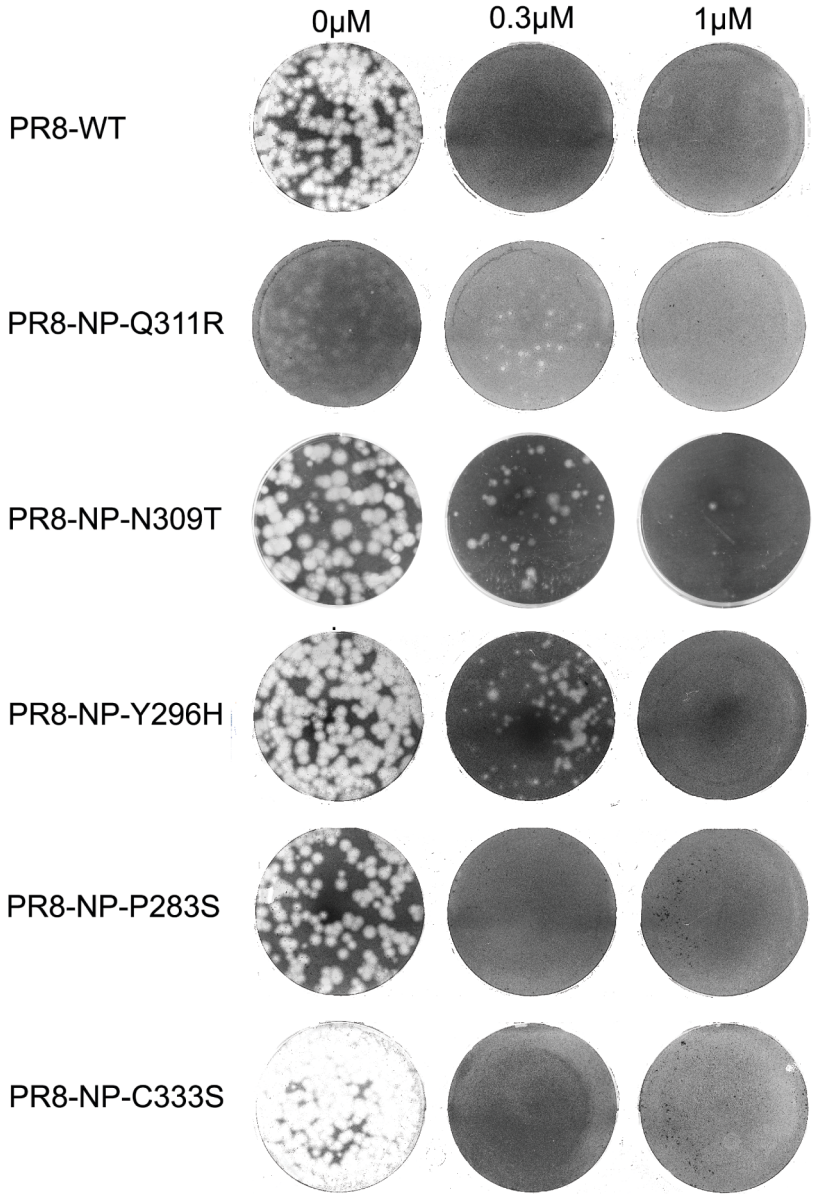

Fig. 4.4. Plaque reduction assays with the NP-mutant viruses. MDCK cells were infected with WT or mutant viruses at 100 PFU/well in the presence (0.3 μM, 1 μM) or absence (0 μM) of KPT-335. 48 h p.i. cells were fixed and stained with toluidine blue and imaged.

calculated and is presented in Fig.4.5.C as a fold change. By this metric, WT virus showed the largest reduction in plaque size after treatment with KPT-335 (Fig. 4.5.BC). N309T, Y296H, P283S and C333S displayed smaller differences in virus spread after drug treatment; however, these changes in plaque size were not significantly different from that of WT virus (Fig. 4.5.C). Notably, Q311R spread was not affected by the presence of compound (in fact the average plaque size was marginally higher in the presence of drug), resulting in a significant difference in fold change compared to the WT (Fig.4.5.C). Overall these results showed that all NP-mutant viruses were less able to spread in tissue culture than the WT virus in the absence of the drug. KPT-335 did not affect the plaque size of the NP-mutant viruses to the same magnitude as with WT which may correlate to the initial smaller plaque size presented by the NP-mutant viruses. The NP-mutant Q311R displayed a similar, if not slightly enhanced, plaque phenotype in the presence of the drug, which may indicate that this drug-resistant mutation came at a fitness cost to the virus.

4.2.4 Immunofluorescent investigation of viral protein localisation during infection with NP-mutant viruses

KPT-335 blocks the nuclear-cytoplasmic transport of vRNPs as shown previously by examination of NP intracellular localisation at late stages of infection. To determine if the NP-mutant viruses were inhibited by KPT-335 at the stage of nuclear export, IF analysis was performed as described in prior chapters. A549 cells were infected with WT or mutant viruses at an MOI of 3 in the absence (DMSO) or presence (0.3 μM or 1μM) of KPT-335. 8 h p.i. cells were fixed, permeabilised and immunofluorescently

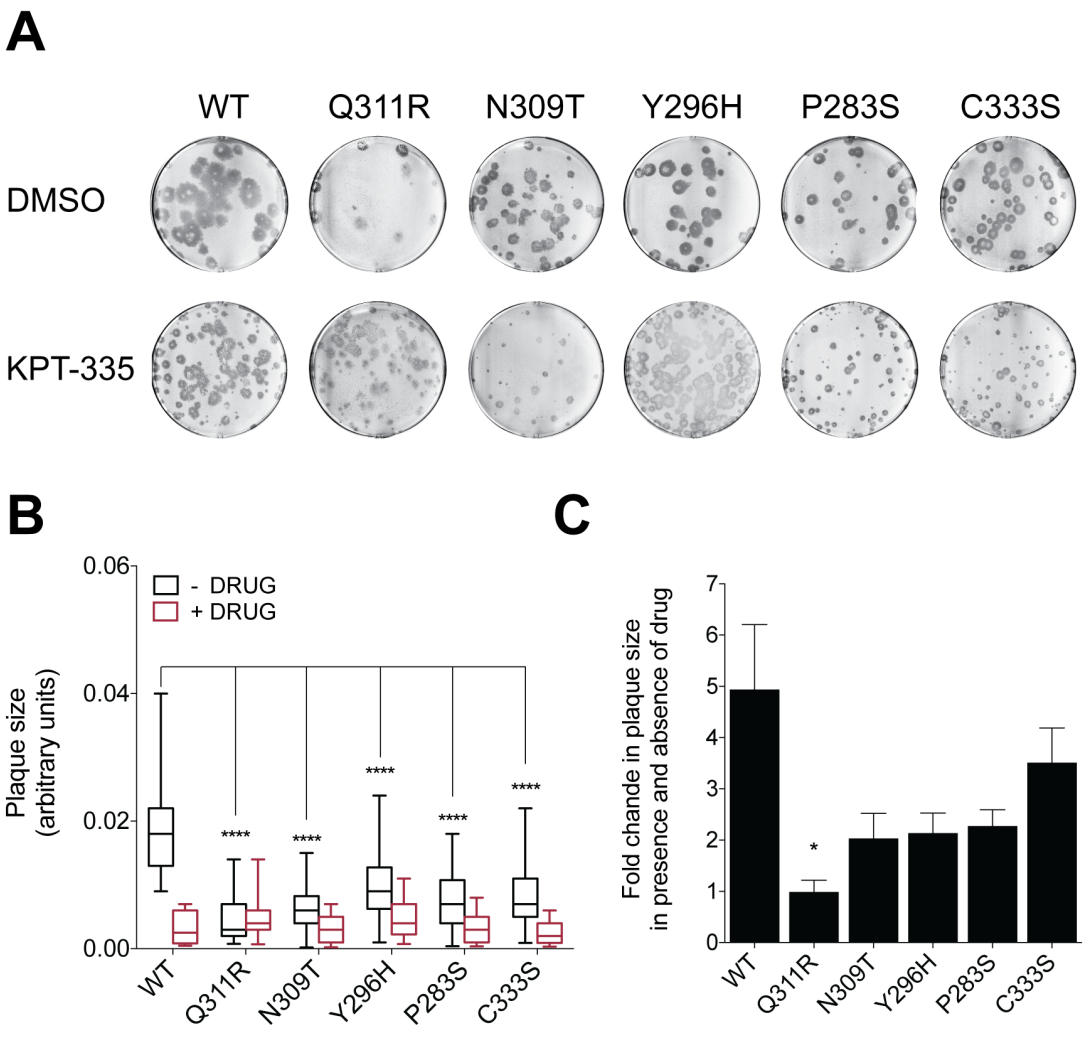

Fig. 4.5 Plaque size of NP-mutant viruses in the presence and absence of KPT-335. (A) Immunostained plaque assays. MDCK cells were infected with 100 PFU/well of WT and the mutant viruses in the presence (0.15μM) or absence (DMSO) of KPT-335. 48 h p.i. cells were fixed and stained with anti-NP to visualise virus spread **(B)** Quantification of plaque size. The diameters of infected foci were measured using ImageJ software. Around 20 plaques were measured per well from three independent experiments. ****<0.0001 in one-way ANOVA. **(C)** Fold change in plaque size in the presence and absence of drug. Data are the mean ± S.E.M of three independent experiments *<0.01 in one-way ANOVA.

stained for NP (green) and a nuclear stain (DAPI; blue). As expected, in the absence of compound, WT infected cells displayed cytoplasmic NP staining, indicating that nuclear export of the replicated viral genome had taken place (Fig. 4.6). A similar cytoplasmic NP pattern was observed for all the mutant viruses in the absence of compound. WT infected cells, in the presence of drug, displayed partial nuclear retention of NP at 0.3 μM and full nuclear NP retention at 1 μM, as shown previously for PR8 virus. In the presence of 0.3 μM compound, Q311R and N309T infected cells displayed noticeably more cytoplasmic NP than the WT virus, suggesting reduced susceptibility to KPT-335 inhibition. Y296H and P283S infected cells gave less cytoplasmic NP than Q311R and N309T but still more than the WT at 0.3 μM. C333S displayed a similar NP pattern to the WT at 0.3 μM, with no visible export. All mutant virus NPs were retained in the nucleus of cells in the presence of the higher concentration of 1 μM drug, suggesting that these mutations alone were not adequate for the virus to fully escape KPT-335-mediated inhibition of the nuclear export process. Overall these results suggest a variance in susceptibility of the NP-mutants, with Q311R and N309T showing the greatest drug-resistant phenotype, Y296H and P283S showing a partial drug-resistant phenotype and C333S displaying a similar phenotype as WT virus.

To assess the reproducibility of the NP intracellular retention data in Fig. 4.6, analyses of multiple dose-response IF assays were carried out. Images were taken as single optical slices through the middle of the cell and areas of cells were chosen at random. Infected cells were scored for whether NP was predominantly and/or partially localised in the nucleus. As previously observed for the WT virus, NP was mostly cytoplasmic in the absence of compound (DMSO) with <10 % of cells showing nuclear retention

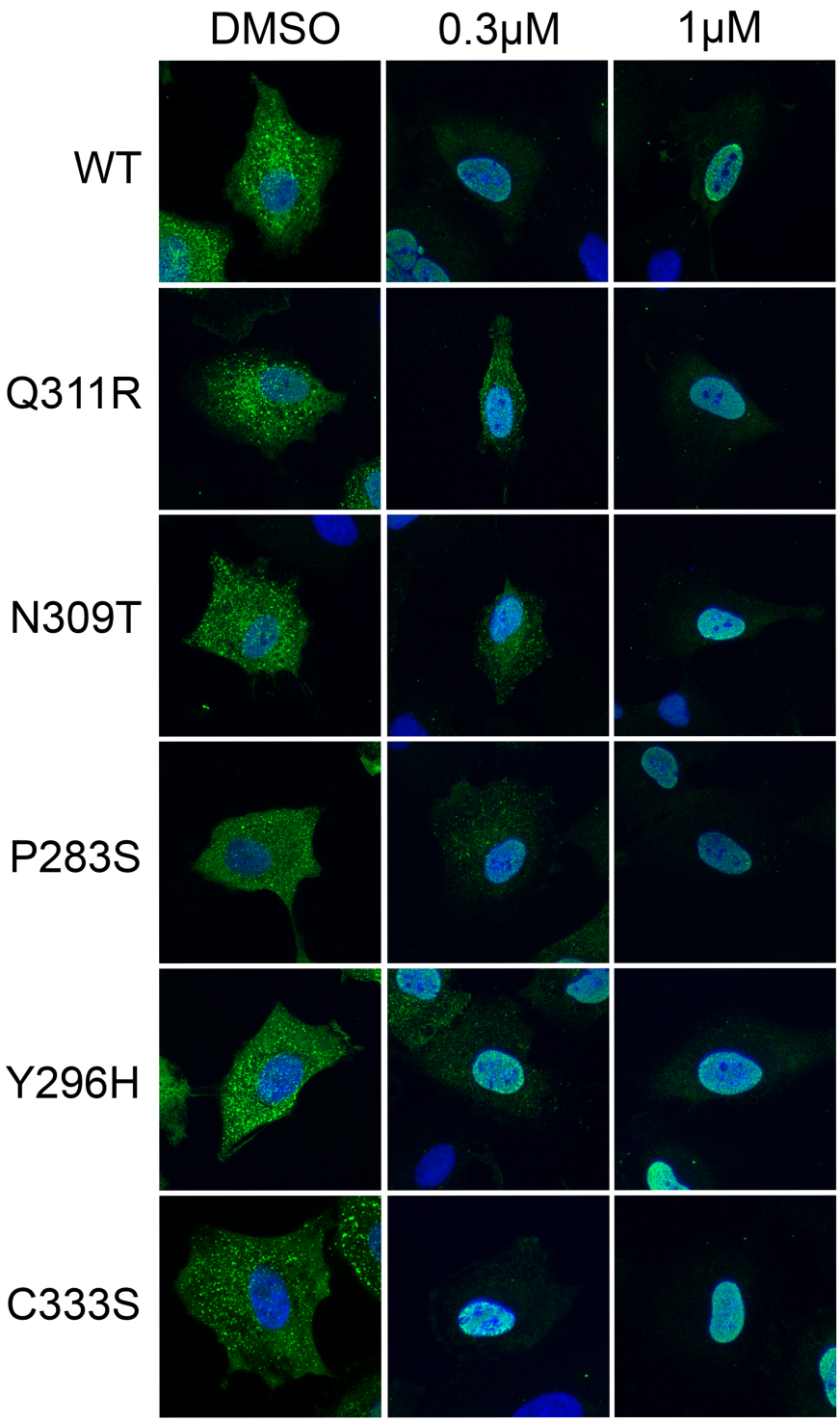

Fig. 4.6. Intracellular localisation of NP during infection with NP-mutant viruses in the presence of KPT-335. A549 cells were infected at MOI 3 with WT or NP-mutant viruses in the presence (0.3μM or 1μM) or absence (DMSO) of KPT-335. 8 h p.i. cells were stained with anti-NP (green) and a nuclear stain (DAPI; blue) and imaged by confocal microscopy. Images shown were taken as single optical slices.

(Fig. 4.7.B). This was similar for all the NP-mutant viruses in the absence of compound. WT virus displayed ~40-50 % of cells with full or partial nuclear NP at 0.3 μM. In comparison, Q311R and N309T infections gave only ~10-20 % of cells with NP nuclear retention, which was significantly lower than the values obtained for WT at this concentration (Fig. 4.7.B). Y296H, P283S and C333S viruses displayed similar NP retention patterns to WT virus. Although there was some evidence of reduced susceptibility for Y296H at 0.3 μM (~30 % retention), none of these viruses had showed a significant difference in the number of cells with RNP nuclear retention in comparison to the WT. All viruses displayed ~70-90 % NP nuclear retention at 1 μM drug with no significant differences between viruses. Notably, a ring-like formation of NP staining around the inner edge of the nucleus was observed for WT, Y296H, P283S and C333S infections in the presence of KPT-335 (Fig. 4.7.A), a similar phenotype observed in chapter 3 for PR8-WT (Fig. 3.8). However, this ring of NP was not evident in Q311R or N309T infected cells. Overall these results indicated that Q311R and N309T were least susceptible to CRM1-inhibiton. In addition, the difference in intranuclear NP distribution presented by Q311R and N309T may suggest a change in normal vRNP export.

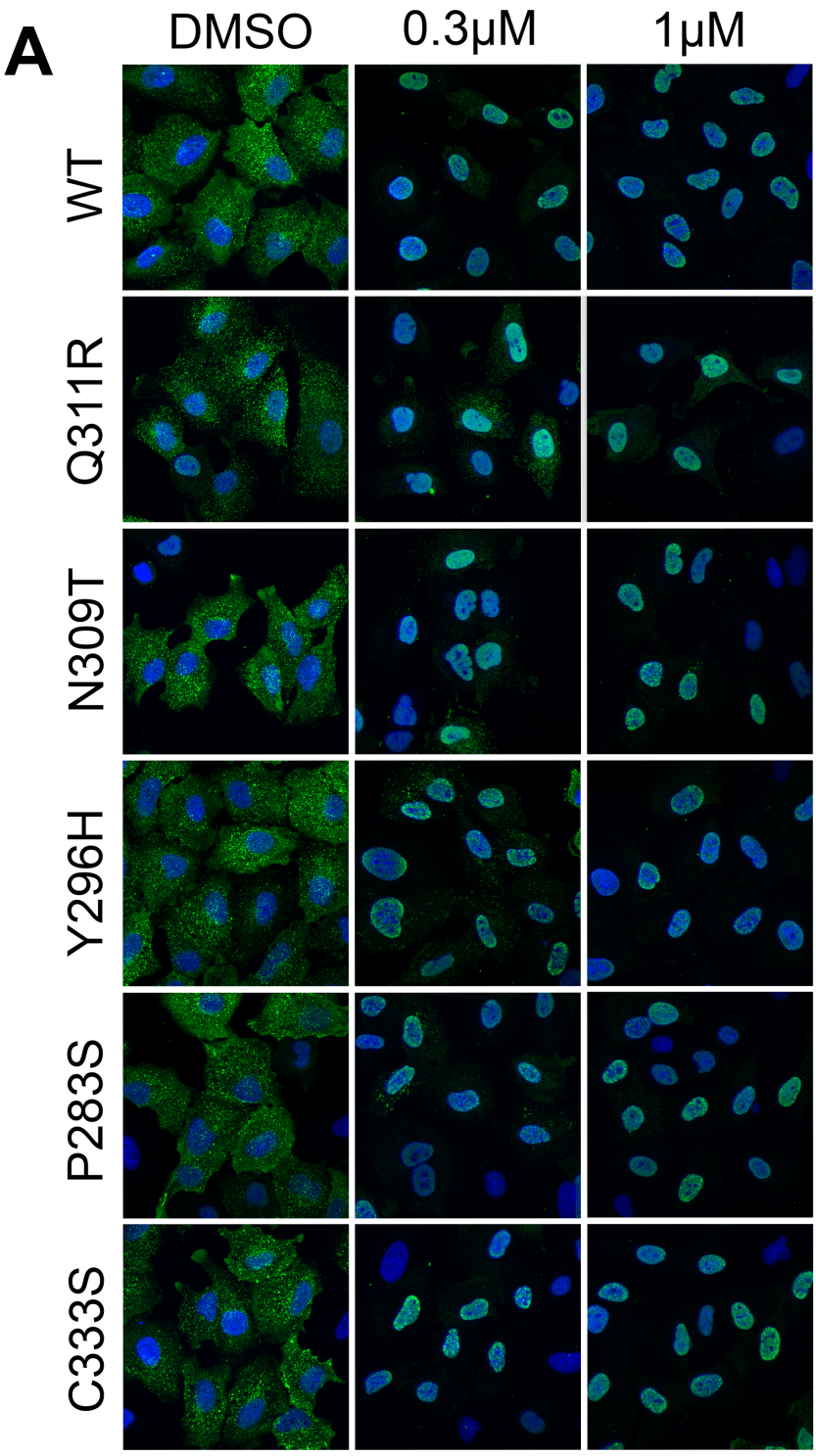

Fig. 4.7. Effect of KPT-335 on intracellular localisation and accumulation of NP in NP-mutant viruses. (A) A549 cells were infected at MOI 3 with WT or NP-mutant viruses in the presence (0.3μM or 1μM) or absence (DMSO) of KPT-335. 8 h p.i. cells were stained with anti-NP (green) and a nuclear stain (DAPI; blue) and imaged by confocal microscopy.

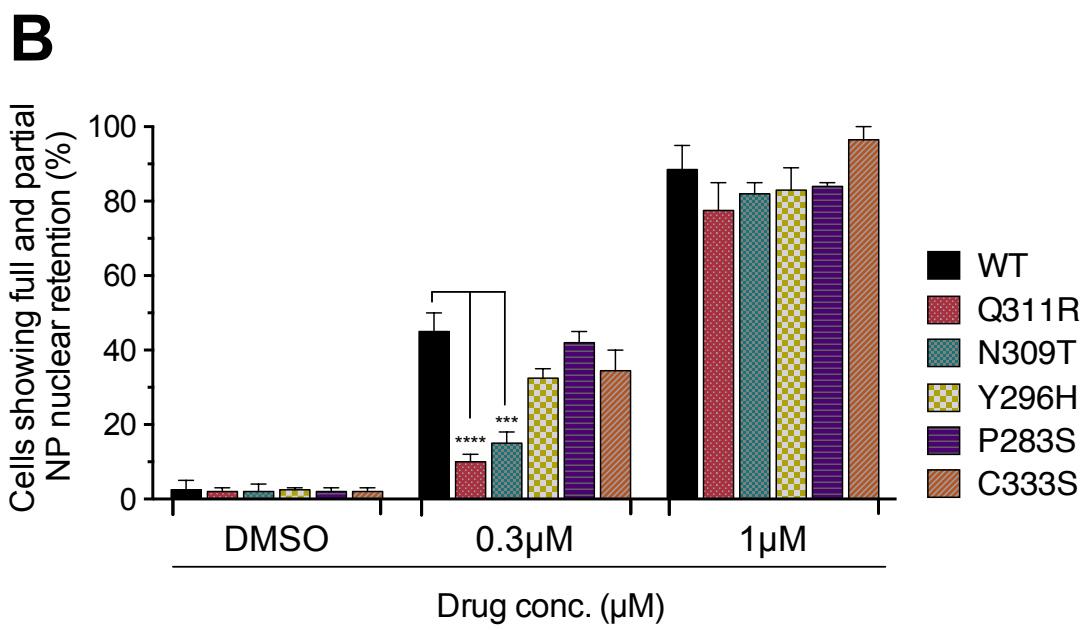

Fig. 4.7. Quantification of the effect of KPT-335 on intracellular localisation of NP with NP-mutant viruses. Quantification of NP nuclear retention after KPT-335 treatment. Cells with predominately nuclear NP were scored. Counts were taken from three images per drug concentration from two independent experiments and are plotted as mean ± S.D. *** p< 0.001, **** p <0.000 1 in one-way ANOVA

Viral proteins M1 and NS2 are described as mediators involved in canonical CRM1-mediated nuclear export of vRNPs (reviewed in Paterson *et al.,* 2012). As previously shown in chapter 2, KPT-335 treatment did not alter the cytoplasmic localisation of M1 and NS2 during late stages of virus infection. To determine whether localisation of M1 and NS2 was altered during infection with the two most phenotypically drug-resistant NP-mutant viruses Q311R and N309T, infected cells were treated with KPT-335 and M1 and NS2 protein localisation examined by IF. As described previously for Fig. 4.6, A549 cells were infected with WT or the mutant viruses at an MOI of 3, in the absence (DMSO, '-') or presence (0.3 μM, '+') of KPT-335. At 8 h p.i., cells were permeabilised and immunofluorescently stained for NP (as a positive control for drug inhibition), M1 or NS2 (green) and a nuclear stain (DAPI; blue). As expected, mock infected cells showed little to no viral protein staining (Fig. 4.8). WT infected cells displayed punctate cytoplasmic NP in the absence of drug and nuclear NP in the presence of drug, indicating successful inhibition of nuclear export. Q311R and N309T infected cells displayed a similar cytoplasmic NP staining pattern to the WT in the absence of drug and some cytoplasmic staining in the presence of 0.3 μM as previously observed (Fig. 4.8), again suggesting that while hindered, RNP nuclear export was not blocked as effectively. However, M1 and NS2 localisation remained unchanged, in the absence and in the presence of KPT-335, displaying a mostly diffuse cytoplasmic localisation for all viruses analysed. Overall these results show that M1 and NS2 localisation was unaffected by CRM1-inhibition (as shown previously) and that the NP Q311R and N309T mutations did not alter normal M1 and NS2 localisation.

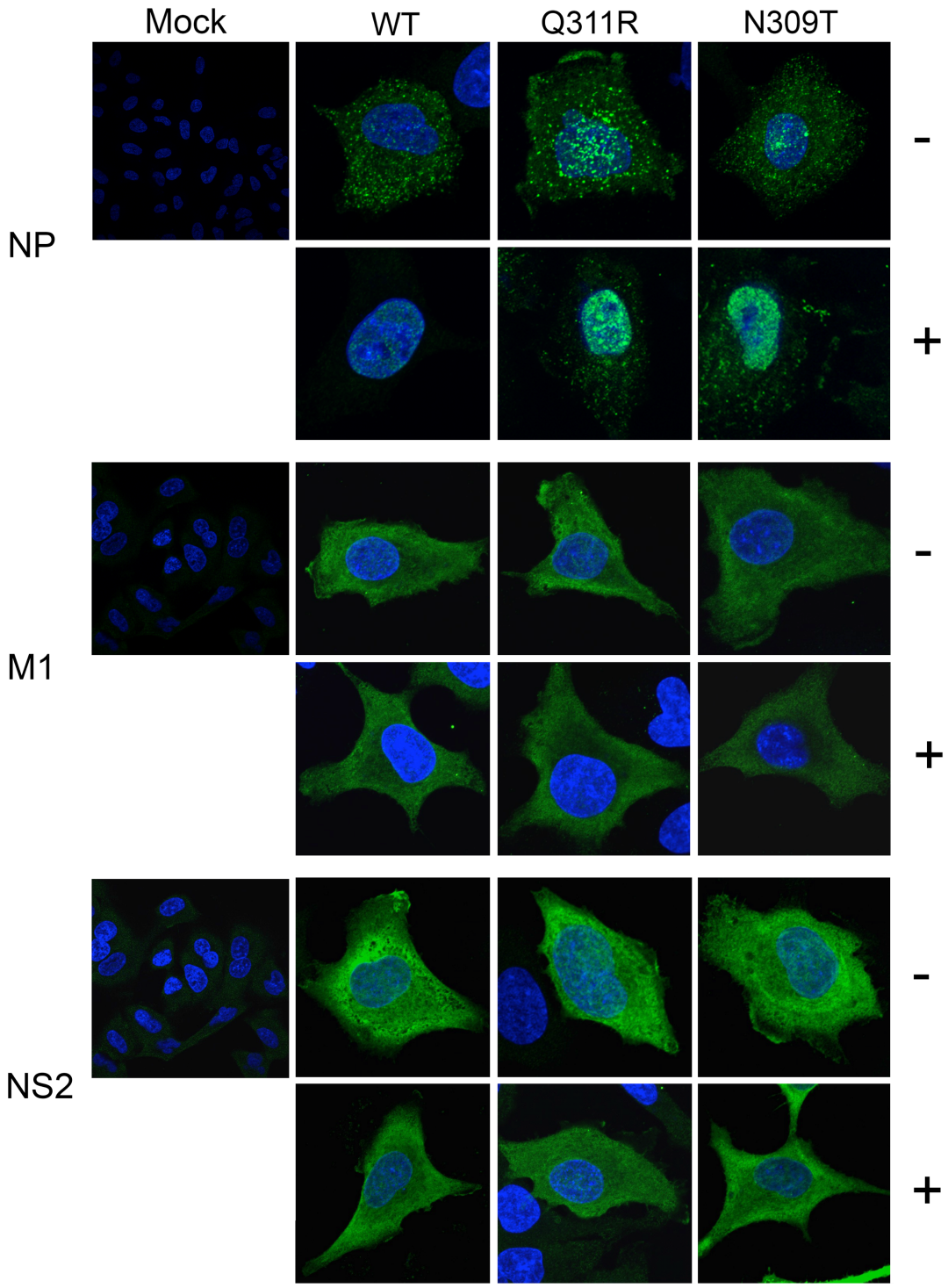

Fig. 4.8. Effect of KPT-335 on localisation of M1 and NS2 during infection with NP-mutant viruses. A549 cells were infected with WT, Q311R or N309T viruses at MOI 3 in the presence 0.3μM (+) or absence (-) of KPT-335. 8 h p.i. cells were stained with anti-NP, anti-M1 and anti-NS2 (all green) and a nuclear stain (DAPI; blue) and imaged by confocal microscopy. Images taken as maximum intensity projections.

4.2.5 Susceptibility of NP-mutant viruses to LMB

LMB is an irreversible inhibitor of CRM1 and therefore a more potent blocker of CRM1-mediated nuclear export than the SINEs. If the NP-mutant viruses escaped the permanent blockade of CRM1 by LMB, it could suggest that the viruses were utilising another cellular nuclear export pathway. A549 cells were infected with WT or the mutant viruses at an MOI of 0.01 and treated with increasing concentrations of LMB, starting at 3 nM and increasing in 0.5-log_{10} increments to 30 nM. At 24 h p.i., virus titre was determined by plaque assay. WT virus was inhibited by LMB in a dose-dependent manner such that 3 nM compound reduced titre by >50 % and 10 nM by nearly 99 % (Fig. 4.9). Curve fitting to the data resulted in an estimated IC_{50} value of 0.3 nM (R^2 value = 0.5) (Fig.4.9). The multicycle LMB IC_{50} value determined in chapter 2 was 6 nM, indicating an inconsistency in antiviral activity of LMB between the two experiments, possibly due to different batches of compound. The Q311R and N309T viruses were also inhibited by LMB in a dose-dependent manner, resulting in IC_{50} values of 0.7 nM and 0.6 nM, respectively. These IC_{50} values were ~2-fold greater than the WT value however, due to low R^2 values (0.5 and 0.4) it could not be confidently concluded that Q311R and N309T were significantly less susceptible to LMB than the WT virus. Y296H and C333S were also inhibited by LMB, although both viruses were more sensitive to low doses of the compound, resulting in ~100 and ~600-fold smaller IC_{50} values than the WT, respectively. P283S was also more sensitive to LMB, especially at the lowest drug concentration tested. However, a suitable dose-response curve could not be fitted and subsequently an IC_{50} value could not be determined. Overall these data conclude that

the NP mutations did not allow the virus to fully escape LMB inhibition and that interestingly three of the mutant viruses (P283S, Y296H and C333S) were more susceptible to irreversible CRM1 inhibition.

4.2.6 Effect of NP-mutants on viral gene expression

The reduction in replicative fitness of the two most phenotypically KPT-335-resistant mutant viruses, Q311R and N309T (Fig 4.2), suggested that the escape mutations came at a cost to virus fitness. To determine if the reduced virus fitness correlated with a reduced ability of the NP-mutant polypeptides to support viral gene expression, their function in RNP reconstitution assays was assessed. This assay indirectly measures mRNA production from synthetic vRNA-like templates encoding a reporter gene by the viral polymerase (Huang *et al.,* 1990). pDUAL plasmids for the protein components of the viral RNP (PB2, PB1, PA and NP; "3PNP") are co-transfected. Transcription of these plasmids by cellular RNA polymerase II produce the viral polypeptides. A vRNA-like luciferase reporter gene construct is also co-transfected, which contains the UTRs of PR8 segment 8 flanking an antisense luciferase gene, all under the control of an RNA polymerase I promoter. This plasmid is transcribed by cellular RNA polymerase I to produce RNA that sufficiently resembles vRNA to the IAV components to be assembled into an RNP. The viral polymerase then transcribes it into mRNA which is translated to produce luciferase (Lutz *et al.,* 2005). The luciferase output is therefore directly proportional to the activity of the viral polymerase, which (importantly for this experiment) is influenced by the support function of NP (Elton *et al.,* 1999).

A

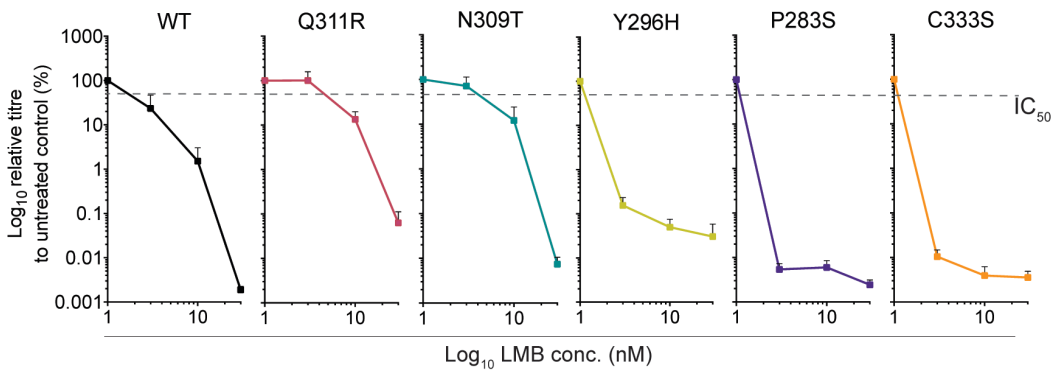

B

Virus	IC_{50} (nM)	95% CI	R^2	IC_{50} fold change to WT
WT	0.3	0.3 to 0.4	0.5	-
Q311R	0.7	Very wide	0.5	↑2.3
N309T	0.6	0.2 to 0.8	0.4	↑2
Y296H	0.003	0.0004 to 0.1	0.5	↓100
P283S	-	-	-	-
C333S	0.0005	0.00001 to 0.1	0.4	↓600

Fig. 4.9. Efficacy of LMB against NP-mutant viruses. (A) Dose response efficacy of LMB against NP-mutant viruses. A549 cells were infected with WT or NP-mutants at MOI 0.01 and treated with increasing concentrations of LMB. 24 h p.i. virus was titred by plaque assay. Data are the mean ± S.E.M of three independent experiments performed with three independent virus rescues. **(B)** Table displaying IC_{50} values and 95% confidence intervals (CI) for the WT and NP-mutant viruses with their corresponding goodness-of-fit R^2 values. Values were determined by a non-linear regression model. The fold change of the NP-mutant viruses IC_{50} values are displayed in comparison to the WT IC_{50} value. Dotted line indicates the ~IC_{50} value on the graph.

Equal numbers of 293T cells were co-transfected in a 24-well plate alongside the pDUAL plasmids of each component of the PR8 RNP (3PNP) using WT segment 5 (NP) or plasmids containing the mutations; Q311R, N309T, Y297H, P283S or C333S, along with the luciferase vRNA reporter plasmid. At 48 h post-transfection, all the cells from each well were lysed and luciferase activity was measured. A 'minus PA' negative control was included, therefore the full polymerase complex would not form and luciferase activity measured would be considered background (data not shown). NP-mutant RNP activity was normalised to the WT value (100 %) (minus background activity). Q311R and N309T NP plasmids gave a 10-30 % reduction in relative luminescence, which was statistically insignificant when compared to the WT (Fig. 4.10). However, Y296H, P283S and C333S had significantly lower relative activity (by ~40-70 %) than WT NP. Interesting, the two least fit and most phenotypically drug-resistant mutants Q311R and N309T did not display a significant difference in gene expression in comparison to the WT as measured by this assay. Thus, KPT-335-resistance and/or reduced replicative fitness did not necessarily correlate to with decreases in the viral gene expression.

4.2.7 Viral gene expression during infection with NP-mutant viruses

To determine if the NP-mutations affected viral gene expression during infection, western blot analyses were performed with infected cell lysates from a single cycle growth assay. MDCK cells were mock infected or infected with WT or the mutant viruses at an MOI of 3. 16 h p.i. cells were lysed and analysed by SDS-PAGE and western blotting for viral proteins PB1, HA, NP, M1, M2, NS1 and NS2 and cellular

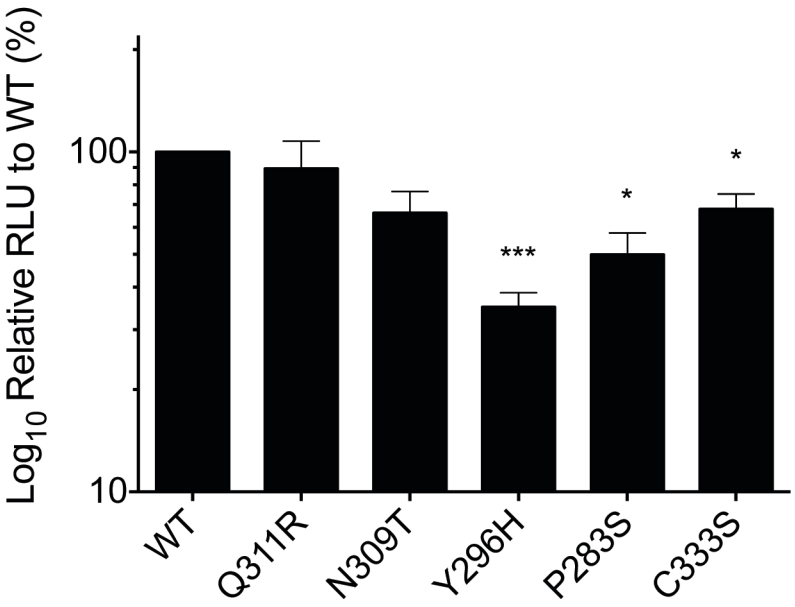

Fig. 4.10. Transcriptional activity of NP-mutants. 293T cells were co-transfected with pDUAL PB1, PB2, PA and WT or mutant NP plasmids along with an RNA polymerase I firefly reporter vRNA plasmid. Luciferase activity was measured 48 h post transfection. Data are the means ± S.E.M of three independent experiments each carried out in triplicate. *p<0.05, ** p<0.01,***p<0.001 (one-way ANOVA with original data values).

tubulin as a loading control. Mock infected samples did not contain any viral proteins, as expected (Fig. 4.11). Comparable amounts of the viral proteins PB1, HA, NP, M2 and NS1 were present in all infected cell lysates. However, Q311R and N309T infections displayed increased accumulation of M1 and NS2, both of which are mediators thought to be involved in nuclear-cytoplasmic export of vRNPs via the CRM1 pathway (reviewed in Eisfeld *et al.*, 2015).

To determine the reproducibility of this apparent difference in M1 and NS2 expression, the amounts of these polypeptides were quantified from five independent experiments and normalised to the tubulin loading control. The Q311R and N309T infected cell lysates consistently presented around twice the amount of M1 in comparison to the WT infection. However, the increase in NS2 (as shown in Fig. 4.11.A) was less reproducible, leading to an average ~1.5-fold increase but with a high standard error. Consequently, the differences in NS2 abundance were not statistically significant when compared to the WT virus. Y296H, P283S and C333S NP-mutant viruses produced similar quantities of both M1 and NS2 relative to the WT virus. Overall the western blot analysis revealed significantly increased M1 expression during a single round of Q311R and N309T virus replication.

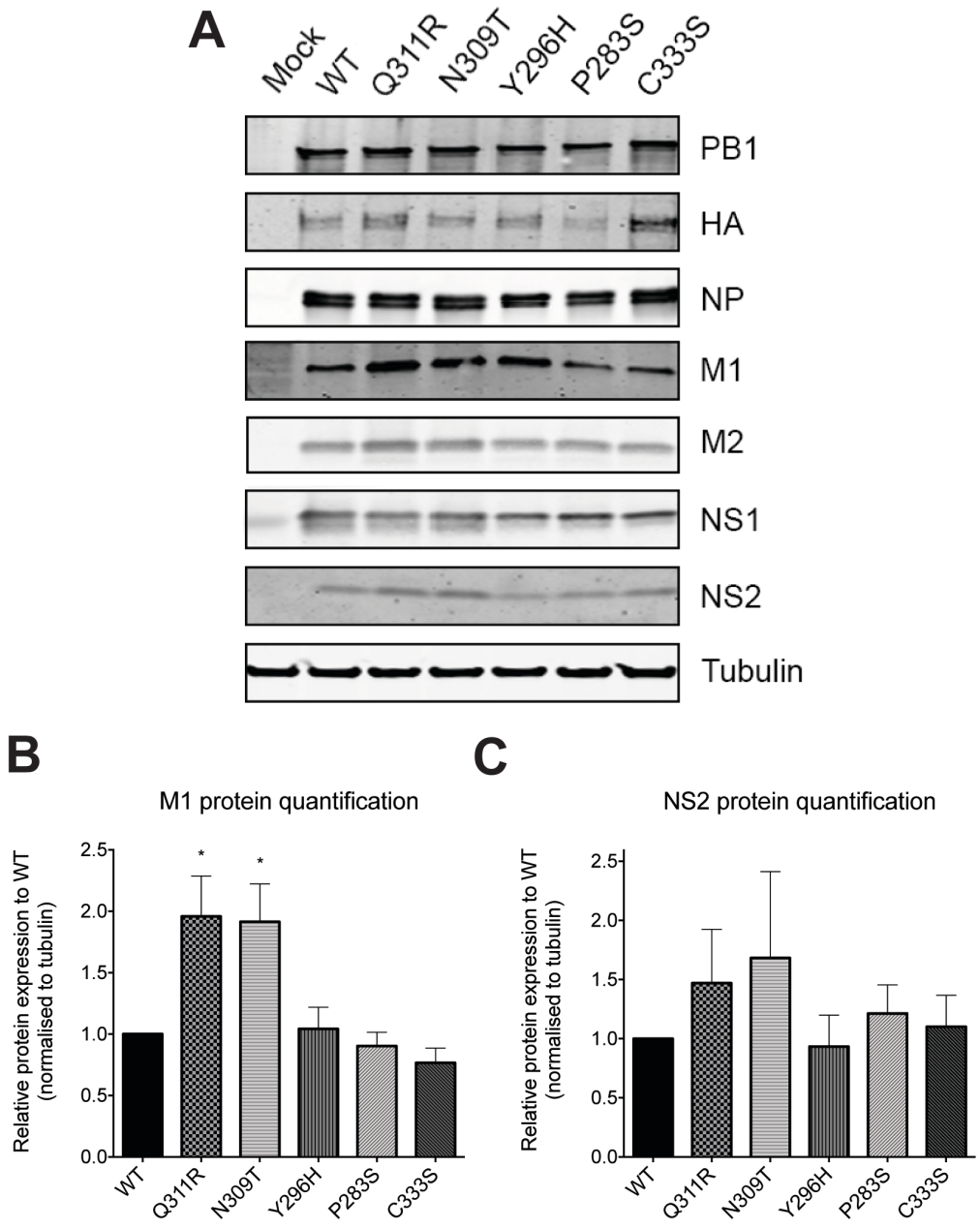

Fig. 4.11. Viral gene expression in a single cycle growth assay. (A) Western blot of infected cell lysates for viral proteins. MDCK cells were infected (or mock infected) with WT or mutant viruses at MOI 3. 16 h p.i. infection cells were lysed and analysed by SDS-PAGE and western blotting for viral proteins PB1, HA, NP, M1, NS1, and NS2 and cellular alpha tubulin as a loading control. **(B)** M1 or **(C)** NS2 protein quantification. Protein bands were quantified using ImageStudio Li-cor software and normalised to tubulin and then the WT data. Data are the mean ± S.E.M of 5 independent experiments. *$p<0.05$ in unpaired t-test.

4.2.8 Virion protein analysis of purified NP-mutant viruses

As presented in the previous section, an increase M1 expression was observed during single cycle infections with the Q311R and N309T viruses (Fig. 4.11). To determine if the increase in the viral M1 protein was represented in released virus particles, purification of the WT and the five NP-mutants was performed to analyse virion composition. To obtain a large volume of virus for purification, viruses were grown in 10-day old embryonated hens' eggs before harvesting 2-days post infection. Allantoic fluid harvested from the mock infected and infected eggs was clarified and initially concentrated through a 60 % sucrose cushion. The pelleted virus was resuspended and purified further by banding on a 15 %-60 % sucrose gradient. Following re-concentration by further ultracentrifugation, the purified viruses were resuspended again and aliquots were separated by SDS-PAGE and stained with Coomassie Brilliant Blue. Viral proteins were identified by their predicted molecular weight. The NP protein of the purified viruses was sequenced to confirm the presence of mutations after growth in eggs.

As expected, the uninfected (mock) purified allantoic fluid did not contain substantial amounts of viral or cellular proteins (Fig. 4.12.A). The major structural polypeptides NP, HA1, M1 and HA2 were readily detected in the purified virus preparations. WT, Y296H, P283S and C333S samples contained similar quantities of the major viral proteins. Notably however, Q311R and N309T viruses displayed a slight increase in both the HA1 and HA2 proteins and (especially Q311R) a considerable increase in the M1 polypeptide. Western blotting analysis with the purified virus preparations was also performed (Fig. 4.12.B). The mock infected sample showed no NP or M1, as

expected (Fig. 4.12.B) and all viruses displayed similar amounts of NP. Q311R presented a clear increase in M1 in comparison to the other viruses. An increase in M1 was not as evident in the N309T preparation as shown in the Coomassie analysis (Fig.4.12.A).

To determine if these results were reproducible, an independent purification was carried out with the WT and Q311R and N309T mutant viruses (data not shown). The NP, M1 and HA protein bands were quantified using ImageJ from the two independent purifications. M1:NP and HA:NP ratios were then calculated for each mutant virus relative to the WT ratio (Fig. 4.12.A.B). Q311R and N309T both displayed a significant increase in relative M1 incorporation, of 3 and 2-fold, respectively (Fig. 4.13.C). Additionally, significant differences in the HA1:NP ratio were observed for both the Q311R and N309T viruses, of ~1.5-2-fold compared to WT (Fig. 4.13.D). Y296H, P283S and C333S NP-mutant viruses displayed no significant difference in M1:NP or HA1/HA2:NP ratios compared to WT (Fig. 4.13.C.D). Overall these results indicated that Q311R and N309T virions contained significantly higher quantities of M1 and HA1 compared to the WT virus.

4.2.9 Morphology of NP-mutant viruses

The increase in M1:NP and HA:NP ratios in Q311R and N309T purified virus preparations (Fig. 4.12) suggested the hypothesis that these NP-mutations changed the morphology of these viruses, since filamentous influenza particles have been reported to contain a higher amount of M1 and HA relative to NP (Badham and Rossman, 2016). Therefore, IF analysis was performed to examine the budding morphology of

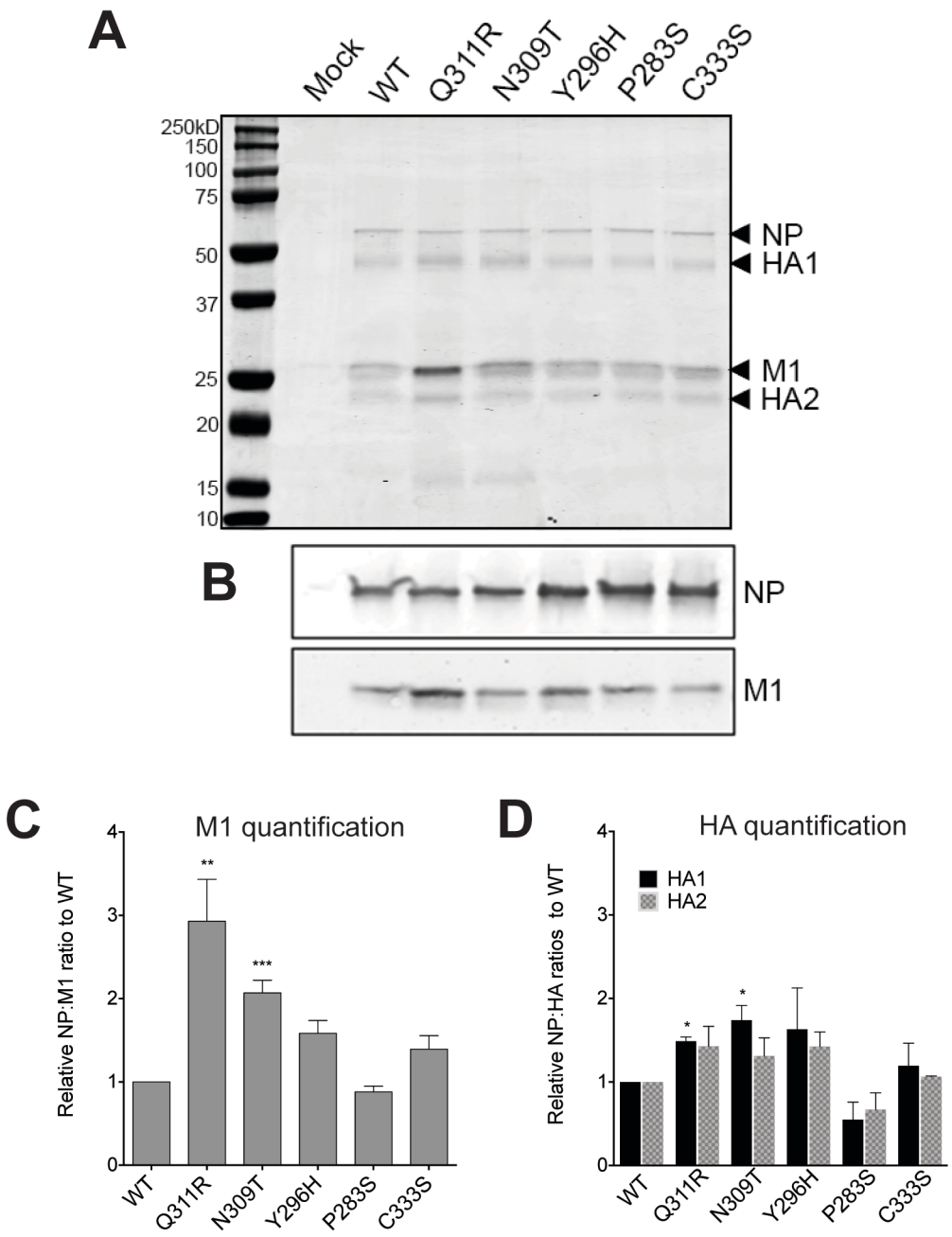

Fig. 4.12. Analysis of purified virus preparations. **(A)** Proteins were separated on a 12 % polyacrylamide gel. Gel was fixed and stained with Coomassie Brilliant Blue. Viral proteins were identified by their predicted molecular weight. **(B)** Western blotting of viral NP and M1 proteins in purified virus preparations. Proteins were separated by SDS-PAGE and western blotting with anti-NP and anti-M1. **(C, D)** NP, M1, HA1 and HA2 bands were quantified using ImageStudio Li-cor software and normalised to NP. Data are the mean ± S.E.M of 2 independently purified virus preparations. **p<0.001 ***p<0.0005 in unpaired t-tests.

the NP-mutant viruses. A549 cells were mock infected or infected with WT or -mutant viruses and 16 h p.i., cells were fixed, left unpermeabilised and immunofluorescently stained with anti-PR8 (green) to detect cell surface HA and a nuclear stain (DAPI; blue). Mock infected cells displayed some focal staining, indicative of some background noise from the PR8 antibody (Fig. 4.13). WT virus-infected cells displayed a stippled punctate array of surface HA, a pattern commonly seen for viruses that only produce spherical virus particles, consistent with previous reports that PR8 is spherical in morphology (Mosely and Wyckoff, 1946, Elton et al., 2001). In contrast, Q311R and N309T viruses presented longer filamentous structures. Q311R displayed multiple, short filaments, while fewer but longer filaments were observed for N309T. Y296H and C333S displayed a slight increase in filament formation in comparison to WT virus but fewer than Q311R and N309T infected cells. P283S presented a similar HA surface staining pattern to the spherical WT virus. Overall these data show that the NP mutations Q311R and N309T altered the spherical budding morphology of the WT-PR8 virus towards a more filamentous phenotype. Thus, suggesting that the increase in structural proteins M1 and HA1 observed for Q311R and N309T did indeed correlate with the filamentous nature of these viruses.

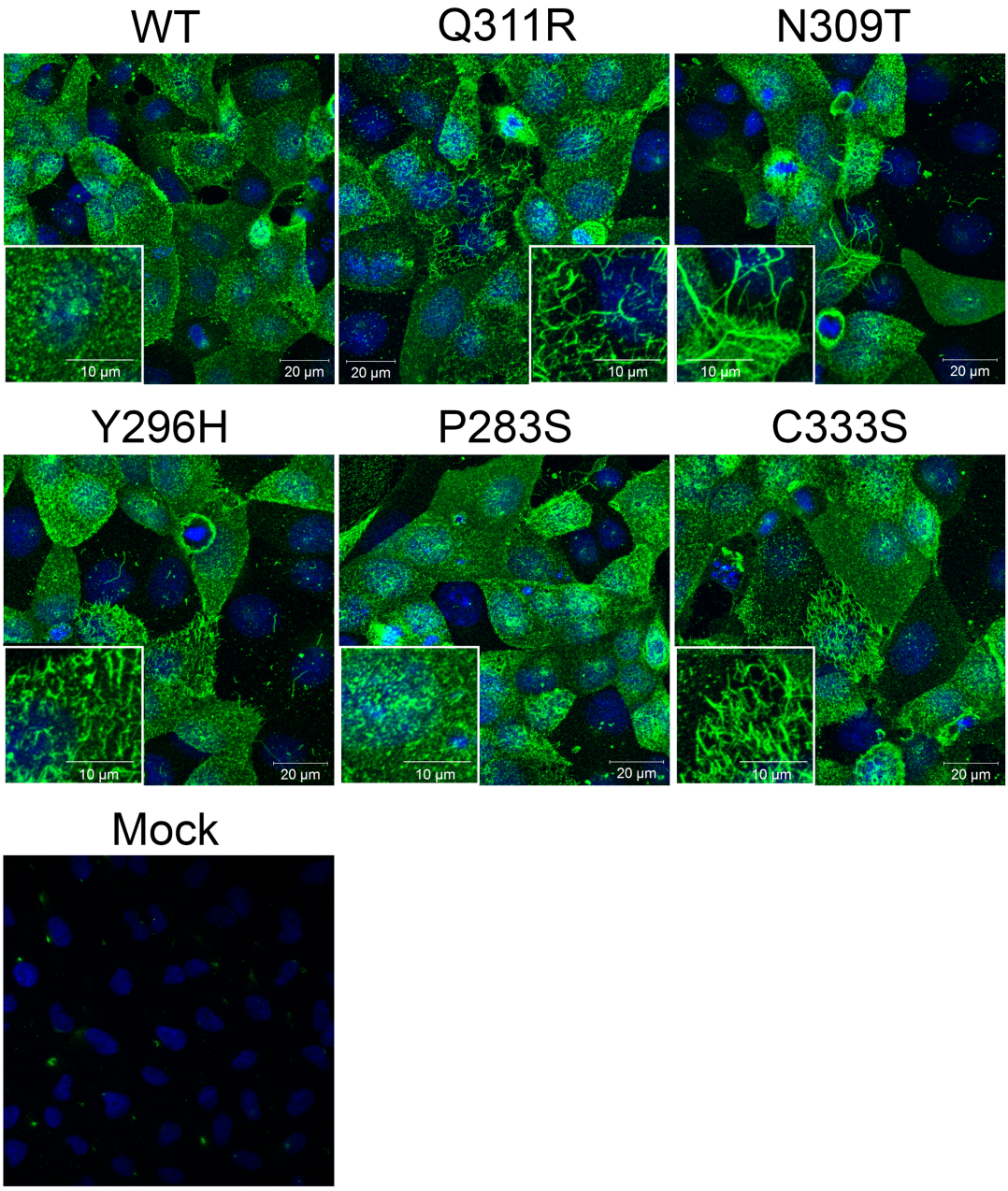

Fig. 4.13. Cells surface staining for virus HA during infection with NP-mutant viruses. A549 cells were infected with WT or NP-mutant viruses at MOI 3. 16 h p.i. unpermeabilised cells were stained with anti-PR8 (green) and a nuclear stain (DAPI; blue). Z-stacks were taken by confocal microscopy. Images shown as maximum intensity projections. Data representative of 2 independent experiments .

4.3 Discussion

In this chapter, it was determined that amino acid substitutions within the NP gene allowed an H1N1 virus to partially escape CRM1-inhibition by the KPT-335 compound. Generation of IAV harbouring potential drug-resistant mutations presented in chapter 3 was necessary to establish whether the amino acid changes contributed to a KPT-335-resistant phenotype. Utilising these recombinant NP-mutant viruses allowed determination of their susceptibility to KPT-335 by dose-response analyses and examination of the drug's mechanism of action by IF. Additionally, further phenotypic assays gave an insight into the possible mechanism of escape from CRM1 inhibition of the NP-mutant viruses.

4.3.1 NP-mutant virus susceptibility to KPT-335

The generated NP-mutant viruses' susceptibility to KPT-335 was tested by multiple phenotypic assays which included plaque reduction assays, dose-response inhibition curves and analysis of NP intracellular localisation. The outcomes of these assays are summarised in Table 4.1. KPT-335 dose-response inhibition analysis revealed that viruses containing the NP amino acid changes Q311R and N309T were the least susceptible to the compound's antiviral activity, with the most resistant phenotype displayed by Q311R (Fig. 4.2). The other NP-mutants Y296H, P283S and C333S were more susceptible to KPT-335; however, the estimated IC_{50} values were higher than the WT, suggesting a possible partial resistant phenotype (Fig. 4.2). The plaque reduction data determined that Q311R, N309T and Y296H were resistant to KPT-335 at 0.3 μM whereas P283S and C333S did not display a resistant phenotype at this concentration

(Fig. 4.3). The WT virus was more susceptible to KPT-335 inhibition when measured by plaque reduction assay compared to the dose-response test. This suggests that plaque reduction assays are a less sensitive method of measuring drug susceptibility, therefore explaining the variance in drug-resistant phenotypes between the two experiments. Examination of NP localisation during infection displayed a greater persistence of cytoplasmic NP in Q311R and N309T infected cells after treatment with 0.3 μM, confirming the KPT-335-resistant phenotype previously observed for these viruses. Complementary to the plaque reduction data (Fig 4.4), nuclear retention of NP occurred at the higher concentration of compound (1 μM), indicating that Q311R and N309T were only partially resistant to KPT-335. Considering the plaque reduction data, dose response and IF analysis, it was concluded that NP amino acid substitutions Q311R, N309T and Y296H caused partial resistance to CRM1 inhibition, with P283S and C333S also displaying a questionable drug-resistant phenotype. Alongside these phenotypic tests, quantification of virus particles in presence of drug analysed by qPCR could be another method in which to assess the partial/questionable resistant phenotype of the NP variants.

4.3.2 NP-mutant virus fitness

The partial drug-resistance phenotype of Q311R, N309T and Y296H viruses suggests that additional mutations would be required to enhance and/or develop a fully resistant IAV strain. Compensatory mutations are likely to develop under serial passage of a pathogen under the selection of a drug and have been described to play an important role in the evolution of pathogens (reviewed in Handel *et al.,* 2006). In this study, additional amino acid substitutions were discovered upon sequencing the serial

Table 4.1 Summary of NP-mutant virus susceptibility to KPT-335

	Plaque reduction	Dose-response inhibition	NP localisation (IF)
WT	✘	✘	✘
Q311R	✓	✓	✓
N309T	✓	✓	✓
Y296H	✓	?	✘
P283S	✘	?	✘
C333S	✘	?	✘

Key: ✘ = not resistant, **?** = questionable resistance, ✓ = partial resistance

Table 4.2 Summary of NP-mutant viral fitness

	Multi-cycle replication	Plaque size		Transcriptional activity
		- drug	+drug	
WT	✘	✘	✘	✘
Q311R	✓	✓	✓	✘
N309T	?	✓	✘	✘
Y296H	?	✓	✘	✓
P283S	?	✓	✘	✓
C333S	✓	✓	✘	✓

Key: ✘ = no fitness loss, **?** = potential fitness loss, ✓ = fitness loss

passaged viruses described in the prior chapter. Mutations which possibly arose as an artefact of virus adapting to the A549 cells during the serial passage included: F551S (PB2), R363G (PB1) and A178T (NP). Generating recombinant viruses containing both the NP-mutations and the potential compensatory changes may enhance the drug-resistant phenotype and/or increase virus fitness. However, testing a larger number of different mutant combinations was judged not be a valuable use of resources. Therefore, to simplify the phenotypic analysis, viruses were generated to contain single NP mutations only.

The NP mutations, Q311R, N309T and Y296H allowed IAV to partially overcome inhibition by KPT-335. However, these amino acid substitutions came at a fitness cost to the virus. The differences in fitness were evident in some or all of multi-cycle replication assays, plaque size analysis and investigations into transcriptional activity (results summarised in Table 4.2). NP-mutant virus C333S replicated to a similar titre as WT whereas N309T, Y296H and P283S displayed a slight reduction in growth and Q311R presented a clear reduction in replicative fitness (Fig. 4.2). Further investigations into this loss of fitness by plaque reduction assay revealed that Q311R did not replicate efficiently in absence of drug, displaying small and hazy plaques (Fig. 4.3); a similar phenotype that was seen in corresponding serial passage experiment (R1) (chapter 3, Fig. 3.3:3.4.). All NP-mutant viruses presented a significant reduction in plaque size compared to WT in the absence of compound (Fig. 4.5). Interestingly, Q311R plaque size remained unchanged in the presence of the compound whereas the plaque size of the other NP-mutant viruses and WT was restricted by KPT-335, indicating that Q311R replication fitness may increase in the presence of a sub-

inhibitory compound concentration. Viral transcription was not affected by NP mutations Q311R and N309T (Fig. 4.10). However, NP-mutants Y296H, P283S, C333S showed a minor reduction in transcriptional activity in comparison to WT, although the corresponding titres suggested a limited loss of replicative fitness for these viruses. Thus, it was hypothesised that the loss of fitness and/or the resistant phenotype observed for Q311R and N309T amino acids substitutions did not correlate to a change in viral transcription.

There are many factors by which amino acid changes could be detrimental to the virus. For example, amino acid substitutions can lead to a loss in enzyme activity, change in the structure/folding of a protein and/or reduction in a polypeptide stability (reviewed in Teng *et al*., 2010). The most drug-resistant mutant virus and also the least fit virus, Q311R had substitution of a hydrophilic, uncharged glutamine (Q) to a positively charged arginine (R). Arginine residues are abundant in protein active and/or binding sites and due to their positive charge, can pair with negatively charged amino acids to create a stable non-covalent bond. Therefore, an amino acid substitution to an arginine may suggest a modification in a protein-protein interaction which could change virus fitness and/or have implications for a mechanism of drug-resistance. Further mechanistic and structural analysis of the NP protein containing the mutations of interest would be required to confirm these suggestions.

The two WHO-approved antiviral classes; adamantanes and NAIs, have had distinct levels of antiviral efficacy with respect to their resistance patterns. Adamantane resistance can occur with a single point mutation within the M2 gene (Bright *et al*,

2006; Deyde *et al*., 2007; Frederick and Hayden, 2006). These resistant strains, containing the S31N mutation, do not have a fitness disadvantage; thus they are transmissible and able to cause disease (Hayden *et al.,* 1989, Mast *et al.,* 1991), explaining the success of adamantane-resistance strains at taking hold within the population. In contrast, NAI escape mutations have been previously shown to significantly reduce viral replication (Burnham *et al*., 2014). Post-pandemic 2009, NAI resistance is not currently prevalent within the population, suggesting that the drug resistance mutations may hinder the ability of the virus to transmit and infect successfully. Considering the resistance patterns for current IAV antivirals, the single point NP mutations found in this study caused a viral fitness defect and therefore the potential of KPT-335 resistance to emerge and transmit efficiently would be predicted to be low.

4.3.2 Effects of the NP mutations and possible mechanism of resistance

Viral NP formed a ring-like pattern at the inner edge of the nucleus during WT infection in the presence of KPT-335 (Fig. 4.7.A). Elton *et al.,* (2001, 2005), Ma *et al.,* (2001) and Watanabe *et al.,* (2001) previously described this specific NP staining pattern inside the nuclear envelope after treatment with LMB. In the absence of LMB, NP appeared more diffuse throughout the nucleus at 3.5 h p.i. which was unchanged by LMB treatment at 3.5 h p.i. However, at late times points of infection (9 h), LMB treatment caused NP to preferentially accumulate at the edge of the nucleus (Elton *et al.,* 2001). In the present study, the NP peripheral ring formation was not noted during infection with Q311R and N309T viruses in the presence of KPT-335 and NP was more evenly distributed throughout the nucleoplasm, suggesting that these amino acid

substitutions have disrupted 'normal' vRNP nuclear-cytoplasmic transport. Bui *et al.,* (2000), have previously suggested that RNP export occurs in two stages. The first stage would involve the release of the vRNPs from cellular chromatin (data supported by Bukrinskaya *et al.,* 1979, Chase *et al.,* 2011, Takizawa *et al.,* 2006), potentially causing the diffuse NP staining at early stages of infection and the second stage would involve translocation of the vRNPs across the nuclear pore. Considering the Elton and Bui data, it could be speculated that as Q311R and N309T NP did not form the ring-like pattern as these substitutions could have slowed the nuclear export process prior to the second (late) stage of nuclear export.

LMB covalently binds to cysteine-529 on CRM1, thus permanently blocking export of proteins that utilise the CRM1 nuclear export pathway. Dose-response inhibition with LMB indicated that the NP-mutant viruses were generally suppressed by the compound. This is consistent with the previous conclusion that the single amino acids changes did not allow the virus to fully escape KPT-335 inhibition and suggests that CRM1-function was most likely still essential for nuclear export of vRNPs. Unlike LMB, KPT-335 transiently binds to CRM1 for ~12 to 24 h (London *et al.,* 2014). Therefore, the transient inhibition of nuclear export would allow for sufficient virus replication and thus the possible accumulation of genetic mutations necessary for resistance. During the serial passage experiments (chapter 3), one passage equated to 48 h of replication in the presence of drug. In chapter 2, it was suggested that another reversible CRM1 inhibitor, KPT-185 had a half-life of <48 h (Fig. 2.7.) Thus, if KPT-335 had a similar half-life, viral replication >24 h p.i may not have occurred in the presence of an active inhibitory concentration of compound, thus increasing the chance

of escape mutations. Consequently, it could be hypothesised that if a similar serial passage experiment was performed with LMB, due to its covalent nature, resistance may be difficult to select for. However, in terms of clinical relevance, LMB is too toxic to be used as an antiviral therapy and therefore, as with most cellular inhibitors, a balance between toxicity, effectiveness and potential for resistance emergence needs to be considered.

A significant increase in M1 accumulation was observed in a single round of replication with Q311R and N309T viruses as analysed by western blot (Fig. 4.11). Analysis of purified viruses by SDS-PAGE established that Q311R and N309T incorporated a higher amount of M1 protein into the virion per NP molecule (Fig. 4.12). The NP mutations Q311R and N309T may increase M1 expression by changing NP interactions with other proteins involved in the nuclear export process. Previous studies indicate that NS2 is responsible for vRNP interaction with CRM1 (O'Neill *et al.,* 1998 Askarsu *et al.,* 2003, Watanabe *et al.,* 2011) for export of vRNP from the nucleus to the cytoplasm. Contradictorily Bui *et al.,* 2000 suggested that vRNP nuclear export could occur in the absence of NS2 and highlighted that the presence of M1 was essential to the late stages of nuclear export. The M1 gene contains a leucine-rich NES domain which is critical for nuclear export of M1 (Cao *et al.,* 2012). The last three residues of the NES motif are surface exposed, indicating a possible interaction with CRM1 and/or another protein involved in nuclear export. Previous studies have demonstrated that NP can directly interact with CRM1 via its NES motif and therefore it is reasonable to speculate that M1 could also interact with CRM1 and/or an adaptor protein via its NES domain. As mentioned previously, Cao and colleagues found that

a M1 NES fusion protein was not sensitive to LMB treatment. The function of most-leucine rich NES can be inhibited by LMB (Kudo *et al.,* 1999). However, there are a few reports that identify NES-containing proteins that are not inhibited by LMB, such as the N protein of canine distemper virus (CDV) and human receptor-interacting protein 3 (RIP3) (Sato *et al.,* 2006, Yang *et al.,* 2004). This may suggest that the M1 NES domain is not sensitive to LMB because the compound does not block the interaction between CRM1 and M1 and/or M1 interacts with a different insensitive NES adapter protein. In this case, it could be hypothesised that if M1 was not sensitive to CRM1 inhibition, an increase in M1 concentration during infection may help the virus overcome CRM1-inhbition by KPT-335.

M1 has been described to control influenza virion morphology (Bourmakina & Garcia-Sastre, 2003. Elleman & Barclay, 2004). This was initially shown by changing a filamentous virus (A/Udorn/72) to a spherical form by a single point mutation in the M1 protein (Zebedee *et al.,* 1988, Zebedee *et al.,* 1989, Roberts *et al*, 1998). However, the exact mechanism by which M1 influences morphology is not well characterised. Investigations into the morphology of the NP-mutant viruses revealed that Q311R and N309T viruses displayed an increase in a filamentous budding phenotype compared to the PR8-WT virus, which usually forms exclusively spherical particles (Mosely & Wyckoff, 1946). The filamentous budding morphology of the NP-mutants could be further characterised by electron microscopy, which would allow for an alternative method of quantifying the differences in the filament size.

The correlation between the increase in M1 incorporation and filamentous virion formation was supported by the examination of the protein profile of a known filamentous virus (PR8 MUd), which contained an increase in M1 and HA structural proteins; similar to Q311R and N309T (data not shown). Bialas *et al.,* (2014) have previously shown that NP amino acid substitutions can affect whether an influenza virus presents a spherical or filamentous budding morphology. The authors identified three NP residues: 214, 217 and 253 that play a role in determining virion morphology and suggested that the minor groove of helical vRNP is the site of interaction with the M1 layer during budding. The NP-M1 interactions have been described to induce a conformational change in M1, possibly by creating an angle between the layers beneath the viral envelope thus changing particle morphology (Bialas *et al.,* 2014). These data suggest the possibility that the NP-mutants presented in this study have modified interactions between NP and M1, thereby creating a filamentous virus. Additionally, it has been previously demonstrated that filamentous viruses are less fit *in vitro* than spherical forms (Seladi-Schulam *et al.,* 2013). Therefore, the smaller plaque phenotype and reduction in replicative fitness presented by Q311R and N309T viruses may in part be a result of their filamentous natures.

The data described in this chapter showed that NP amino acid changes Q311R, N309T and Y296H allowed an H1N1 virus to partially escape KPT-335 CRM1-inhibition. The NP mutations did not select for a fully KPT-335-resistant virus strain, indicating the virus could not easily escape the consequences of CRM1 inhibition with a single point mutation. Additionally, drug-resistant mutations Q311R and N309T, came at a replicative fitness cost to the virus. This apparently higher genetic barrier for drug-

resistance makes CRM1 a promising antiviral therapy target. The next chapter investigates the reduced fitness phenotype further and possible mechanisms of resistance of the NP-mutant viruses.

Chapter 5 Investigating the sensitivity of KPT-335-resistant NP-mutant influenza A viruses to the antiviral protein, MxA.

5.1 Introduction

In the previous chapter, individual single NP amino acid substitutions Q311R, N309T and Y296H were found to elicit a resistant phenotype to the drug KPT-335, which otherwise blocks the nuclear export of vRNPs by targeting the cellular protein, CRM1. A literature search for other studies that highlighted the same amino acid residues within NP that were altered upon serial passage of IAV in the presence of KPT-335 (311, 309, 296, 283 and 333) was carried out. This search revealed a limited number of published studies which discussed the NP residues of interest (Table 5.1). However, three papers referenced an area on the surface of the NP protein (Fig. 5.1) that determined the sensitivity of IAV to the innate immune antiviral factor, myxovirus resistance gene A (MxA) (Ashenberg *et al.,* 2017; Götz *et al.,* 2016; Mänz *et al*., 2013), which correlated well with the KPT-335-resistant NP mutations found in this study.

MxA is a human innate immune protein that's expression is induced by the activation of the IFN response. MxA inhibits influenza replication by targeting the viral NP protein (Matzinger *et al.,* 2013; Nigg & Pavlovic, 2015; Turan *et al.*, 2004; Zimmermann *et al.,* 2011; Verhelst *et al.*, 2012; Xiao *et al.,* 2013), however the exact mechanism of

Table 5.1 NP mutation amino acid positions referenced in published papers

AA	SUMMARY OF FINDINGS	PAPER
309	▪ Mutations were identified that facilitate growth of avian IAV in humans ▪ An influenza (dk/AB/76) (H1N1) virus was adapted to a high-growth phenotype (N309K)	(Danzy *et al.,* 2014)
296	▪ Phosphorylation of Y296 caused nuclear retention of NP by reducing the interaction between NP and CRM1 ▪ Y296F ablated tyrosine phosphorylation of NP during the early stage of virus infection	(Zheng *et al.,* 2015)
283	▪ Deep mutational scanning identified surface exposed sites within the NP that affected viral inhibition by MxA (includes 283 and 309). Further information in table 5.2. ▪ IAV strains containing the NP human-adaptive amino acid residues: 100I/V, 283P, 313Y were restricted by MxA ▪ Introduction of 100I/V, 283P, 313Y into the NP of an MxA-sensitive influenza virus (KAN-1)/04 (H5N1) resulted in a gain of MxA resistance and a decrease in viral replication fitness. ▪ Reassortant viruses with the PB2, PA and NP of human influenza isolates were generated in the genetic background of an avian H5N1 virus to determine effect on pathogenicity in mice. ▪ 100I/V and 283P did not enhance pathogenicity in mice	(Ashenberg *et al*., 2017) (Götz *et al.*, 2016) (Mänz *et al.,* 2013) (Kim *et al.,* 2010)
333	▪ Mutational analysis examined the roles of highly conserved amino acids within NP ▪ C333A had little to no effect on virus growth	(Li *et al.,* 2009)
311, 309, 296, 283	▪ Identified 7 potential nuclear export signal (NES) motifs with striking similarity to leucine-rich NES motifs ▪ Potential motif [289-314] was not sufficient to a direct the fusion protein from the nucleus to cytoplasm and therefore was confirmed as a novel NES motif	(Yu *et al.,* 2012)

the inhibitory interaction between NP and MxA is incompletely understood. Two strategies in which influenza viruses overcome MxA restriction have been described; blockage of the upregulation of the IFN response which drives the expression of MxA (Hale *et al.*, 2010) and more specifically, by acquiring amino acid mutations within NP which can reduce sensitivity to MxA (Dittmann *et al*., 2008; Mänz *et al.*, 2013). Manz *et al*, described human influenza viruses to be more resistant to MxA restriction than avian viruses and identified a small set of amino acid differences within NP that defined this sensitivity (100I/V, 283P and 313Y). Additionally, a deep mutational scanning study on the NP of an H3N2 virus identified amino acids clustered on the polypeptide surface that appeared to be important for MxA recognition (Ashenberg *et al.,* 2017). 12 amino acid sites identified from the screen were confirmed to either increase or decrease the sensitivity of the virus to MxA restriction (Fig. 5.1.B). The MxA recognition amino acid positions from Mänz *et al.,* (shown in blue) and Ashenberg *et al*., (shown in red) were mapped to the crystal structure of the NP protein (Fig. 5.1A). This illustrates that these amino acids lie in close proximity to the surface exposed NP mutations established in this study with two of the positions coinciding (N309T and P283S; shown in green). Therefore, it was hypothesised that the surface exposed NP mutations identified in this study (Q311R, N309T, Y296H, P283S) would influence IAV sensitivity to MxA restriction.

The aim of this section was to determine whether the KPT-335-resistant NP-mutations altered the sensitivity of IAV to the innate immune antiviral protein, MxA. The mechanism by which MxA may restrict the NP-mutant viruses was investigated, as well as determining whether the NP-mutant viruses were suppressed by IFN-I

stimulation. Most of the work in the chapter was performed using an MxA over-expressing cell line which was kindly gifted from Dr Dave Jackson's laboratory, University of St. Andrews. (Xiao *et al.*, 2013).

A

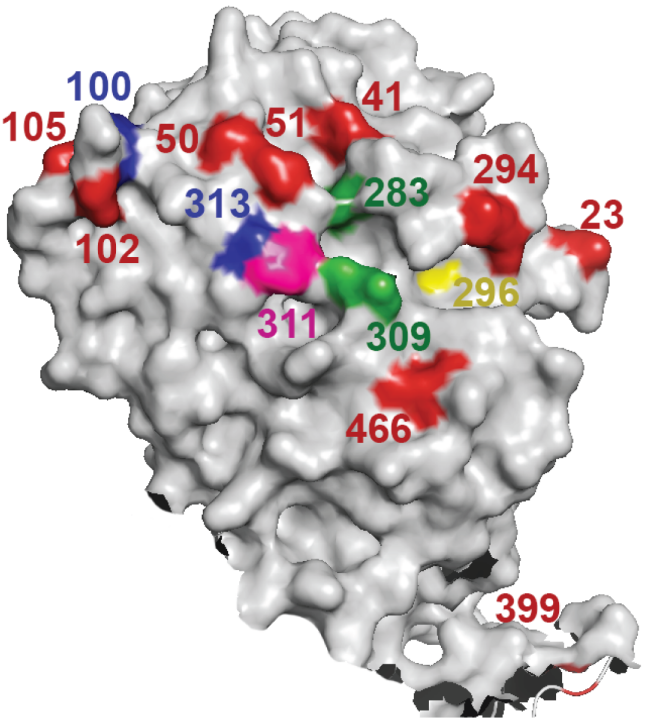

B

	Amino acid substitution	KPT-335 susceptibility
NP-mutants discovered upon serial passage with nuclear export inhibitor, KPT-335 (chapter 3)	Q311R and N309T	Resistant
	Y296H and P283S	Partial resistance
	C333S	Questionable resistance
		MxA sensitivity
MxA escape mutants (Manz *et al.,* 2013)	100I/V, 283P and 313Y	Resistant
NP residues with MxA recognition (Ashenberg *et al.,* 2017)	D51N, E294R, N309R, L466G, Q4Y, M105G, Q12S, T23H, S50C	Sensitive
	I41T, Q399R and R102A	Resistant

Fig. 5.1. NP amino acid residues involved in MxA recognition in relation to KPT-335-resistant mutants. (A) Crystal structure of the NP monomer surface annotated with amino acids residues from Mänz *et al.,* (shown in blue), Ashenberg *et al.,* (shown in red) and overlapping mutations from this study and published work (shown in green). 311 (pink) and 296 (yellow). **(B)** Table indicating the amino acid changes required for KPT-335 and MxA resistance/susceptibility (Q4Y and Q12S not mapped).

5.2 Results

5.2.1 Antiviral activity of MxA during NP-mutant virus infection

The IFN-induced innate immune factor, MxA, can restrict IAV replication at early stages of infection (Xiao *et al.,* 2013). As previously described, mutations within the NP protein can determine IAV sensitivity to MxA antiviral activity. To establish the effect MxA had on the NP-mutant viruses generated in chapter 4, virus replication was examined in a cell line which overexpressed the MxA protein (MxA-A549). Prior to infections in the MxA-A549 cells, the increased expression of MxA in the engineered cell line compared to normal A549s was confirmed by western blotting cellular lysates for MxA and tubulin as a loading control (Fig 5.2.B). In addition, an immunofluorescence assay was utilised to confirm that the majority of cells in the overexpressing cell line produced high levels of MxA (Fig 5.2.A).

To determine if the NP-mutant viruses were susceptible or resistant to MxA restriction, multi-cycle growth infections were performed in naïve and MxA-A549 cells. Cells were infected with PR8 (WT) or the mutant viruses at an MOI of 0.01. At 24 h p.i., viral supernatant was harvested and the titre was determined by plaque assay. In naïve-A549 cells, WT, Y296H, P283S and C333S viruses all replicated to ~10^7 PFU/ml, while Q311R and N309T grew to ~10^6 PFU/ml (Fig. 5.2.C), consistent with previous data (Fig. 5.3). The WT virus replicated to ~10^6 PFU/ml in the MxA-A549 cells. This 1-$\log_{10}$ reduction in titre is comparable with previous reports that PR8 was partially resistant to MxA restriction (Manz *et al.,* 2015). Y296H and P283S viruses also replicated to ~10^6 PFU/ml in the MxA cells, similar to the WT virus, suggesting that

they were also partially resistant to MxA. However, the two mutant viruses that had the strongest drug-resistant phenotypes, Q311R and N309T were notably more susceptible to MxA antiviral activity, resulting in a 3-$\log_{10}$ (to 10^3 PFU/ml) and 2-$\log_{10}$ (to 10^4 PFU/ml) reductions in titre, respectively. Interestingly, the C333S virus was not affected by MxA restriction and replicated to a similar titre as in the naïve cells (10^7 PFU/ml).

To give a clearer view of any differences in susceptibility, the fold changes in virus titre between naïve and MxA A549 cells were analysed (Fig. 5.2.D). These results displayed a greater fold decrease in titre for Q311R than the WT virus in all three independent experiments, indicating that the former virus was more sensitive to MxA restriction (Fig. 5.2.D). N309T also displayed a generally greater decrease in titre than the WT virus, however the spreads of individual data points from the two viruses overlapped suggesting this change may not be significantly different. Y296H and P283S viruses presented little difference in fold change, with the spread of values similar to that of the WT. Notably, C333S displayed a significantly smaller set of fold-change values to the WT, indicating that this mutant virus was more resistant to MxA antiviral activity. Overall, these results indicated that NP amino acid changes Q311R, N309T and C333S altered the virus' sensitivity to MxA restriction thus supporting the hypothesis that NP KPT-335-resistance mutations could influence IAV sensitivity to MxA restriction.

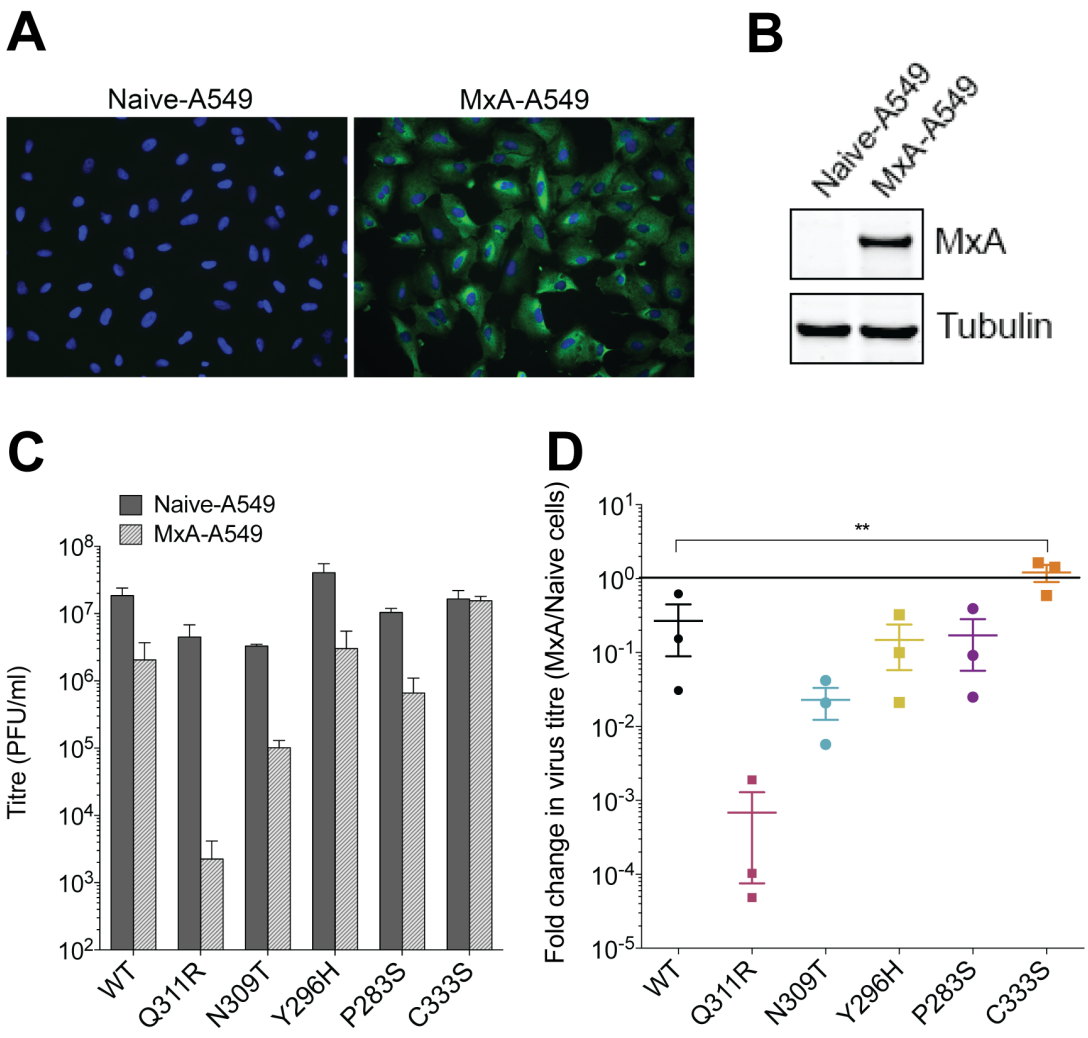

Fig. 5.2 Growth of NP-mutant viruses in an MxA over-expressing cell line. (A) Immunofluorescent staining of MxA. Naïve-A549 and MxA-A549 cells were fixed, permeabilised and stained with anti-MxA (green) and a nuclear stain (DAPI; blue). **(B)** Western blot detection of MxA. Cell lysates were analysed by SDS-PAGE and western blotting with anti-MxA and anti-tubulin as a loading control. **(C)** Virus replication in MxA cells. Naïve or MxA-A549 cells were infected with WT or NP-mutant viruses at MOI 0.01. Virus supernatant was harvested at 24 h and titred by plaque assay. Data are the mean ± S.E.M. of three independent experiments. **(D)** Fold change in virus titre (MxA cells vs naïve cells) ** $p<0.05$ in one way ANOVA.

5.2.2 Ability of NP-mutant viruses to infect MxA overexpressing cells

To investigate further the difference in sensitivity of the NP mutant viruses Q311R and N309T to MxA, IF analysis of infection levels was performed in the overexpressing cell line to determine if the mutant viruses were able initiate viral infection (as measured by expression of the "early" class viral gene product NP) with similar efficiency to the WT virus. Naïve and MxA-A549 cells were infected with WT or the mutant viruses at an MOI of 3. At 8 h p.i., cells were stained with anti-NP (red), anti-MxA (green) and a nuclear stain (DAPI; blue). The naïve cells expressed low levels of MxA, as expected (Fig. 5.3). All viruses displayed similar amounts of NP in the cytoplasm of the naïve cells, representing comparable infection levels between the viruses and also indicating that nuclear export of vRNPs had taken place (Fig. 5.3). The MxA-A549 cells displayed an abundance of MxA in the cytoplasm confirming that the cells overexpressed the protein. WT, Y296H, P283S and C333S displayed cytoplasmic NP in the MxA-overexpressing cell line, similarly to the infected naïve cells, indicating that these viruses were able to replicate in the presence of MxA. In contrast, Q311R infection gave very few NP-positive cells in the MxA cell line, indicating that the presence of the antiviral protein restricted the ability of the virus to establish infection. N309T infected MxA cells displayed a reduced number of NP-positive cells and interestingly, the NP was localised to the nucleus rather than the cytoplasm as observed for the WT and the other NP-mutants. Overall the IF analysis confirmed that Q311R was highly sensitive to MxA restriction during a single round of replication. The N309T virus was also less able to establish infection in the presence of high levels of MxA, but even in cells where viral gene expression was clearly

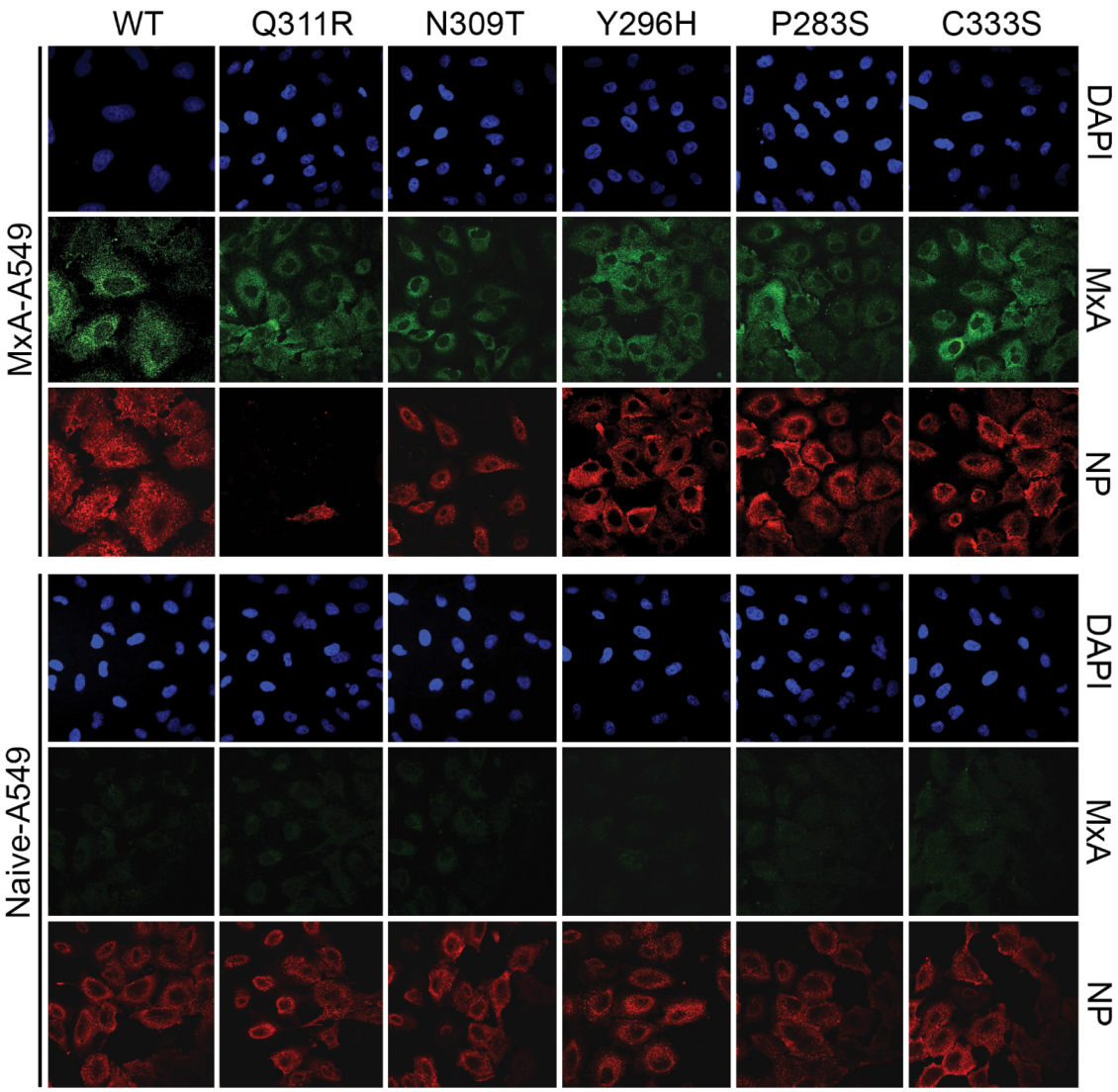

Fig. 5.3. Immunofluorescent staining of viral NP during infection in MxA-A549 cells. Naive-A549 or MxA-A549 cells were infected with WT or NP-mutant viruses at MOI 3. 8 h p.i. cells were fixed, permeabilised and stained and with anti-NP (red), anti-MxA (green) and a nuclear stain (DAPI; blue). Images are representative of 2 independent experiments.

present, the presence of nuclear NP suggested that normal vRNP nuclear-cytoplasmic transport was disrupted in the presence of MxA.

5.2.3 Investigation into mechanism of action of MxA sensitivity

MxA is thought to inhibit IAV by acting upon two stages of the viral life cycle; preventing transcription by incoming vRNPs (primary transcription), most likely by blocking their transport into the nucleus (Matzinger *et al.,* 2013, Xiao *et al.,* 2013), as well as by inhibiting amplification of vRNA from cRNA copies (genome replication), possibly by sequestering newly synthesized NP and PB2 in the cytoplasm (Huang *et al*., 2012; Pavlovic *et al.*, 1990; Verhelst *et al*., 2012). To determine if the NP-mutant viruses were blocked by MxA at the stage of RNP nuclear import, investigation into the ability of the viruses to transport vRNPs into the nucleus was determined utilising the MxA cell line. For this experiment, cells were infected in the presence of cycloheximide (a protein synthesis inhibitor) to allow immunofluorescent-tracking of incoming vRNP complexes into the nucleus.

Naïve and MxA-A549 cells were infected with purified WT or NP-mutant viruses (Q311R and N309T) in the presence of CHX. 3.5 h p.i. cells were fixed and stained with anti-NP (green), anti-MxA (red) and a nuclear stain (DAPI; blue). Naïve cells infected with WT virus in the absence of CHX (-CHX) were used as a positive control for nuclear import of vRNPs and the efficacy of CHX treatment. Naïve cells treated with importazole and CHX (+IMP, +CHX) were used as a positive control for inhibition of vRNP import as IMP specifically targets the cellular importin-β pathway thus blocking their nuclear import (Soderholm *et al.,* 2011). As expected, mock

infected naïve and MxA cells showed no NP staining (Fig. 5.4.A), and MxA was abundant in the overexpressing cell line (Fig. 5.4.A.B). WT virus in the absence of CHX displayed bright staining of nuclear and cytoplasmic NP, indicating normal infection had taken place (Fig. 5.4.A). WT virus treated with IMP (+CHX) presented much fainter NP-staining largely in the form of cytoplasmic puncta, indicating that nuclear import of vRNPs had been blocked by the compound (Fig. 5.4.A). Infections with WT, Q311R and N309T in naïve cells (+CHX) gave NP staining predominantly in the nucleus demonstrating typical import of vRNPs (Fig. 5.4.B). In the MxA cells, WT RNP was still localised to the nucleus, indicating nuclear import had occurred even in the presence of MxA. However, in the MxA cells, NP staining from Q311R and N309T viruses was mostly cytoplasmic with little to no evidence of RNPs in the nucleus of the cells. Thus, both Q311R and N309T NP-mutant viruses were blocked at the stage of nuclear import during infection of a MxA overexpressing cell line. Therefore, the MxA restriction observed in the multi-cycle replication assay (Fig. 5.2) and IF analysis (Fig. 5.3) for Q311R and N309T was, at least in part, from MxA antiviral activity acting at the stage of RNP nuclear import.

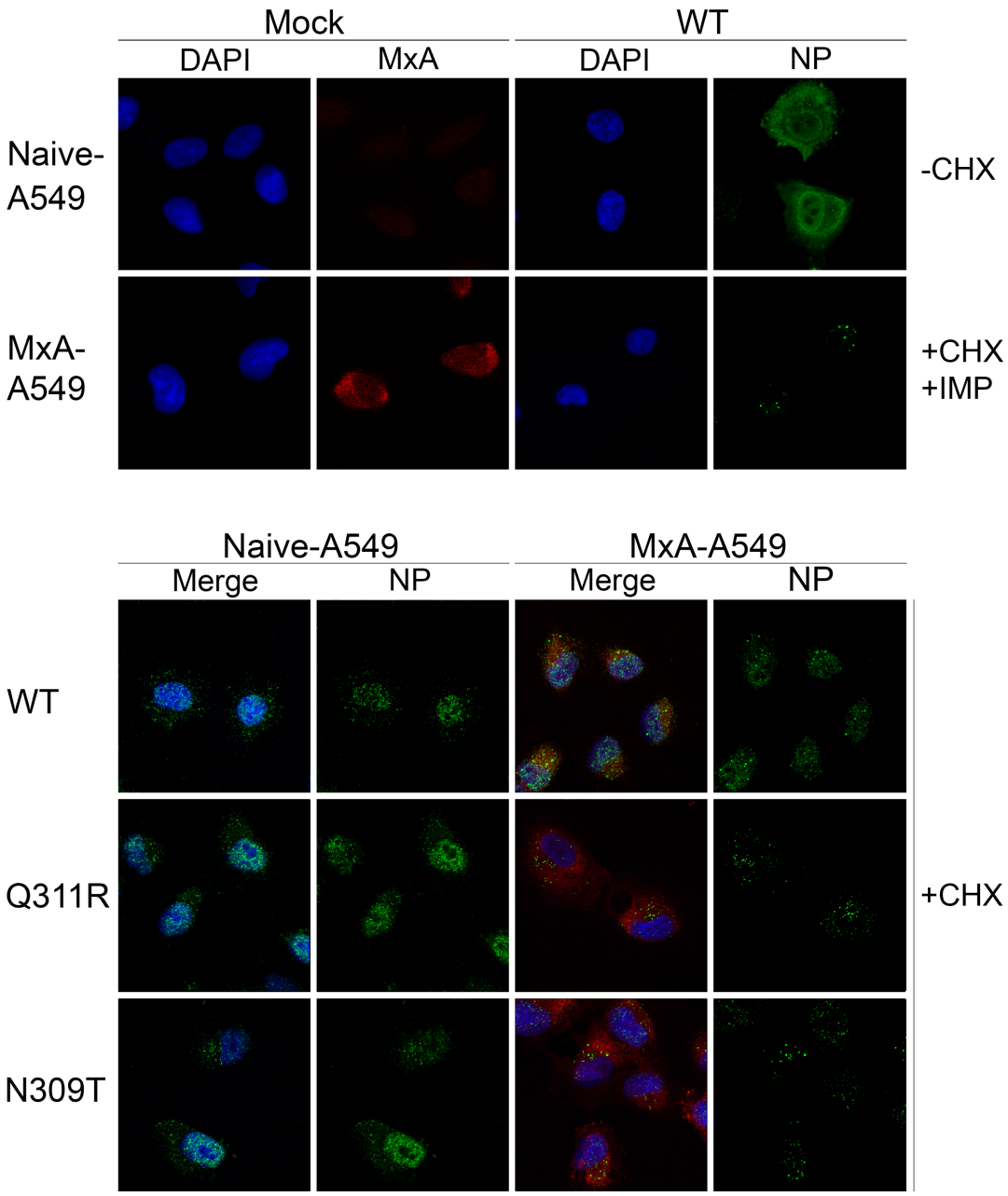

Fig. 5.4. Import of viral NP into the nucleus during infection in MxA-A549 cells. Naïve or MxA-A549 cells were infected with purified WT or NP-mutant viruses. 3.5 h p.i. cells were stained with anti-NP (green), anti-MxA (red) and a nuclear stain (DAPI; blue). **(A)** Mock and WT infected naïve and MxA-A549 cells. WT infected cells in the absence of cycloheximide (-CHX) were used as a positive control for import of NP. Cells were treated with 100μM of importazole (+IMP/+CHX) as a positive control for blocking import of NP. **(B)** Infections were carried out in the presence of CHX (+CHX) to stop translation of newly synthesised proteins.

5.2.4 Expression of innate immune factors during infection with NP-mutant viruses

During IAV infection, the virus typically modulates the innate responses, restricting upregulation of antiviral factors such as MxA (Pauli *et al*., 2008). To determine if the NP-mutant viruses could suppress upregulation of MxA, its expression was analysed after a single round of virus replication. Naïve and MxA-A549 cells were uninfected (mock) or infected with WT or the NP-mutant viruses at an MOI of 3. 16 h p.i. cellular lysates were analysed by SDS-PAGE and western blotting with anti-MxA and anti-tubulin as a loading control. Mock infected naïve-A549 cells did not contain MxA indicating the protein was not intrinsically present at detectable levels in uninfected A549 cells (Fig. 5.5). As expected, MxA was expressed to high levels in the MxA-A549 cells, with no visible difference MxA abundance between the viruses analysed. All viruses induced a low level of MxA expression in the naïve cells, excluding Q311R where a prominent band was observed. This suggested that the Q311R virus could possibly upregulate MxA expression and/or lacked the capability to suppress the IFN-I signalling pathway thus upregulating interferon stimulated genes (ISGs).

To determine if the increase in MxA expression present during infection with Q311R was specific, two other ISGs; protein kinase R (PKR) and ISG-15 were analysed by western blotting. Like MxA, PKR and ISG-15 are both IFN-induced anti-viral proteins that are normally suppressed during IAV infection (reviewed in Iwasaki & Pillai, 2014). A549 cells were left uninfected (mock) or infected with WT and the NP-mutant viruses at an MOI of 3. Samples of mock and WT infected cells were also pre-treated with IFN-I (100 U/ml) for 16 h pre-infection as a positive control for upregulation of

ISG expression. At 16 h p.i., cellular lysates were analysed by SDS-PAGE and western blotting for anti-MxA, anti-PKR, anti-ISG-15 and anti-tubulin as a loading control. As expected, IFN-I-stimulated uninfected and cells infected with WT virus to express high levels of all three ISGs examined, with slightly increased ISG expression in the infected cells (Fig. 5.6). As previously observed in Fig 5.5, infected cells displayed low levels of MxA in the absence of exogenous IFN-I, apart from those infected with Q311R. Similarly, PKR and ISG-15 levels were also elevated in Q311R infected cells. Thus, the western blot data suggested that the Q311R NP-mutant virus may have a wider influence on the IFN signalling pathway.

5.2.5 Quantification of secreted IFN-I during infection with NP-mutant viruses

To determine if the increase in ISG expression during Q311R infection was a result of greater triggering of the IFN-I response, levels of active IFN-I secreted during virus infection were examined using a bioassay. The reporter cell line HEK-blue IFN- α/β has been transfected with human STAT1 and IRF8 genes to obtain a fully active IFN-I signalling pathway and also engineered to express secreted alkaline phosphatase (SEAP) under the control of an ISG54 promoter (Ahmed *et al*., 2016). Thus, stimulation of the HEK blue cell line with IFN-I activates the JAK-STAT/ISGF3 pathway and induces the production of SEAP which can be measured by colorimetry following the addition of substrate.

A549 cells were mock infected or infected with WT or the NP-mutant viruses at an MOI of 3. A PR8 NS1 RNA binding mutant virus (containing the mutations: R38A,

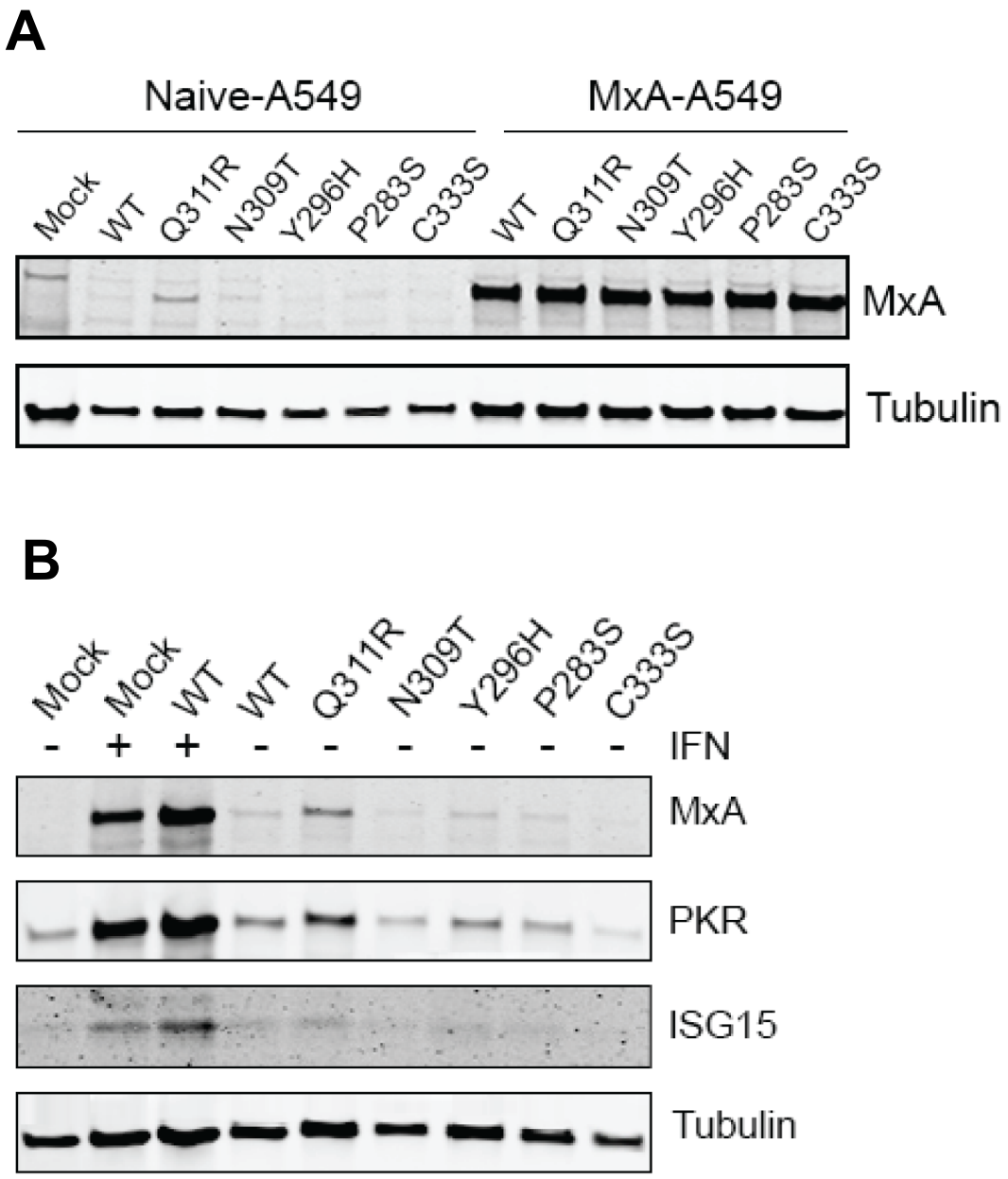

Fig. 5.5. ISG expression during infection with NP-mutant viruses (A) MxA expression during virus infection. Naïve or MxA-A549 cells were infected at MOI 3. At 16 h p.i., cellular lysates were analysed by SDS-PAGE and western blotting for MxA and tubulin. **(B)** ISG expression during virus infection. A549 cells were infected with WT or mutant viruses at MOI 3. Cells were pre-treated with IFN (100 U/ml) for 16 h pre-infection as a positive control for ISG expression (+) or left untreated (-). 16 h p.i. cellular lysates were analysed by SDS-PAGE and western blotting for MxA, PKR, ISG-15 and cellular loading control, tubulin.

K41A) which is deficient in IFN-antagonism was included as a positive control for the detection of secreted IFN-I (Talon *et al.,* 2000; Newby *et al.,* 2007). At 24 h p.i., viral supernatants were quantified for the presence of IFN-I using the HEK-Blue reporter assay. A standard curve of recombinant human IFN-I was also incubated on the HEK-Blue cells, starting at a concentration of 7.8 U/ml and increasing in 2-fold increments to 1000 U/ml. Media and cells only samples were also included as negative controls to determine the background level of the assay. SEAP activity from the HEK-Blue cells increased with increasing concentrations of exogenous IFN-I treatment, as expected. The media and cells only controls indicated that the limit of detection of the assay was ~80 U/ml of IFN-I, as determined by the standard curve (Fig. 5.6). Mock infected cells displayed similar amounts of SEAP activity as the media and cells only controls. The positive control NS1 mutant virus infection resulted in high levels of IFN secretion, equivalent to at least 1000 U/ml of IFN-I. WT, N309T, Y296H, P283S and C333S viruses induced comparable amounts of SEAP activity to the mock infected and negative controls, suggesting that these viruses efficiently supressed the IFN-I response. Notably, the Q311R virus displayed a significant increase in SEAP activity which equated to ~200 U/ml of IFN-I. These results demonstrated that Q311R either lacked the ability to suppress IFN-I secretion during infection and/or the virus enhanced the activation of the innate immune response.

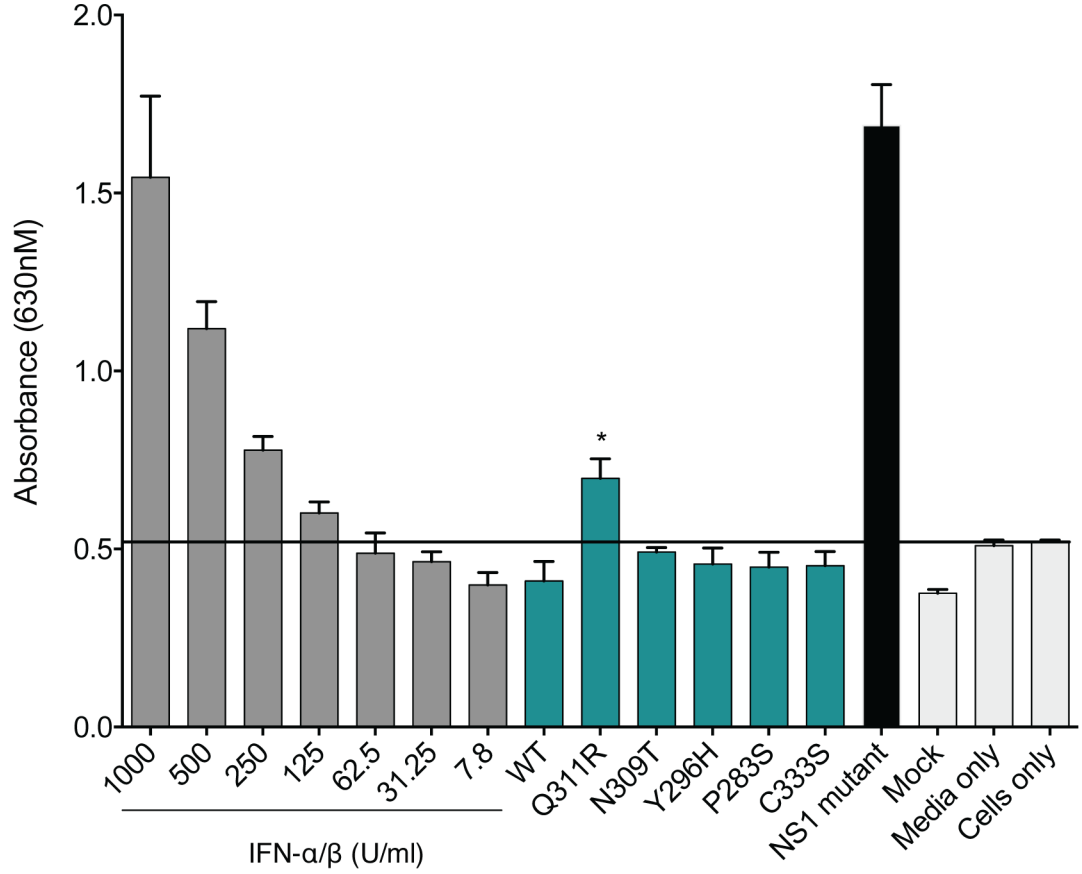

Fig. 5.6. HEK-Blue reporter assay to quantify IFN-I upregulation during infection with NP-mutant viruses. A549 cells were infected at MOI 3 for 24 h. Cell supernatants were quantified for IFN-I using a HEK-Blue cell reporter assay (absorbance read at 680 nm). The black line indicates the limit of detection. Data are the mean ± S.E.M from three independent experiments. *p<0.05 in unpaired t-test

5.2.6. Effect of NP-mutant viruses on the global IFN response

Following detection of the virus by the host innate immune system via pathogen-associated molecular patterns (PAMPs), IFN-I is secreted which upregulates hundreds of different ISGs (reviewed in Iwasaki & Pillai, 2014). Therefore, it could be hypothesised that the MxA sensitive mutation, Q311R, may also be more sensitive to global IFN-I antiviral activity. Prior to testing the effect IFN-I induction had on NP-mutant virus replication, a IFN-I dose response assay was performed to determine an optimal IFN-I concentration to inhibit virus replication. A549 cells were left untreated or pre-treated with increasing concentrations of IFN-I starting at 10 U/ml and increasing in 0.5-$\log_{10}$ increments to 1000 U/ml. At 16 h post-treatment, cells were infected with PR8-WT at an MOI of 0.01. 24 h p.i. virus supernatant was harvested and titre was determined by plaque assay. As expected, pre-treatment with IFN-I inhibited virus replication in a dose-dependent manner (Fig. 5.7.A). From the dose-response curve, it was determined that 100 U/ml was optimal as inhibition of the virus plateaued at concentrations somewhere between 100-300 U/ml suggesting saturation of IFN-I antiviral activity.

To determine the effect of IFN-I stimulation on NP-mutant virus replication, A549 cells were pre-treated with IFN-I (100 U/ml) or left untreated. 16 h post-treatment, cells were infected with WT or the NP-mutant viruses at an MOI of 0.01. 24 h p.i. virus supernatant was harvested and titre was determined by plaque assay (Fig. 5.7.B). The fold change in virus replication was determined by calculating the difference in titre from cells untreated and treated with IFN-I (Fig. 5.7.C). In untreated A549 cells,

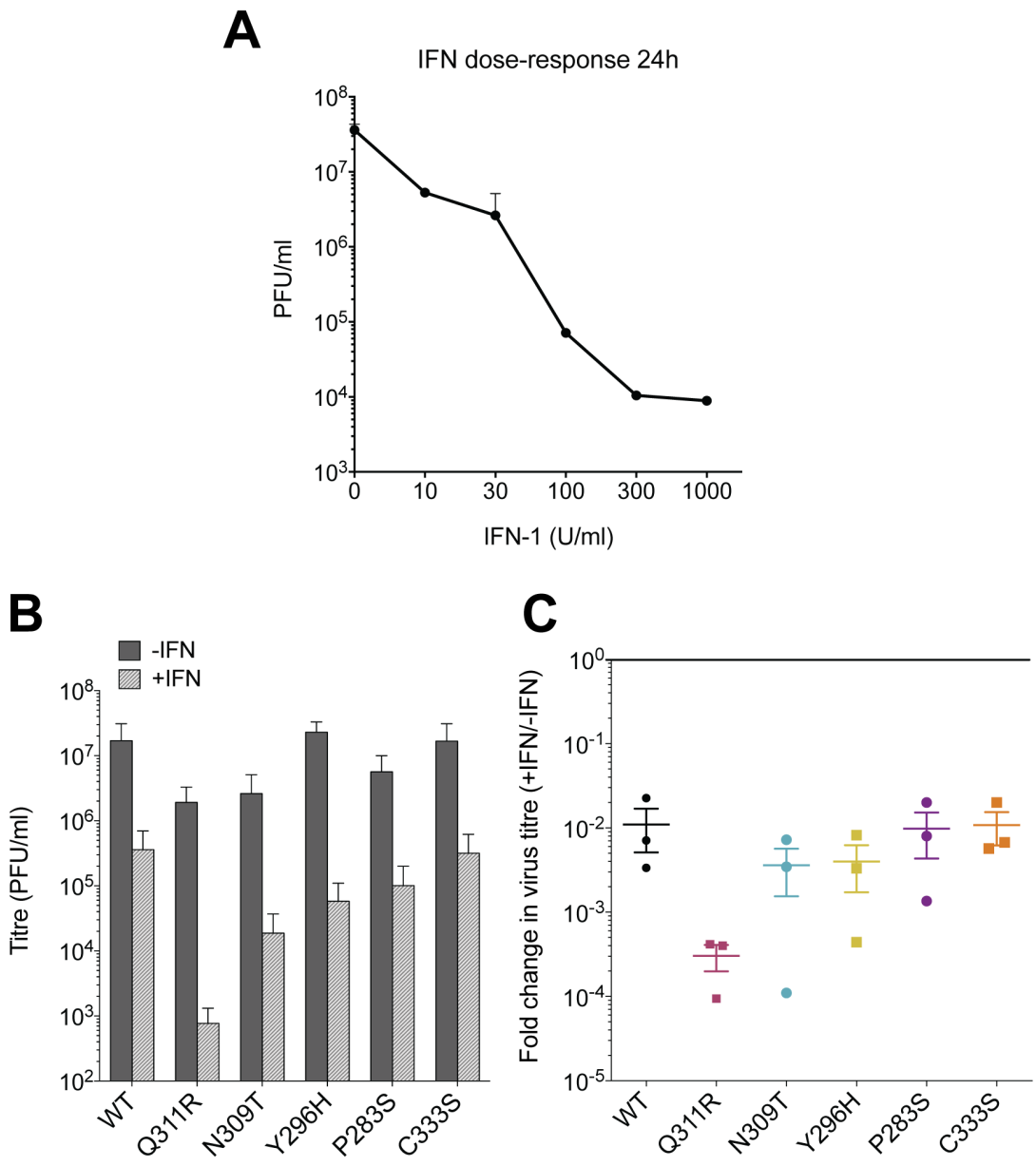

Fig. 5.7 Effect of IFN-I pre-treatment on virus growth. **(A)** IFN-I dose inhibition curve. A549 cells were pre-treated with increasing concentrations of IFN-I. 16 h post-treatment, cells were infected with PR8 virus at MOI 0.01. Virus supernatant was harvested at 24h and titre determined by plaque assay. Data are the mean and range of two independent experiments. **(B)** Virus replication in IFN-I stimulated cells. A549 cells were pre-treated with 100 U/ml of IFN-I (+IFN) or left untreated (-IFN). 16 h post-treatment, cells were infected with WT or NP-mutant viruses at MOI 0.01. Virus supernatant was harvested at 24 h and titred by plaque assay. Data are the mean ± S.E.M of three independent experiments. **(C)** Fold change in virus titre (presence/absence of IFN). Data n.s. as analysed by one-way ANOVA.

WT, Y296H, P283S and C333S viruses all replicated to ~10^7 PFU/ml and as expected, Q311R and N309T displayed a 1-$\log_{10}$ reduction in replication (to ~10^6 PFU/ml). As determined by the dose-response inhibition curve in Fig. 5.7.A, 100 U/ml of IFN-I pre-treatment inhibited WT virus by ~2-$\log_{10}$ to ~10^5 PFU/ml (Fig. 5.7.B). This reduction in titre was similar for N309T, Y296H, P283S and C333S viruses after IFN pre-treatment. Notably, the NP-mutant virus that had the strongest drug-resistant phenotype, Q311R, was also the most susceptible to IFN induction, resulting in a 3-$\log_{10}$ decrease down to only 10^3 PFU/ml. A greater fold decrease in titre by Q311R was observed when compared to the WT virus and the other NP-mutant viruses, indicating that this mutant virus was more sensitive to IFN pre-treatment (Fig. 5.7.D). Overall, these results indicated that the NP amino acid change Q311R increased IAV sensitivity to IFN-I inhibition and suggests the susceptibility of this virus to MxA restriction (Fig. 5.2.C.D) may not be specific to this ISG alone.

5.3 Discussion

In this chapter, it was discovered that the nuclear export inhibitor escape mutant viruses Q311R and N309T were more sensitive to MxA restriction compared to the partially MxA-resistant PR8-WT virus. Previous studies have demonstrated that amino acid substitutions within the NP gene can greatly influence the antiviral activity of MxA. Surface exposed amino acid residues on the NP protein, defined by Manz *et al.,* (2015) and Ashenberg *et al.,* (2017) clustered in the same region as the amino acid changes isolated in this study (Fig. 5.1).

KPT-335 escape NP-mutant viruses, Q311R and N309T, displayed an increase in susceptibility to MxA restriction as determined by multi-cycle replication assays and measurement of infection levels in an MxA-A549 overexpressing cell line (Fig. 5.2;5.3). An NP N309R mutation has been shown previously to produce a MxA sensitive strain (Ashenberg *et al.,* 2017). In this study, N309 mutated to a threonine (T) also altered the virus' susceptibility to MxA, thus supporting the previous data that the 309 side chain is involved in MxA recognition. While N309T did not cause a significant reduction in virus replication in the MxA cells (Fig. 5.2), analysis of infection levels by IF showed that NP remained localised predominately in the nucleus (Fig. 5.3), suggesting that the N309T substitution may have somehow slowed nuclear export of vRNPs. A proline (P) at amino acid position 283 within NP has been described to help the virus escape MxA restriction (Mänz *et al.,* 2015). P283 is naturally present in the PR8 (H1N1) strain and as shown in Fig. 5.2., WT virus was only partially restricted by MxA. Additionally, a substitution of 283 P to serine (S) did

not change the PR8 partial resistance phenotype (Fig. 5.2, 5.3). Q311R appeared the most susceptible to MxA restriction (Fig. 5.2, 5.3). NP amino acid residue 311 has not been previously identified as a MxA recognition site, thus adding a novel NP residue to the list if those that can affect the virus' sensitivity to MxA. The altered sensitivity to MxA caused by Q311R and N309T mutations further supports the current published studies that this region on the surface of NP may specifically interact with MxA and/or an adaptor protein involved in MxA's mechanism of action.

The amino acid residues involved in NP and MxA interaction and the mechanism by which this interaction restricts IAV is currently unknown. Previous studies regarding other viruses show a relation between MxA and nucleoproteins. MxA can inhibit thogotovirus (THOV) infection via interaction with THOV nucleocapsids and thereby blocking their cytoplasmic-nuclear import (Kochs and Haller, 1999). Additionally, it has been demonstrated that MxA and NP directly interact during La Crosse virus infection (Kochs *et al.*, 2002). Recently, Gao *et al.,* (2016) solved the crystal structure of MxA which revealed that it oligomerizes into ring-like structures and have been suggested to assemble around incoming vRNPs. It was hypothesised that these MxA rings would interfere with RNP nuclear import and/or primary transcription. The authors found that attenuated MxA escape viruses disturbed intracellular trafficking of incoming vRNPs, thus supporting one of their hypotheses. Here, it was determined that MxA sensitive viruses Q311R and N309T were blocked at the stage of RNP nuclear import in an MxA-overexpressing cell line (Fig. 5.4). This outcome is comparable with the Gao *et al.,* study, in that MxA may restrict viral propagation by

blocking vRNPs at the stage of nuclear import, however the exact details of MxA antiviral mechanism of action are still not fully elucidated.

Q311R infected cell lysates contained an increased amount of in MxA and two other ISGs; ISG-15 and PKR (Fig. 5.5), indicating upregulation of these antiviral proteins and/or the incapability of the virus to control the IFN-response. Quantification of IFN-I secretion indicated that Q311R increased IFN-I levels (Fig. 5.6). This may suggest that the Q311R mutation has enhanced IFN induction, for example by allowing vRNA to be more exposed to PRRs (as discussed below) or that the mutation has reduced the ability of the virus to suppress the IFN-I response. Additionally, it was discovered that Q311R was significantly more susceptible to the IFN-I innate immune response (Fig. 5.7), indicating that Q311R may not be exclusively restricted by MxA. The viral NS1 protein is a potent virulence factor that helps 'mask' the virus from the innate immune response by multiple mechanisms (Tisoncik *et al.*, 2011). It is the most important IFN-antagonist protein encoded by the virus. The Ortin and Fodor laboratories, demonstrated that NS1 can interact with NP within the RNP complex (Marion *et al.,* 1997; Robb *et al.,* 2010) which suggests the hypothesis that NP surface mutation Q311R may affect NS1 IFN-antagonism by altering the interaction between NP and NS1. However, there is limited knowledge on the interaction of these two proteins. It could be speculated that the mechanism by which the NP-mutant virus, Q311R has overcome inhibition of nuclear-cytoplasmic transport of vRNPs has somehow altered NS1's ability to shuttle between the nucleus and cytoplasm; possibly necessary for a mechanism of action of NS1 IFN-antagonism. Therefore, an alternation in normal

nuclear-cytoplasmic transport may potentially have limited the ability of NS1 to prevent an efficient IFN response and expression of ISGs.

The main PRR that recognises IAV is the cytoplasmic retinoic acid-inducible gene I (RIG-I) (Kato *et al.*, 2006). RIG-I responds to strongly to dsRNA and binds immediately after RNPs are released from the endosomes into the cytoplasm (Li *et al.,* 2014), resulting in antiviral signalling. Therefore, it could be speculated that Q311R triggered a greater IFN response (Fig. 5.6) because of an enhanced detection of the RNPs via RIG-I. As suggested previously, MxA may restrict IAV by forming ring-like structures around the vRNPs, thus if a virus was more sensitive to MxA restriction, expression of MxA could potentially 'hold' RNPs in the cytoplasm for easier recognition by RIG-I. Thus, in turn RIG-I would upregulate expression of IFNs and ISGs.

As determined in chapter 4, the MxA sensitive viruses, Q311R and N309T, contained a higher relative amount of the viral M1 protein in the virion (Fig. 4.11). Presently, there is limited evidence to suggest an interaction between MxA and M1. However, one study demonstrated that MxA inhibition of IAV replication did not affect the synthesis of PA, PB1, PB2, HA, NA and NP primary transcripts but increased M1 and NS2 primary transcripts by 2-3-fold (Pavlovic *et al.*, 1992). Additionally, despite the higher abundance of M1 and NS2 transcripts, these proteins were still efficiently exported and translated. Therefore, it could be hypothesised that the increase in M1 expression in Q311R and N309T NP-mutants may somehow relate to the mechanism of action of MxA thus increasing their susceptibility to MxA restriction.

MxA can also interfere with the function of cellular host proteins. Wisskirchen *et al.,* (2011) demonstrated that UAP56, a cellular ATP-dependent RNA helicase protein, co-immunoprecipitated with human MxA. UAP56 is a nuclear-cytoplasmic shuttling protein which plays an important role during assembly of the spliceosome and nuclear export of both spliced and unspliced mRNAs into the cytoplasm (Thomas *et al.*, 2011). A direct interaction between NP and MxA has yet to be described (Turan *et al.*, 2004) therefore, Wisskirchen *et al.,* suggested that the cellular protein UAP56 was the missing link between NP and MxA; a hypothesis which was suggested by previous studies showing that UAP56 can bind directly to free NP and vRNPs (Momose *et al.,* 2001; Mayer *et al.,* 2007). UAP56 is also required during influenza infection to prevent accumulation of dsRNA in the cytoplasm of cells and therefore assists the virus to overcome evasion of the IFN-I response (Wisskirchen *et al.,* 2011). In the context of this study, if the possible linker nuclear-cytoplasmic protein UAP56 was involved in the NP-MxA interactions it may be hypothesised that surface exposed NP-mutation Q311R has altered NP's interaction with UAP56 and therefore has disrupted the transport of dsRNA, increasing dsRNA accumulation in the cytoplasm thus increasing IFN-I expression and upregulation of ISGs.

NP amino acids substitutions Q311R and N309T confer a resistant phenotype to the selective nuclear export inhibitor, KPT-335 but at a replication fitness cost to the virus. In this chapter, it was discovered that the Q311R and N309T mutations limit the ability of the virus to escape the IFN-induced innate immune restriction factor MxA and Q311R was susceptible IFN-I pre-treatment and showed increased MxA, PKR and

ISG-15 expression. The increased sensitivity of the KPT-335-resistant NP-mutant viruses to MxA suggested that there could be an evolutionary trade-off if KPT-335 resistance virus variants emerged. MxA may pose a barrier during human IAV infection if the virus obtained CRM1-inhibition escape mutations and therefore, in a clinical environment, it may be difficult for the virus to overcome both drug selection pressures and human innate immune response restrictions by escape mutations.

Chapter 6 Discussion

6.1 Conclusion

The aim of this project was to investigate the potential of two cellular nuclear export inhibitors; KPT-335 (verdinexor) and KPT-185 as novel therapeutic agents against IAV infection. The data described in this thesis provided pre-clinical evidence of efficacy for both compounds. KPT-335 and KPT-185 inhibited an H1N1 virus in a dose-dependent manner by blocking CRM1-mediated RNP nuclear export, with limited cytotoxic effects *in vitro*. Additionally, KPT-335 was effective against a wide range of both human and animal IAV strains suggesting that the host protein, CRM1 is utilised by all influenza viruses. Investigations into the potential for drug-resistance revealed the emergence of apparently resistant virus variants after 9-10 passages in the presence of KPT-335. Sequencing analysis of independently derived resistant virus clones showed that IAV acquired four surface mutations within the NP protein (Q311R, N309T, Y296H, P282S). The NP amino acid changes: Q311R and N309T presented the strongest drug resistant phenotype. However, they came at a fitness cost to virus replication. Interestingly, both mutations caused an increase in M1 levels during infection, increased M1:NP ratios in the virion and also induced a filamentous budding morphology at the final stage of virus replication. Furthermore, the NP surface mutations were found to cluster in a region reported to have a role in interactions with the cellular antiviral protein MxA. The Q311R and N309T viruses showed an increase in susceptibility to MxA restriction compared to WT virus and

Q311R also induced higher levels of IFN-I during infection. Taken together with Karyopharm's promising data on KPT-335 (https://www.karyopharm.com/pipeline/oralverdinexor-kpt-335), this thesis confirms the potential of KPT-335 as a therapeutic agent against IAV infection in humans. Additionally, if KPT-335 drug-resistance was to emerge within the population it could be hypothesised that the virus may not be able to overcome both the drug selection pressures and the increased innate immune response faced by escape mutations. Thus, KPT-335 could be a successful novel antiviral to overcome the resistance problem as seen with current anti-influenza therapies.

6.2 Future directions

6.2.1 Advancing KPT-335 as a therapeutic anti-influenza agent

Preclinical efficacy guidance for the development of a novel antiviral compound are shown in Table 6.1. These guidelines have been taken and adapted from the FDA recommendations for "Guidance for Industry - Antiviral Product Development" (https://www.fda.gov/ohrms/dockets/98fr/05d-0183-gdl0002-01.pdf). Each aim is outlined and the relevant preceding studies with KPT-335 as well as the work presented in the thesis are summarised. Brief suggestions of future work related to each objective are also discussed.

Table 6.1. Summary of the pre-clinical efficacy of KPT-335

INVESTIGATION	AIM	PREVIOUS WORK	THIS STUDY	FUTURE WORK
Mechanism of action	Demonstrate the compounds ability to specifically inhibit viral replication by establishing the site of the products action	The compound blocked nuclear export of vRNPs by disrupting CRM1-NS2 binding (Perwitasari *et al.,* 2014)	vRNPs were retained in the nucleus of the cell after treatment with the compound. A known CRM1 inhibitor, LMB was used as positive control for blockade of nuclear export	Determine if there are any possible off target effects Investigate the *in vitro* half-life of the compound
Antiviral activity	Assess the antiviral activity of the compound against a broad range of clinical and laboratory viral isolates *in vitro*	The compound inhibited replication of both influenza A and B viruses including a pandemic H1N1 virus and an H5N1 avian influenza virus (Perwitasari *et al.,* 2014)	The compound was effective against a wide range of both human and animal strains including swine, avian and equine IAVs	Investigate the antiviral activity of the compound against other viruses that also utilise the CRM1 pathway such as HSV-1 and HCMV
	Measure the viral titres after treatment in animal model systems to assess the antiviral activity of compound *in vivo*	Prophylactically and therapeutically protected mice against disease pathology (Perwitasari *et al.,* 2014) Virus shedding and pro-inflammatory cytokine expression were reduced in both mouse and ferret models after treatment with compound (Perwitasari *et al.,* 2016)	-	*In vivo* efficacy established
Cytotoxicity and	Cytotoxicity tests using increasing concentrations of antiviral compound to determine the	A CC_{50} value of 26.8 μM was determined in A549 cells (Perwitasari *et al.,* 2014)	CC_{50} values of 2.6 μM (A549 cells) and 9.8 μM (MDCK cells) were determined	*In vitro* cytotoxicity well established

Therapeutic Indexes	concentration that results in death of 50% of the host cells (CC_{50})			
	Determine the relative effectiveness of the compound in inhibiting viral replication compared to inducing cell death - selective index (SI) (CC_{50}/IC_{50})	SI range = 64-2680 (Perwitasari *et al.,* 2014)	SI range = 87-130	*In vitro* selective index established
Combination activity analysis	Evaluate the antiviral activity of the compound in two-drug combinations with other approved antivirals	*In vivo* efficacy was enhanced with a combination of oseltamivir and KPT-335 compared to KPT-335 alone (Perwitasari *et al.,* 2016)	-	Further evaluation of combination efficacy with current antivirals/experimental agents (*in vitro* and *in vivo*)
Resistance	Select for drug-resistant virus variants *in vitro*	Serial passage with 0.2 μM of KPT-335 was performed for 10 passages however drug-resistance viral variants did not emerge (Perwitasari *et al*., 2016)	Resistant virus variants emerged after 9-10 passages in the presence of 0.15 μM and 0.3 μM of compound	Characterise resistance in several genetic backgrounds (i.e., strains, subtypes) to determine if the same or different patterns of resistance mutations would develop
	Genotypic analysis of resistant viruses selected *in vitro* to determine if mutations contribute to a reduced susceptibility to the compound	-	Five mutations found within the NP gene (four of which were surface exposed) Additional possible compensatory/resistance mutations were also found in PB2, PB1 and NP	Next generation sequencing of passaged viruses and host cells
	Phenotypic analysis to determine if mutant viruses have reduced susceptibility to the compound	-	NP mutations Q311R and N309T elicited a drug resistant phenotype. Y296H and P283S a partial drug-resistant phenotype	Generate viruses containing multiple drug-mutations to determine if there would be an enhanced resistant phenotype

6.2.2 Investigations into the molecular mechanism of drug-resistance to a CRM1 inhibitor

The mechanism by which IAV escaped inhibition of the CRM1 pathway was unclear. Possible mechanisms of resistance to KPT-335 are presented in Fig 6.1. Evidence to support each hypothesised mechanism and future experiments to explore the possibility of each are discussed below. Information on how the virus overcomes CRM1-inhibition would enhance the ability to troubleshoot if resistance was to occur in humans; i.e. target another cellular pathway that the virus has adapted to use and/or a novel cellular/viral mediator protein involved in the nuclear export process. This would potentially allow for the use of a combination therapy and/or allow the selection of alternative therapies based on knowledge of the mechanism of resistance.

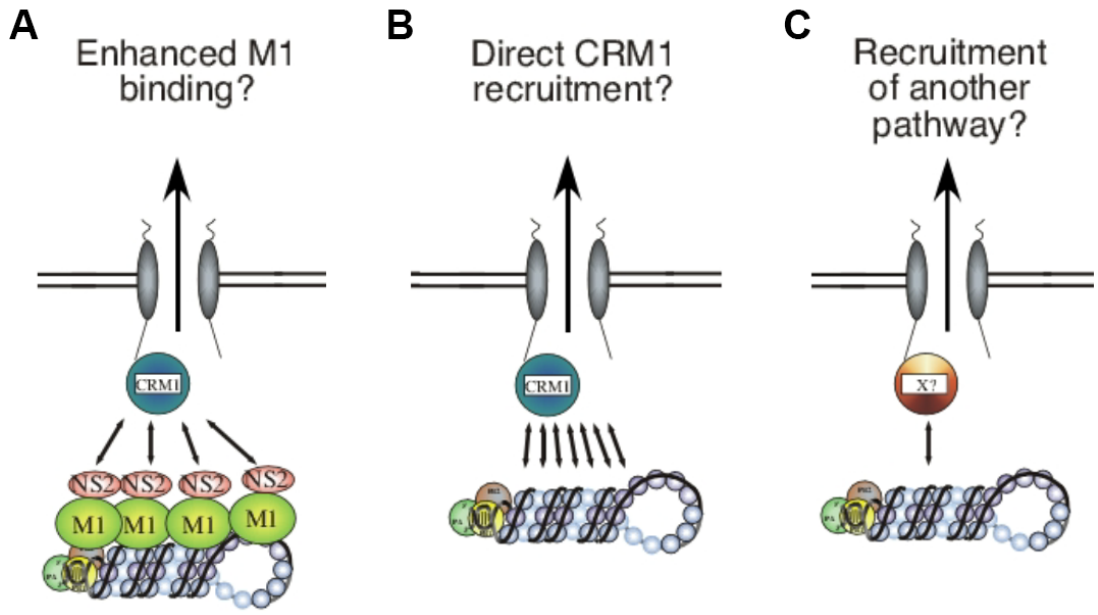

Figure 6.1. Possible mechanisms of KPT-335 resistance. (A) Enhanced binding and/or recruitment of M1. **(B)** Direct binding of NP to CRM1. **(C)** Nuclear export involving another pathway. Cartoon drawn by Prof. Paul Digard.

A. Enhanced canonical nuclear export

The current 'daisy chain' model for nuclear export of vRNPs suggests that NP within the vRNP complex binds to M1 which in turn binds to NS2. The NS2 protein contains the NES domain which then interacts with CRM1. KPT-335 disrupts the binding between NS2 and CRM1 thus blocking nuclear export. Work presented in chapter 4 showed that viruses harbouring the KPT-335-resistant NP mutations Q311R and N309T produced increased levels of M1 during infection as well as yielding virus particles containing an increase in the M1:NP ratio. Thus, it may be hypothesised that the amino acid changes within NP caused an alteration in NP-M1 interaction which could increase M1 recruitment and/or binding for enhanced daisy chain export (as shown in Fig. 6.1A). It could also be speculated that the increase in M1 incorporation into the virion was an artefact of resistance to CRM1 inhibition, in which the NP mutations caused a change in the interaction with M1 and thereby changed the morphology of the virus to form to filaments. Subsequently, more membrane-associated structural proteins such as M1 would be incorporated into the virion. To determine if there was an alternation in the interaction between the NP-mutants the WT virus, the *in vitro* binding could be analysed between NP and CRM1 and/or NP and NS2/M1. Radiolabelling of CRM1, M1 and NS2 plasmids and subsequently incubating them with WT NP and mutant NP plasmids alongside Sepharose beads would reveal the bound material as analysed by SDS-PAGE and autoradiography. The co-immunoprecipitation between NP (WT and mutants) with the virus proteins and host protein would reveal if there was an increased interaction with the mutant NP and other polypeptides involved in the daisy chain model.

B. Viral NP binds directly to CRM1

As KPT-335 disrupts the interaction between NS2 and CRM1, it could be hypothesised that the NP surface mutations have allowed the RNP to bind directly to CRM1, thereby overcoming the inhibition of this interaction (Fig 6.1.B). As discussed in chapter 3, published studies have shown that that NP can directly bind to CRM1 (Elton *et al.,* 2001, Chutiwitoonchai *et al.,* 2014; Kakisaka *et al*., 2015), however whether this is essential for CRM1-mediated export of RNPs has yet to be determined. To establish if the mutations within the NP protein caused the virus to directly interact with CRM1, biochemical assays could be performed to compare binding efficacy of the NP-mutants with CRM1 to the WT NP. Additionally, investigation into the effect of CRM1 overexpression on mutant vs WT NP localisation may determine an increase in binding to CRM1. For example, if there was an increase in cytoplasmic accumulation of NP after CRM1 overexpression, this would support the hypothesis that NP interacts with CRM1 nuclear export in absence of other viral proteins.

C. Involvement of an unknown mediator and/or pathway

Another mechanism by which the virus may have overcome CRM1 inhibition could be that it has adapted to utilise another nuclear export pathway (Fig 6.1.C). To date there is limited evidence to suggest that nuclear export of vRNPs is CRM1-independent. However, there are a wide range of cellular export pathways that are utilised by other viruses for the export of several different types of RNA. For example, Mason-Pfizer monkey virus (MPMV) RNA nuclear export involves the human Tap protein (Kang and Cullen, 1999) Thus, it could be speculated that the virus has changed to interact with another cellular export factor. To determine if the NP-mutants

interacted with an unknown host protein, a pull-down assay could be carried out and mass spectrometry performed to determine which cellular proteins bound to the NP mutants.

Additionally, a paper by Mulhbauer *et al.,* (2015), described that influenza viruses can CRM1-independently passively transport their RNPs across the nuclear pore at later stages of infection by inducing caspase activation. The authors describe that during infection caspases can enlarge the cellular nuclear pores, which in turn can facilitate the translocation of large protein complexes such as vRNPs across the nuclear membrane. Therefore, suggesting that vRNP nuclear export could occur via a CRM1-independent mechanism.

Chapter 7 Materials and Methods

7.1 Materials

7.1.1 Plasmids

Table 7.1 Plasmids

Name	Description		Source
pDUAL	Reverse genetics 8-plasmid system for A/Puerto Rico/8/1934 (H1N1). RNA pol I and pol II bidirectional promoters at either side of insert to allow for mRNA and vRNA-like RNA synthesis		Prof. Ron Fouchier, (Erasmus University Medical Center, Rotterdam, Netherlands)
	Segment	**Accession number**	de Wit *et al*., 2004
	PB2	EF467818	
	PB1	EF467819	
	PA	EF467820	
	HA	EF467821	
	NA	EF467822	
	M	EF467823	
	NS	EF467824	
	NP-Q311R	-	This study
	NP-309T	-	
	NP-Y296H	-	
	NP-P283S	-	
	NP-C333S	-	
pHH21 and pcDNA3.1	Reverse genetics 12-plasmid system for A/Udorn/1971 (H3N2)		Prof. Robert Lamb (Department of Molecular Biosciences, North-western

<table>
<tr><td></td><td colspan="2"></td><td>University, Illinois, USA)</td></tr>
<tr><td rowspan="10">pHH21</td><td colspan="2">Pol I promoter leads to vRNA-like RNA synthesis</td><td>Prof. Robert Lamb</td></tr>
<tr><td>Segment</td><td>Accession number</td><td rowspan="9">Chen et al., 2007</td></tr>
<tr><td>PB2</td><td>CY009643</td></tr>
<tr><td>PB1</td><td>CY009642</td></tr>
<tr><td>PA</td><td>CY009641</td></tr>
<tr><td>HA</td><td>CY009636</td></tr>
<tr><td>NP</td><td>CY009639</td></tr>
<tr><td>NA</td><td>CY009638</td></tr>
<tr><td>M</td><td>CY009637</td></tr>
<tr><td>NS</td><td>CY009640</td></tr>
<tr><td rowspan="6">pcDNA3.1</td><td colspan="2">CMV pol II promoter upstream of insert allows for constitutively high protein expression</td><td>Prof. Robert Lamb</td></tr>
<tr><td>Segment</td><td>Accession number</td><td rowspan="5">Chen et al., 2007</td></tr>
<tr><td>PB2</td><td>CY009643</td></tr>
<tr><td>PB1</td><td>CY009642</td></tr>
<tr><td>PA</td><td>CY009641</td></tr>
<tr><td>NP</td><td>CY009639</td></tr>
<tr><td>pPol I Luc</td><td colspan="2">Reporter for minireplicon assay. Contains firefly luciferase reporter gene in reverse orientation. Flanked by UTRs of PR8 segment 8 under the control of a pol I promotor.</td><td>Prof. Laurence Tiley (University of Cambridge, UK)</td></tr>
</table>

7.1.2 Oligonucleotides

DNA oligonucleotides were synthesised by and purchased from Sigma.

7.1.2.1 Sequencing primers

Table 7.2 Sequencing primers

Primer	Sequence (5' to 3')
Uni 12	AGCAAAAGCAGG
pDUAL forward	ATGTCGTAACAACTCCGCCC
pDUAL reverse	TTTTTGGGGACAGGTGTCCG
PR8 PB2 internal forward	TCAAGGAACATGCTGGGAACA
PR8 PB2 internal reverse	CCTCCTCGGGAGACAGTAGT
PR8 PB1 internal forward	GGGAAGCTAAAACGGAGAGCA
PR8 PB1 internal reverse	TGTCACCTCTATGGCATCGG
PR8 PA internal forward	GCAGAACTGCAGGACATTGA
PR8 PA internal reverse	AGTTGTGGAGATGCATACAAGC

7.1.2.2 Mutagenesis primers

Table 7.3 Mutagenesis primers

Primer	Sequence (5' to 3')
PR8 NP-Q311R forward	CTGATTAGGCTGTACACTCGGCTGTTTTGAAGCAGTC
PR8 NP-Q311R reverse	CTGATTAGGCTGTACACTCGGCTGTTTTGAAGCAGTC
PR8 NP-N309T forward	CTGTACACTTGGCTGGTTTGAAGCAGTCTGAAAGGG
PR8 NP-N309T reverse	CCCTTTCAGACTGCTTCAAACCAGCCAAGTGTACAG
PR8 NP-Y296H forward	CACTGGCTACGGCAGATCCATACACACAGGC
PR8 NP-Y296H reverse	GCCTGTGTGTATGGATCTGCCGTAGCCAGTG
PR8 NP-P283S forward	CACTGGCTACGGCAGATCCATACACACAGGC

PR8 NP-P283S reverse	GCCTGTGTGTATGGATCTGCCGTAGCCAGTG
PR8 NP-C333S forward	CGGCAGAATGGCTTGCCATCCACACCAGTT
PR8 NP-C333S reverse	AACTGGTGTGGATGGCAAGCCATTCTGCCG

7.1.3 Antibodies

7.1.3.1 Primary antibodies to IAV proteins

Table 7.4 Primary antibodies and antisera raised against IAV proteins

Antibody	Application	Source
Rabbit polyclonal anti-MBP-NP (2915)	WB (1:500), Plaque immunostaining (1:1000)	(Noton *et al.,* 2007)
Rabbit polyclonal anti-PR8 M1	WB (1:500)	(Amorim *et al.,* 2007)
Rabbit polyclonal anti-PB1(V19)	WB (1:500)	(Digard *et al.,* 1989)
Rabbit polyclonal anti-PB2 (2N580)	WB (1:500)	(Carrasco *et al.,* 2004)
Rabbit polyclonal anti-PR8	IF 1:1000	(Amorim *et al.,* 2007)
Rabbit polyclonal anti-PR8 NS1	WB (1:500), IF (1:1000)	(Carrasco *et al.,* 2004)
Mouse monoclonal anti-NP (AA5H)	IF (1:1000)	Abcam (ab20343)
Mouse monoclonal anti-M2 (14C2)	WB (1:1000)	Abcam (ab5416)
Mouse monoclonal anti-M1 (GA2B)	IF (1:500)	Abcam (ab22396)
Rabbit monoclonal anti-NS2	WB (1:1000), IF (1:500)	GeneTex (GTX125952)

7.1.3.2 Primary antibodies to cellular proteins

Table 7.5 Primary antibodies against cellular proteins

Antibody	Application	Source
Goat polyclonal anti-MxA	WB (1:1000), IF (1:500)	R&D Systems (AF7946)
Rat monoclonal anti-tubulin	WB (1:1000)	Serotec (MCA77G)
Rabbit monoclonal anti-PKR	WB (1:500)	Millipore (07-886)
Rabbit polyclonal anti-ISG-15	WB (1:500)	Invitrogen (PA5-17461)

7.1.3.3 Secondary antibodies

Table 7.6 Secondary antibodies

Antibody	Application	Source
Donkey anti-mouse IgG (H+L) Secondary antibody, Alexa Fluor® 488 conjugate	IF (1:1000)	ThermoFisher (A-21202)
Donkey anti-rabbit IgG (H+L) Secondary antibody, Alexa Fluor® 488 conjugate	IF (1:1000)	ThermoFisher (A-21206)
Donkey anti-mouse IgG (H+L) Secondary antibody, Alexa Fluor® 595 conjugate	IF (1:1000)	ThermoFisher (A-21202)
IRDye® 800CW Donkey anti-Mouse IgG (H+L)	WB (1:10000)	LiCor (925-32212)
IRDye® 800CW Donkey anti-Rabbit IgG (H+L)	WB (1:10000)	LiCor (925-32213)
IRDye® 800CW Donkey anti-Goat IgG (H+L)	WB (1:10000)	LiCor (925-32214)

IRDye® 680CW Donkey anti-Rabbit IgG (H+L)	WB (1:10000)	LiCor (926-68071)
IRDye® 680CW Donkey anti-Rat IgG (H+L)	WB (1:10000)	LiCor (926-68029)
Goat Anti-Rabbit IgG (H+L)-HRP conjugate	Plaque assay (1:1000)	Bio-Rad (1721019)

7.1.3.4 Fluorescent dyes

Table 7.7 Fluorescent dyes

Dye	Application	Source
Prolong Gold Antifade Mountant with DAPI	IF (neat)	Thermo Fisher
DAPI D1306	IF (1:10000)	Thermo Fisher

7.1.4 Eukaryotic cells

Table 7.8 Eukaryotic cell lines

Cell	Description	Source
MDCK	Madin-Darby Canine Kidney cells	Sigma
A549	Human Adenocarcinomic Alveolar Basal Epithelial cells	Sigma
293T	Human Embryonic Kidney cells	Sigma
HEK-Blue	HEK293-Blue IFN-α/β cells	InvivoGen
MxA-A549	A549 cells constitutively expressing MxA	Dr Dave Jackson (University of St Andrews, UK)

Naïve-A549	A549 cells	Dr Dave Jackson (University of St Andrews,UK)

7.1.5 Viruses

Table 7.9 IAV virus strains

Strain	Subtype	Source
A/PR/8/34	H1N1	Reverse genetics virus (de Wit *et al.,* 2004)
A/Udorn/72	H3N2	Reverse genetics virus (Chen *et al.,* 2007)
PR8 MUd	H1N1 (PR8 containing seg7 from Udorn)	Reverse genetics virus
A/swine/England/453/06	H1N1	Prof. James Wood, University of Cambridge
A/duck/England/62	H4N6	Prof. Wendy Barclay, Imperial College London
A/duck/Singapore/5/97	H5N3	Prof. Wendy Barclay (Imperial College London, UK)
A/equine/Miami/53	N3N8	Animal Health Trust (AHT)
PR8-NP-Q311R mutant	H1N1	This study
PR8-NP-N309T mutant	H1N1	
PR8-NP-Y296H mutant	H1N1	
PR8-NP-P283S mutant	H1N1	
PR8-NP-C333S mutant	H1N1	

7.1.6 Drugs

Table 7.10 Compounds

Drug	Mechanism	Source
KPT-335	Selective inhibitor of nuclear export	Karyopharm Therapeutics
KPT-185	Selective inhibitor of nuclear export	Karyopharm Therapeutics
KPT-301	Enantiomer of KPT-185	Karyopharm Therapeutics
Leptomycin B	Cytotoxic inhibitor of nuclear export	Cambridge Bioscience (1814-025)
Importazole	Selective inhibitor of nuclear import	Sigma-Aldrich (SML0341)
Cycloheximide	Eukaryote protein synthesis inhibitor	Sigma-Aldrich (C7698)

7.2 Methods

7.2.1 Cell culture

7.2.1.1 Eukaryotic cell culture

MDCK cells, 293T cells, A549 cells and Naïve-A549 cells were grown in complete Dulbecco's Modified Eagle Medium (D-MEM) (D-MEM supplemented with 10 % (v/v) foetal bovine serum (FBS), 2 mM glutamine, 100 U/ml penicillin and 100 U/ml streptomycin) at 37 ˚C in 5 % CO_2. HEK-Blue cells were cultured in complete D-MEM with 30 µg/ml blasticidin and 100 µg/ml Zeocin. MxA-A549 cells were cultured in complete D-MEM with 2 µg/ml puromycin. Cells were typically passaged twice weekly by washing cells 2 x PBS and detached using 0.25 % trypsin-EDTA solution (ThermoFisher, cat# 25200056) or without trypsin for HEK-Blue cells. Cells were resuspended in complete D-MEM and typically split 1 in 10.

7.2.1.2 Cell counting

Cells were counted using a Neubauer chamber which consists of 4 x 4 grids which was visualised using the 10X objective lens in a light microscope. Cell suspension was added to the chamber under a glass coverslip. The number of cells was counted in a 4 x 4 grid and the cell concentration was calculated (N x 10^4 cells/ml).

7.2.2 Virus work

7.2.2.1 Generation of P0 stocks

Reverse genetics pDUAL 8-plasmid sets were transfected into 75-90 % confluent 293T cells in 6-well plates. Media from 293T cells was replaced with 1 ml of Opti-MEM (reduced serum media) 1 h before transfection. Reverse genetics plasmids (250 ng/µl of each plasmid) were diluted in 100 µl Opti-MEM. 4 µl Lipofectamine2000 (Invitrogen, cat# 11668) per 100 µl Opti-MEM was incubated for 5 min at room temperature then mixed with the diluted DNA for 30 min. The transfection mix was slowly dropped over the 293T cells. Media was replaced 5-6 h post-transfection with 2.5 ml of D-MEM supplemented with 0.3 % BSA, 2 mM glutamine, 100 U/ml penicillin and 100 U/ml streptomycin and incubated at 37 ˚C in 5 % CO_2. Trypsin-TPCK (Sigma, cat# 4352157) was added to the cells 2 days post-transfection at 1 µg/ml in 500 µl D-MEM with 0.3 % BSA, 2 mM glutamine, 100 U/ml penicillin and 100 U/ml streptomycin. Cell supernatant was harvested 3 days post-transfection and spun at 1200 rpm for 5 min to clarify the supernatant. P0 stocks were aliquoted and stored at -80 ˚C to be used to make P1 virus stocks.

7.2.2.2 Generation of P1 stocks

MDCK cells were grown to 90 % confluency in T75 flasks. Cells were washed 2 x 10 ml serum-free D-MEM (D-MEM containing 2 mM glutamine, 100 U/ml penicillin and 100 U/ml streptomycin) before adding 300 µl of P0 stock with 3 ml of virus growth media (D-MEM supplemented with 0.14 % BSA, 2 mM glutamine, 100 U/ml penicillin, 100 U/ml streptomycin and 1 µg/ml TPCK trypsin) for 1 h. After the incubation, 18 ml of virus growth media was added and cells were incubated for 48 h

at 37 ˚C in 5 % CO_2. Supernatants were harvested and cells clarified at 3000 rpm for 5 min. P1 stocks were aliquoted and stored at -80 ˚C.

7.2.2.3 Egg grown virus stocks

Embryonated hen eggs (Henry Stewart & Co.) were incubated at 37 ˚C in 40-50 % humidity for 10 days. Prior to infection, eggs were candled to check viability of the embryo. The shell was sterilised with 70 % ethanol (v/v) and two small holes were punctured in the egg shell, one just below the line of the air sac and one at the top of the egg. Virus was diluted to 100 PFU/ml in serum-free D-MEM and using a 1 ml syringe and 25 G needle 100 µl of diluted virus stock was inoculated into the allantoic cavity. The two punctures were sealed with Scotch Magic Tape and eggs were incubated for a further 48 h at 37 ˚C in 40-50 % humidity. Before harvesting the allantoic fluid, the eggs were chilled overnight at 4 ˚C. The top of the shell was removed using curved forceps and the air sac membrane was punctured. Allantoic fluid was collected using a P1000 Gilson, clarified at 4000 rpm for 10 min and stored at -80 ˚C.

7.2.2.4. Virus purification by ultracentrifugation

Eggs were infected as described above *7.2.2.3 Egg grown virus stocks*. 4 eggs were infected with 100 PFU of virus per egg to obtain ~20-50 ml of allantoic fluid for purification. The allantoic fluid was clarified twice at 2,100 x g for 10 min then 23 ml of allantoic fluid was loaded onto a 30 % sucrose/PBS cushion and spun at 30,000 rpm for 90 min at 4 ˚C using a SW28Ti rotor (Beckman). The resulting pellet was washed with 1 x PBS and resuspended in 50 µl of PBS overnight. The virus was further

purified by loading 200 µl of 30 % sucrose purified virus sample onto a 15-60 % sucrose/PBS gradient and spun for 38,000 rpm for 40 min at 4 ˚C, without a brake using a SA41Ti rotor (Beckman). The virus band was extracted from the gradient using a 1 ml syringe and 19 G needle. The extracted virus was loaded on to PBS and spun at 30,000 rpm for 9 min at 4 ˚C. The resulting pellet was resuspended in 100 µl of PBS overnight at 4 ˚C. Purified virus sample was stored at 4 ˚C for up to 10 days.

7.2.2.5 Infections

Cells were grown to ~90 % confluency in 24-well plates. Cells were washed 2 x 1 ml serum-free D-MEM and 200 µl of virus diluted in serum free D-MEM was added for 1 h at 37 ˚C in 5 % CO_2. For a multi-cycle infection, cells were infected with virus at an MOI of 0.01 and overlaid with virus growth media. For a single cycle infection, cells were infected with virus at an MOI of 3, virus inoculum was removed and an acid wash buffer (10 mM HCL, 150 mM NaCl (pH 3.0)) was applied for 1 min to inactive non-internalised virus particles. Cells were then washed 3 x 1 ml PBS and overlaid with complete DMEM. Supernatants were harvested at various time points post-infection and stored at -80 ˚C for downstream analyses.

7.2.2.6 Plaque assays

MDCK cells were seeded in 6-well plates and grown to 100 % confluency. Prior to infection cells were washed 1 x 2 ml serum D-MEM. Virus samples were serially diluted 10-fold in serum free D-MEM. Virus dilutions (400 µl per well) were added to the cells and incubated for 1 h at 37 ˚C in 5 % CO_2. After incubation, 2 ml of Avicel overlay (virus growth media supplemented with 1.2% (w/v) Avicel (FMC

BioPolymer, cat# 9004-34-6) was added to each well and incubated a further 48 h at 37 ˚C in 5 % CO_2. Cells were then fixed with 2 ml 10 % neutral buffered formalin per well and incubated for 20 min – 24 h. After fixation, the formalin/overlay was removed and cells were stained with 0.1 % (w/v) toluidine blue for 20 min – 1 h. Toluidine blue stain was then removed and cells were washed with water before counting the number of plaques per well (PFU/ml).

7.2.3 Drug analyses

7.2.3.1 Cytotoxicity assays

Drug cytotoxicity analyses were performed using the CellTiter-Glo viability assay (Promega, cat# G7570), which quantifies the ATP content of cells. A549 cells were seeded at 1 $x10^4$ cells/well in a 96-well flat clear bottom, opaque-walled plate (Corning, cat# 07-200-587). The following day, cells were incubated with 2-fold increasing concentrations of drug and/or DMSO in serum-free DMEM at 37 ˚C in 5 % CO_2 for 24 h. Equal volumes of the CellTiter-Glo reagent were added to each well and mixed for 2 min on an orbital shaker to induce cell lysis. The plate was incubated at room-temperature for 10 min to stabilise the luminescent signal before imaging with a micro plate reader (GloMax, Promega). An integration time of 0.24 sec per well was used.

7.2.3.2 Drug-dose inhibition assays

After a 1 h incubation with virus (as described in section *7.2.2.5 Infections*), inoculum was removed and 1 ml of media was added containing concentration of drug of interest. Drugs were typically diluted in 0.5-log_{10} increments. For multi-cycle dose response curves, compound was added to virus growth media and incubated for 24 h. For single cycle dose response curves, compound was added to complete media and incubated for 16 h. Virus supernatants were then harvested and titre was determined by plaque assay. To determine the IC_{50} values, data was converted to a % of the untreated control and plotted against a log_{10} inhibitor concentration. Dose-response curves were then fitted by a non-linear regression using the program GraphPad Prism.

7.2.3.3 Time of drug addition assays

A549 cells were seeded at 2 $x10^5$ cells/well in a 24-well plate and at $1x10^5$ cells/well on to 13 mm round coverslips. The following day, cells were washed 1 x 1 ml serum-free D-MEM and incubated with virus at an MOI of 3 for 1 h at 37 ˚C in 5 % CO_2. Cells were incubated with either DMSO or with KPT-335 (0.3 μM) an hour prior to infection, at time of infection or 2, 4, 6 and 8 h post-infection (p.i.). For infections carried out on coverslips, cells were fixed at 8 h p.i. and immunofluorescence analysis was performed as described in *7.2.6.3. Immunofluorescence staining*. For infections carried out in the 24-well plates, viral supernatant was harvested at 16 h p.i. and virus titre was determine by plaque assay.

7.2.3.4 Plaque reduction assays

MDCK cells were seeded at $1x10^6$ cells/well in 6-well plates. The following day, cells were washed 1 x 2 ml serum-free D-MEM and incubated with ~100-1000 PFU of virus for 1 h at 37 ˚C in 5 % CO_2. Virus inoculum was removed and cells were incubated with Avicel overlay containing either DMSO or KPT-335 (0.3 μM or 1 μM) for 48 h at 37 ˚C in 5 % CO_2. After incubation, the plaque reduction assays were processed and analysed as described for *7.2.2.6 Plaque assays*.

7.2.3.5 Serial passage

A549 cells were seeded at $1x10^6$ cells/well in a 6-well plate. The following day, cells were washed with 1 x 2 ml serum-free D-MEM and incubated with 200 μl of virus at an MOI of 0.001 for 1 h at 37˚C in 5% CO_2. Virus inoculum was removed and cells were overlaid with virus growth media containing DMSO, KPT-335 (0.15 μM or 0.3 μM) or amantadine (30 μM). 48 h p.i., virus supernatant was harvested and titre was determined by plaque assay as described above *7.2.2.6 Plaque assays.* After titre determination, the harvested viral supernatant was subject to further rounds of replication under the same conditions as described above. This was performed for 9-10 passages.

7.2.3.6 Plaque isolation

Plaque assays with serial passaged viruses were performed similarly as described above *6.2.2.5 Plaque assays* using an agarose overlay in place of the Avicel overlay. For agarose plaque assays, 7.5 ml of 2 % (w/v) boiled agar was mixed with 17.5 ml of minimum essential media (MEM) supplemented with 0.3 % (w/v) BSA, 0.2 % (v/v)

sodium bicarbonate, 10 mM HEPES, 0.007 % (w/v) Dextran, 3 mM L-glutamine, 140 U/ml penicillin, 140 µg/ml streptomycin and 1.4 µg/ml *N*-acetylated trypsin (NAT) and was incubated for 1 h at 37 ˚C in 5 % CO_2. Virus inoculum was removed and 2 ml of agarose overlay was added per well. Once agarose had set, plates were inverted and incubated at 37 ˚C in 5 % CO_2 for 48 h. Single plaques were then picked from the live cells using a cut P1000 tip and the isolated plaque was then ejected onto fresh MDCK cells in 24-well plate in 0.5 ml of virus growth media. Cells were incubated at 37 ˚C in 5 % CO_2 for 24 h to allow for virus propagation.

7.2.4 Molecular techniques

7.2.4.1 RNA extraction from viral supernatant

Extraction of viral RNA (vRNA) from virus supernatant was performed using a QIAamp viral RNA Mini Kit (Qiagen, cat# 52906), as per manufacture's instructions. Isolated vRNA was eluted in 30 µl of nuclease-free water and stored at -20 ˚C.

7.2.4.2 Reverse Transcription (RT)

vRNA was transcribed into complementarily DNA (cDNA) using a Verso cDNA Synthesis Kit (Thermo Scientific, cat# AB1453A) and a universal oligonucleotide primer (Uni12, *5'-AGCAAAAGCAGG-3'*), which binds to the 12 conserved nucleotides at the 3' end of influenza segments. 1 ng vRNA and 0.5 µM Uni12 primer were added to nuclease free water to make up a reaction volume of 10 µl. The vRNA/primer mix was incubated at 65 ˚C for 10 min and then a Verso reaction mix containing 20 % (v/v) cDNA synthesis buffer, 0.5 mM dNTPs and 1 µl Verso enzyme was added to give a

final reaction volume of 20 µl. The mix was further incubated for 1 h at 65 ˚C. RT reactions were stored at -20 ˚C.

7.2.4.3 Polymerase chain reaction (PCR)

Amplification of IAV gene segments was carried out using Taq DNA polymerase (Invitrogen, cat# 18038042). Forward and reverse oligonucleotide primers were designed to complement ends of the coding regions for segments 1, 2, 3, 5, 7 and 8 of A/PR/8/34 (Table 7.1.2.1) and sets of internal primers for segments 1, 2 and 3 were designed to amplify the middle regions of these larger genes (Table 7.1.2.1). Each reaction contained: 1 mM of each dNTP, 1.5 mM $MgCl_2$, 0.2 µM of each primer and 0.05 % buffer W1. Thermocycling condition were as follows: 94 ˚C for 2 min, followed by 94 ˚C for 1 min, 55 ˚C for 1 min and 72 ˚C for 3 min for 30 cycles and a final incubation at 72 ˚C for 10 min. PCR reactions were stored at 4 ˚C.

7.2.4.4 PCR purification

Before sequencing, the PCR product was purified using a QIAquick PCR purification kit (Qiagen, cat# 28104) as per manufacturer's instructions. PCR product was eluted in 30 µl of nuclease-free water and stored at -20 ˚C.

7.2.4.5 Site-directed mutagenesis of plasmid DNA

To generate DNA plasmids containing nucleotide changes of interest, mutagenesis was performed using a QuikChange Lightning Site-Directed Mutagenesis kit (Agilent, cat# 210518). Two complementary oligonucleotides were synthesised containing the desired mutation, flanked by the unmodified nucleotide sequence (Table 7.1.2.1).

Sample reactions were prepared as follows; 5 µl 10 x reaction buffer, 10-100 ng dsDNA template, 125 ng primer 1, 124 ng primer 2, 1 µl dNTP mix, 1.5 µl QuikSolution reagent and nuclease free water to a final volume of 50 µl. 1 µl of QuikChange lightning enzyme was added per reaction. Reactions were then cycled using the following conditions; first step, 95 ˚C for 2 min then 95 ˚C for 20 sec, 60 ˚C for 10 sec and 68 ˚C for 30 sec/kb of plasmid length for 18 cycles, followed by a final step at 68 ˚C for 5 min. 2 µl of Dpn I restriction enzyme was added directly to each amplification reaction and incubated at 37 ˚C for 5 min. Dpn I-treated DNA was then transformed as below; *7.2.4.6 Transformation of competent DH5α.*

7.2.4.6 Transformation of competent DH5α

Plasmid DNA (250 ng) or 2 µl of Dpn I-treated DNA (for mutagenesis reactions) was added to 10 µl of competent DH5α cells and was gently mixed and incubated 5-15 min on ice. The plasmid and cell mixture was incubated for 45 sec at 42 ˚C and immediately placed back on ice for 2 min. 900 µl of LB broth (15 g/l agar, 10 g/l tryptone, 5 g/l yeast extract, and 10 g/l sodium chloride (pH 7)) was added to the cells and placed in a shaker (200 rpm) for 1 h at 37 ˚C. Cells were pelleted using centrifugation (13,000 rpm for 1 min) and ~800 µl of supernatant was removed. The remaining cells were resuspended in the remaining supernatant and then spread on an agar plate with the appropriate antibiotic using a sterile spreader in the presence of a Bunsen burner flame to prevent contamination. Transformation plates were incubated at 37 ˚C for >16 h.

7.2.4.7 DNA gel electrophoresis

1 % (w/v) agarose was boiled in 1 x TAE running buffer (40 mM Tris, 20 mM acetic acid and 1mM EDTA) and 1:10,000 dilution of SYBR Safe DNA gel stain (ThermoFisher, cat# S33102) was added. DNA samples were mixed with 1 x DNA loading dye (6 x, 10 mM Tris-HCl (pH7.6), 0.15 % (w/v) Orange G dye, 0.03 % (w/v) xylene cyanol FF, 60 % (v/v) glycerol and 60 mM EDTA) and loaded into the set agarose gel alongside a 1kb DNA ladder (Promega, cat#G5711). Gels were run at 100 V for 45-60 min in TAE running buffer.

7.2.4.8 Sequencing of DNA

5 µl of template DNA (100 ng/ml plasmid DNA or 20-80 ng/ml of PCR reaction) was added to 5 µl of appropriate primer (5 µM) (Table 7.1.2.1). The sequencing mix was sent for Sanger sequencing performed by GATC Biotech (Germany). Sequencing results were analysed using the DNASTAR Lasergene 9 core suite.

7.2.5 Protein analyses

7.2.5.1 SDS-PAGE

Proteins were separated by molecular weight using sodium dodecyl sulfate polyacrylamide gel electrophoresis (SDS-PAGE). SDS-PAGE apparatus and reagents were supplied by Bio-Rad (Mini-Protean tetra system). Generally, 2 x 10^5 cells/well in a 24-well plate were lysed with 200 µl of Laemmli buffer (20 % (v/v) glycerol, 2 % (w/v) SDS, 100 mM DTT, 24 mM Tris and 0.016 % (v/v) xylene cyanol solution). Prior to SDS-PAGE, cell lysates were boiled at 95 ˚C for 5 min, vortexed briefly and

centrifuged for 1 min. 8-30 µl of sample was loaded per lane and separated on a 4-20 % gradient Protean TGX gel (Bio-Rad). For virion analysis, 2-10 µl of gradient purified virus was loaded per lane and separated on a 12 % Protean TGX gel (Rio-Rad). Gels were run at a constant voltage of 100 V for ~2 h in Tris-Glycine running buffer (25 mM Tris, 192 mM glycine and 0.1 % (w/v) SDS). Proteins were identified using a Precision Plus Protein dual colour molecular marker (Bio-Rad, cat#1610374). Proteins were visualised by Coomassie Brilliant Blue staining or western blot analysis (see below).

7.2.5.2 Coomassie blue protein staining

Protein samples separated by SDS-PAGE were fixed using a fixing solution (50 % (v/v) methanol, 10 % (v/v) acetic acid in deionised water). Gels were washed 3 x 15 min in fixing solution and were then stained using 0.2 % (w/v) Coomassie Brilliant Blue (R-250) in fixing solution for 30 min. Gels were then de-stained using a destaining solution (25 % (v/v) methanol, 5 % (v/v) acetic acid in deionised water) for 6 – 24 h before imaging on the LiCor Odyssey imaging platform.

7.2.5.3. Western Blotting

Proteins separated by SDS-PAGE were blotted onto 0.2 µM nitrocellulose membrane by semi-dry transfer using the Trans-Blot Turbo TM Transfer System (Bio-Rad). The transfer membrane and stacks were immersed in ~100 ml of transfer buffer for 2-3 min. The nitrocellulose membrane was placed on the polyacrylamide gel (positive cathode side) and placed between two ion reservoir stacks (Bio-Rad) in the cassette. The transfer was run at 2.5 A, 25.0 V for 7 min. Membranes were blocked with 5 %

skimmed milk/0.1 % Tween20/PBS for 20 min. Blocked membranes were washed 3 x 0.1 % Tween20/PBS (v/v) then incubated with the appropriate primary antibody diluted in 0.1 % Tween20/PBS (v/v) for 1 h at room temperature or 4 ˚C overnight. Membranes were washed as above and incubated at room temperature for 45 min with the appropriate secondary antibodies conjugated with near-infrared dye. Membranes were washed as above and analysed on the LiCor Odyssey imaging platform.

7.2.6 Immunofluorescent microscopy

7.2.6.1 High MOI infection

A549 cells were seeded onto 13 mm round coverslips at 1 x 10^5 cells/coverslip. The following day, cells were washed 1 x 1 ml serum free D-MEM and incubated with 200 µl of virus at an MOI of 3 for 1 h at 37 ˚C in 5 % CO_2. Virus inoculum was then removed and cells were overlaid with 1 ml complete media. 8 h p.i., cells were washed 3 x PBS and then fixed with 4 % (v/v) formaldehyde in PBS. Fixed cells were stained and analysed as described in *7.2.6.3. Immunofluorescent staining.*

7.2.6.2 Import assay

A549 cells were seeded onto coverslips (as described above) and washed 1 x 1 ml serum free D-MEM. Cells were then incubated with 2-10 µl of gradient purified virus (nominal MOI) for 1 h at 37 ˚C in 5 % CO_2. Infections were performed in the presence or absence of 100 µg/ml cycloheximide (CHX) to inhibit protein synthesis and 100 µM importazole (IMP) to inhibit nuclear import. Virus inoculum was then removed and cells were overlaid with 1 ml complete media. 3.5 h p.i., cells were washed 3 x

1ml PBS and then fixed with 4 % (v/v) formaldehyde in PBS. Fixed cells were stained and analysed as below *7.2.6.3. Immunofluorescent staining.*

7.2.6.3 Immunofluorescent staining

After infection, cells were washed 1 x 1 ml PBS (pre-warmed) and fixed using 250 µl 4% formaldehyde/PBS (v/v) for 20 min. Fixed cells were washed 3 x 1 ml 0.1% FBS/PBS (v/v) and permeabilised using 250 µl 0.2% Triton X-100 (v/v) for 5 min. Permeabilised cells were washed 3 x 1 ml 0.1% FBS/PBS (v/v) and stained with the appropriate primary antibody diluted in 0.1% FBS/PBS (v/v) for 1 h at room temperature. Cells were washed as above and incubated with appropriate fluorescent-labelled secondary antibody for 45 min at room temperature covered in foil to protect fluorophores from photobleaching. Cells were washed as before and stained with nuclei dye DAPI for 5 min at room temperature. Coverslips were mounted on a glass microscopy slide using ~3 µl ProLong Gold Antifade reagent (ThermoFisher, cat#P36934). Slides were cured at room temperature for at least 24 h before imaging.

7.2.6.4 Microscopy

Images were taken on either Leica DMLB microscope (x20 or x40 objective lens) or on a Zeiss LSM 710 confocal microscope (x63 objective lens). Fluorescence settings were kept consistent throughout the imaging of each experiment.

7.2.7 Molecular assays

7.2.7.1. Minireplicon

293T cells were seeded at 1 x 10^5 cells/well in a 24-well plate. The following day, 50ng pDUAL plasmids (PB2, PB1, PA and NP) and 20 ng firefly reporter plasmid (pPol I Luciferase) were diluted in 50 µl Opti-MEM for transfection. 1 µl lipofectamine2000 was mixed with 50 µl Opti-MEM and incubated for 5-10 min at room temperature. The lipofectamine2000 mixture was added to the plasmid mix and incubated for 30 min. Medium on the 293T cells was removed and 500 µl of Opti-MEM was added per well. 100 µl of transfection mix was added dropwise into each well and cells were incubated for 48 h at 37 ˚C in 5 % CO_2. The medium was then removed and cells were lysed with 100 µl of 1 x Reporter Lysis Buffer (Promega, cat# E4030). Cells were scraped and plates were centrifuged at 12000 x g for 2 min at 4 ˚C. 60 µl of cell lysate was added to an opaque 96-well plate (Corning, cat# CLS3362). 25 µl of 0.6 mM beetle luciferin (Promega, cat# E1601) was injected per well using a GloMax luciferase reader (GloMax, Promega) to measure luciferase activity (200 µl/sec injection speed, 0.5 sec gap and 5 sec integration time).

7.2.8 Interferon assays

7.2.8.1 IFN-type I dose inhibition experiments

A549 cells were seeded at 1 x 10^5 cells/well in a 24-well plate for 12 h. Cells were then treated with varying concentrations of exogenous universal Type I IFN (PBL Assay Science, cat# 11200) diluted in complete media. 24 h after treatment, cells were washed 1 x 1 ml serum free D-MEM and infected with virus at an MOI of 0.01 in 200

µl of serum free D-MEM for 1 h at 37 ˚C in 5 % CO_2. 24 h p.i., virus supernatant was harvested for titre determine and cell lysates were generated for western blot analysis.

7.2.8.2 IFN-I HEK-blue assays

A549 cells were seeded in 24-well plates at 2 x 10^5 cells/well. The following day, cells were infected with virus at an MOI of 3 as described in *7.2.2.5 Infections*. 24 h p.i. virus supernatant was harvested, clarified (3000 rpm, 5 min) and stored at -80 ˚C prior to assaying. To determine the IFN-I levels in the supernatant of infected cells, 20 µl of sample was incubated with 180 µl of HEK-Blue cell suspension (2.5 x 10^5 cells/ml) in a 96-well plate for 24 h at 37 ˚C in 5 % CO_2. 20 µl of HEK Blue cell supernatant was then incubated with 180 µl of Quanti-Blue substrate in a 96-well plate for 2 h at 37 ˚C. Absorbance (630 nm) was read using a microplate reader (GloMax, Promega) as a read-out for bioactive IFN-I levels in the samples. An IFN-I standard curve was produced by incubating known quantities of exogenous IFN-I alongside the infected cell supernatants.

7.2.9 Statistical analyses

All statistical tests were performed using GraphPad Prim 6 or Microsoft excel software.

References

Ahmen, N., Barrow, C., & Suphioglu, C. (2016). Exploring the Effects of Omega-3 and Omega-6 Fatty Acids on Allergy Using a HEK-Blue Cell Line. *International Journal of Molecular Sciences*, *17*(2), 220. http://doi.org/10.3390/ijms17020220

Akarsu, H., Burnmeister, W., Petosa, C., Petit, I., Muller, C., Ruigrok, R. W. H., & Baudin, F. (2003). Crystal structure of the M1 protein-binding domain of the in ̄uenza A virus nuclear export protein (NEP/NS2). *The EMBO Journal*, 1–10.

Alamares-Sapuay, J. G., Martinez-Gil, L., Stertz, S., Miller, M. S., Shaw, M. L., & Palese, P. (2013). Serum- and glucocorticoid-regulated kinase 1 is required for nuclear export of the ribonucleoprotein of influenza A virus. *Journal of Virology*, *87*(10), 6020–6026. http://doi.org/10.1128/JVI.01258-12

Alame, M. M., Massaad, E., & Zaraket, H. (2016). Peramivir: A Novel Intravenous Neuraminidase Inhibitor for Treatment of Acute Influenza Infections. *Frontiers in Microbiology*, *7*(e0131412), 647–14. http://doi.org/10.3389/fmicb.2016.00450

Amorim, M. J., Bruce, E. A., Read, E. K. C., Foeglein, A., Mahen, R., Stuart, A. D., & Digard, P. (2011). A Rab11- and Microtubule-Dependent Mechanism for Cytoplasmic Transport of Influenza A Virus Viral RNA. *Journal of Virology*, *85*(9), 4143–4156. http://doi.org/10.1128/JVI.02606-10

Amorim, M.-J., Read, E. K., Dalton, R. M., Medcalf, L., & Digard, P. (2006). Nuclear Export of Influenza A Virus mRNAs Requires Ongoing RNA Polymerase II Activity. *Traffic*, *8*(1), 1–11. http://doi.org/10.1111/j.1600-0854.2006.00507.x

Ashenberg, O., Padmakumar, J., Doud, M., & Bloom, J. (2017). Deep mutational scanning identifies sites in influenza nucleoprotein that affect viral inhibition by MxA. *PLoS Pathogens*, *13*(3), e1006288. http://doi.org/10.1371/-journal.ppat.1006288

Badham, M. D., & Rossman, J. S. (2016). Filamentous Influenza Viruses. *Current Clinical Microbiology Reports*, *3*(3), 155–161.

Balgi, A. D., Wang, J., Cheng, D. Y. H., Ma, C., Pfeifer, T. A., Shimizu, Y., et al.

(2013). Inhibitors of the Influenza A Virus M2 Proton Channel Discovered Using a High-Throughput Yeast Growth Restoration Assay. *PLoS ONE*, *8*(2), e55271–9. http://doi.org/10.1371/journal.pone.0055271

Baranovich, T., Saito, R., Suzuki, Y., Zaraket, H., Dapat, C., Caperig-Dapat, I., et al. (2010). Emergence of H274Y oseltamivir-resistant A(H1N1) influenza viruses in Japan during the 2008?2009 season. *Journal of Clinical Virology*, *47*(1), 23–28. http://doi.org/10.1016/j.jcv.2009.11.003

Baudin, F., Bach, C., Cusack, S., & Ruigrok, R. (1994). Strcuture of influenza virus RNP. I. Influenza virus nucleoprotein melts secondary structure in panhandle RNA and exposes the bases to the solvent. *The EMBO Journal*, *13*(13), 3158–3165.

Baudin, F., Petit, I., Weissenhorn, W., & Ruigrok, R. W. H. (2001). In Vitro Dissection of the Membrane and RNP Binding Activities of Influenza Virus M1 Protein. *Virology*, *281*(1), 102–108. http://doi.org/10.1006/viro.2000.0804

Baxter, R., Patriarca, P. A., Ensor, K., Izikson, R., Goldenthal, K. L., & Cox, M. M. (2011). Evaluation of the safety, reactogenicity and immunogenicity of FluBlok® trivalent recombinant baculovirus-expressed hemagglutinin influenza vaccine administered intramuscularly to healthy adults 50â€“64 years of age. *Vaccine*, *29*(12), 2272–2278. http://doi.org/10.1016/j.vaccine.2011.01.039

Beck, M., & Hurt, E. (2017). The nuclear pore complex: understanding its function through structural insight, *18*(2), 73–89. http://doi.org/10.1038/nrm.2016.147

Belardo, G., Cenciarelli, O., La Frazia, S., Rossignol, J.-F., & Santoro, M. G. (2015). Synergistic effect of nitazoxanide with neuraminidase inhibitors against influenza A viruses in vitro. *Antimicrobial Agents and Chemotherapy*, *59*(2), 1061–1069. http://doi.org/10.1128/AAC.03947-14

Belongia, E. A., Kieke, B. A., Donahue, J. G., Greenlee, R. T., Balish, A., Foust, A., et al. (2009). Effectiveness of Inactivated Influenza Vaccines Varied Substantially with Antigenic Match from the 2004–2005 Season to the 2006–2007 Season. *The Journal of Infectious Diseases*, *199*(2), 159–167. http://doi.org/10.1086/595861

Belshe, R. B., Smith, M. H., Hall, C. B., Betts, R., & Hay, A. J. (1988). Genetic basis of resistance to rimantadine emerging during treatment of influenza virus infection. *Journal of Virology*, *62*(5), 1508–1512.

Belshe, R., Edwards, K., Vesikari, T., Black, S., Walker, R., Hultquist, M., et al. (2007). Live Attenuated versus Inactivated Influenza Vaccine in Infants and Young Children. *The New England Journal of Medicine*, *356*, 685–696.

Bialas, K. M., Bussey, K. A., Stone, R. L., & Takimoto, T. (2014). Specific Nucleoprotein Residues Affect Influenza Virus Morphology. *Journal of Virology*, *88*(4), 2227–2234. http://doi.org/10.1128/JVI.03354-13

Bier, K., York, A., & Fodor, E. (2011). Cellular cap-binding proteins associate with influenza virus mRNAs. *Journal of General Virology*, *92*(7), 1627–1634. http://doi.org/10.1099/vir.0.029231-0

Blass, D., Patzelt, E., & Kuechler, E. (1982). Cap-Recognizing Protein of Influenza Virus. *Virology*, *116*, 339–348.

Bouloy, M., Plotch, S., & Krug, R. (1978). Globin mRNAs are primers for the transcription of influenzaviral RNA *in vitro*. *Proc. Natl. Acad. Sci, USA*, *75*(10), 48886–44890.

Bourmakina, S. V., & García-Sastre, A. (2003). Reverse genetics studies on the filamentous morphology of influenza A virus. *Journal of General Virology*, *84*(Pt 3), 517–527. http://doi.org/10.1099/vir.0.18803-0

Braam, J., Ulmanen, I., & Krug, R. M. (1983). Molecular model of a eucaryotic transcription complex: functions and movements of influenza P proteins during capped RNA-primed transcription. *Cell*, *34*(2), 609–618.

Bright, R. A. (2006). Adamantane Resistance Among Influenza A Viruses Isolated Early During the 2005-2006 Influenza Season in the United States. *Jama*, *295*(8), 891–894. http://doi.org/10.1001/jama.295.8.joc60020

Bright, R., Shay, D., Shu, B., Cox, N., & Klimov, A. (2006). Adamantane Resistance Among Influenza A Viruses Isolated Early During the 2005-2006 Influenza Season in the United States. *The JAMA Network*, *295*(8), 891–894.

Brown, D., & Rose, J. (1992). Sorting of GPI-anchored proteins to glycolipid-enriched membrane subdomains during transport to the apical cell surface. *Cell*, *68*(3), 533–544.

Bui, M., Wills, E., Helenius, A., & Whittaker, G. (2000). Role of the Influenza Virus M1 Protein in Nuclear Export of Viral Ribonucleoproteins. *Journal of Virology*,

74(4), 1781–1786.

Bukrinskaya, A. G., Vorkunova, G. K., & Vorkunova, N. K. (1979). Cytoplasmic and nuclear input virus RNPs in influenza virus-infected cells. *Journal of General Virology*, *45*(3), 557–567. http://doi.org/10.1099/0022-1317-45-3-557

Burnham, A. J., Baranovich, T., Marathe, B. M., Armstrong, J., Webster, R. G., & Govorkova, E. A. (2014). Fitness costs for Influenza B viruses carrying neuraminidase inhibitor-resistant substitutions: underscoring the importance of E119A and H274Y. *Antimicrobial Agents and Chemotherapy*, *58*(5), 2718–2730. http://doi.org/10.1128/AAC.02628-13

Cacoub, P., Saadoun, D., Limal, N., Sene, D., Lidove, O., & Piette, J. (2005). PEGylated interferon alfa-2b and ribavirin treatment in patients with hepatitis C virus-related systemic vasculitis. *Arthritis and Rheumatism*, *52*(3), 911–915. http://doi.org/10.1002/art.20958

Cady, S. D., Wang, J., Wu, Y., DeGrado, W. F., & Hong, M. (2011). Specific Binding of Adamantane Drugs and Direction of Their Polar Amines in the Pore of the Influenza M2 Transmembrane Domain in Lipid Bilayers and Dodecylphosphocholine Micelles Determined by NMR Spectroscopy. *Journal of the American Chemical Society*, *133*(12), 4274–4284. http://doi.org/10.1021/ja102581n

Calder, L., Wasilewski, S., Berriman, J., & Rosenthal, P. (2010). Structural organization of a filamentous influenza A virus, *107*(23), 1–61065–1069. http://doi.org/10.1073/pnas.1002123107/-/DCSupplemental/sm01.mp4

Calderia, D., Alarcao, J., Vaz-Carnerio, A., & Costa, J. (2012). Risk of pneumonia associated with use of angiotensin converting enzyme inhibitors and angiotensin receptor blockers: systematic review and meta-analysis. *Bmj*, *345*, e4260.

Calfee, D., & Hayden, F. (1998). New approaches to influenza chemotherapy. Neuraminidase inhibitors. *Drugs*, *56*(4), 537–553.

Cao, S., Liu, X., Yu, M., Li, J., Jia, X., Bi, Y., et al. (2012). A Nuclear Export Signal in the Matrix Protein of Influenza A Virus Is Required for Efficient Virus Replication. *Journal of Virology*, *86*(9), 4883–4891. http://doi.org/10.1128/JVI.06586-11

Campbell, P. J., Danzy, S., Kyriakis, C. S., Deymier, M. J., Lowen, A. C., & Steel, J.

(2014). The M Segment of the 2009 Pandemic Influenza Virus Confers Increased Neuraminidase Activity, Filamentous Morphology, and Efficient Contact Transmissibility to A/Puerto Rico/8/1934-Based Reassortant Viruses. *Journal of Virology*, *88*(7), 3802–3814. http://doi.org/10.1128/JVI.03607-13

Capparelli, E. V., & Syed, S. S. (2008). Nitazoxanide treatment of Cryptosporidium parvum in human immunodeficiency virus-infected children. *The Pediatric Infectious Disease Journal*, *27*(11), 1041. http://doi.org/10.1097/-INF.0b013e3181862ae1

Centers for Disease Control and Prevention (CDC), 2009. Seasonal Influenza. [Online] Available; https://www.cdc.gov/flu/pandemic-resources/index.htm

Chase, G. P., Rameix-Welti, M.-A., Zvirbliene, A., Zvirblis, G., Götz, V., Wolff, T., et al. (2011). Influenza Virus Ribonucleoprotein Complexes Gain Preferential Access to Cellular Export Machinery through Chromatin Targeting. *PLoS Pathogens*, *7*(9), e1002187–14. http://doi.org/10.1371/journal.ppat.1002187

Chen, W., Calvo, P. A., Malide, D., Gibbs, J., Schubert, U., Bacik, I., et al. (2001). A novel influenza A virus mitochondrial protein that induces cell death. *Nature Medicine*, *7*(12), 1306–1312. http://doi.org/10.1038/nm1201-1306

Cheng, C., Rayner, J., Smith, G., Wang, P., Naipospos, T., Zhang, J., et al. (2006). Distribution of amantadine-resistant H5N1 avian influenza variants in Asia. *The Journal of Infectious Diseases*, *193*(12), 1626–1629. http://doi.org/-10.1086/504723

Chutiwitoonchai, N., Kakisaka, M., Yamada, K., & Aida, Y. (2014). Comparative Analysis of Seven Viral Nuclear Export Signals (NESs) Reveals the Crucial Role of Nuclear Export Mediated by the Third NES Consensus Sequence of Nucleoprotein (NP) in Influenza A Virus Replication. *PLoS ONE*, *9*(8), e105081–13. http://doi.org/10.1371/journal.pone.0105081

Colman, P. (1994). Influenza virus neuraminidase: Structure, antibodies, and inhibitors. *Protein Science*, *3*, 1687–1696.

Compans, R., Content, J., & Duesberg, P. (1972). Structure of the Ribonucleoprotein of Influenza Virus. *Journal of Virology*, *10*(4), 795–800.

Couch, R., Keitel, W., & Cate, T. (1997). Improvement of Inactivated Influenza Virus Vaccines. *The Journal of Infectious Diseases*, *176*, 176: S38–44.

Cox, J., Hampson, A., & Hamilton, R. (1980). An Immunoflurescence Study of Influenza Virus Filament Formation. *Archives of Virology*, *63*, 275–284.

Cox, M. M. J., Patriarca, P. A., & Treanor, J. (2008). FluBlok, a recombinant hemagglutinin influenza vaccine. *Influenza and Other Respiratory Viruses*, *2*(6), 211–219. http://doi.org/10.1111/j.1750-2659.2008.00053.

Cros, J., García-Sastre, A., & Palese, P. (2005). An Unconventional NLS is Critical for the Nuclear Import of the Influenza A Virus Nucleoprotein and Ribonucleoprotein. *Traffic*, *6*, 205–213. http://doi.org/10.1111/j.1600-0854.2004.00263.x

Dapat, C., Kondo, H., Dapat, I. C., Baranovich, T., Suzuki, Y., Shobugawa, Y., et al. (2013). Neuraminidase inhibitor susceptibility profile of pandemic and seasonal influenza viruses during the 2009â€“2010 and 2010â€“2011 influenza seasons in Japan. *Antiviral Research*, *99*(3), 261–269. http://doi.org/10.1016-/j.antiviral.2013.06.003

Danzy, S., Studdard, L. R., Manicassamy, B., Solorzano, A., Marshall, N., García-Sastre, A., et al. (2014). Mutations to PB2 and NP proteins of an avian influenza virus combine to confer efficient growth in primary human respiratory cells. *Journal of Virology*, *88*(22), 13436–13446. http://doi.org/10.1128/JVI.01093-14

Das, A., Wei, G., Parikh, K., & Liu, D. (2015). Selective inhibitors of nuclear export (SINE) in hematological malignancies. *Experimental Hematology & Oncology*, *4*(1), 7. http://doi.org/10.1186/s40164-015-0002-5

Davies, W. L., Grunert, R. R., Haff, R F., Mcgahen, J. W., Neumayer, E. M., Paulshock, M., et al. (1964). Antiviral activity of 1-adamantanamine (amantadine). *Science*, *144*(3620), 862–863.

De Villiers, P. J. T., Steele, A. D., Hiemstra, L. A., Rappaport, R., Dunning, A. J., Gruber, W. C., & Forrest, B. D. (2009). Efficacy and safety of a live attenuated influenza vaccine in adults 60 years of age and older. *Vaccine*, *28*(1), 228–234. http://doi.org/10.1016/j.vaccine.2009.09.092

de Wit, E., Spronken, M. I. J., Bestebroer, T. M., Rimmelzwaan, G. F., Osterhaus, A. D. M. E., & Fouchier, R. A. M. (2004). Efficient generation and growth of influenza virus A/PR/8/34 from eight cDNA fragments. *Virus Research*, *103*(1-2), 155–161. http://doi.org/10.1016/j.virusres.2004.02.028

Dennis, E., & Norris, P. (2015). Eicosanoid storm in infection and inflammation. *Nature Reviews. Immunology*, *15*(8), 511–523. http://doi.org/10.1038/nri3859

Deyde, V. M., Xu, X., Bright, R. A., Shaw, M., Smith, C. B., Zhang, Y., et al. (2007). Surveillance of resistance to adamantanes among influenza A(H3N2) and A(H1N1) viruses isolated worldwide. *The Journal of Infectious Diseases*, *196*(2), 249–257. http://doi.org/10.1086/518936

Dias, A., Bouvier, D., Crépin, T., McCarthy, A. A., Hart, D. J., Baudin, F., et al. (2009). The cap-snatching endonuclease of influenza virus polymerase resides in the PA subunit. *Nature*, *458*(7240), 914–918. http://doi.org/10.1038/nature07745

Dittmann, J., Stertz, S., Grimm, D., Steel, J., García-Sastre, A., Haller, O., & Kochs, G. (2008). Influenza A virus strains differ in sensitivity to the antiviral action of Mx-GTPase. *Journal of Virology*, *82*(7), 3624–3631. http://doi.org/-10.1128/JVI.01753-07

Dobson, J., Whitley, R., Pocock, S., & Monto, A. (2015). Articles Oseltamivir treatment for influenza in adults: a meta-analysis of randomised controlled trials. *The Lancet*, *385*(9979), 1729–1737. http://doi.org/10.1016/S0140-6736(14)62449-1

Dong, X., Biswas, A., & Chook, Y. M. (2009). Structural basis for assembly and disassembly of the CRM1 nuclear export complex. *Nature Structural & Molecular Biology*, *16*(5), 558–560.

Dong, G., Peng, C., Luo, J., Wang, C., Han, L., Wu, B., et al. (2015). Adamantane-Resistant Influenza A Viruses in the World (1902–2013): Frequency and Distribution of M2 Gene Mutations. *PLoS ONE*, *10*(3), e0119115–20. http://doi.org/10.1371/journal.pone.0119115

Dunning, J., Baillie, J. K., Cao, B., & Hayden, F. G. (2014). Antiviral combinations for severe influenza. *The Lancet Infectious Diseases*, *14*(12), 1259–1270. http://doi.org/10.1016/S1473-3099(14)70821-7

Duval, X., de Werf, S., Blanchon, T., Mosnier, A., Bouscamber-Duchamp, M., Tibi, A., et al. (2010). Efficacy of oseltamivir-zanamivir combination compared to each monotherapy for seasonal influenza: a randomized placebo-controlled trial. *PLoS Medicine*, *7*(11), e1000362. http://doi.org/10.1371/journal.pmed.1000362

Duxbury, A., Hampson, A., & Sievers, J. (1968). Antibody Response in Humans to Deoxycholate-Treated Influenza Virus Vaccine. *The Journal of Immunology*, *101*, 62–67.

ECDC. (2016). Expert Opinion on neuraminidase inhibitors for prevention and treatment of influenza, 1–39.

Edinger, T. O., Pohl, M. O., & Stertz, S. (2014). Entry of influenza A virus: host factors and antiviral targets. *Journal of General Virology*, *95*(Pt_2), 263–277. http://doi.org/10.1099/vir.0.059477-0

Edmond, J., Johnston, R., Kidd, D., Rylance, H., & Sommerville, R. (1966). The inhibition of neuraminidase and antiviral action. *British Journal of Pharmacology Chemotherpy*, *27*, 415–426.

Eefje J A Schrauwen, R. A. M. F., & Fouchier, R. A. M. (2014). Host adaptation and transmission of influenza A viruses in mammals. *Emerging Microbes & Infections*, *3*(2), e9 http://doi.org/10.1038/emi.2014.9

Eierhoff, T., Hrincius, E. R., Rescher, U., Ludwig, S., & Ehrhardt, C. (2010). The Epidermal Growth Factor Receptor (EGFR) Promotes Uptake of Influenza A Viruses (IAV) into Host Cells. *PLoS Pathogens*, *6*(9), e1001099–16. http://doi.org/10.1371/journal.ppat.1001099

Eisfeld, A. J., Neumann, G., & Kawaoka, Y. (2014). At the centre: influenza A virus ribonucleoproteins. *Nature Publishing Group*, *13*(1), 28–41. http://doi.org/10.1038/nrmicro3367

Elleman, C. J., & Barclay, W. S. (2004). The M1 matrix protein controls the filamentous phenotype of influenza A virus. *Virology*, *321*(1), 144–153. http://doi.org/10.1016/j.virol.2003.12.009

Elton, D., & Bishop, K. (1999). Modulation of Nuclear Localization of the Influenza Virus Nucleoprotein through Interaction with Actin Filaments. *Journal of Virology*, *73*(3), 2222–2231.

Elton, D., Simpson-Holley, M., Archer, K., Medcalf, L., Hallam, R., McCauley, J., & Digard, P. (2001). Interaction of the Influenza Virus Nucleoprotein with the Cellular CRM1-Mediated Nuclear Export Pathway. *Journal of Virology*, *75*(1), 408–419. http://doi.org/10.1128/JVI.75.1.408-419.2001

Elton, D., Amorim, M.-J., Medcalf, L., & Digard, P. (2005). “Genome gating;” polarized intranuclear trafficking of influenza virus RNPs. *Biology Letters*, *1*(2), 113–117. http://doi.org/10.1098/rsbl.2004.0253

Fedson, D. (2009). Confronting the next influenza pandemic with anti-inflammatory and immunomodulatory agents: why they are needed and how they might work. *Influenza and Other Respiratory Viruses*, *3*(4), 129–142.

Fischer, U., Huber, J., Boelens, W. C., Mattaj, I. W., & Luhrmann, R. (1995). The HIV-1 Rev activation domain is a nuclear export signal that accesses an export pathway used by specific cellular RNAs. *Cell*, *82*(3), 475–483.

Fodor, E., Devenish, L., Engelhardt, O. G., Palese, P., Brownlee, G. G., & García-Sastre, A. (1999). Rescue of influenza A virus from recombinant DNA. *Journal of Virology*, *73*(11), 9679–9682.

Fodor, E. (2013). The RNA polymerase of influenza A virus: mechanisms of viral transcription and replication. *Acta Virologica*, *57*(02), 113–122. http://doi.org/10.4149/av_2013_02_113

Frederick, G., & H, H. (2006). Antiviral Resistance in Influenza Viruses - Implications for Management and Pademic Response. *The New England Journal of Medicine*, *354*(8), 785–788.

Fujii, K., Fujii, Y., Noda, T., Muramoto, Y., Watanabe, T., Takada, A., et al. (2005). Importance of both the coding and the segment-specific noncoding regions of the influenza A virus NS segment for its efficient incorporation into virions. *Journal of Virology*, *79*(6), 3766–3774. http://doi.org/10.1128/JVI.79.6.3766-3774.2005

Fujii, Y., Watanabe, T., Yoshida, T., & Kawaoka, Y. (2003). Selective incorporation of influenza virus RNA segments into virions. *Proc. Natl. Acad. Sci, USA*, *100*(4), 2002–2007.

Furuta, Y., Gowen, B. B., Takahashi, K., Shiraki, K., Smee, D. F., & Barnard, D. L. (2013). Favipiravir (T-705), a novel viral RNA polymerase inhibitor. *Antiviral Research*, *100*(2), 446–454. http://doi.org/10.1016/j.antiviral.2013.09.015

Galabov, A. S., Mileva, M., Simeonova, L., & Gegova, G. (2016). Combination activity of neuraminidase inhibitor oseltamivir and -tocopherol in influenza virus A (H3N2) infection in mice. *Antiviral Chemistry and Chemotherapy*, *24*(3-4), 83–91. http://doi.org/10.1177/2040206616656263

Garten, R., Davis, C., Russel, C., Shu, B., Lindstorm, S., Balish, A., Sessions, W., et al. (2009). Antigenic and genetic characteristics of swine-origin 2009 A(H1N1) influenza viruses circulating in humans. *Science*, *325*(5937), 197–201. http://doi.org/10.1126/science.11762

Gorse, G., Otto, E., Powers, D., Chambers, G., Eickhoff, C., & Newman, F. (1996). Induction of Mucosal Antibodies by Live Attenuated and Inactivated Influenza Virus Vaccines in the Chronically. *The Journal of Infectious Diseases*, *173*, 285–290.

Gottschalk, A. (1959). On the mechanism underlying initiation of influenza virus infection. *Ergebnisse Der Mikrobiologie, Immunitatsforschung Und Experimentellen Therapie*, *32*, 1–22.

Götz, V., Magar, L., Dornfeld, D., Giese, S., Pohlmann, A., Höper, D., et al. (2016). Influenza A viruses escape from MxA restriction at the expense of efficient nuclear vRNP import. *Nature Publishing Group*, *6*, 1–15. http://doi.org/10.1038/srep23138

Govorkova, E. A., Fang, H.-B., Tan, M., & Webster, R. G. (2004). Neuraminidase inhibitor-rimantadine combinations exert additive and synergistic anti-influenza virus effects in MDCK cells. *Antimicrobial Agents and Chemotherapy*, *48*(12), 4855–4863. http://doi.org/10.1128/AAC.48.12.4855-4863.2004

Greenhawt, M. (2014). Influenza vaccination in asthmatic patients. *Journal of Allergy and Clinical Immunology*, *133*(4), 1233–1234.e3. http://doi.org/10.1016-/j.jaci.2014.02.009

Gubareva, L. V., Webster, R. G., & Hayden, F. G. (2001). Comparison of the activities of zanamivir, oseltamivir, and RWJ-270201 against clinical isolates of influenza virus and neuraminidase inhibitor-resistant variants. *Antimicrobial Agents and Chemotherapy*, *45*(12), 3403–3408. http://doi.org/10.1128/AAC.45.12.3403-3408.2001

Gulick, R. (2002). Structured Treatment Interruption in Patients Infected with HIV. *Current Opinion in Drugs*, *62*(2), 245–253.

Haffizulla, J., Hartman, A., Hoppers, M., Resnick, H., Samudrala, S., Ginocchio, C., et al. (2014). Effect of nitazoxanide in adults and adolescents with acute uncomplicated influenza: a double-blind, randomised, placebo-controlled, phase

2b/3 trial. *The Lancet Infectious Diseases*, *14*(7), 609–618. http://doi.org/10.1016/S1473-3099(14)70717-0

Hale, B. G., Randall, R. E., Ortin, J., & Jackson, D. (2008). The multifunctional NS1 protein of influenza A viruses. *Journal of General Virology*, *89*(10), 2359–2376. http://doi.org/10.1099/vir.0.2008/004606-0

Hale, B. G., Albrecht, R. A., & García-Sastre, A. (2010). Innate immune evasion strategies of influenza viruses. *Future Microbiology*, *5*(1), 23–41. http://doi.org/10.2217/fmb.09.108

Hamilton, B. S., Whittaker, G. R., & Daniel, S. (2012). Influenza Virus-Mediated Membrane Fusion: Determinants of Hemagglutinin Fusogenic Activity and Experimental Approaches for Assessing Virus Fusion. *Viruses*, *4*(12), 1144–1168. http://doi.org/10.3390/v4071144

Han, H., Cui, Z. Q., Wang, W., Zhang, Z. P., Wei, H. P., Zhou, Y. F., & Zhang, X. E. (2010). New regulatory mechanisms for the intracellular localization and trafficking of influenza A virus NS1 protein revealed by comparative analysis of A/PR/8/34 and A/Sydney/5/97. *Journal of General Virology*, *91*(12), 2907–2917. http://doi.org/10.1099/vir.0.024943-0

Handel, A., Regoes, R. R., & Antia, R. (2006). The Role of Compensatory Mutations in the Emergence of Drug Resistance. *PLoS Computational Biology*, *2*(10), e137.

Hao, L., Sakurai, A., Watanabe, T., Sorensen, E., Nidom, C. A., Newton, M. A., et al. (2008). Drosophila RNAi screen identifies host genes important for influenza virus replication. *Nature*, *454*(7206), 890–893. http://doi.org-/10.1038/nature07151

Hara, K., Schmidt, F. I., Crow, M., & Brownlee, G. G. (2006). Amino acid residues in the N-terminal region of the PA subunit of influenza A virus RNA polymerase play a critical role in protein stability, endonuclease activity, cap binding, and virion RNA promoter binding. *Journal of Virology*, *80*(16), 7789–7798. http://doi.org/10.1128/JVI.00600-06

Harada, S., Yokomizo, K., Monde, K., Maeda, Y., & Yusa, K. (2007). A broad antiviral neutral glycolipid, fattiviracin FV-8, is a membrane fluidity modulator. *Cellular Microbiology*, *9*(1), 196–203. http://doi.org/10.1111/j.1462-5822.2006.00781.x

Harris, A., Cardone, G., Winkler, D., Haymann, B., Brecher, M., White, J., & Steven, A. (2006). Influenza virus pleiomorphy characterized by cryoelectron tomography, *103*(50), 19123–19127.

Hayden, F., & Hay, A. (1992). Emergence and transmission of influenza A viruses resistant to amantadine and rimantadine. *Current Topics in Microbiology and Immunology*, *176*, 119–130.

Helenius, A. (1992). Unpacking the incoming influenza virus. *Cell*, *69*(4), 577–578.

Huang, T., Palese, P., & Krystal, M. (1990). Determination of influenza virus proteins required for genome replication. *Journal of Virology*, *64*(11), 5669–5673.

Huang, T., Chen, J., Chen, Q., Wang, H., Yao, Y., Chen, J., & Chen, Z. (2012). A Second CRM1-Dependent Nuclear Export Signal in the Influenza A Virus NS2 Protein Contributes to the Nuclear Export of Viral Ribonucleoproteins. *Journal of Virology*, *87*(2), 767–778. http://doi.org/10.1128/JVI.06519-11

Hughes, M. (2000). Influenza A virus NS2 protein mediates vRNP nuclear export through NES-independent interaction with hCRM1. *The EMBO Journal*, 1–8.

Hause, B. M., Ducatez, M., Collin, E. A., Ran, Z., Liu, R., Sheng, Z., et al. (2013). Isolation of a Novel Swine Influenza Virus from Oklahoma in 2011 Which Is Distantly Related to Human Influenza C Viruses. *PLoS Pathogens*, *9*(2), e1003176–11. http://doi.org/10.1371/journal.ppat.1003176

Hayden, F. G., & Hay, A. J. (1992). Emergence and transmission of influenza A viruses resistant to amantadine and rimantadine. *Current Topics in Microbiology and Immunology*, *176*, 119–130.

Hoffman, P., Sisson, G., Croxen, M., Welch, K., Harman, W., Cremades, N., & Morash, M. (2007). Antiparasitic Drug Nitazoxanide Inhibits the Pyruvate Oxidoreductases of Helicobacter pylori, Selected Anaerobic Bacteria and Parasites, and Campylobacter jejuni. *Antimicrobial Agents and Chemotherapy*, *51*(3), 868–876.

Hogner, K., Wolff, T., Pleschka, S., Plog, S., Gruber, A. D., Kalinke, U., et al. (2013). Macrophage-expressed IFN-beta contributes to apoptotic alveolar epithelial cell injury in severe influenza virus pneumonia. *PLoS Pathogens*, *9*(2), e1003188. http://doi.org/10.1371/journal.ppat.1003188

Hsu, M., Parvin, J., Gupta, S., Krystal, M., & Palese, P. (1987). Genomic RNAs of influenza viruses are held in a circular conformation in virions and in infected cells by a terminal panhandle. *Proc. Natl. Acad. Sci, USA*, *84*, 8140–8144.

Huang, S., Chen, J., Chen, Q., Wang, H., Yao, Y., Chen, J., & Chen, Z. (2012). A Second CRM1-Dependent Nuclear Export Signal in the Influenza A Virus NS2 Protein Contributes to the Nuclear Export of Viral Ribonucleoproteins. *Journal of Virology*, *87*(2), 767–778. http://doi.org/10.1128/JVI.06519-11

Hurt, A. C., Besselaar, T. G., Daniels, R. S., Ermetal, B., Fry, A., Gubareva, L., et al. (2016). Global update on the susceptibility of human influenza viruses to neuraminidase inhibitors, 2013;2015. *Antiviral Research*, *132*(C), 178–185. http://doi.org/10.1016/j.antiviral.2016.06.001

Hussain, M., Galvin, H., Haw, T. Y., Nutsford, A., & Husain, M. (2017). Drug resistance in influenza A virus: the epidemiology and management. *Infection and Drug Resistance*, *Volume 10*, 121–134. http://doi.org/10.2147/IDR.S105473

Hutchinson, E. C., Charles, P. D., Hester, S. S., Thomas, B., Trudgian, D., Mart nez-Alonso, M. N., & Fodor, E. (2014). Conserved and host-specific features of influenza virion architecture. *Nature Communications*, *5*, 4816–25. http://doi.org/10.1038/ncomms5816

Hutten, S., & Kehlenbach, R. H. (2007). CRM1-mediated nuclear export: to the pore and beyond. *Trends in Cell Biology*, *17*(4), 193–201. http://doi.org/-10.1016/j.tcb.2007.02.003

Hwang, I., Scott, J., Kakarla, T., Duriancik, D., Choi, S., Cho, C., Lee, T., Park, H., French, A., Beli, E., Gardner, E., & Kim, S. (2012). Activation mechanisms of natural killer cells during influenza virus infection. *PLoS ONE*, *7*(12), e51858.

Ilyushina, N. A., Hay, A., Yilmaz, N., Boon, A. C. M., Webster, R. G., & Govorkova, E. A. (2008). Oseltamivir-Ribavirin Combination Therapy for Highly Pathogenic H5N1 Influenza Virus Infection in Mice. *Antimicrobial Agents and Chemotherapy*, *52*(11), 3889–3897.

Ilyushina, N. A., Hoffmann, E., Salomon, R., Webster, R. G., & Govorkova, E. A. (2007). Amantadine-oseltamivir combination therapy for H5N1 influenza virus infection in mice. *Antiviral Therapy*, *12*(3), 363–370.

Iwasaki, A., & Pillai, P. S. (2014). Innate immunity to influenza virus infection. *Nature*

Publishing Group, *14*(5), 315–328. http://doi.org/10.1038/nri3665

Jagger, B. W., Wise, H. M., Kash, J. C., Walters, K. A., Wills, N. M., Xiao, Y. L., et al. (2012). An Overlapping Protein-Coding Region in Influenza A Virus Segment 3 Modulates the Host Response. *Science*, *337*(6091), 199–204. http://doi.org/10.1126/science.1222213

Jackson, D., Murray, J., White, D., & Gerhard, W. (1982). Enumeration of antigenic sites of influenza virus hemagglutinin. *Infection and Immunity*, *37*(3), 912–918.

Jefferson, T., Jones, M., Doshi, P., Spencer, E. A., Onakpoya, I., & Heneghan, C. J. (2014). Oseltamivir for influenza in adults and children: systematic review of clinical study reports and summary of regulatory comments. *Bmj*, *348*(apr09 2), g2545–g2545. http://doi.org/10.1136/bmj.g2545

Jenning, O., Finch, J., & Roberston, J. (1983). Does the higher order structure of the influenza virus ribonucleoprotein guide sequence rearrangements in influenza viral RNA? *Cell*, *34*(2), 619–627.

Jewel, N., Vaghefi, N., Mertz, S., Akter, P., Peebles, R, Bakaletz, L., et al. (2007). Differential type I interferon induction by respiratory syncytial virus and influenza a virus in vivo. *Journal of Virology*, *81*(18), 9790–9800. http://doi.org/10.1128/JVI.00530-07

Jorba, N. R., Coloma, R. O., & Ort n, J. (2009). Genetic trans-Complementation Establishes a New Model for Influenza Virus RNA Transcription and Replication. *PLoS Pathogens*, *5*(5), e1000462–14. http://doi.org/10.1371/-journal.ppat.1000462

Joseph, U., Su, Y. C. F., Vijaykrishna, D., & Smith, G. J. D. (2016). The ecology and adaptive evolution of influenza A interspecies transmission. *Influenza and Other Respiratory Viruses*, *11*(1), 74–84. http://doi.org/10.1111/irv.12412

Kallfass, C., Lienenklaus, S., Weiss, S., & Staeheli, P. (2013). Visualizing the beta interferon response in mice during infection with influenza A viruses expressing or lacking nonstructural protein 1. *Journal of Virology*, *87*(12), 6925–6930. http://doi.org/10.1128/JVI.00283-13

Kakisaka, M., Sasaki, Y., Yamada, K., Kondoh, Y., Hirokazu, H., & Osada, H. (2015). A Novel Antiviral Target Structure Involved in the RNA Binding, Dimerization, and Nuclear Export Functions of the Influenza A Virus Nucleoprotein. *PLoS*

Pathogens, *11*(7), e1005062.

Kashiwagi, S., Watanabe, A., Ikematsu, H., Uemori, M., & Awamura, S. (2016). Long-acting Neuraminidase Inhibitor Laninamivir Octanoate as Post-exposure Prophylaxis for Influenza. *Clinical Infectious Diseases*, *63*(3), 330–337. http://doi.org/10.1093/cid/ciw255

Kato, H., Takeuchi, O., Sato, S., Yoneyama, M., Yamamoto, M., Matsui, K., et al. (2006). Differential roles of MDA5 and RIG-I helicases in the recognition of RNA viruses. *Nature*, *441*(7089), 101–105. http://doi.org/10.1038/nature04734

Kawaguchi, A., Matsumoto, K., & Nagata, K. (2012). YB-1 functions as a porter to lead influenza virus ribonucleoprotein complexes to microtubules. *Journal of Virology*, *86*(20), 11086–11095. http://doi.org/10.1128/JVI.00453-12

Killingley, B., & Nguyen-Van-Tam, J. (2013). Routes of influenza transmission. *Influenza and Other Respiratory Viruses*, *7*(7083), 42–51. http://doi.org/10.1111/irv.12080

Kim, J. H., Hatta, M., Watanabe, S., Neumann, G., Watanabe, T., & Kawaoka, Y. (2010). Role of host-specific amino acids in the pathogenicity of avian H5N1 influenza viruses in mice. *Journal of General Virology*, *91*(Pt 5), 1284–1289. http://doi.org/10.1099/vir.0.018143-0

Kim, W., Young, S., Huh, J., Kim, M., Kim, Y., Kim, H., Rya, Y., et al. (2011). Triple-combination antiviral drug for pandemic H1N1 influenza virus infection in critically ill patients on mechanical ventilation. *Antimicrobial Agents and Chemotherapy*, *55*(12), 5703–5709. http://doi.org/10.1128/AAC.05529-11

Kochs, G., & Haller, O. (1999). Interferon-induced human MxA GTPase blocks nuclear import of Thogoto virus nucleocapsids. *Proceedings of the National Academy of Sciences of the United States of America*, *96*(5), 2082–2086.

Kochs, G., Janzen, C., Hohenberg, H., & Haller, O. (2002). Antivirally active MxA protein sequesters La Crosse virus nucleocapsid protein into perinuclear complexes. *Proceedings of the National Academy of Sciences of the United States of America*, *99*(5), 3153–3158. http://doi.org/10.1073/pnas.052430399

Kudo, N., Matsuoka, Y., Taoka, H., Fujiwara, D., Schreiner, E. P., Wolff, B., et al. (1999). Leptomycin B inactivates CRM1/exportin 1 by covalent modification at cysteine residue in the central conserved region. *Cell Biology*, 1–6.

Kumar, N., Liang, Y., Parslow, T. G., & Liang, Y. (2011). Receptor tyrosine kinase inhibitors block multiple steps of influenza a virus replication. *Journal of Virology*, *85*(6), 2818–2827. http://doi.org/10.1128/JVI.01969-10

Kuo, R.-L., Li, L.-H., Lin, S.-J., Li, Z.-H., Chen, G.-W., Chang, C.-K., et al. (2016). Role of N Terminus-Truncated NS1 Proteins of Influenza A Virus in Inhibiting IRF3 Activation. *Journal of Virology*, *90*(9), 4696–4705. http://doi.org/10.1128/JVI.02843-15

Kurokawa, M., Ochiai, H., Nakajima, K., & Niwayama, S. (1990). Inhibitory effect of protein kinase C inhibitor on the replication of influenza type A virus. *Journal of General Virology*, *71*, 2149–2155.

Kuruvilla, J., Savona, M., Baz, R., Mau-Sorensen, P. M., Gabrail, N., Garzon, R., et al. (2017). Selective inhibition of nuclear export with selinexor in patients with non-Hodgkin lymphoma. *Blood*, *129*(24), 3175–3183. http://doi.org/10.1182/blood-2016-11-750174

Lakdawala, S. S., Lamirande, E. W., Suguitan, A. L., Wang, W., Santos, C. P., Vogel, L., et al. (2011). Eurasian-Origin Gene Segments Contribute to the Transmissibility, Aerosol Release, and Morphology of the 2009 Pandemic H1N1 Influenza Virus. *PLoS Pathogens*, *7*(12), e1002443–14. http://doi.org/10.1371/journal.ppat.1002443

Larsen, S., Bui, S., Perez, V., Mohammad, A., Medina-Ramirez, H., & Newcomb, L. L. (2014). Influenza polymerase encoding mRNAs utilize atypical mRNA nuclear export. *Virology Journal*, *11*(1), 154–11. http://doi.org/10.1186/1743-422X-11-154

Leneva, I. A., Russell, R. J., Boriskin, Y. S., & Hay, A. J. (2009). Characteristics of arbidol-resistant mutants of influenza virus: Implications for the mechanism of anti-influenza action of arbidol. *Antiviral Research*, *81*(2), 132–140. http://doi.org/10.1016/j.antiviral.2008.10.009

Li, Z., Watanave, T., Hatta, M., Watanbe, S., Nando, A., Ozawa., M., et al. (2009). Mutational analysis of conserved amino acids in the influenza A virus nucleoprotein. *Journal of Virology*, *83*(9), 4153–4162. http://doi.org/10.1128/JVI.02642-08

Li, W., Chen, H., Sutton, T., Obadan, A., & Perez, D. (2014). Interactions between the

Influenza A Virus RNA Polymerase Components and Retinoic Acid-Inducible Gene I. *Journal of Virology*, *88*(18), 10432–10447.

Liang, Yuying, Hong, Y., & Parslow, T. G. (2005). cis-Acting packaging signals in the influenza virus PB1, PB2, and PA genomic RNA segments. *Journal of Virology*, *79*(16), 10348–10355. http://doi.org/10.1128/JVI.79.16.10348-10355.2005

Lohse, N., Hansen, A.-B. E., Pedersen, G., Kronborg, G., Gerstoft, J., Sorensen, H. T., et al. (2007). Survival of persons with and without HIV infection in Denmark, 1995-2005. *Annals of Internal Medicine*, *146*(2), 87–95.

London, C. A., Bernabe, L. F., Barnard, S., Kisseberth, W. C., Borgatti, A., Henson, M., et al. (2014). Preclinical evaluation of the novel, orally bioavailable Selective Inhibitor of Nuclear Export (SINE) KPT-335 in spontaneous canine cancer: results of a phase I study. *PLoS ONE*, *9*(2), e87585. http://doi.org/10.1371/journal.pone.0087585

Loucaides, E., von Kirchback, J., Foeglein, A., Sharps, J., Fodor, E., & Digard, P. (2009). Nuclear dynamics of influenza A virus ribonucleoproteins revealed by live-cell imaging studies. *Virology*, *394*(1), 154–163. http://doi.org/10.1016/j.virol.2009.08.015

Lundberg, L., Pinkham, C., Baer, A., Amaya, M., Narayanan, A., Wagstaff, K., Jans, D., & Kehn-Hall, K. (2013). Nuclear import and export inhibitors alter capsid protein distribution in mammalian cells and reduce Venezuelan Equine Encephalitis Virus replication. *Antiviral Research*, *100*(3), 662–672. http://doi.org/10.1016/j.antiviral.2013.10.004

Lutz, A., Dyall, J., Olivo, P. and Pekosz, A. (2005). Virus-inducible reporter genes as a tool for detecting and quantifying influenza A virus replication. *Journal of Virological Methods*, *126*(1-2), 13–20. http://doi.org/10.1016/-j.jviromet.2005.01.016

Ma, K., Roy, M., & Whittaker, G. R. (2001). Nuclear Export of Influenza Virus Ribonucleoproteins: Identification of an Export Intermediate at the Nuclear Periphery. *Virology*, *282*(2), 215–220. http://doi.org/10.1006/viro.2001.0833

Magnus, von, P. (1954). Incomplete Forms of Influenza Virus. *Advances in Virus Research*, *2 IS* -, 59–79.

Malakhov, M. P., Aschenbrenner, L. M., Smee, D. F., Wandersee, M. K., Sidwell, R. W., Gubareva, L. V., et al. (2006). Sialidase fusion protein as a novel broad-spectrum inhibitor of influenza virus infection. *Antimicrobial Agents and Chemotherapy*, *50*(4), 1470–1479. http://doi.org/10.1128/AAC.50.4.1470-1479.2006

Marjuki, H., Alam, M., Ehrhart, C., Wagner, R., Planz, O., Klenk, H., et al. (2006). Membrane Accumulation of Influenza A Virus Hemagglutinin Triggers Nuclear Export of the Viral Genome via Protein Kinase C-alpha-mediated Activation of ERK Signaling. *The Journal of Biological Chemistry*, *281*(24), 16707–16715.

Marjuki, H., Yen, H.-L., Franks, J., Webster, R. G., Pleschka, S., & Hoffmann, E. (2007). Higher polymerase activity of a human influenza virus enhances activation of the hemagglutinin-induced Raf/MEK/ERK signal cascade. *Virology Journal*, *4*(1), 134–19. http://doi.org/10.1186/1743-422X-4-134

Martin, K., & Helenius, A. (1991). Nuclear Transport of Influenza Virus Ribonucleoproteins: The Viral Matrix Protein (Ml) Promotes Export and Inhibits Import. *Cell*, *67*, 117–130.

Masihi, K. N., Schweiger, B., Finsterbusch, T., & Hengel, H. (2007). Low dose oral combination chemoprophylaxis with oseltamivir and amantadine for influenza A virus infections in mice. *Journal of Chemotherapy (Florence, Italy)*, *19*(3), 295–303. http://doi.org/10.1179/joc.2007.19.3.295

Matsumoto, K., & Wolffe, A. (1998). Gene regulation by Y-box proteins: coupling control of transcription and translation. *Trends in Cell Biology*, *8*, 318–323.

Matsuyama, A., Arai, R., Yashiroda, Y., Shirai, A., Kamata, A., Sekido, S., et al. (2006). ORFeome cloning and global analysis of protein localization in the fission yeast Schizosaccharomyces pombe, *24*(7), 841–847. http://doi.org/10.1038/nbt1222

Matsuzaki, Y., K, M., Aoki, Y., Suto, A., Abiko, C., Sanjoh, K., et al. (2010). A two-year survey of the oseltamivir-resistant influenza A(H1N1) virus in Yamagata, Japan and the clinical effectiveness of oseltamivir and zanamivir. *Virology Journal*, *7*(54), 1–8.

Matzinger, S. R., Carroll, T. D., Dutra, J. C., Ma, Z.-M., & Miller, C. J. (2013). Myxovirus resistance gene A (MxA) expression suppresses influenza A virus replication in alpha interferon-treated primate cells. *Journal of Virology*, *87*(2),

1150–1158. http://doi.org/10.1128/JVI.02271-12

Mänz, B., Dornfeld, D., Götz, V., Zell, R., Zimmermann, P., Haller, O., et al. (2013). Pandemic Influenza A Viruses Escape from Restriction by Human MxA through Adaptive Mutations in the Nucleoprotein. *PLoS Pathogens*, *9*(3), e1003279–16. http://doi.org/10.1371/journal.ppat.1003279

Mayer, D., Molawi, K., MArtinez-Sobrido, L., Ghanem, A., Thomas, S., Baginsky, S., et al. (2007). Identification of cellular interaction partners of the influenza virus ribonucleoprotein complex and polymerase complex using proteomic-based approaches. *Journal of Proteome Research*, *6*(2), 672–682. http://doi.org/10.1021/pr060432u

McCauley, J. W., & Mahy, B. W. (1983). Structure and function of the influenza virus genome. *Biochemical Journal*, *211*(2), 281–294.

McCown, M. F., & Pekosz, A. (2006). Distinct domains of the influenza a virus M2 protein cytoplasmic tail mediate binding to the M1 protein and facilitate infectious virus production. *Journal of Virology*, *80*(16), 8178–8189. http://doi.org/10.1128/JVI.00627-06

McKimm-Breschkin, J. L. (2000). Resistance of influenza viruses to neuraminidase inhibitors — a review. *Antiviral Research*, *47*, 1–17.

McMichael, A. J., & Haynes, B. F. (2013). Influenza vaccines: mTOR inhibition surprisingly leads to protection, *14*(12), 1205–1207. http://doi.org/-10.1038/ni.2764

Mehrbod, P., Omar, A. R., Hair-Bejo, M., Haghani, A., & Ideris, A. (2014). Mechanisms of action and efficacy of statins against influenza. *BioMed Research International*, *2014*(11), 872370–8. http://doi.org/10.1155/2014/872370

Miller, P. E., Rambachan, A., Hubbard, R. J., Li, J., Meyer, A. E., Stephens, P., et al. (2013). Supply of neuraminidase inhibitors related to reduced influenza A (H1N1) mortality during the 2009-2010 H1N1 pandemic: summary of an ecological study. *Influenza and Other Respiratory Viruses*, *7*(s2), 82–86. http://doi.org/-10.1111/irv.12092

Mills, J., Chanock, R. M., & Alling, D. W. (1969). Mutants of influenza virus. *British Medical Journal*, *4*(5684), 690.

Momose, F., Basler, C., O'Neill, R., Iwamatsu, A., Palese, P., & Nagata, K. (2001). Cellular splicing factor RAF-2p48/NPI-5/BAT1/UAP56 interacts with the influenza virus nucleoprotein and enhances viral RNA synthesis. *Journal of Virology*, *75*(4), 1899–1908. http://doi.org/10.1128/JVI.75.4.1899-1908.2001

Momose, F., Sekimoto, T., Ohkura, T., Jo, S., Kawaguchi, A., Nagata, K., & Morikawa, Y. (2011). Apical Transport of Influenza A Virus Ribonucleoprotein Requires Rab11-positive Recycling Endosome. *PLoS ONE*, *6*(6), e21123–15. http://doi.org/10.1371/journal.pone.0021123

Monto, A. S., McKimm-Breschkin, J. L., Macken, C., Hampson, A. W., Hay, A., Klimov, A., et al. (2006). Detection of influenza viruses resistant to neuraminidase inhibitors in global surveillance during the first 3 years of their use. *Antimicrobial Agents and Chemotherapy*, *50*(7), 2395–2402. http://doi.org/-10.1128/AAC.01339-05

Mortensen, E., Nakashima, B., Cornell, J., Copeland, L., Pugh, M., Anzueto, A., et al. (2012). Population-based study of statins, angiotensin II receptor blockers, and angiotensin-converting enzyme inhibitors on pneumonia-related outcomes. *Clinical Infectious Diseases*, *55*(11), 1466–1473. http://doi.org/10.1093/cid/cis733

Mosley, M., & Wyckoff, R. (1946). Electron micrography of the virus of influenza. *Nature*, *157*, 263.

Moss, R. B., Hansen, C., Sanders, R. L., Hawley, S., Li, T., & Steigbigel, R. T. (2012). A phase II study of DAS181, a novel host directed antiviral for the treatment of influenza infection. *The Journal of Infectious Diseases*, *206*(12), 1844–1851. http://doi.org/10.1093/infdis/jis622

Muramoto, Y., Noda, T., Kawakami, E., Akkina, R., & Kawaoka, Y. (2013). Identification of Novel Influenza A Virus Proteins Translated from PA mRNA. *Journal of Virology*, *87*(5), 2455–2462.

Mutka, S. C., Yang, W. Q., Dong, S. D., Ward, S. L., Craig, D. A., Timmermans, P. B. M. W. M., & Murli, S. (2009). Identification of Nuclear Export Inhibitors with Potent Anticancer Activity In vivo. *Cancer Research*, *69*(2), 510–517. http://doi.org/10.1158/0008-5472.CAN-08-0858

Muz, B., Azab, F., Puente, P., Landesman, Y., & Azab, A. (2017). Selinexor Overcomes Hypoxia-Induced Drug Resistance in Multiple Myeloma.

Translational Oncology, *10*(4), 632–640. http://doi.org/-10.1016/j.tranon.2017.04.010

Nair, J., Musi, E., & Schwartz, G. (2017). Selinexor (KPT-330) Induces Tumor Suppression through Nuclear Sequestration of IκB and Downregulation of Survivin. *Clinical Cancer Research*. http://doi.org/10.1158/1078-0432.CCR-16-2632

Nayak, D. P., Balogun, R. A., Yamada, H., Zhou, Z. H., & Barman, S. (2009). Influenza virus morphogenesis and budding. *Virus Research*, *143*(2), 147–161. http://doi.org/10.1016/j.virusres.2009.05.010

Nelson, M., & Vincent, A. (2015). Reverse zoonosis of influenza to swine: new perspectives on the human-animal interface. *Trends in Microbiology*, *23*(3), 142–153. http://doi.org/10.1016/j.tim.2014.12.002

Neumann, G., Castrucci, M., & Kawaoka, Y. (1997). Nuclear Import and Export of Influenza Virus Nucleoprotein. *Journal of Virology*, *71*(12), 9690–9700.

Neumann, G., Hughes, M., & Kawaoka, Y. (2000). Infuenza A virus NS2 protein mediates vRNP nuclear export through NES-independent interaction with hCRM1. *The EMBO Journal*, *19*(24), 6751–6758.

Neumann, G., Noda, T., & Kawaoka, Y. (2009). Emergence and pandemic potential of swine-origin H1N1 influenza virus. *Nature*, *459*(7249), 931–939. http://doi.org/10.1038/nature08157

Newby, C., Sabin, L., & Pekosz, A. (2007). The RNA binding domain of influenza A virus NS1 protein affects secretion of tumor necrosis factor alpha, interleukin-6, and interferon in primary murine tracheal epithelial cells. *Journal of Virology*, *81*(17), 9469–9480. http://doi.org/10.1128/JVI.00989-07

Nguyen, A. M., & Noymer, A. (2013). Influenza mortality in the United States, 2009 pandemic: burden, timing and age distribution. *PLoS ONE*, *8*(5), e64198. http://doi.org/10.1371/journal.pone.0064198

National Health Service (NHS), 2016 [Online] Available: http://www.nhs.uk-/Conditions/vaccinations/Pages/flu-influenzavaccine.aspx

Nicholson, K. G., Wood, J. M., & Zambon, M. (2003). Influenza. *The Lancet*, *362*(9397), 1733–1745. http://doi.org/10.1016/S0140-6736(03)14854-4

Nigg, P. E., & Pavlovic, J. (2015). Oligomerization and GTP-binding Requirements of MxA for Viral Target Recognition and Antiviral Activity against Influenza A Virus. *Journal of Biological Chemistry*, *290*(50), 29893–29906. http://doi.org/10.1074/jbc.M115.681494

Nishi, K., Yoshida, M., & Fujiwara, D. (1994). Leptomycin B targets a regulatory cascade of crm1, a fission yeast nuclear protein, involved in control of higher order chromosome structure and gene expression, 1–5.

Noda, T., Sagara, H., Yen, A., Takada, A., Kida, H., Cheng, R. H., & Kawaoka, Y. (2006). Architecture of ribonucleoprotein complexes in influenza A virus particles. *Nature*, *439*(7075), 490–492. http://doi.org/10.1038/nature04378

Noton, S. L., Medcalf, E., Fisher, D., Mullin, A. E., Elton, D., & Digard, P. (2007). Identification of the domains of the influenza A virus M1 matrix protein required for NP binding, oligomerization and incorporation into virions. *Journal of General Virology*, *88*(8), 2280–2290. http://doi.org/10.1099/vir.0.82809-0

Nguyen, J., Smee, D., Barnard, D., Julander, J., Gross, M., Jong, M., & Went, G. (2012). Efficacy of Combined Therapy with Amantadine, Oseltamivir, and Ribavirin In Vivo against Susceptible and Amantadine-Resistant Influenza A Viruses. *PLoS ONE*, *7*(1), e31006. http://doi.org/10.1371/journal.pone.0031006

O'Neill, R., Jaskunas, R., Blobel, G., Palese, P., & Moroianu, J. (1995). Nuclear Import of Influenza Virus RNA Can Be Mediated by Viral Nucleoprotein and Transport Factors Required for Protein Import. *The Journal of Biological Chemistry*, *270*(39), 22701–22704.

O'Neill, R., Talon, J., & Palese, P. (1998). The influenza virus NEP (NS2 protein) mediates the nuclear export of viral ribonucleoproteins. *The EMBO Journal*, 1–9.

Okomo-Adhiambo, M., Sleeman, K., Ballenger, K., Nguyen, H. T., Mishin, V. P., Sheu, T. G., et al. (2010). Neuraminidase Inhibitor Susceptibility Testing in Human Influenza Viruses: A Laboratory Surveillance Perspective. *Viruses*, *2*(10), 2269–2289. http://doi.org/10.3390/v2102269

O'Reilly, M., Oguin, T., Scott, S., Thomas, P., Locuson, C., Morrison, R., Daniels, J., Brown, H., & Lindsley, C. (2014). Discovery of a highly selective PLD2 inhibitor (ML395): a new probe with improved physiochemical properties and broad-spectrum antiviral activity against influenza strains. *ChemMedChem*, *9*(12), 2633–

2637. http://doi.org/10.1002/cmdc.201402333

Osterholm, M., Kelley, N., Sommer, A., & Belongia, E. (2011). Efficacy and effectiveness of influenza vaccines: a systematic review and meta-analysis. *The Lancet Infectious Diseases*, *12*(1), 36–44. http://doi.org/10.1016/S1473-3099(11)70295-X

Palese, P., Tobita, K., & Ueda, M. (1974). Characterization of Temperature Sensitive Influenza Virus Mutants Defective in Neuraminidase. *Virology*, *61*, 397–410.

Parikh, K., Cang, S., Sekhri, A., & Lui, D. (2014). Selective inhibitors of nuclear export (SINE)--a novel class of anti-cancer agents. *Journal of Hematology & Oncology*, *7*, 78. http://doi.org/10.1186/s13045-014-0078-0

Pavlovic, J., Haller, O., & Staeheli, P. (1992). Human and mouse Mx proteins inhibit different steps of the influenza virus multiplication cycle. *Journal of Virology*, *66*(4), 2564–2569.

Pavlovic, J., Zurcher, T., Haller, O., & Staeheli, P. (1990). Resistance to influenza virus and vesicular stomatitis virus conferred by expression of human MxA protein. *Journal of Virology*, *64*(7), 3370–3375.

Pauli, E.-K., Schmolke, M., Wolff, T., Viemann, D., Roth, J., Bode, J. G., & Ludwig, S. (2008). Influenza A Virus Inhibits Type I IFN Signaling via NF-κB-Dependent Induction of SOCS-3 Expression. *PLoS Pathogens*, *4*(11), e1000196.

Paterson, D., & Fodor, E. (2012). Emerging roles for the influenza A virus nuclear export protein (NEP). *PLoS Pathogens*, *8*(12), e1003019.

Pathak, K. B., & Nagy, P. D. (2009). Defective Interfering RNAs: Foes of Viruses and Friends of Virologists. *Viruses*, *1*(3), 895–919. http://doi.org/10.3390/v1030895

Perwitasari, O., Johnson, S., Yan, X., Howerth, E., Shacham, S., Landesman, Y., et al. (2014). Verdinexor, a Novel Selective Inhibitor of Nuclear Export, Reduces Influenza A Virus Replication In Vitro and In Vivo. *Journal of Virology*, *88*(17), 10228–10243. http://doi.org/10.1128/JVI.01774-14

Perwitasari, O., Johnson, S., Yan, X., Register, E., Crabtree, J., Gabbard, J., et al. (2016). Antiviral Efficacy of Verdinexor In Vivo in Two Animal Models of Influenza A Virus Infection. *PLoS ONE*, *11*(11), e0167221–14. http://doi.org/10.1371/journal.pone.0167221

Peternel, L., Kotnik, M., Prezelj, A., & Urleb, U. (2009). Comparison of 3 Cytotoxicity Screening Assays and Their Application to the Selection of Novel Antibacterial Hits. *Journal of Biomolecular Screening*, *14*(2), 142–150. http://doi.org/10.1177/1087057108329452

Pica, N., & Palese, P. (2013). Toward a Universal Influenza Virus Vaccine: Prospects and Challenges. *Annual Review of Medicine*, *64*(1), 189–202. http://doi.org/10.1146/annurev-med-120611-145115

Pleschka, S., Wolff, T., Ehrhart, C., Hobom, G., Planz, O., Rapp, U., & Ludwig, S. (2001). Influenza virus propagation is impaired by inhibition of the Raf/MEK/ERK signalling cascade. *Nature Cell Biology*, *3*, 301–305.

Plotch, S., Bouloy, M., & Krug, R. (1979). Transfer of 5'-terminal cap of globin mRNA to influenza vural complementary RNA during transcription *in vitro*. *Proc. Natl. Acad. Sci, USA*, *76*(4), 1618–1622.

Plotch, S., Bouloy, M., Ulmanen, I., & Krug, R. (1981). A Unique Cap(m7GpppXm)-Dependent Influenza Virion Endonuclease Cleaves Capped RNAs to Generate the Primers That Initiate Viral RNA Transcription. *Cell*, *23*, 847–858.

Poehling, K., Edwards, K., Weinberg, G., Szilagyi, P., Staat, M., Iwane, M., et al. (2006). The Underrecognized Burden of Influenza in Young Children. *The New England Journal of Medicine*, *355*, 31–40.

Pollard, V. W., & Malim, M. H. (1998). The HIV-1 Rev protein. *Annual Review of Microbiology*, *52*(1), 491–532. http://doi.org/10.1146/annurev.micro.52.1.491

Poon, L., Pritlove, D., Fodor, E., & Brownlee, G. (1999). Direct Evidence that the Poly(A) Tail of Influenza A Virus mRNA Is Synthesized by Reiterative Copying of a U Track in the Virion RNA Template. *Journal of Virology*, *73*(4), 3473–3476.

Portela, A., & Digard, P. (2002). The influenza virus nucleoprotein: a multifunctional RNA-binding protein pivotal to virus replication. *Journal of General Virology*, *83*, 723–734.

Pronker, E. S., Claassen, E., & Osterhaus, A. D. M. E. (2012). Development of new generation influenza vaccines: Recipes for success? *Vaccine*, *30*(51), 7344–7347. http://doi.org/10.1016/j.vaccine.2012.09.071

Raboud, J. M., Harris, M., Rae, S., & Montaner, J. (2002). Impact of adherence on duration of virological suppression among patients receiving combination antiretroviral therapy. *HIV Medicine*, *3*(2), 118–124. http://doi.org/10.1046-/j.1468-1293.2002.00109.x

Read, E. K. C., & Digard, P. (2010). Individual influenza A virus mRNAs show differential dependence on cellular NXF1/TAP for their nuclear export. *Journal of General Virology*, *91*(5), 1290–1301. http://doi.org/10.1099/vir.0.018564-0

Roberts, P., Lamb, R., & Compans, R. (1998). The M1 and M2 Proteins of Influenza A Virus Are Important Determinants in Filamentous Particle Formation, *240*, 127–137.

Robertson, J., Schubert, M., & Lazzerini, R. (1981). Polyadenylation Sites for Influenza Virus mRNA. *Journal of Virology*, *38*(1), 157–163.

Rossignol, J., Elfert, A., El-Gohary, Y., & Keeffe, E. (2009). Improved Virologic Response in Chronic Hepatitis C Genotype 4 Treated With Nitazoxanide, Peginterferon, and Ribavirin. *Gastroenterology*, *136*(3), 856–862.

Rossignol, J. (2014). Nitazoxanide: A first-in-class broad-spectrum antiviral agent. *Antiviral Research*, *110 IS* -, 94–103.

Rossman, J. S., Jing, X., Leser, G. P., & Lamb, R. A. (2010). Influenza Virus M2 Protein Mediates ESCRT-Independent Membrane Scission. *Cell*, *142*(6), 902–913. http://doi.org/10.1016/j.cell.2010.08.029

Sakaguchi, A., Hirayama, E., Hiraki, A., Ishida, Y. O.-I., & Kim, J. (2003). Nuclear export of influenza viral ribonucleoprotein is temperature-dependently inhibited by dissociation of viral matrix protein. *Virology*, *306*(2), 244–253. http://doi.org/10.1016/S0042-6822(02)00013-2

Salk, J., & Salk, D. (1977). Control of Influenza and Poliomyelitis with Killed Virus Vaccines. *Science*, *195*, 834–847.

Sato, H., Masuda, M., Miura, R., Yoneda, M., & Kai, C. (2006). Morbillivirus nucleoprotein possesses a novel nuclear localization signal and a CRM1-independent nuclear export signal. *Virology*, *352*(1), 121–130. http://doi.org/10.1016/j.virol.2006.04.013

Satterly, N., Tsau, P., Deursen, J., Nussenzveig, D., Wang, Y., Faria, P., et al. (2007).

Influenza virus targets the mRNA export machinery and the nuclear pore complex. *Proc. Natl. Acad. Sci, USA*, *104*(6), 1853–1858.

Schnell, J. R., & Chou, J. J. (2008). Structure and mechanism of the M2 proton channel of influenza A virus. *Nature*, *451*(7178), 591–595. http://doi.org/10.1038/nature06531

Scholtissek, C., Becht, H., & Rott, R. (1971). Inhibitionof Influenza RNA Polymerase by Specific Antiserum. *Virology*, *43*, 137–143.

Schroeder, C., Heider, H., Hegenscheid, B., Schoffel, M., Bubovich, V. I., & Rosenthal, H. A. (1985). The anticholinergic anti-Parkinson drug Norakin selectively inhibits influenza virus replication. *Antiviral Research*, *Suppl 1*, 95–99.

Seladi-Schulman, J., Steel, J., & Lowen, A. C. (2013). Spherical Influenza Viruses Have a Fitness Advantage in Embryonated Eggs, while Filament-Producing Strains Are Selected In Vivo. *Journal of Virology*, *87*(24), 13343–13353. http://doi.org/10.1128/JVI.02004-13

Selman, M., Dankar, S., Forbes, N., Jia, J., & Brown, E. (2012). Adaptive mutation in influenza A virus non-structural gene is linked to host switching and induces a novel protein by alternative splicing. *Journal Title*, *1*(11), e42. http://doi.org/10.1038/emi.2012.38

Shaw, M. L., Stone, K. L., Colangelo, C. M., Gulcicek, E. E., & Palese, P. (2008). Cellular proteins in influenza virus particles. *PLoS Pathogens*, *4*(6), e1000085. http://doi.org/10.1371/journal.ppat.1000085

Sheu, T. G., Deyde, V. M., Okomo-Adhiambo, M., Garten, R. J., Xu, X., Bright, R. A., et al. (2008). Surveillance for neuraminidase inhibitor resistance among human influenza A and B viruses circulating worldwide from 2004 to 2008. *Antimicrobial Agents and Chemotherapy*, *52*(9), 3284–3292. http://doi.org/10.1128/AAC.00555-08

Shimizu, T., Takizawa, N., Watanabe, K., Nagata, K., & Kobayashi, N. (2011). Crucial role of the influenza virus NS2 (NEP) C-terminal domain in M1 binding and nuclear export of vRNP. *FEBS Letters*, *585*(1), 41–46. http://doi.org/10.1016/j.febslet.2010.11.017

Sidwell, R. W., Bailey, K. W., Wong, M.-H., Barnard, D. L., & Smee, D. F. (2005).

In vitro and in vivo influenza virus-inhibitory effects of viramidine. *Antiviral Research*, *68*(1), 10–17. http://doi.org/10.1016/j.antiviral.2005.06.003

Smee, D. F., Bailey, K. W., Morrison, A. C., & Sidwell, R. W. (2002). Combination treatment of influenza A virus infections in cell culture and in mice with the cyclopentane neuraminidase inhibitor RWJ-270201 and ribavirin. *Chemotherapy*, *48*(2), 88–93.

Smee, D., Hurst, B., Wong, M., Bailey, K., & Morrey, D. (2009). Effects of double combinations of amantadine, oseltamivir, and ribavirin on influenza A (H5N1) virus infections in cell culture and in mice. *Antimicrobial Agents and Chemotherapy*, *53*(5), 2120–2128. http://doi.org/10.1128/AAC.01012-08

Smee, D. F., Hurst, B. L., Wong, M.-H., Tarbet, E. B., Babu, Y. S., Klumpp, K., & Morrey, J. D. (2010). Combinations of oseltamivir and peramivir for the treatment of influenza A (H1N1) virus infections in cell culture and in mice. *Antiviral Research*, *88*(1), 38–44. http://doi.org/10.1016/j.antiviral.2010.07.003

Smee, D. F., Wong, M.-H., Bailey, K. W., & Sidwell, R. W. (2006). Activities of oseltamivir and ribavirin used alone and in combination against infections in mice with recent isolates of influenza A (H1N1) and B viruses. *Antiviral Chemistry and Chemotherapy*, *17*(4), 185–192. http://doi.org/10.1177/095632020601700403

Stouffer, A. L., Acharya, R., Salom, D., Levine, A. S., Di Costanzo, L., Soto, C. S., et al. (2008). Structural basis for the function and inhibition of an influenza virus proton channel. *Nature*, *451*(7178), 596–599. http://doi.org/10.1038/nature06528

Takizawa, N., Watanabe, K., Nouno, K., Kobayashi, N & Nagata, K. (2006). Association of functional influenza viral proteins and RNAs with nuclear chromatin and sub-chromatin structure. *Microbes and Infection*, *8*(3), 823–833. http://doi.org/10.1016/j.micinf.2005.10.005

Taiwo, B., Murphy, R. L., & Katlama, C. (2010). Novel antiretroviral combinations in treatment-experienced patients with HIV infection: rationale and results. *Drugs*, *70*(13), 1629–1642. http://doi.org/10.2165/11538020-000000000-00000

Taubenberger, J. K., & Morens, D. M. (2006). Influenza revisited. *Emerging Infectious Diseases*, *12*(1), 1–2. http://doi.org/10.3201/eid1201.051442

Teng, S., Wang, L., Srivastava, A., Schwartz, C., & Alexov, E. (2010). Structural Assessment of the Effects of Amino Acid Substitutions on Protein Stability and

Protein-Protein Interaction. *International Journal of Computational Biology and Drug Design*, *3*(4), 334–349.

Thomas, M., Lischka, P., Müller, R., & Stamminger, T. (2011). The Cellular DExD/H-Box RNA-Helicases UAP56 and URH49 Exhibit a CRM1-Independent Nucleocytoplasmic Shuttling Activity. *PLoS ONE*, *6*(7), e22671. http://doi.org/10.1371/journal.pone.0022671

Tisoncik, J. R., Billharz, R., Burmakina, S., Belisle, S. E., Proll, S. C., Korth, M. J., et al. (2011). The NS1 protein of influenza A virus suppresses interferon-regulated activation of antigen-presentation and immune-proteasome pathways. *Journal of General Virology*, *92*(Pt 9), 2093–2104. http://doi.org/10.1099/vir.0.032060-0

Tong, S., Yan, L., Rivailler, P., Conrardy, C., Castillo, D., Chen, L., et al. (2012). A distinct lineage of influenza A virus from bats. *PLoS Pathogens*, *109*(11), 4269–4274. http://doi.org/10.1073/pnas.1116200109/-/DCSupplemental/sapp.pdf

Tong, S., Zhu, X., Li, Y., Shi, M., Zhang, J., Bourgeois, M., et al. (2013). New World Bats Harbor Diverse Influenza A Viruses. *PLoS Pathogens*, *9*(10), e1003657. http://doi.org/10.1371/journal.ppat.1003657.t001

Triana-Baltzer, G., Gubareva, L., Nicholls, J., Pearce, M., Mishin, V., Belser, J., et al. (2009). Novel Pandemic Influenza A(H1N1) Viruses Are Potently Inhibited by DAS181, a Sialidase Fusion Protein. *PLoS ONE*, *4*(11), e7788. http://doi.org/10.1371/journal.pone.0007788

Turan, K., Mibayashi, M., Suguyama, K., Saito, S., Numajiri, A., & Nagata, K. (2004). Nuclear MxA proteins form a complex with influenza virus NP and inhibit the transcription of the engineered influenza virus genome. *Nucleic Acids Research*, *32*(2), 643–652.

Turner, D., Wailoo, A., Nicholson, K., Cooper, N., Sutton, A., & Abrams, K.. (2003). Systematic review and economic decision modelling for the prevention and treatment of influenza A and B. *Health Technology Assessment (Winchester, England)*, *7*(35), iii–iv– xi–xiii– 1–170.

Turner, J. G., Dawson, J. L., Grant, S., Shain, K. H., Dalton, W. S., Dai, Y., et al. (2016). Treatment of acquired drug resistance in multiple myeloma by combination therapy with XPO1 and topoisomerase II inhibitors. *Journal of Hematology & Oncology*, *9*(1), 2648–11. http://doi.org/10.1186/s13045-016-0304-z

Tynell, J., n, K. M., & Julkunen, I. (2014). Mutations within the conserved NS1 nuclear export signal lead to inhibition of influenza A virus replication. *Virology Journal*, *11*(1), 1–12. http://doi.org/10.1186/1743-422X-11-128

Varghese, J., Laver, W., & Colman, P. (1983). Structure of the influenza virus glycoprotein antigen neuraminidase at 2.9 A resolution. *Nature*, *303*(5912), 35–40.

Velthuis, te, A. J. W., & Fodor, E. (2016). Influenza virus RNA polymerase: insights into the mechanisms of viral RNA synthesis. *Nature Publishing Group*, *14*(8), 479–493. http://doi.org/10.1038/nrmicro.2016.87

Verhelst, J., Parthoens, E., Schepens, B., Fiers, W., & Saelens, X. (2012). Interferon-inducible protein Mx1 inhibits influenza virus by interfering with functional viral ribonucleoprotein complex assembly. *Journal of Virology*, *86*(24), 13445–13455. http://doi.org/10.1128/JVI.01682-12

Vijayakrishnan, S., Loney, C., Jackson, D., Suphamungmee, W., Rixon, F. J., & Bhella, D. (2013). Cryotomography of Budding Influenza A Virus Reveals Filaments with Diverse Morphologies that Mostly Do Not Bear a Genome at Their Distal End. *PLoS Pathogens*, *9*(6), e1003413–11. http://doi.org/10.1371/journal.ppat.1003413

Vreede, F. T., Jung, T. E., & Brownlee, G. G. (2004). Model suggesting that replication of influenza virus is regulated by stabilization of replicative intermediates. *Journal of Virology*, *78*(17), 9568–9572. http://doi.org/10.1128/JVI.78.17.9568-9572.2004

Wang, P., & Palese, P. (1997). The NPI-1/NPI-3 (Karyopherin-a) Binding Site on the Influenza A Virus Nucleoprotein NP is a Noncoventional Nuclear Localization Signal. *Journal of Virology*, *71*(3), 1850–1856.

Wang, B., Rekosh, D., & Hammarskjold, M.-L. (2015). Evolutionary conservation of a molecular machinery for export and expression of mRNAs with retained introns. *Rna*, *21*(3), 426–437. http://doi.org/10.1261/rna.048520.114

Wang, M., Wang, S., Wang, W., Wang, Y., Wang, H., & Zhu, W. (2017). Inhibition effects of novel polyketide compound PPQ-B against influenza A virus replication by interfering with the cellular EGFR pathway. *Antiviral Research*, *143*, 74–84. http://doi.org/10.1016/j.antiviral.2017.04.007

Wasilewski, S., Calder, L. J., Grant, T., & Rosenthal, P. B. (2012). Distribution of surface glycoproteins on influenza A virus determined by electron cryotomography. *Vaccine*, *30*(51), 7368–7373. http://doi.org/10.1016-/j.vaccine.2012.09.082

Watanabe, K., Takizawa, N., Masaki, K., Kohtaro, H., Kobayashi, N., & Nagata, K. (2001). Inhibition of nuclear export of ribonucleoprotein complexes of influenza virus by leptomycin B. *Virus Research*, 1–12.

Watanabe, T., & Kawaoka, Y. (2015). Influenza virus–host interactomes as a basis for antiviral drug development. *Current Opinion in Virology*, *14*, 71–78. http://doi.org/10.1016/j.coviro.2015.08.008

Watanabe, T., Watanabe, S., Noda, T., Fujii, Y., & Kawaoka, Y. (2003). Exploitation of nucleic acid packaging signals to generate a novel influenza virus-based vector stably expressing two foreign genes. *Journal of Virology*, *77*(19), 10575–10583. http://doi.org/10.1128/JVI.77.19.10575-10583.2003

Webster, R. G., Bean, W. J., Gorman, O. T., Chambers, T. M., & Kawaoka, Y. (1992). Evolution and ecology of influenza A viruses. *Microbiological Reviews*, *56*(1), 152–179.

Webster, R. G., Yakhno, M., Hinshaw, V., Bean, W., & Murti, G. (1978). Intestinal Influenza: Replication and Characterization of Influenza Viruses in Ducks. *Virology*, *84*, 268–278.

White, C. A. J. (2004). Nitazoxanide: a new broad spectrum antiparasitic agent. *Expert Review of Anti-Infective Therapy*, *2*(1), 43–49.

Whittaker, G. R., Matthew, B., & Helenius, A. (1996). Nuclear Trafficking of Influenza Virus Ribonucleoproteins in Heterokaryons. *Journal of Virology*, 1–14.

Wise, H. M., Hutchinson, E. C., Jagger, B. W., Stuart, A. D., Kang, Z. H., Robb, N., et al. (2012). Identification of a Novel Splice Variant Form of the Influenza A Virus M2 Ion Channel with an Antigenically Distinct Ectodomain. *PLoS Pathogens*, *8*(11), e1002998–14. http://doi.org/10.1371/journal.ppat.1002998

Wisskirchen, C., Ludersdorfer, T. H., Muller, D. A., Moritz, E., & Pavlovic, J. (2011). The cellular RNA helicase UAP56 is required for prevention of double-stranded RNA formation during influenza A virus infection. *Journal of Virology*, *85*(17),

8646–8655. http://doi.org/10.1128/JVI.02559-10

Wong, S. S., & Webby, R. J. (2013). Traditional and new influenza vaccines. *Clinical Microbiology Reviews*, *26*(3), 476–492. http://doi.org/10.1128/CMR.00097-12

World Health Organisation (WHO), 2006 [Online] Available: http://www.who.int-/influenza/en/

Worobey, M., Han, G.-Z., & Rambaut, A. (2014). Genesis and pathogenesis of the 1918 pandemic H1N1 influenza A virus. *Proceedings of the National Academy of Sciences of the United States of America*, *111*(22), 8107–8112. http://doi.org/10.1073/pnas.1324197111

Wu, W. W. H., Weaver, L. L., & Pant eacute, N. (2009). Purification and Visualization of Influenza A Viral Ribonucleoprotein Complexes. *Journal of Visualized Experiments*, (24), 1–3. http://doi.org/10.3791/1105

Xiao, H., Killip, M. J., Staeheli, P., Randall, R. E., & Jackson, D. (2013). The Human Interferon-Induced MxA Protein Inhibits Early Stages of Influenza A Virus Infection by Retaining the Incoming Viral Genome in the Cytoplasm. *Journal of Virology*, *87*(23), 13053–13058.

Yamaguchi, M., Danev, R., Nishiyama, K., Sugawara, K., & Nagayama, K. (2008). Zernike phase contrast electron microscopy of ice-embedded influenza A virus. *Journal of Structural Biology*, *162*(2), 271–276. http://doi.org/10.1016/j.jsb.2008.01.009

Yamaya, M., Shimotai, Y., Hatachi, Y., Kalonji, N., Tandio, Y., Kitajima, Y., et al. (2015). The serine protease inhibitor camostat inhibits influenza virus replication and cytokine production in primary cultures of human tracheal epithelial cells. *Pulmonary Pharmacology & Therapeutics*, *33*, 66–74. http://doi.org/10.1016/j.pupt.2015.07.001

Yamayoshi, S., Watanabe, M., Goto, H., & Kawaoka, Y. (2015). Identification of a Novel Viral Protein Expressed from the PB2 Segment of Influenza A Virus. *Journal of Virology*, *90*(1), 444–456. http://doi.org/10.1128/JVI.02175-15

Yang, Y., Ma, J., Chen, Y., & Wu, M. (2004). Nucleocytoplasmic shuttling of receptor-interacting protein 3 (RIP3): identification of novel nuclear export and import signals in RIP3. *Journal of Biological Chemistry*, *279*(37), 38820–38829. http://doi.org/10.1074/jbc.M401663200

Ye, Q., Krug, R. M., & Tao, Y. J. (2006b). The mechanism by which influenza A virus nucleoprotein forms oligomers and binds RNA. *Nature*, *444*(7122), 1078–1082. http://doi.org/10.1038/nature05379

York, A., & Fodor, E. (2014). Biogenesis, assembly, and export of viral messenger ribonucleoproteins in the influenza A virus infected cell. *RNA Biology*, *10*(8), 1274–1282. http://doi.org/10.4161/rna.25356

Yu, M., Liu, X., Cao, S., Zhao, Z., Zhang, K., Xie, Q., et al. (2012). Identification and Characterization of Three Novel Nuclear Export Signals in the Influenza A Virus Nucleoprotein. *Journal of Virology*, *86*(9), 4970–4980. http://doi.org/10.1128/JVI.06159-11

Zambon, M., & Hayden, F. (2001). Position statement: global neuraminidase inhibitor susceptibility network. *Antiviral Research*, *49*, 147–156.

Zebedee, S. L., & Lamb, R. A. (1988). Influenza A virus M2 protein: monoclonal antibody restriction of virus growth and detection of M2 in virions. *Journal of Virology*, *62*(8), 2762–2772.

Zebedee, S., & Lamb, R. (1989). Nucleotide sequences of influenza A virus RNA segment 7: a comparison of five isolates. *Nucleic Acids Research*, *17*(7), 2870.

Zimmermann, O., Manz, B., Haller, O., Schwemmle, M., & Kocks, G. (2011). The viral nucleoprotein determines Mx sensitivity of influenza A viruses. *Journal of Virology*, *85*(16), 8133–8140. http://doi.org/10.1128/JVI.00712-11

Zhao, H., Ekstrom, M., & Garoff, H. (1998). The M1 and NP proteins of influenza A virus form homo- but not heterooligomeric complexes when coexpressed in BHK-21 cells. *Journal of General Virology*, *79*, 2435–2446.

Zhang, K., Wang, M., Tamayo, A. T., Shacham, S., Kauffman, M., Lee, J., et al. (2013). Novel selective inhibitors of nuclear export CRM1 antagonists for therapy in mantle cell lymphoma. *Experimental Hematology*, *41*(1), 67–78.e4. http://doi.org/10.1016/j.exphem.2012.09.002

Zheng, B.-J., Chan, K.-W., Lin, Y.-P., Zhao, G.-Y., Chan, C., Zhang, H.-J., et al. (2008). Delayed antiviral plus immunomodulator treatment still reduces mortality in mice infected by high inoculum of influenza A/H5N1 virus. *Proceedings of the National Academy of Sciences of the United States of America*, *105*(23), 8091–

8096. http://doi.org/10.1073/pnas.0711942105

Zheng, W., Li, J., Wang, S., Cao, S., Jiang, J., Chen, C., et al. (2015). Phosphorylation Controls the Nuclear-Cytoplasmic Shuttling of Influenza A Virus Nucleoprotein. *Journal of Virology*, *89*(11), 5822–5834. http://doi.org/10.1128/JVI.00015-15